UNIVERSITÀ DEGLI STUDI DI PADOVA

DIPARTIMENTO DI INGEGNERIA CIVILE, EDILE ED AMBIENTALE

CORSO DI LAUREA MAGISTRALE IN INGEGNERIA CIVILE

Tesi di Laurea Magistrale in

Ingegneria Civile

Indirizzo Strutture

RELIABILITY-BASED CALIBRATION OF PARTIAL SAFETY FACTORS FOR CFRP STRENGTHENING IN BENDING OF RC BRIDGES

Relatori: Ch.mo Prof. Joan Ramon Casas

Ch.mo Prof. Carlo Pellegrino

Laureanda: Caterina Trentin

Anno Accademico 2012/2013

Contents

Summary

It is not easy to establish a value for safety factors in the design of structural members, whatever the resisting mechanism they work through. Indeed, safety factor values are often based on the experience of competent designers and are rarely supported by statistical studies. Even though this is not a major problem for easy predictable resisting models, imprecise safety factor estimates may lead to significant consequences in the case of more complicated resisting models, which are affected by high levels of uncertainty, just as the debonding models for flexural strengthening of reinforced concrete members with FRPs.

Over the last years, this phenomenon has been studied closely, and more and more precise models predicting the FRP debonding have been developed. However the uncertainty underpinning the issue is hardly impossible to remove. This is why both a correct estimate of the design values of the safety factors and a better knowledge of the accuracy of the models are extremely important.

This work deals with the calibration of the design safety factor at the Ultimate Limit State for two intermediate crack-induced debonding models, Casas and Pascual (2006) [9] and Said and Wu (2007) [29]. A reliability-based method is adopted and the *model error* is for the first time considered in the procedure as one of the main random variables participating in the problem.

A brief Introduction is dedicated to the state of art and to the Objectives of the paper.

In the first Chapter, CFRP properties are described and the various failure modes of flexurally-strengthened reinforced-concrete members are discussed, focusing on the debonding failure.

In Chapter 2, seven reinforced-concrete bridges (four girder bridges and three slab bridges) are presented. The data about their geometry and reinforcements are taken from a Spanish national catalogue of the ‘40s. In order to verify if the resisting moment of the existing bridges satisfies the actual code requirements, the amount of tensile steel that each bridge should have is calculated according to the Eurocode 1 [6]: all the bridges present different percents of steel lack and need to be strengthened.

In Chapter 3, five intermediate crack-induced debonding models are presented: Teng and Chen (2003) [33], Casas and Pascual (2006), Said and Wu (2007), ACI 440.2R-08 (2008) [2], CNR DT/200 R1/2013 (2013) [14]. The ultimate debonding strain is calculated for each model, inserting the required data corresponding to each bridge. Both a prefabricated and a wet-lay up systems are considered, with a composite/fiber thickness ranging from 0,1 to 5 mm. The comparison is made through the development of *debonding strain vs. composite thickness* graphs, that help to understand which are the main parameters influencing the debonding and the relation between the different models.

Next, in Chapter 4, the strengthening of the bridges included in the study is designed, according to both the CNR Italian guidelines and the American software XTRACT. This is done for two main reasons: first, to verify the reliability of the created design Excel files; second, to obtain results to be used as a basis for further comparison with the reliability approach's outcomes.

An introduction concerning the concept and the evaluation of structural reliability is developed in Chapter 5. The most common methods used to carry out a reliability-based analysis are briefly explained, and a Monte Carlo simulation is chosen to run the calibration.

In Chapter 6, the main variables participating in the limit state function and their probability density functions are presented (composite/fiber elastic modulus, tensile steel resistance, etc.).

Chapter 7 begins with an introduction to the model error variable. The latter is available only for two of the five debonding models introduced: Casas and Pascual's model and Said and Wu's model.

The calibration is then performed for two reliability index targets, β=3,5 and β=4. Three different methods are followed, that differ for the position of the safety factor in the design formula and of the *model error* in the resisting moment equation of the Monte Carlo simulation. The studied models are three: Casas and Pascual, Said and Wu and CNR DT/200 R1/2013. However, the latter model is analyzed only in the first procedure, in which the systemic uncertainties are not considered, since no values of the model error are available in the literature.

The last method, which turns out to be the correct one, consists in multiplying the model error variable for the entire resisting moment of the limit state equation; for the sake of coherence, the safety factor is placed before the whole resisting moment in the design formula.

It is possible to obtain results only for Said and Wu's model. They are commented and design values for the safety factors of the model are proposed. For Casas and Pascual, instead, no results are drawn and the reasons why this happens are explained in details in the last section. Eventually, all the proposed solutions and observations are summarized in the Conclusions Chapter, in which also some suggestions for further investigations are presented.

Introduction

Over the last 20 years, the use of fiber-reinforced polymers (FRP) for the strengthening, repair and seismic retrofit of existing structures has widely increased. This has been possible thanks to the huge research activity conducted, focused mainly on the FRPs mechanical characteristics and capacity on collaborating with other materials largely used in civil engineering, such as reinforced concrete, wood and masonry.

The strengthening with FRPs results very attractive since the composites present high mechanical characteristics, high properties as thermic and electric insulators, immunity to corrosion and efficiency of application. The use of FRPs is moreover not invasive, since the composites are bonded externally on existing structures in form of laminates, without altering heavily the facility configuration, size and weight.

The way they are applied to the existing structures is different depending on the action they have to contrast. FRPs are placed on the tension face of elements subject to bending, bonded reproducing a U-shape strengthening for elements subject to shear, attached to create a confinement for elements subject to shear and elements subject to torsion.

When testing flexurally-strengthened reinforced concrete elements, several different collapse modes have been observed [21]. The most problematic failure is the so-called *debonding*, which is generated in the vicinity of intermediate cracks or near one of the plate ends. Indeed, the high stress concentration at these points initiates the phenomenon, which propagates in the superficial concrete layer to which the composite plates are bonded. The debonding generally occurs before the ultimate tensile stress in the FRP is reached, therefore, it has often to be considered as the critical collapse mode in the design. Unfortunately, this failure mode is very difficult to predict and depends on numerous factors, so that is not easy to determine positively an ultimate limit value for the debonding stress.

Over the years, many models predicting debonding failures of RC concrete strengthened members have been developed. Each model counts for more or less parameters and has a certain degree of precision. Going from the strength of the fiber to the resin properties, from the ratio of the plate width over the concrete width to the effective bond length, the

factors affecting the debonding behavior are so many that is really difficult to create a model that counts them all accurately.

The large number of studies conducted to verify the goodness of the proposed models has pointed out the high uncertainty of the phenomenon, which makes really complicated to establish a design formula for national guidelines, that is, more specifically, to determine the right safety factor which should be used when designing with a certain debonding model.

Until now, most of the times, safety factors have been determined on the basis of generic statistical studies or of designers' experience, but the high variability related to the debonding problem would require a more precise approach, or better a *reliability-based approach*.

The term "*reliability*" means the capacity of a structure to perform required functions under stated conditions for a specified period of time. The measure of the structure reliability is given by the reliability index β, which assumes different values, depending on the importance of the strengthened structure and the sum of money available for the renewal [16].

When an existing structure is strengthened, it should be decided a reliability target index and it should be verified for which quantity of composite strengthening this target is reached. The check is done by setting the limit state function:

$$G = R - S \geq 0$$

where R is the resistance of the structural member and S represents the acting loads effect. When the limit state function is higher than zero ($G \geq 0$), the member is in the safe domain, otherwise it is in the unsafe domain ($G < 0$), which corresponds to the failure of the element. Depending on the method adopted (Monte Carlo simulation, FOSM or FORM, etc.), after calculating the probability of failure, it is possible to evaluate the β corresponding to the strengthened member.

The calibration of the safety factor is done by calculating the coefficient that minimizes the scatter between the fixed target β and the real β of the strengthened member.

A reliability-based approach for reinforced concrete elements, externally bonded with CFRPs (*carbon fiber-reinforced polymers*), was proposed for the first time by Triantafillou in 1992 [34], and then faced again in Plevris et al. in 1995 [28], in which a

Monte Carlo simulation was conducted in order to determine the strength reduction factor for a typical cross-section of RC beams strengthened in bending. Various design cases were considered, modifying conveniently the acting parameters; anyway, only the failure modes for CFRP rupture and concrete crushing were analyzed, saying that uncertainties in debonding failure could be substantially limited by a high level of control when applying the CFRP plate to the soffit of the beam.

Okeil et al. [27] conducted a similar study in 2002, this time for girder bridges cross-sections. The reliability of three simply-supported reinforced concrete bridges, with different levels of steel corrosion, was investigated in order to determine a resistance model for strengthened RC beams and estimate a strength reduction design factor. A Monte Carlo simulation led to the calculation of the resistant moment, while a first-order reliability method was used to obtain the reliability index β. Again the CFRP rupture failure mode was modeled, without considering any other type of failure, such as shear or debonding.

A more detailed procedure for calibrating safety factors when designing with FRP was proposed by Monti and Santini [24] in 2002. Their aim was to give an easy and general framework, that could be followed regardless of the different types of applications and strengthening used (flexure, shear, …). Unlikely, their method is difficult to solve, mainly because thought for different limit states and so multiple load and capacity situations that a simultaneous calibration should be done, implying a remarkable computational effort. Monti and Santini themselves applied the procedure in a flexural strengthening example by introducing some simplifications, strictly violating the purpose of the method they proposed.

In 2003, the problem was faced again by Val et al. [35], which made a FORM analysis in order to determine a force reduction factor for FRP-confined column design.

The drawbacks of all these studies mainly consist in four points:

- they consider only prefabricated systems, neglecting the variability which can affect the problem in case of a wet-lay up system (with the exception of Val et al. [35]);
- they did not propose a final design value, so that the calculation of safety factors and the development of reliability-based methods can be said meaningless;

- they did not consider the degradation of the FRP due to the environmental exposure;
- they did not take into account the real critical failure, i.e., the debonding.

All these problems were known by Atadero and Karbhari [3] which proposed a methodology for the calibration of the preliminary resistance factors for externally-bonded wet-lay up CFRP, by following the load and factor design (LRFD), given in the American Code. They studied the bending strengthening of 20 reinforced-concrete T beams bridge girders, hypothesizing different types of applications, accounting for the environmental exposure and aiming to three different target reliability factors, $\beta = 2{,}5$, 3,0 and 3,5. The collapse mode they investigated was the debonding failure.

They started from the modified LFRD equation they had already proposed in their previous article [4]:

$$\sum \gamma_i Q_i \leq \Phi R(\dots, \psi x_{FRP})$$

where:

- Q_i and R are the load effect and the resistance;
- γ_i is the load factor;
- Φ is the general resistance factor;
- ψ is the composite specific factor;
- x_{FRP} is the contribute of FRP to the resistance.

They proposed different design values of the composite specific factors for constant general resistance factors, pooling the analyzed bridges in more design groups, depending on the percent of steel loss. They suggested also to consider the mean value of laboratory test results as the characteristic value of the contribution of the composite to the resistance. The mean value is indeed independent from the COV and allows to assign all the variability of the problem to the composite resistance factor.

As observed by Ceci et al. [12], the drawback of the procedure followed by Atadero and Karbhari is that there is not a specific accounting for the modeling uncertainties (or systemic uncertainties), which in many cases play a significant role in the strengthening design with CFRP.

The model error can be quantified by the definition of a random variable, statistically determined, which is characterized by a specific mean and coefficient of variation (COV). Unfortunately, the systemic uncertainties are not evaluated for many models, therefore most of the times a reliability-based method cannot be applied with an appropriate level of safety.

Objectives

The purpose of this research is to determine the design safety factors of two intermediate crack-induced debonding models for flexurally strengthened reinforced-concrete members (i.e. Casas and Pascual [9, 11], Said and Wu [29]) at the Ultimate Limit State, following a reliability-based approach.

To perform a proper reliability-based analysis it is necessary to define accurately the independent random variables participating in the limit state function and their probability density functions. Indeed, the higher or lower number of independent variables can change significantly the speed of convergence of the analysis. In this paper, for the first time, one of the main objectives is to ass a further random variable to the others usually considered in a reliability-based approach (e.g. the material resistance and the acting loads): the *model error* variable. As already explained in the introduction paragraph, the model error takes into account all the systemic uncertainties related to the used resisting model and is a fundamental factor to quantify properly the accuracy of the prediction made. Until now, this variable has never been considered in the calibration of design safety factors for intermediate crack-induced debonding models; this is why the design values proposed for the most common existing models cannot be considered enough reliable, though based on the judgment of expert designers and the observation of multiple experimental results.

The innovation of the procedure introduced entails a particular effort in the understanding of the *model error* role: how should it be taken into account? And how does it affect the results?

The way it is determined suggests that it should be considered affecting the whole *concrete-steel-composite* system, and, therefore, it should be placed to multiply the whole resisting moment of the strengthened section in the limit state function. However, it could

be interesting to study also those situations in which it does not participate at all in the problem, or it simply affects just the composite resistance contribution. This would help in comprehending the importance of the model error and its effects on the results.

Moreover, a comparison between the design equations of the studied debonding models could give a further help to understand the model error's influence. This comparison could be made through the development of *debonding strain vs. composite thickness* graphs, which can be a useful reference for the analysis of the reliability approach's outcomes.

Indispensable for the performing of the calibration is also the development of proper design equations in parallel to the setting of the limit state equation. Results will be influenced strongly by the position of the safety factors themselves and by the resisting model adopted.

First, for sake of coherence, the position of the safety factor in the design equation should be the same of the model error in the corresponding limit state equation. Second, it is of vital importance to assume a cross-section resisting model as precise as possible.

The calibration will be here performed considering the flexural strengthening of T-shape reinforced-concrete members. It can be deduced from now that it would be necessary to introduce a specific model for the compressive concrete resistance. Indeed, it is known that generally, in T-shape sections, the debonding occurs before the ultimate compressive strength of the concrete is reached. Moreover, usually concrete strains are so low that the simplified rectangular stress-block cannot be used and it is necessary to refer to another stress-strain relation.

Therefore, an additional objective of the present research is to develop a simplified linear concrete stress-strain relation. This will allow to simplify the design equations, reducing significantly the computational effort, otherwise required.

As it can be understood from the considerations made, due to the innovation of the proposed procedure and to the multiplicity of aspects to be considered, the treated issue could appear complex and really hard to deal with.

This is why another objective is also to make the problem as easy as possible, giving a general framework for the calibration of safety factors, that can be easily applicable in many different situations.

Chapter 1

CFRP systems and failure modes of RC elements strengthened in bending

1.1 Carbon-Fiber-Reinforced Polymers (CFRPs)

The acronym CFRP indicates a composite material made up of carbon fibers embedded in a polymeric matrix to protect fibers and provide load transfer. The low specific gravity (polymers ensure a low density) and the good mechanical properties obtained by the combination of the two materials make CFRPs, and FRPs in general, an innovative and attractive technology for various technical fields.

From a structural design point of view, the most important characteristics are:

- the anisotropic an heterogeneous behavior;
- the high mechanical resistance, with an elastic constitutive relation until rupture;
- the elevated resistance to corrosion;
- the high properties as thermic and electric insulator;
- the facility of its application and the good adaptability to any surface shape.

The anisotropic behavior can increase significantly the material resistance if the fibers are properly aligned along the direction of the acting stress, otherwise it can be dangerous for the material performance. Furthermore, the heterogeneity can be synonymous of a scarce adherence between fibers and matrix, hence, it is necessary to choose carefully the combined materials. Generally, the matrix is made of an epoxy resin since it guarantees a good insulation and an optimum bond between fibers; moreover, it is thermosetting and enables to reach high performances even under high temperatures.

Carbon fibers differ from the other materials used as reinforcements (glass fibers, aramid fibers, ceramic fibers and basalt fibers) because of their higher elastic modulus and mechanical resistance. To obtain these properties, the fiber is subject to thermic treatments, such as the carbonization (1500-2000°C, to increase the critical load) and the graphitization (2500-3000°C, to increase the elastic modulus).

It is possible to produce different typologies of carbon fibers:

- High tenacity carbon fibers (HT), maximum tensile stress = 5000 MPa; tensile elastic modulus = 240 GPa; elongation at rupture = 1,5%; density = 1,78 g/cm^3;
- High modulus carbon fibers (HM), maximum tensile stress = 3000 MPa; tensile elastic modulus = 390 GPa; elongation at rupture = 0,8%; density = 1,80 g/cm^3;
- Ultra high modulus carbon fibers (UHM), maximum tensile stress = 1500 MPa; tensile elastic modulus = 640 GPa; elongation at rupture > 0,5%; density = 2,10 g/cm^3.

The drawback in the use of carbon fiber-reinforced polymers is their fragile behavior at rupture, dangerous for ultimate limit state design. Anyway, the mentioned qualities of the composite make it one of the most successful and valued material in civil engineering and its application is widely increasing.

1.2 The use of carbon fibers

The prevalent use of carbon fibers consists in repair, strengthening and retrofit of existing structures, while its exclusive employment in the construction of structural bearing elements is still not common.

The retrofit of existing structures by carbon fibers can be done basically in two ways:

- By using externally bonded laminates (*Figure 1.1*);
- By bonding external carbon fibers bars (*Near-Surface Mounted Bars* –NSMB- *Figure 1.2*).

Figure 1.1 Externally-bonded laminates.

Figure 1.2. Bonding external carbon fibers bars.

The second method is not frequent, mainly because more invasive and rather recent compared to the first one, and therefore considered less reliable. The bonding of CFRP plates, more in general with FRP, is instead so largely diffused that many countries have believed necessary to give guidelines for design with FRP, even if only few of them have a real official code.

1.3 Externally-bonded CFRP systems

CFRP strengthening plate systems can be divided into three main groups:

- Prefabricated systems (pre-cured);
- Wet-lay up systems (cured *in situ*);
- Pre-peg systems (pre-impregnated).

These systems differ in the constituent materials, form and procedure of application and the choice of one rather than another depends on the type of structure that have to be strengthened.

1.3.1 Prefabricated systems (*Figure 1.3*)

Manufactured off site, they exist in the market as unidirectional laminate sheets, multidirectional grids and shells. Their application is made using an adhesive, along with the primer and putty. In order to follow the right installation procedure, the manufacturer should be contacted.

Figure 1.3 Pre-cured system.

Since in this type of application the volume of the resin is known precisely, in calculations designers will refer to the proprieties of the entire composite, usually given by manufacturers.

1.3.2 Wet-lay up systems (*Figure 1.4*)

Common types of wet-lay up systems consist generally in dry unidirectional fiber sheets, dry multidirectional fiber sheets or fabrics and dry fiber tows (untwisted bundles of continuous fibers). These products are impregnated with a suturing resin on site, which, together with the primer and putty, creates the bonding of the FRP to the element surface.

The wetted fabric is therefore applied directly to the substrate, with the result that the bonding of the material and the cure of composite converge into one step. In field-manufactured systems is difficult to control precisely the quantity of resin used in the application, so, in calculations, designers have to refer to the area of the dry fiber.
This method allows to strengthen easily surfaces of different shapes, thanks to the flexibility of the wetted fabric. This is why wet-lay up systems result attractive to the designers, though the high degree of uncertainty associated with them.

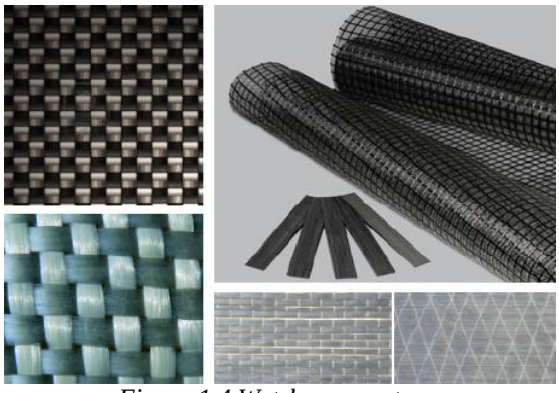

Figure 1.4 Wet-lay up systems.

Figure 1.5 Pre-peg system.

1.3.3 Pre-peg systems (*Figure 1.5*)

Pre-peg FRP systems consist of partially cured unidirectional or multidirectional fiber sheets or fabrics that are pre-impregnated with a suturing resin in the manufacturer's facility. They are bonded with or without an additional resin, depending on the specific application and cured *in situ* like wet-lay up systems.

1.4 Failure modes of RC elements strengthened in bending with FRP

The collapse behavior of reinforced concrete elements strengthened with CFRP is discussed below, in order to make clear the assumptions and considerations that will be made in the following chapters when designing the strengthening of reinforced concrete bridges. The failure modes of a RC element strengthened in flexure with externally-bonded CFRP reinforcement, at-large with FRP, can be divided in two classes:

1- Those where full composite action of concrete and FRP is maintained until the concrete reaches crushing in compression or the FRP fails in tension;

2- Those where the peeling-off of the FRP prevents the composite action of the two materials.

1.4.1 Full composite action

This type of failure is very similar to the classical flexural failure of RC beams, even if there are some small differences due to the brittle behavior of the FRP plate. FRP rupture generally occurs when the longitudinal steel bars are already yielded, although it depends on the location of the steel bars, which may be placed far away from the tension face.
There can be three failure modes:

a- Steel yielding followed by concrete crushing (FRP intact);
b- Crushing of the concrete in compression before yielding of the steel reinforcement (FRP intact). This type of failure occurs for relatively high reinforcement ratios, it is brittle and so unwanted.
c- Steel yielding followed by rupture of the FRP plate.

1.4.2 Loss of composite action

The role played by the adherence of composite and concrete is very important, since delamination or peeling-off is a fragile failure. Speaking of resistance hierarchy, this mechanism of crisis should not precede flexural or shear failure of the reinforced element. Delamination may occur at different interfaces between the concrete and the FRP reinforcement (*Figure 1.6*):

- **At the interfaces between concrete and adhesive or adhesive and FRP,** due to insufficient surface preparation during the application of the FRP process. This leads to a cohesion strength of epoxy resin lower than the adhesion strength.
- **In the adhesive.** Delamination will set in the adhesive only if its force gets lower than the concrete one and this can happen under particular conditions, such as high temperatures and very resistant concretes.
- **In the FRP**. It is called interlaminar shear failure and involves the debonding between fibers and resin in the composite. For example, if concrete has a high strength, the crack propagation could be energetically more convenient in the FRP than in the concrete.

By the way, this is a secondary failure mode, which occurs after the bond crack has initiated in the concrete.

- **In the concrete.** The resin has a tensile and shear strength higher than that of the concrete. A layer of concrete will remain on the FRP plate, and its thickness can vary between few millimeters to the entire concrete cover. As many experimental data show, this is the most common debonding failure, due mainly to the availability of strong adhesives that bond well to FRP and concrete.

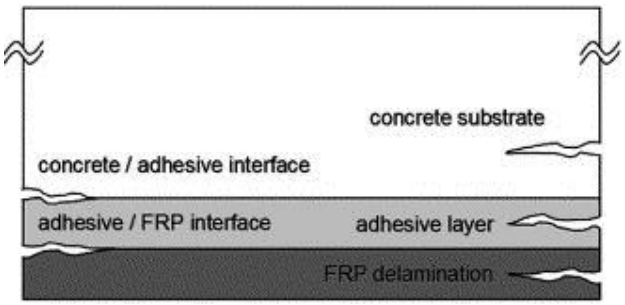

Figure 1.6. Delamination at different interfaces in the strengthened RC element.

The occurring of one bond failure rather than another one depends on the behavior of the RC strengthened member.

It is possible to identify two main groups of delamination modes:

a- Plate-end debonding failures;

b- Intermediate crack-induced interfacial debonding.

1.4.2.1 Plate-end debonding

It starts at or near the plate-end and two principal mechanisms can be observed. The most common is the concrete cover separation (*Figure 1.7*), due to the formation of a crack at or near the plate end, where there are high interfacial shear and normal stresses caused by the sudden termination of the plate. The crack propagates to the tensile steel and then continues horizontally along the steel line, provoking the concrete cover separation. Another plate-end debonding failure mode is the plate-end interfacial debonding (*Figure 1.8*), which is less frequent. As the former, this peeling is initiated by the presence of interfacial shear and normal stresses at or near the plate ends, which are higher than the

strength of the weakest material, generally the concrete. Characteristic of this type of failure is a thin layer of concrete that remains attached to the FRP plate (it could be questioned the choice of the failure name). This kind of delamination is increased by adhesives of poor quality and concrete surfaces not well-prepared.

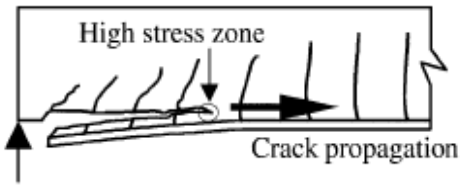

Figure 1.7. Concrete cover separation [31].

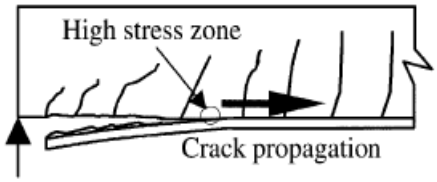

Figure 1.8. Plate-end interfacial debonding [31].

1.4.2.2 Intermediate crack-induced debonding

Delamination initiates at a flexural or a mixed flexural shear crack away from the plate end, generally where the maximum moment acts. The crack propagates from the intermediate zone to the end of the plate and causes the debonding. Failure occurs at the concrete level, adjacent to the adhesive-to-concrete interface, so that a thin layer of concrete remains attached to the FRP composite.

Interfacial debonding differentiates depending on which of the mentioned crack caused it: flexural (*Figure 1.9*) or mixed flexural-shear (*Figure 1.10*).

In the first case the high local interfacial stresses generated by the formation of the crack initiate the debonding, which progresses towards the plate end, usually the nearest one.

The widening of the cracks can be considered the driving force for the propagation of the debonding. In the second case, the presence of additional peeling stresses should be taken into account. They are those provoked by relative vertical displacements between the two faces of the crack. Anyway it is believed that these additional peeling stresses are not relevant as those generated by the widening of the crack.

This is because the FRP sheet is very thin and has a low flexural stiffness. Therefore it works as a membrane when subject to downward pushing force and develops in-plane tensile stresses rather than transverse shear stresses in the plate. This means that even if at the initiation of debonding tensile transverse stresses are high, they are expected to decrease rapidly as debonding propagates.

Hence, it is possible to say that intermediate flexural-shear crack debonding and intermediate flexural-crack debonding basically have a very similar behavior.

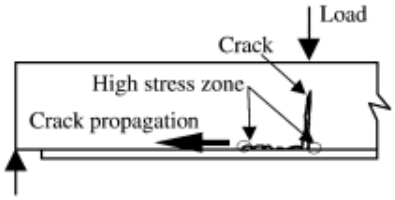

Figure 1.9. Intermediate flexural crack induced interfacial debonding [31].

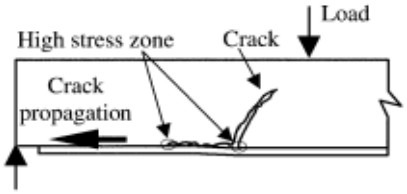

Figure 1.10. Intermediate flexural-shear crack induced interfacial debonding [31].

Chapter 2
Description of the analyzed bridges

2.1 The bridges and the used nomenclature

Debonding models are generally checked in specimens of small size, that do not represent properly the real structures to which the FRP strengthening is applied. It has been shown in several experiments that the maximum strain in the FRP at debonding is related to the dimensions of the specimens. This is why it is chosen to not perform the calibration for simple beams, but for structural elements that have a large cross-section depth, such as members of bridges.

In order to consider an appropriate range of geometries to calibrate the safety factors, seven different reinforced concrete bridges are studied:

- four girder bridges;
- three slab bridges.

These are not existing bridges, but they are designed by considering the most common typologies of existing bridges in Spain, built in the 1940's.

In order to simplify the references to the bridges, the following notation will be used, as suggested even in [11].

The first letter of the abbreviation corresponding to each bridge indicates the shape of its cross-section:

- "B", which means "beam", for girder bridges;
- "S", which means "slab", for slab bridges.

The first symbol is followed by numbers, which represent the span lengths in meters. There will be two digits for simply supported bridges and four digits for continuous bridges. Eventually the last two letters "RC" state the material of the bridge, which is reinforced concrete.

The concrete has a characteristic compressive strength equal to $f_{ck} = 20\ MPa$, while the characteristic yielding strength of the steel is $f_{yk} = 216\ MPa$ [8]. These values are very low and this is because at that time no materials with better properties were available.

2.2 Girders bridges

The four girder bridges belong to a bridge national catalogue, written in the 40's by Casado [8]. In this catalogue were suggested some standard solutions for the cross-section geometry and reinforcement amount of girder bridges, in order to give a design guideline in a country so far lacking of adequate design codes. That is the reason why nowadays in Spain existing bridges present, in the most of the cases, those suggested characteristics.

The analyzed bridges are simply supported and have the same width of the cross-section, which counts six principal beams. There are three transverse beams, two at the ends and one at the mid span.

The bridges differ in span length and principal and transverse beams height (*Figure 2.1-2.3*).

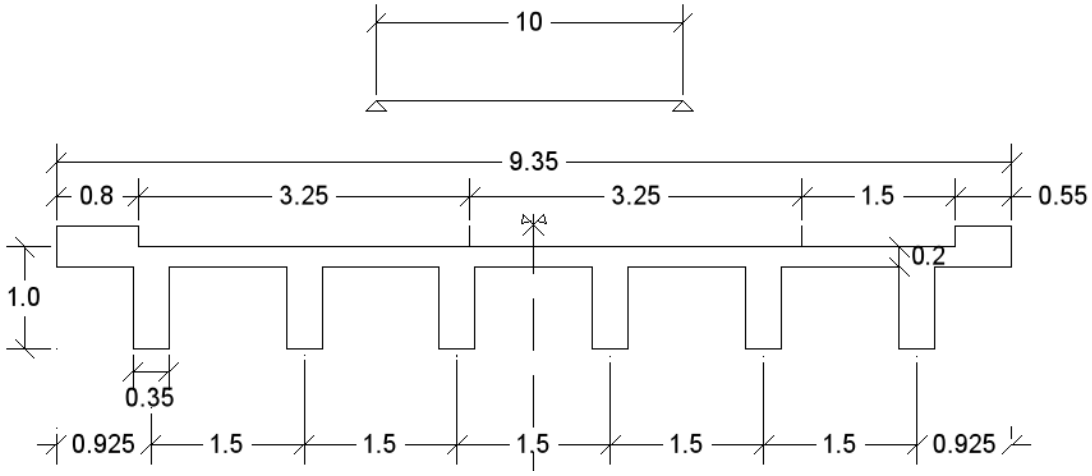

Figure 2.1. B10RC (dimensions in m).

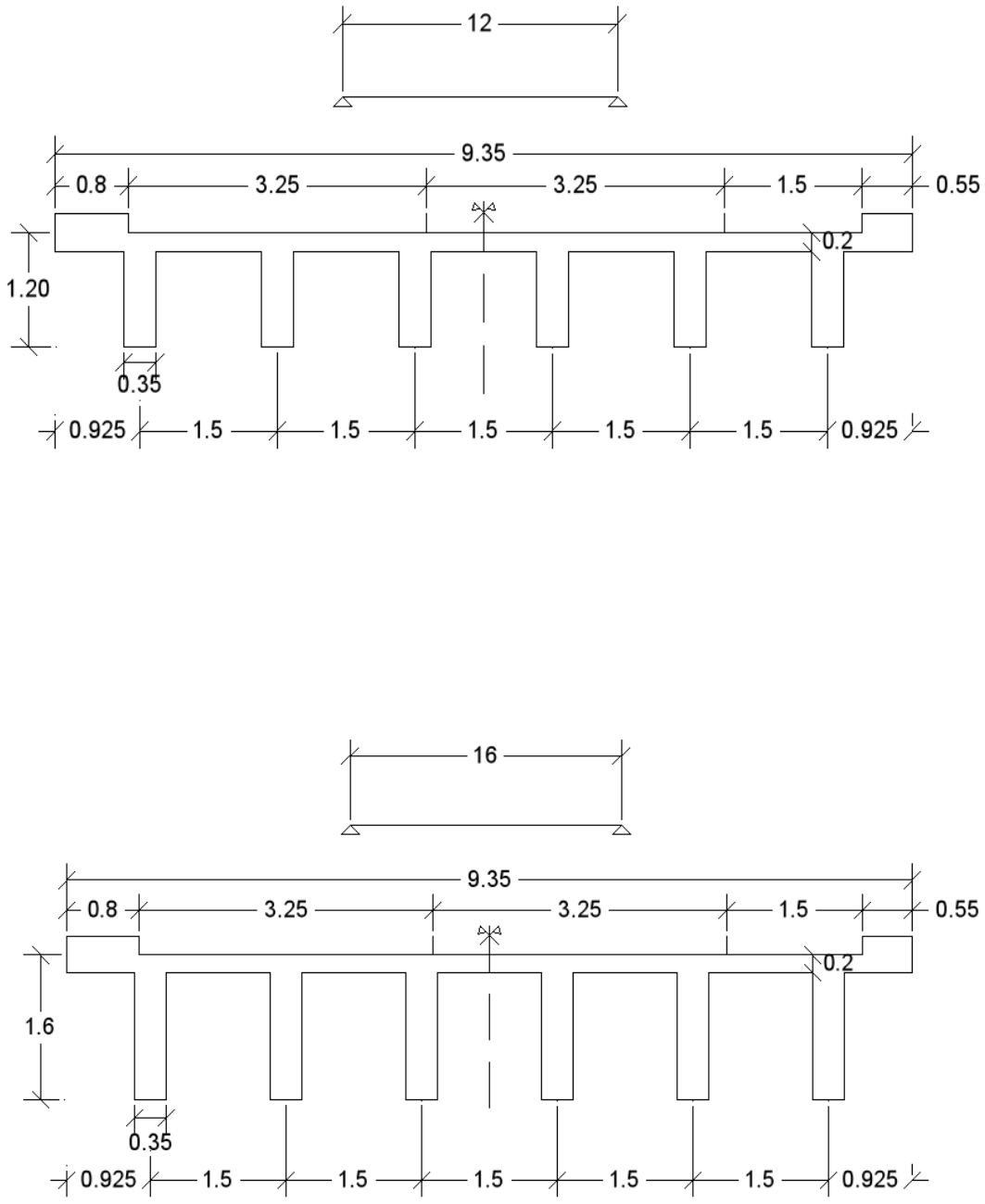

Figure 2.2. B12RC and B16RC (dimensions in m).

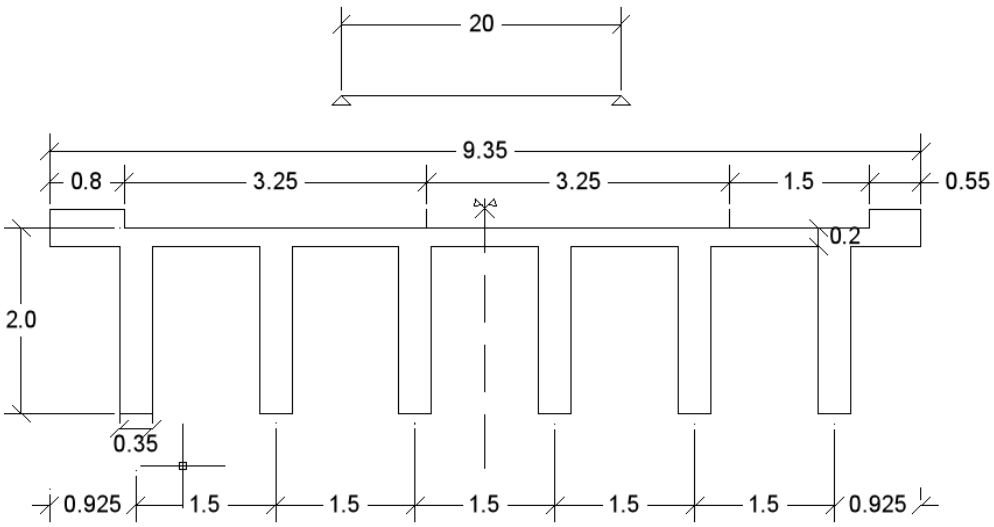

Figure 2.3. B20RC (dimensions in m).

As first step, in order to verify if the bridges can satisfy the actual code requirements, all the acting loads are calculated again according to the Eurocode [6].

It is found out that there are sensible differences between new and old load calculations. Indeed, those conducted according to the Eurocode give higher values and show the necessity of an increase in the quantity of steel reinforcement. This increment results to have a mean of 32% for tensile steel. The increase in the compressive steel quantity is neglected, since its contribute to the section resistance is not crucial.

As said, the total amount of the existing reinforcement is available and so the geometric details of the section [8]. The resisting moments of the old bridges are given from old tables, too. As for loads, resistance is checked following the current normative, in order to see if the new code requirements are fulfilled.

The comparison between old and new resisting moments is made for the mid span section (the most loaded) of one of the principal longitudinal beams. The considered acting moment is the mean one, obtained by dividing the global moment acting on the mid-span of the bridge by the number of the beams. The moment is not increased by any Massonnet's coefficient, which should take into consideration the effect of the live load eccentricity, particularly significant for the exterior beams. This is not done since the

increment of the load due to the Massonnet's coefficient would be different for each bridge, while here it is wanted to calibrate a safety factor that could be applied to any situation, independently from each specific design case.

The final values are showed in *Table 2.1*, where M_{sd} is the acting moment according to the Eurocode, M_{Rd} is the resisting moment an A_s is the area of the tensile steel.

All the drawings and detailed calculations are reported in *Annex A*.

Bridge	M_{sd} [KNm]	**Old calculations**		**New calculations**		**Tensile steel increment** [%]
		M_{Rd} [KNm]	A_s $[cm^2]$	M_{Rd} [KNm]	A_s $[cm^2]$	
B10RC	5572	4396	255	6060	370	45,10
B12RC	7647	6390	295	7722	386	30,85
B16RC	13016	10836	386	13296	489	26,68
B20RC	20296	17208	488	21150	611	25,20
Mean increment of the area of tensile reinforcement: 31,96						~ 32 %

Table 2.1. Old and new resisting moments of the analyzed girder bridges.

2.3 Slab bridges

As well as for girder bridges, the section geometry is taken from the national catalogue by introducing little modifications [8] (*Figures 2.4-2.5*).

One of the slab bridges is simply supported, while the others are statically indeterminable, with 3 spans. The difference is that, in this case, the "existing" amount of reinforcement is unknown. Therefore, at first, the quantity of tensile reinforcement needed to obtain a resisting moment higher than the acting one is calculated according to the Eurocode [6]. Then this quantity is reduced of the 32%, the percent which relates old and new reinforcements in the girder bridges. In this way the "existing" reinforcement is obtained (*Table 2.2*).

Again, only the tensile steel is taken into account, since it gives the most important contribute to the resistance.

For the section characteristics and calculations, see *Annex A.*

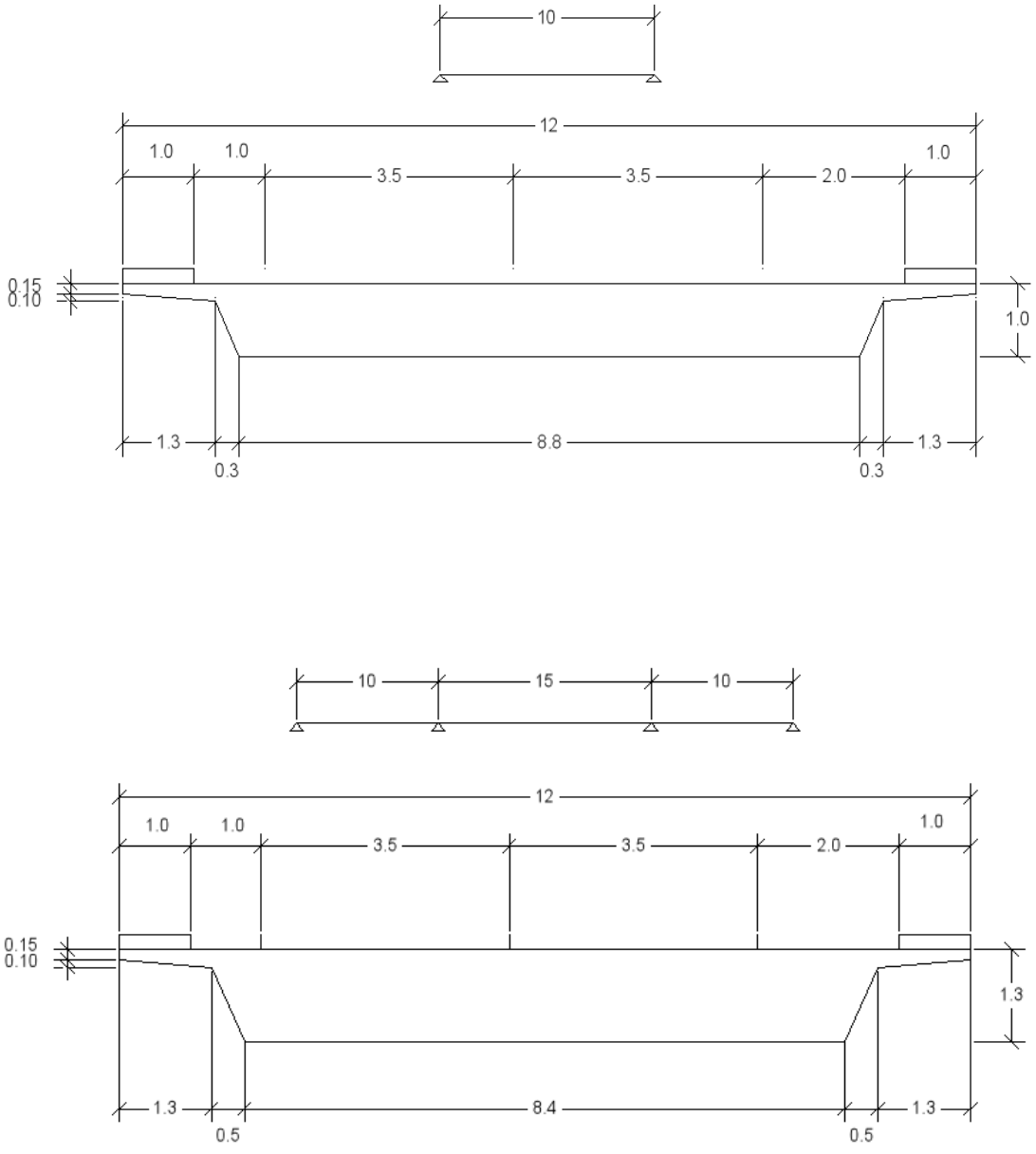

Figure 2.4. S10RC and S15RC (dimensions in m).

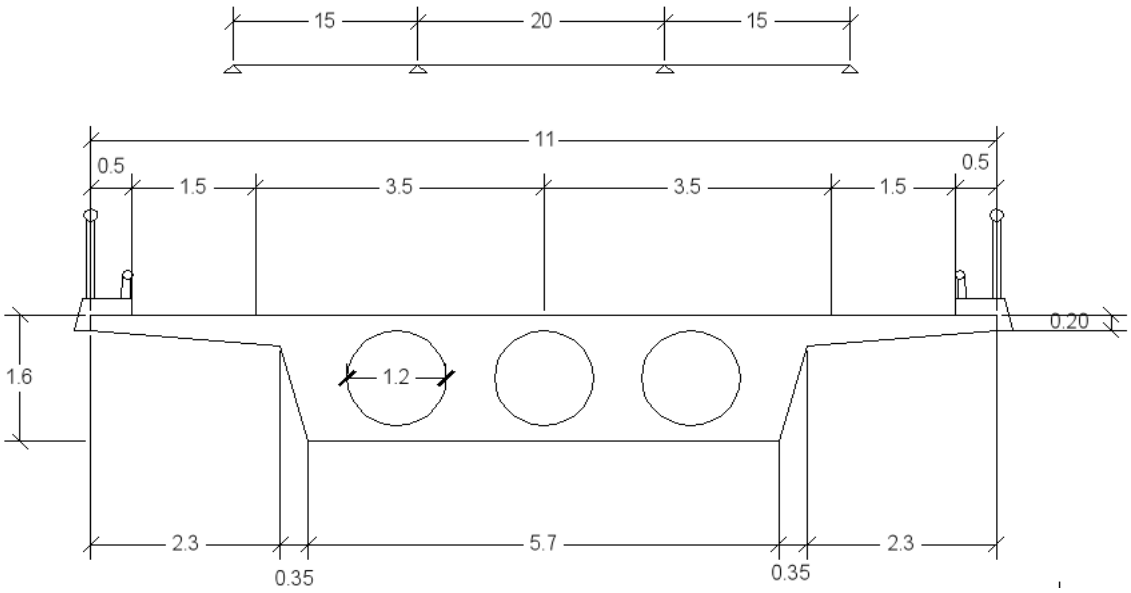

Figure 2.5. S1520RC (dimensions in m).

Bridge	M_{sd} [KNm]	**Fictitious old calculations**		**New calculations**		**Tensile steel increment** [%]
		M_{Rd} [KNm]	A_s $[cm^2]$	M_{Rd} [KNm]	A_s $[cm^2]$	
S10RC	8698	6519	388	9179	570	32
S1015RC	9625	6899	303	9878	446	32
S1520RC	12289	9479	335	13599	493	32

Table 2.2. Old and new resisting moments of the analyzed slab bridges.

Chapter 3
Comparison of 5 intermediate crack-induced debonding models

3.1 Ultimate debonding strain models

When the FRP reinforcement of a member subject to flexure is designed for ULS, one of the most important parameters which describe the composite is the ultimate strain ε_{fu}. This value is easy to know, obtainable from the ultimate strain provided by manufacturers, then arranged with opportune factors given by codes.

Nevertheless, the maximum strain in the FRP when delamination occurs may be lower than the ultimate strain and this controls the ultimate resistance of the strengthened element. On the contrary, its value is not easy to determine. Indeed, debonding failure depends on several parameters, such as the stiffness of the FRP, the presence of cracks, the stiffness of the substrate and the stiffness of the bonding resin. Since all these factors participate in the failure, it is complicated to develop a unique model that considers them all.

Hence, various models have been developed in order to predict delamination, some giving more importance to a factor rather than to another, with the result that they present different degree of accuracy and it is not easy to understand which of them could be the best one.

They are usually divided into two main groups:

a- models which predict plate-end crack-induced debonding;

b- models which predict intermediate crack-induced debonding (IC debonding).

Until now, the most reliable model for plate-ends debonding are considered to be those presented by Oehlers [26] and Smith and Teng [33].

Casas and Pascual's model [9], one of the models compared in the next section, was developed both as a plate-end and an intermediate crack-induced debonding model, characteristic that makes it different from all the others. Moreover, this model is the only one which takes into account the properties of the bonding materials. Casas and Pascual is here considered when predicts intermediate debonding.

3.2 The main parameters affecting the intermediate crack-induced debonding

The modulus of elasticity and thickness of the composite play obviously a decisive role in debonding, such as the mechanical proprieties of the concrete. In addition to these, there are other two factors, to which the right importance has been given only recently.

One of the most important aspect of bond behavior is that there is an effective bond length L_e, beyond which an increase in the bond length does not lead to any increment in the bond strength. This concept makes external strengthening with FRP plates very different from internal reinforcement, for which, in case of sufficient concrete cover, the bond length can be designed for its full tensile strength.

The main deficiency showed by many of the developed methods consists exactly in neglecting or wrongly estimating this important parameter.

Another critical factor, identified for the first time by Chen and Teng [13], is the ratio of the width of the bonded plate b_f to the width of the concrete element b_c. Indeed, if the term $\frac{b_f}{b_c} > 1$, nonuniform stresses are generated across the width of the concrete element when the force is transferred from the plate to the concrete.

In fact, the thinner b_f the higher the shear stress in the adhesive at failure, because of the contribute of the concrete outside the bond area.

In addition to the parameters mentioned above, there are other two important factors, which are considered in Casas and Pascual, but they are not in other debonding models:

- the size effect;
- the resin properties.

How and through which terms they are taken into account will be explained below when Casas and Pascual's model is described.

3.3 The 5 analyzed IC debonding models

Casas and Pascual's equation for the maximum debonding force is here illustrated together with other four intermediate debonding models. After a brief description, the models are applied to the cross-section of the studied bridges and then compared between them, through a diagram debonding deformation, ε_{fd}, against composite thickness, t_f.

The analyzed models (in chronological order) are:

1- **Chen and Teng**, 2003 [33];
2- **Casas and Pascual**, 2006 [9];
3- **Said and Wu**, 2007 [29];
4- **ACI 440.2R-08**, 2008 [2];
5- **C.N.R. DT200 R1/2013**, 2013 [14].

3.3.1 Chen and Teng's model (2003)

J.G. Teng et al. in the article [33] proposed a correction to the model developed by Chen and Teng, already presented in another previous article [13].

In the antecedent work, indeed, the maximum force that can be transmitted from the concrete to the FRP without having IC debonding is expressed as:

$$T_u = \alpha\beta_p\beta_l\sqrt{f_c}b_f L_e = 0{,}427\beta_p\beta_l\sqrt{f_c}b_f L_e \qquad (3.1)$$

where :

$$\beta_p = \sqrt{\frac{2-\frac{b_f}{b_c}}{1+\frac{b_f}{b_c}}}$$

$$\beta_l \begin{cases} 1 & if\ L \geq L_e \\ \sin\left[\frac{\pi L}{2L_e}\right] & if\ L < L_e \end{cases}$$

$$L_e = \sqrt{\frac{E_f t_f}{\sqrt{f_c}}} \quad [mm]$$

in which E_f, t_f and b_f are the elastic modulus (MPa), thickness (mm) and width of the bonded plate; f_c and $b_c$are the cylinder compressive strength (MPa) and width (mm) of the concrete block; L is the bond length (mm) and L_e the effective bond length (mm).

In the same paper, Teng and Chen also suggest a different equation from the one above, recommended for practical design. This formula introduces a reduction to the 95 percent characteristic value of the factor 0,427, that becomes 0,315 and gives a more conservative ultimate strength for design use:

$$T_u = \frac{0{,}315\beta_p\beta_l\sqrt{f_c}b_f L_e}{\gamma_b} \quad (3.2)$$

Where γ_b is a safety factor specific for FRP flexural strengthening and assumed equal to 1,25.

The problem is that the model, as emphasized by the authors themselves, presents some drawbacks which can compromise the precision in prediction of IFC debonding failure. Indeed, the proposed formula was developed by referring to shear test specimens, that don't present bending deformation and flexural reinforcement. Furthermore, the interaction between multiple cracks cannot be well-represented and the assumption of plane section in the cracked section analysis is no more valid. Last remark can be contested though. In fact, when debonding starts to propagate the load-carrying capacity of the beam increases little or not at all so that the plane section assumption can be judged reasonable.

Deficiencies listed above are wanted to be taken into account by a modification of the coefficient α. In [33] the value of α is therefore re-calibrated. The new proposed design value both for slabs and beams is 0,48, number which derives from an analysis conducted over beam and slab tests for IFC debonding. The 95% fractile just for beams is instead 0,544.

3.3.2 Casas and Pascual's model (2006)

Most of the models, that were developed in order to determine the maximum strain in FRP when delamination occurs, are based on tests, which were conducted on specimens of small sizes. The risk of taking small specimens is that most of the time they cannot really be representative of what happens in buildings and real structures. In fact, it has been seen that the dimensions of the specimens play an important role in the value of the maximum strain at debonding. Casas and Pascual's model considers this and gives a simplified method to calculate the debonding strain in elements with large cross-section depth. In these elements, the distance between bending cracks (s) is larger than the effective bond length of the FRP (l_e), hence the condition at a crack is independent on the situation in the closer ones. Anyway, even if the interaction between the cracks was not

neglected, another simplification could be made, by the introduction of a new parameter (θ).

What makes Casas and Pascual's model more precise, if compared with other models, is that in the developed equations are taken into account also the properties of the bonding resin .

Single crack model

The behavior of the FRP close to a single crack or joint is here illustrated (*Figure 3.1*). Debonding occurs when the maximum shear stress is reached (τ_{max}), which corresponds to a maximum force per unit width in the FRP:

$$T_u = \tau_{max} L_e \tag{3.3}$$

Where τ_{max}=η$\sqrt{f_c}$, with f_c= compressive strength of concrete and η = coefficient experimentally determined.

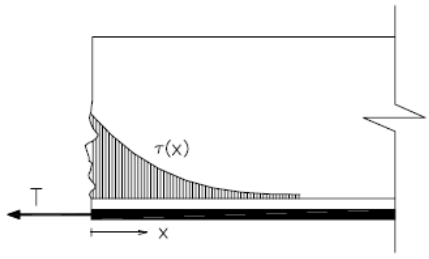

Figure 3.1. Distribution of shear stresses in the concrete-FRP interface for a single crack [9].

If the stiffness of the strengthened concrete element is higher than the FRP stiffness, the effective bond length L_e is given by

$$L_e = \sqrt{\frac{k_f}{g_b}} \tag{3.4}$$

where

- $k_f = E_f t_f$ is the stiffness of the FRP for unit length;
- $g_b = \frac{g_r g_c}{g_r + g_c}$ is the shear joint stiffness of concrete plus adhesive resin;

with

- $g_r = \frac{G_r}{t_r}$, shear stiffness of the resin;

- $g_c = \frac{G_c}{t_{ce}}$, shear stiffness of concrete.

G_r and G_c are the shear modulus of the resin and the concrete. Poisson's coefficients for both materials are taken respectively as 0,38 and 0,5; t_r is the resin thickness and t_{ce} is the concrete thickness, calculated as suggested in [22]:

$$t_{ce} = b_f + 50{,}8 \leq \frac{h}{2}\,[\text{mm}] \tag{3.5}$$

Where b_f is the width of the FRP and h is the cross-section depth. The constant 50,8 mm represents the concrete cover thickness (2 in.) and this value is an approximate average value of covers observed in common bridges. Poisson's coefficient value for the concrete is due to the fact that the concrete is considered to be in a plastic range. If $g_c \gg g_r$, the shear deformation of the concrete can be neglected and $g_b = g_r$, so that

$$L_e = \frac{1}{\alpha} = \sqrt{\frac{E_f t_f}{g_r}} \tag{3.6}$$

The higher the FRP and adhesive stiffness the lower the debonding resistance: the parameter is a good estimator of the stiffness of the system and of the influence of cracking in the element.

Proposed equations

The multiple cracks model is not here explained in detail, since it won't be applied in this work, but the general simplified formula is in any event reported below, together with the final equation proposed for the single crack model.

What determines the use of the single crack model rather than of multiple cracks model is the value of the ratio $\frac{s}{L_e}$. Indeed, it was seen that if this ratio assumes a value that is about 2 or lower, the presence of multiple cracks has a positive effect on the debonding strength and this is increased even of the 50-60%. That is true until the cross-section depth does not become too large, because in the case of ratios bigger than 4, the cracks interaction have no influence on the debonding behavior (*Figure 3.2*) and the model is a single crack model (this is generally the case of slab and beam bridges).

The parameter *s* can be calculated as $\frac{d}{2}$, where d is the effective height of the beam.

The results obtained by experimental tests can be summarized in the following definition of the force per unit width at FRP when failure due to debonding occurs:

- If $\frac{s}{L_e} \geq 4$, then $T_u = 0{,}996\sqrt{f_c}L_e$ (3.7)

- If $\frac{s}{L_e} < 4$, then $T_u = 0{,}996\beta\sqrt{f_c}L_e$ (3.8)

where $= \frac{\xi_1}{(1-\xi_2\xi_3)}$,$\xi_1 = \frac{e^{\frac{s}{L_e}} - e^{-\frac{s}{L_e}}}{e^{\frac{s}{L_e}} + e^{-\frac{s}{L_e}}}$,$\xi_2 = \frac{2}{e^{\frac{s}{L_e}} + e^{-\frac{s}{L_e}}}$,

$\xi_3 = 1 - \theta\frac{k}{k'}(1-r)$, with $\theta = \frac{2}{3}$

k= slope of the diagram moment-tension in the FRP before yielding of reinforcing steel

k'= slope of the diagram moment-tension in the FRP after yielding of reinforcing steel and up to FRP failure (*Figure 3.3*).

Because of the dimensions of the reinforced concrete bridges, normally $\frac{s}{L_e} \geq 4$ and therefore the simplest formula is used, revealing Casas and Pascual as a method of a very easy application.

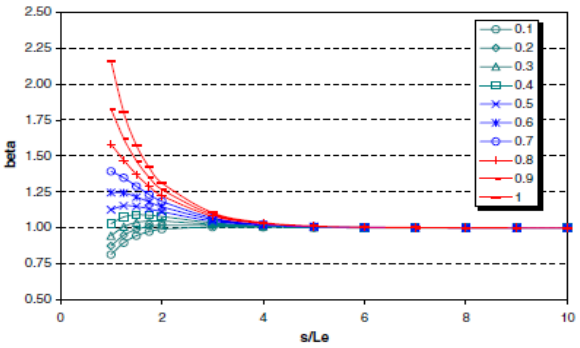

Figure 3.2. Values of β as a funtion of ξ_3 and s/Le.

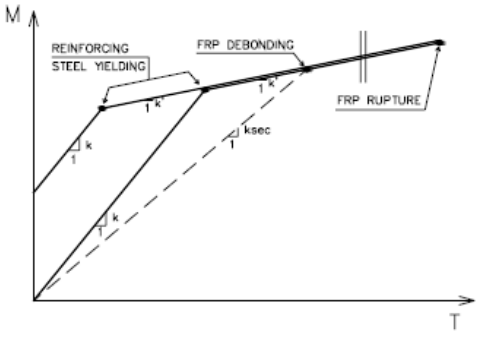

Figure 3.3. Relationship moment-tension in the FRP. Definition of k, k' and ksec.

3.3.3 Said and Wu's model (2007)

In [29] Said and Wu investigated five typical IC debonding models and identified many problems in their application. As a solution to these deficiencies, the authors proposed a new method for predicting failure load due to IC debonding, a method which is defined as "reliable and simple".

The FRP strain at debonding ε_{deb} is expressed in a general form by the following equation:

$$\varepsilon_{deb} = \frac{C1(f_c)^{C2}}{(E_f t_f)^{C3}} \tag{3.9}$$

where C1, C2 and C3 are constants determined from experimental data.

Said and Wu discovered that the compressive strength of the concrete does not have a significant effect on IC debonding and that the high level of data dispersion which characterizes the majority of the other investigated models is mainly due to the excessive role given to concrete in causing IC delamination.

By referring to over 200 testing data the constants appearing in the formula above are determined:

$$\varepsilon_{deb} = \frac{0{,}23(f_c)^{0{,}2}}{(E_f t_f)^{0{,}35}} \tag{3.10}$$

where $f_c$is the characteristic compressive strength of the concrete. This model is calibrated over mean values, while the other considered models are calibrated over characteristic values (95% fractile).

3.3.4 ACI 440.2R-08 model (2008)

ACI defines the maximum strain for preventing intermediate crack-induced debonding failure, ε_{fd} , which is defined as follows:

$$\begin{aligned} \varepsilon_{fd} &= 0.083\sqrt{\frac{f'_c}{nE_f t_f}} \le 0.9\varepsilon_{fu} \quad \text{in in.-lb units} \\ \varepsilon_{fd} &= 0.41\sqrt{\frac{f'_c}{nE_f t_f}} \le 0.9\varepsilon_{fu} \quad \text{in SI units} \end{aligned} \tag{3.11}$$

The formula above is a modified form of the equation of Teng et al (2001, 2004), based on committee evaluation of a significant database for flexural beam tests when FRP debonding failure occurs.

When designing with FRP, a reduction coefficient ψ_f should be introduced, before the FRP contribute to flexural strength. This factor takes into consideration the different failure modes of FRP and improves the reliability of the strength prediction.

3.3.5 C.N.R. DT200 R1/2013 model

The Italian guidelines consider the concept of the effective bond length as well as Casas and Pascual's model. Indeed, l_e is that length beyond which a further increase of bond length l_b does not increase the bond strength (*Figure 3.4*).

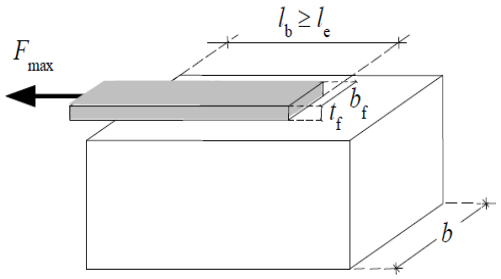

Figure 3.4. Maximum transmittable force for a FRP reinforcement [14].

This leads to the definition of an optimal anchorage length, which design value is given by:

$$l_{ed} = min\left\{\frac{1}{\gamma_{Rd} f_{bd}}\sqrt{\frac{\pi^2 E_f t_f \Gamma_{Fd}}{2}}, 200\ mm\right\} \tag{3.12}$$

where:

- E_f and t_f are the elastic modulus along the direction of the force and the thickness of the composite;
- Γ_{Fd} is the design value of the crack energy;

- $f_{bd} = \frac{2\Gamma_{Fd}}{s_u}$, with $s_u = 0{,}25\ mm$ the ultimate value of the sliding between FRP and support;

- $\gamma_{Rd} = 1{,}25$ is a corrective coefficient.

The design value of the crack energy, Γ_{Fd}, can be expressed as:

$$\Gamma_{Fd} = \frac{k_b k_g}{FC}\sqrt{f_{cm} f_{ctm}} \tag{3.13}$$

where the introduced factors have the following meaning:

- f_{cm} and f_{ctm} are respectively the medium value of the compressive and tensile resistance of the concrete, evaluated *in situ*. In the case of lack of experimental data, the medium compressive resistance of the concrete can be calculated as stated in the current code;

- FC is an opportune factor of confidence;

- k_b is a geometric parameter, function of the width of the reinforced beam, b, and that of the composite b_f.

$$k_b = \sqrt{\frac{2-\frac{b_f}{b}}{1+\frac{b_f}{b}}} \geq 1 \tag{3.14}$$

if $\frac{b_f}{b} \geq 0{,}25$, otherwise the value of k_b with $\frac{b_f}{b} = 0{,}25$ should be taken ($k_b = 1{,}18$).

- k_G is a coefficient calibrated on the base of experimental results and it has to assumed equal to 0,023 mm for pultruted FRP, 0,037 mm for wet-lay up systems.

In case of flexural strengthening of a slab, achieved by the use of FRP strips placed side by side, each with a width equal to b_f, factor k_b can be calculated from the equation above, by assuming b as the center to center distance of two close strips.

ULS resistance for intermediate delamination

To avoid the failure for intermediate debonding, it should be verified that the variation of stress $\Delta\sigma_f$ in the FRP between two cracks is smaller than a specific limit value, $\Delta\sigma_R$.

The latter depends on the characteristics of the adherence, on the distance between consecutive cracks and on the level of tension σ_f in the composite.

A valid alternative could be to follow a simplified procedure that consists in verifying that, at SLU, the tension in the reinforcement does not exceed the value $f_{dd,2}$:

$$f_{\mathrm{fdd,2}} = \frac{k_q}{\gamma_{\mathrm{f,d}}} \cdot \sqrt{\frac{E_{\mathrm{f}}}{t_{\mathrm{f}}} \cdot \frac{2 \cdot k_{\mathrm{b}} \cdot k_{\mathrm{G,2}}}{FC} \cdot \sqrt{f_{\mathrm{cm}} \cdot f_{\mathrm{ctm}}}} \quad (3.15)$$

Where

- $\gamma_{f,d}$ is a material partial safety factor, used to prevent delamination, which value is assumed equal to 1,2 or 1,5 depending on the designer's judgment;
- $k_{G,2}$is a corrective coefficient calibrated on the base of experimental results, assumed as 0,10 mm for any typology of reinforcement;
- k_q is a coefficient which takes into account the load conditions, equal to 1,25 for distributed loads and 1 for all the other cases.

The corresponding value of FRP design strain, ε_{fdd}, is:

$$\varepsilon_{\mathrm{fdd}} = \frac{f_{\mathrm{fdd,2}}}{E_{\mathrm{f}}} \quad (3.16)$$

In flexural strengthening calculations, the FRP maximum strain to consider is determined as:

$$\varepsilon_{\mathrm{fd}} = \min\left\{\eta_{\mathrm{a}} \cdot \frac{\varepsilon_{\mathrm{fk}}}{\gamma_{\mathrm{f}}}, \varepsilon_{\mathrm{fdd}}\right\} \quad (3.17)$$

where

- η_a an environmental conversion factor, which assumes different values depending on the environmental conditions (table 3-2, §3.5.1, CNR DT200 R1/2013);

- $\gamma_f$is a material partial safety factor used to calculate the ultimate tensile strain of the composite and its value is taken equal to 1,1 .

- ε_{fk} is the characteristic FRP strain at failure and ε_{fdd} is the maximum deformation for intermediate delamination.

3.4 Comparison between the models applied to the analyzed bridges

Models described above are compared here in a diagram of the *maximum debonding strain vs CFRP thickness*. In order to get comparable data, no safety factors are taken into account. The terms concurring in the equations of the models are assumed with their nominal value, each of them taken from the corresponding code the model refers to.

Hence, CNR DT200 R1/2013 addresses to the NTC2008, ACI 440 2008 to the code itself, Casas and Pascual, Chen and Teng and Said and Wu's model again to ACI 440 2008.

The comparison is made for each of the studied bridge section, in order to see what happens when the principal parameters acting on intermediate debonding phenomenon change.

3.4.1 Materials

CFRP

The composite has a brittle behavior, hence the stress-strain relation of the material is linear up to reaching the ultimate strain.

Precured and wet lay-up systems present different characteristics, summarized in *Table 3.1*. It has to be remembered that for prefabricated systems the characteristics are those of the composite, while for wet-lay up systems, due to the uncertainty in the resin quantity, the data refers only to the fiber. In order to underline this difference, a diverse nomenclature is used, that is *frp* for the composite and *f* for the fiber. It is chosen a high tenacity (or low modulus) CFRP.

Prefabricated systems:

E_{frp} [MPa]	160000
ε_{frpu}	1,6 %
σ_{frpu} [MPa]	2800

Wet-lay up systems:

E_f [MPa]	230000
ε_{fu}	1,6 %
σ_{fu} [MPa]	3900

Table 3.1. Material properties for prefabricated and wet-lay up systems.

Concrete

Concrete properties were already defined when the studied bridges were presented. The only data necessary for the comparison between the models is the characteristic compressive strength $f_{ck} = 20\ MPa$.

3.4.2 Maximum IC debonding strain vs. composite thickness

Precured systems

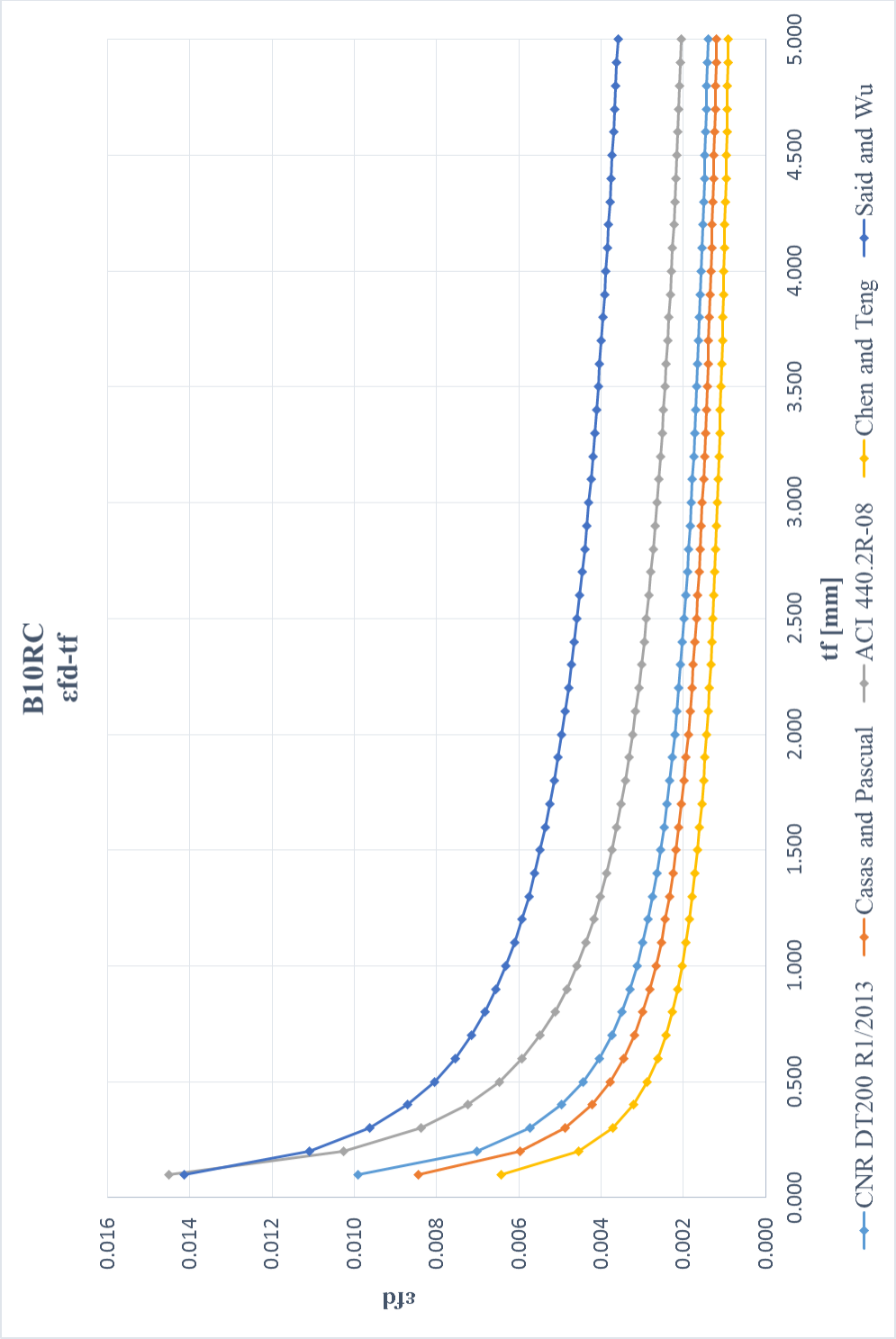

Figure 3.5. Debonding strain vs. composite thickness for bridge B10RC.

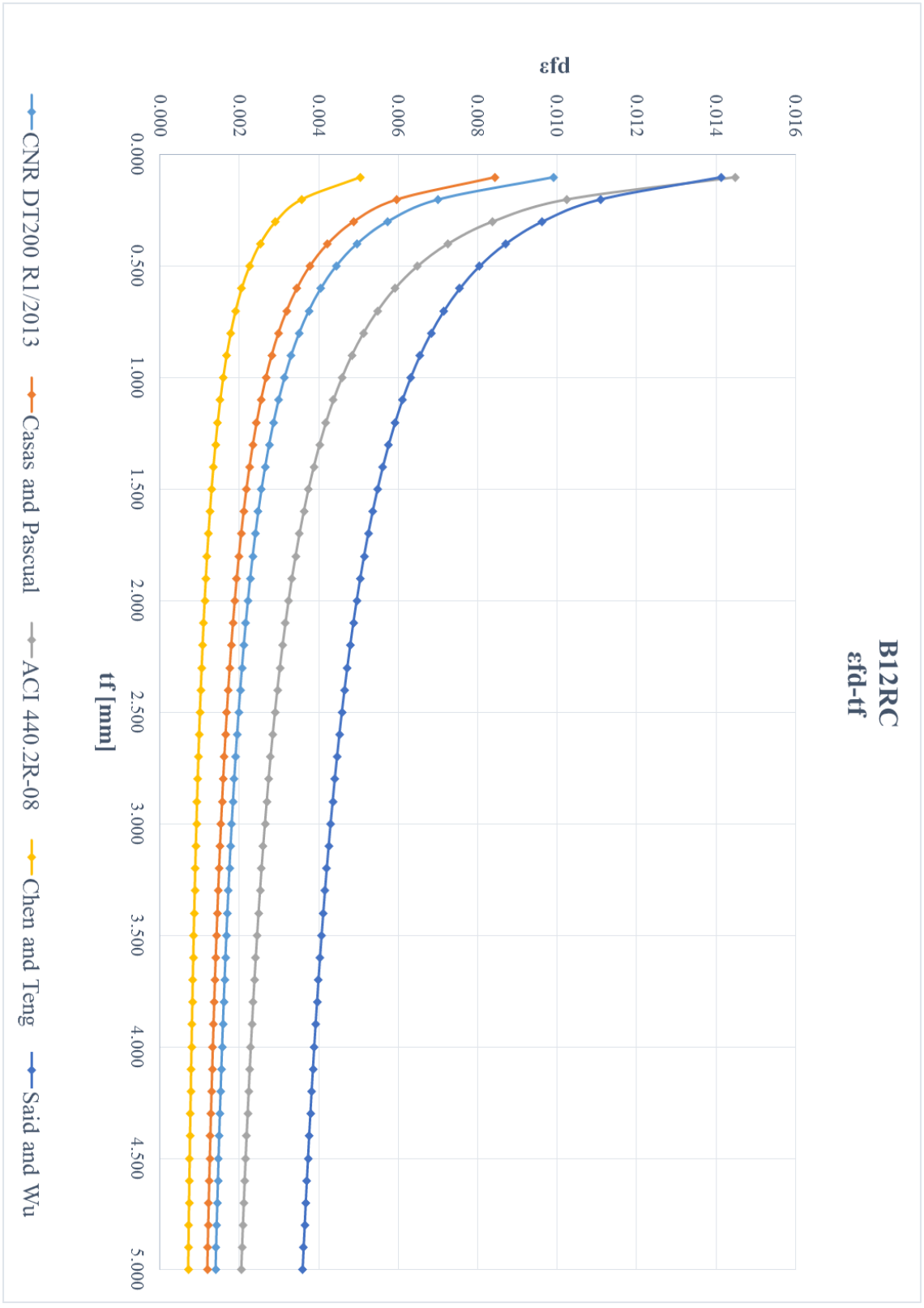

Figure 3.6. Debonding strain vs composite thickness for bridge B12RC.

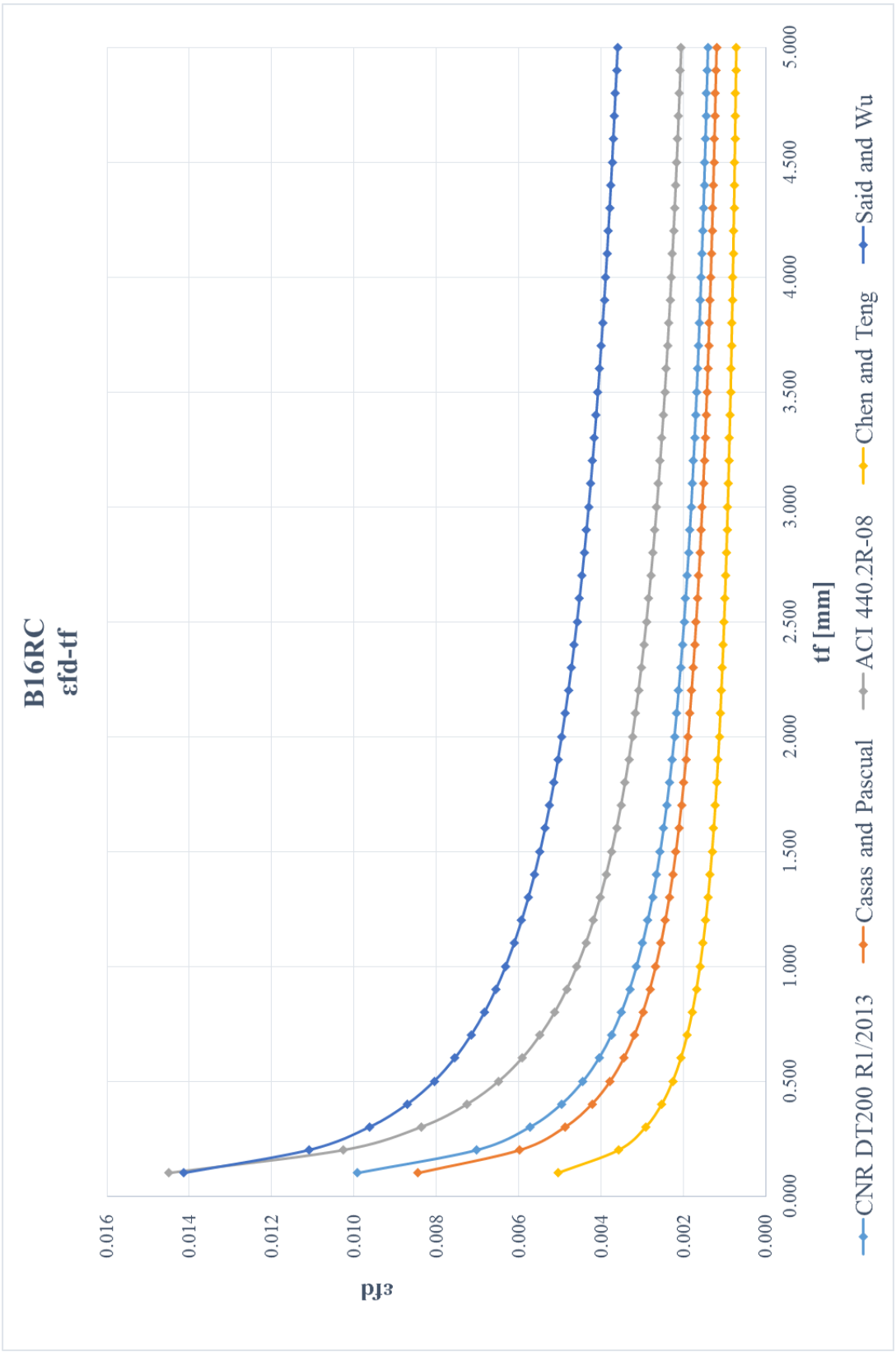

Figure 3.7. Debonding strain vs. composite thickness for bridge B16RC.

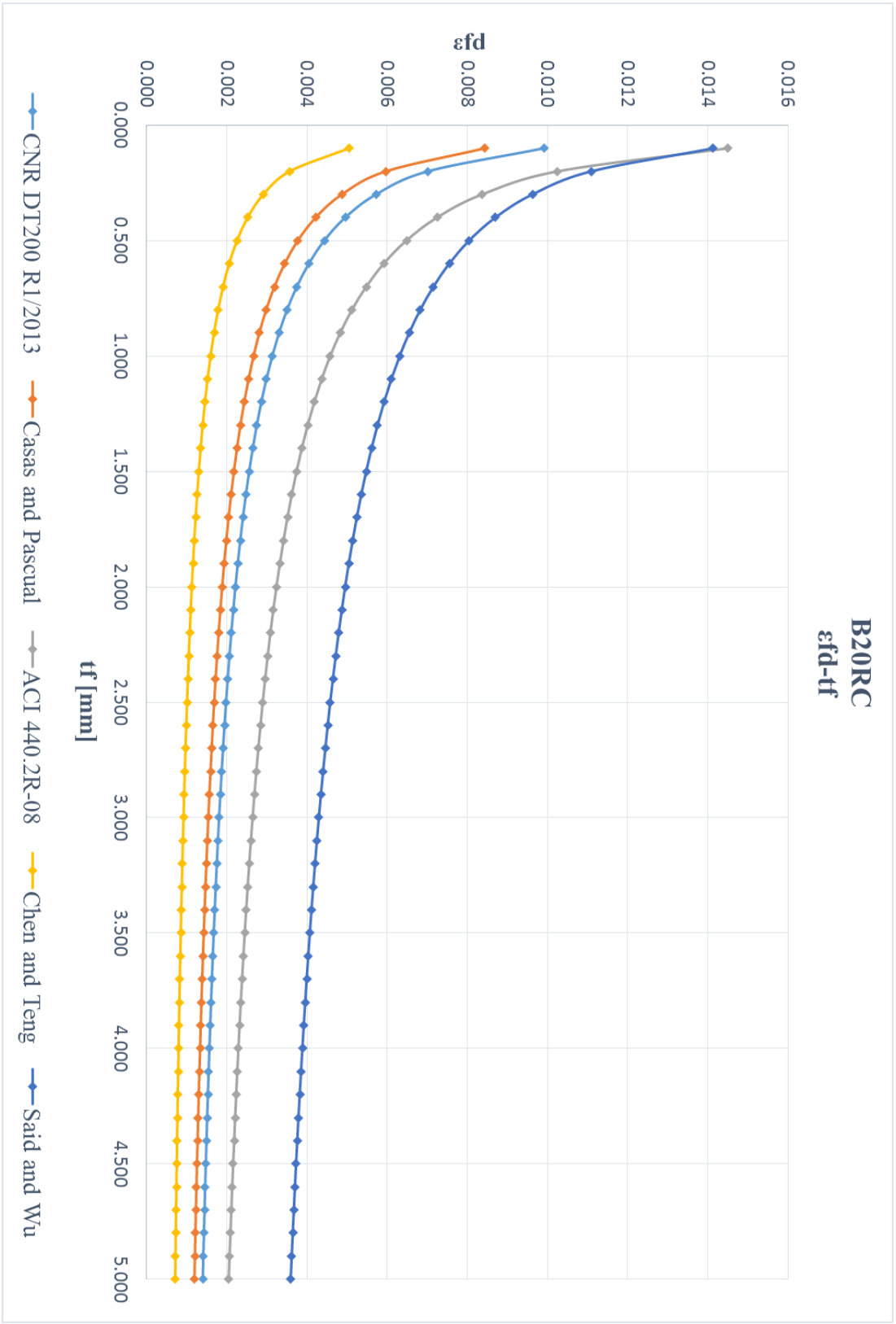

Figure 3.8. Debonding strain vs. composite thickness for bridge B20RC.

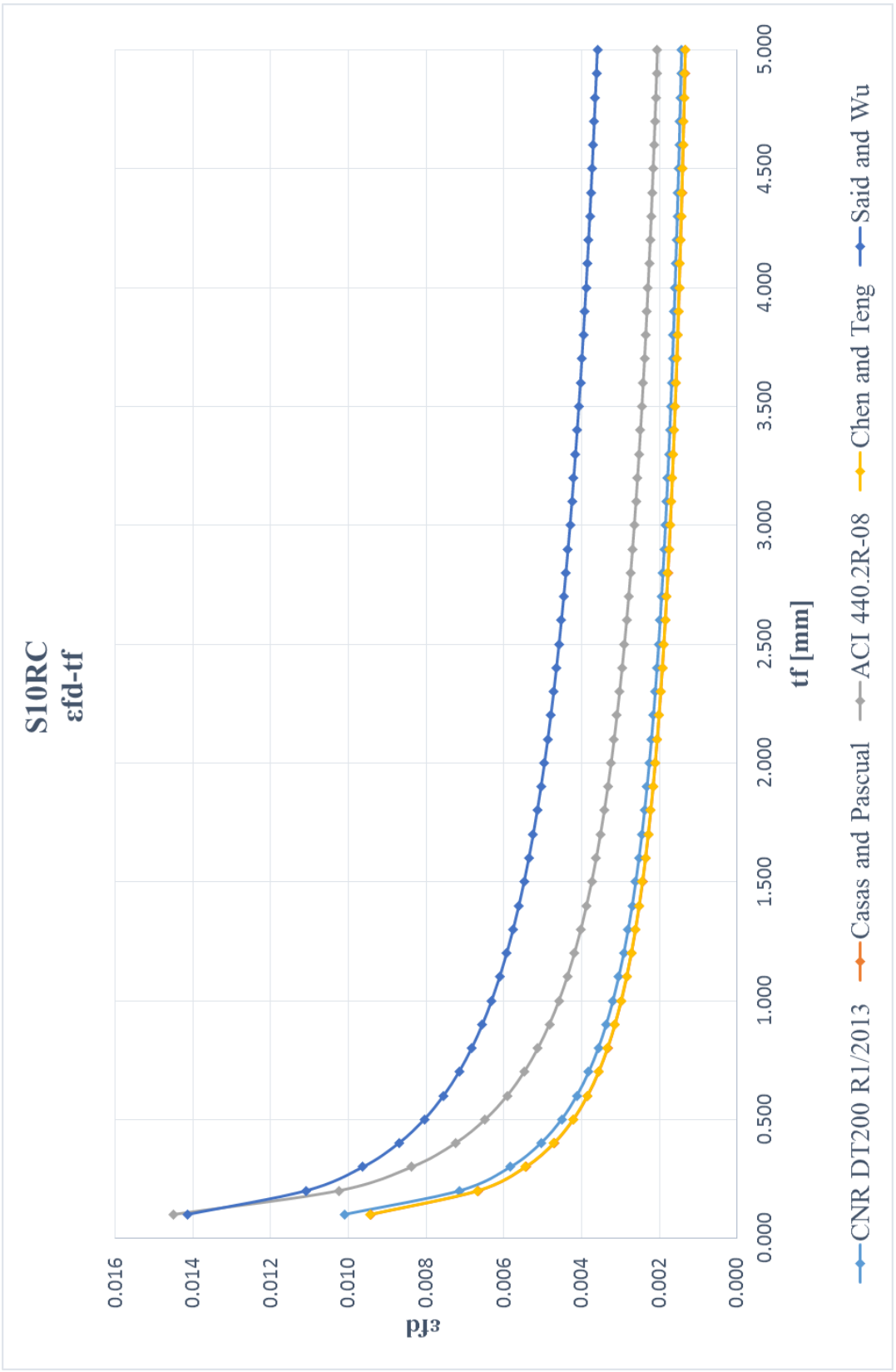

Figure 3.9. Debonding strain vs. composite thickness for bridge S10RC.

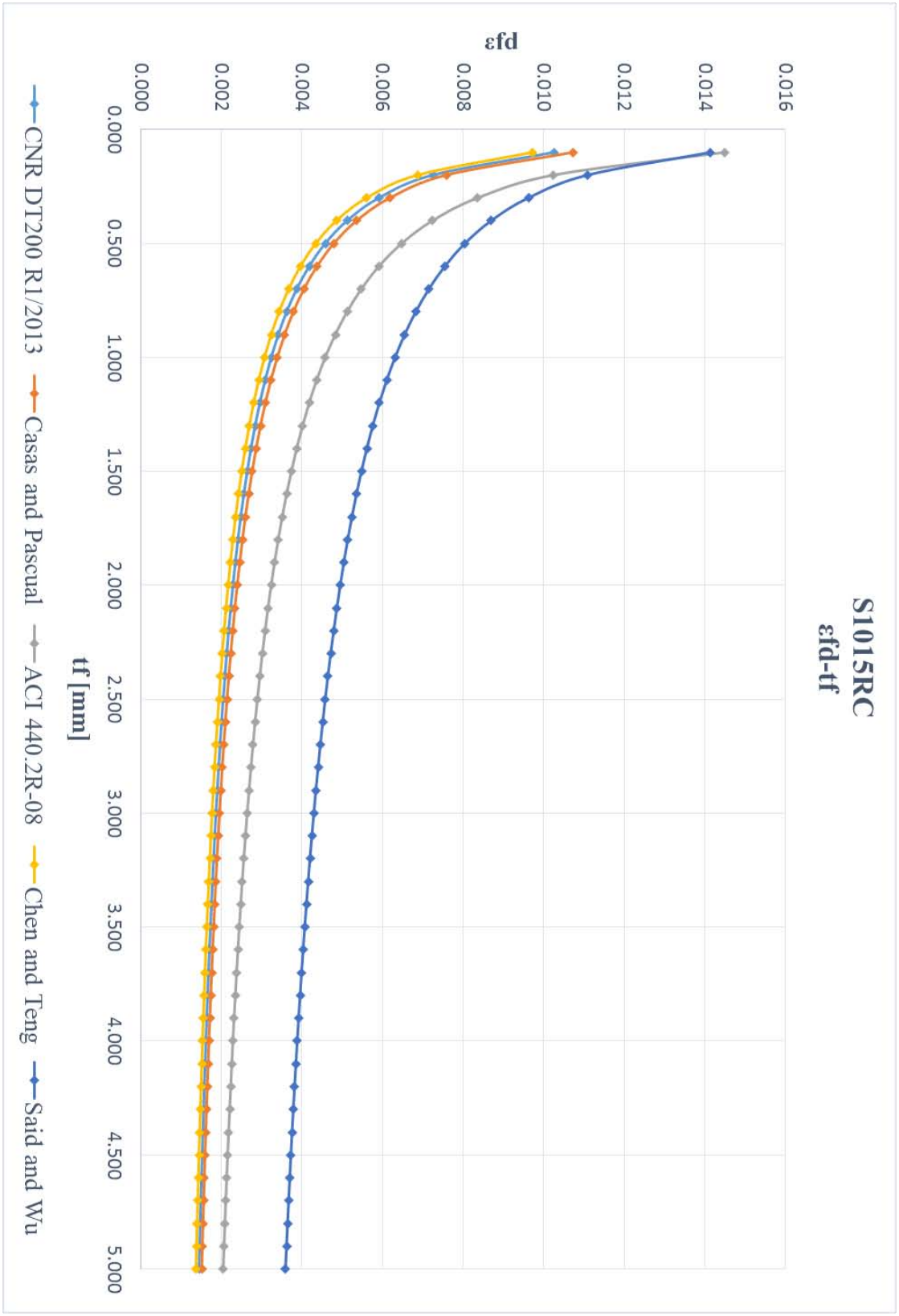

Figure 3.10. Debonding strain vs. composite thickness for bridge S1015RC.

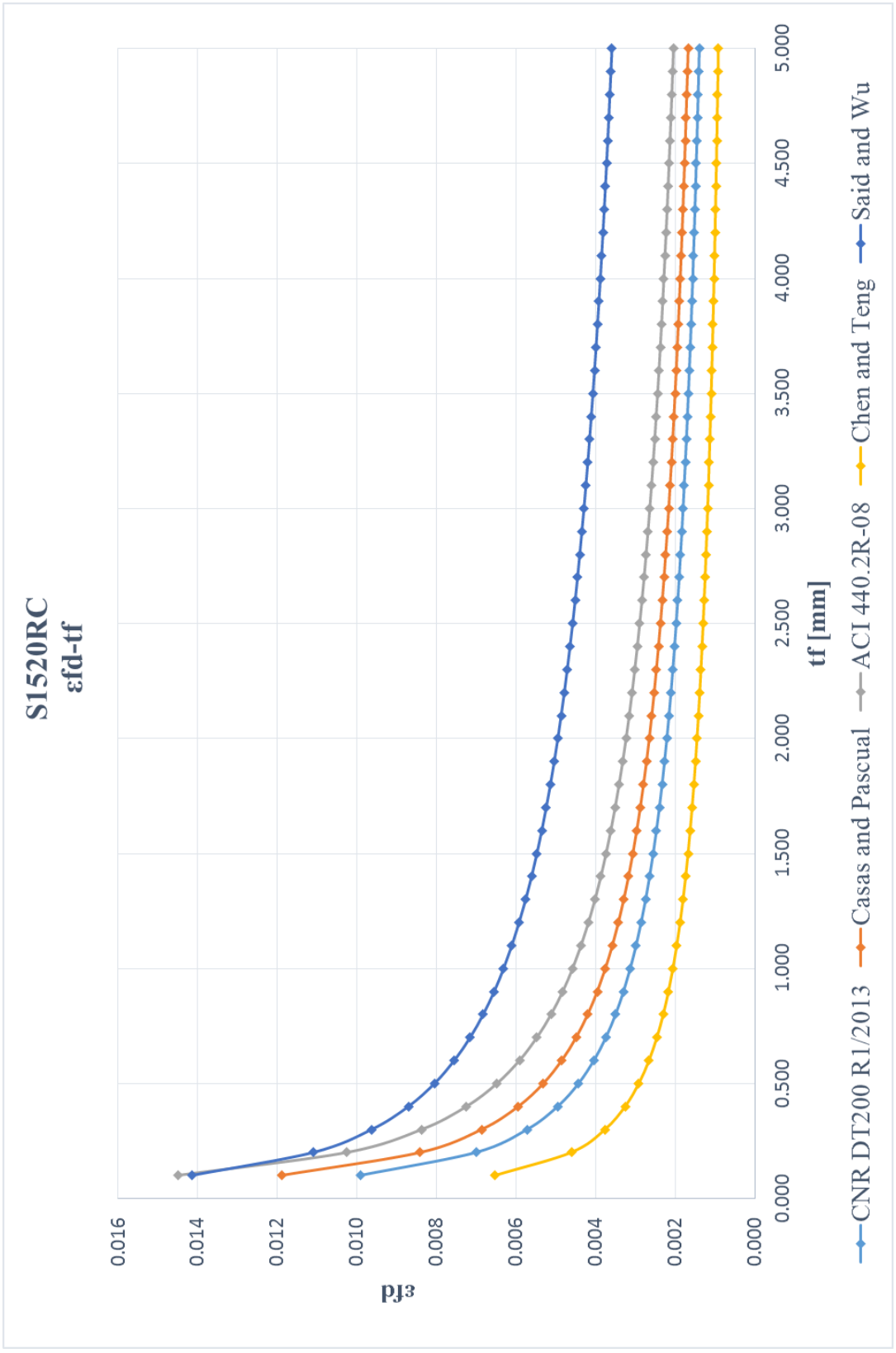

Figure 3.11. Debonding strain vs. composite thickness for bridge S1520RC.

From the diagrams above (*Figure 3.5-3.11*), it can be seen that IC debonding deformation decreases very rapidly as FRP thickness increases. This happens until the thickness of the composite reaches a value more or less equal to 3 mm. A further increase of the thickness does not lead to substantial changes in the ultimate debonding strain. Hence, the risk of incurring in debonding for high thicknesses remains almost the same after a certain value is achieved. The trend of the graph suggests that debonding failures occur for higher thicknesses and that a design with relatively thin FRP sheets is desirable, as confirmed by various tests presented in scientific articles of research.

For girder bridges the relative positions of the curves of the models do not change from one bridge to another, since the variables appearing in the models equations either do not vary or vary in the same way for each of them.

Chen and Teng's model results the safest, whereas Said and Wu's and ACI models give the highest deformations, showing a less conservative approach. Casas and Pascual's and CNR models set at an intermediate position.

The results showed by the graphs reflect the degree of precision of each model (if, for example, parameters such as the effecting bond length and the ratio $\frac{b_f}{b_c}$ participate into the calculation of the debonding strain), but not only. Indeed, at the base of the higher or lower conservatism there is the decision made by the authors of calibrating the model on mean values (as Said and Wu's model) or characteristic values (such as Casas and Pascual's, Chen and Teng's and CNR models).

The difference of the degree of precision between the models, in terms of number of important parameters taken into account, is more evident when comparing the results for slab bridges.

In fact, for girder bridges the ratio $\frac{b_f}{b_c}$ remains unaltered and equal to 1 and the effective bond length $L_e$equally does not vary from bridge to bridge as the value of composite thickness remains the same. In reality, the effective bond length has a constant value even for slab bridges, with the exception of one model, the Casas and Pascual's one. Indeed, in this model L_e is expressed as:

$$L_e = \sqrt{\frac{k_f}{g_b}}$$

where the term g_b contains in its definition the parameter concrete thickness t_{ce}, which value is limited by the cross-section depth:

$$t_{ce} = b_f + 50{,}8 \leq \frac{h}{2}$$

with b_f the width of the composite sheet, expressed in mm.

So, leaving aside Said and Wu's and ACI models, for which the maximum intermediate debonding deformations are not subject to any variation going from girder to slab bridges, the attention is now focused on the behavior of the curve trend of the other three models. CNR curve shifts up or down depending on the change in the value of the parameter $\frac{b_f}{b_c}$, such as Chen and Teng's curve. The bigger scatter between the models is for S1015RC and it is due to the limitations imposed by the CNR to the factor $k_b (= \beta_p)$.

For both S10RC and S1015RC, the ratio $\frac{b_f}{b_c}$ is low (0,444, 0,404) and the factor $k_b = \beta_p >$ 1. On the contrary, for S1520RC, $\frac{b_f}{b_c} = 0{,}980$ and $k_b$is equal to 0,718. But CNR limits the value of $k_b \geq 1$, while Chen and Teng do not impose any lower bound. The result is that Chen and Teng's model is more conservative and basically this is what determines the difference between the two models, also in girder bridges.

Looking at the Casas and Pascual's model, instead, there is an additional parameter which influences the trend of the curve, the size dimensions of the section. In fact, for slab bridges, the factor t_{ce} , which remained constant for girder bridges and always lower than $\frac{h}{2}$, assumes here values so big that the limiting value of $\frac{h}{2}$ has to be taken for calculations. Going from S10RC to S1520RC, that is, going from the shortest cross-section depth to the highest, the model passes from assuming the safest values, together with Chen and Teng's model, to an intermediate position between Chen and Teng's model and CNR. This means that the concrete which can contrast the debonding with its shear stiffness has a limited height, that is exactly one half of the depth of the section. Taking an higher value

of the concrete thickness would mean to overestimate the resistance of the section and therefore to obtain results that are unsafe.

3.4.2 Maximum IC debonding strain vs. fiber thickness

Wet-lay up systems

From a designing point of view, what changes between precured and wet-lay up FRP systems is the uncertainty in the determination of the resin volume that characterizes the latters. For this reason, it cannot be say with certain knowledge which is the area of the composite and in the calculation it is necessary to refer to the area of the dry fibers. This leads to a higher E_f and ultimate tension f_f.

The Italian guidelines CNR DT200 R1/2013 consider the difference between precured and wet-lay up systems when define the crack energy Γ_{Fd}, assuming the value for $k_G = 0{,}037\ mm$. Anyway, this parameter does not affect the value of the maximum debonding strain.

The situation described by the diagrams below is the same as the previous case, with the only difference that the maximum strain decreases, due to the higher rigidity of the composite.

The diagrams *debonding strain vs fiber thickness* are represented in *figures 3.12-3.18*.

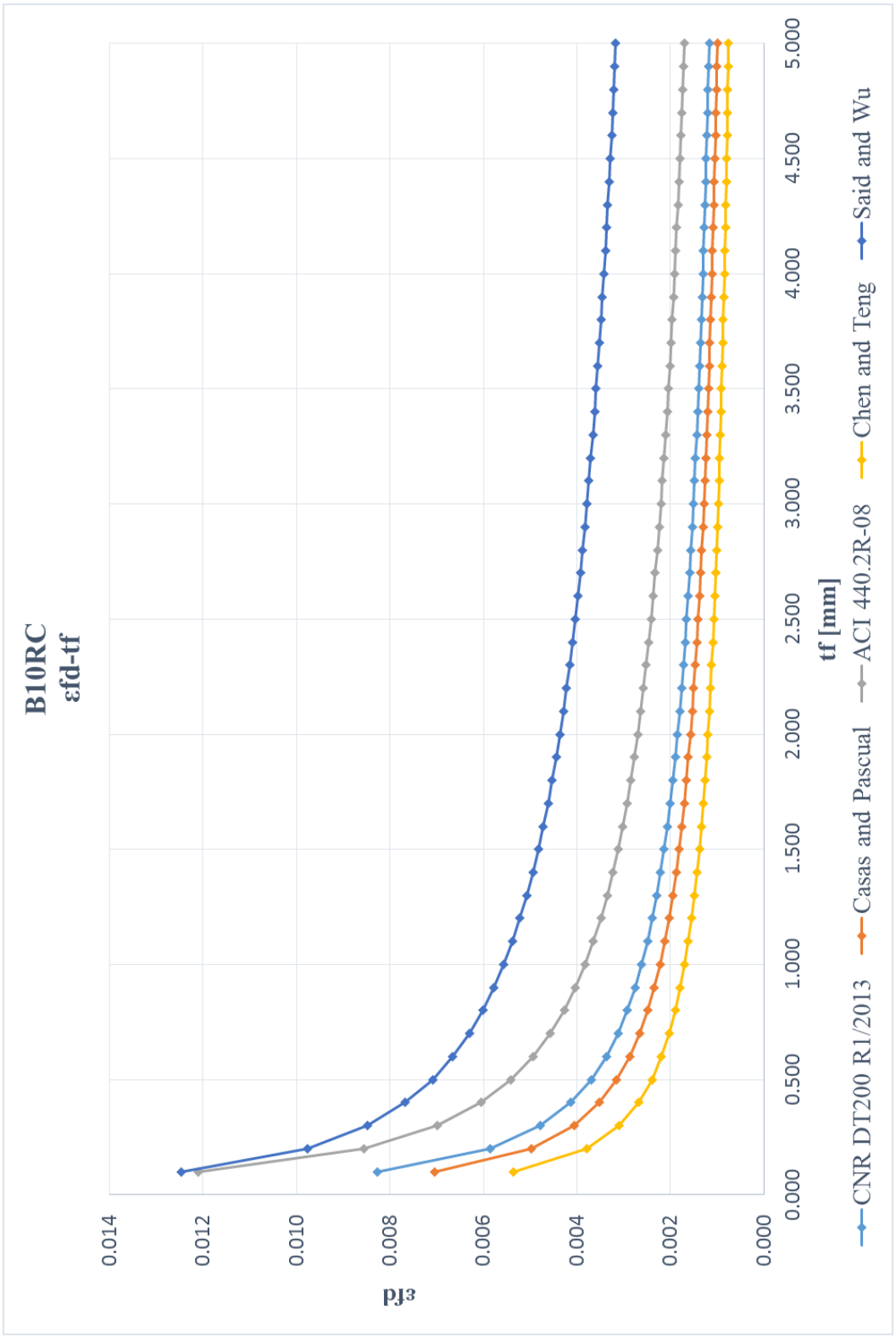

Figure 3.12. Debonding strain vs. fiber thickness for bridge B10RC.

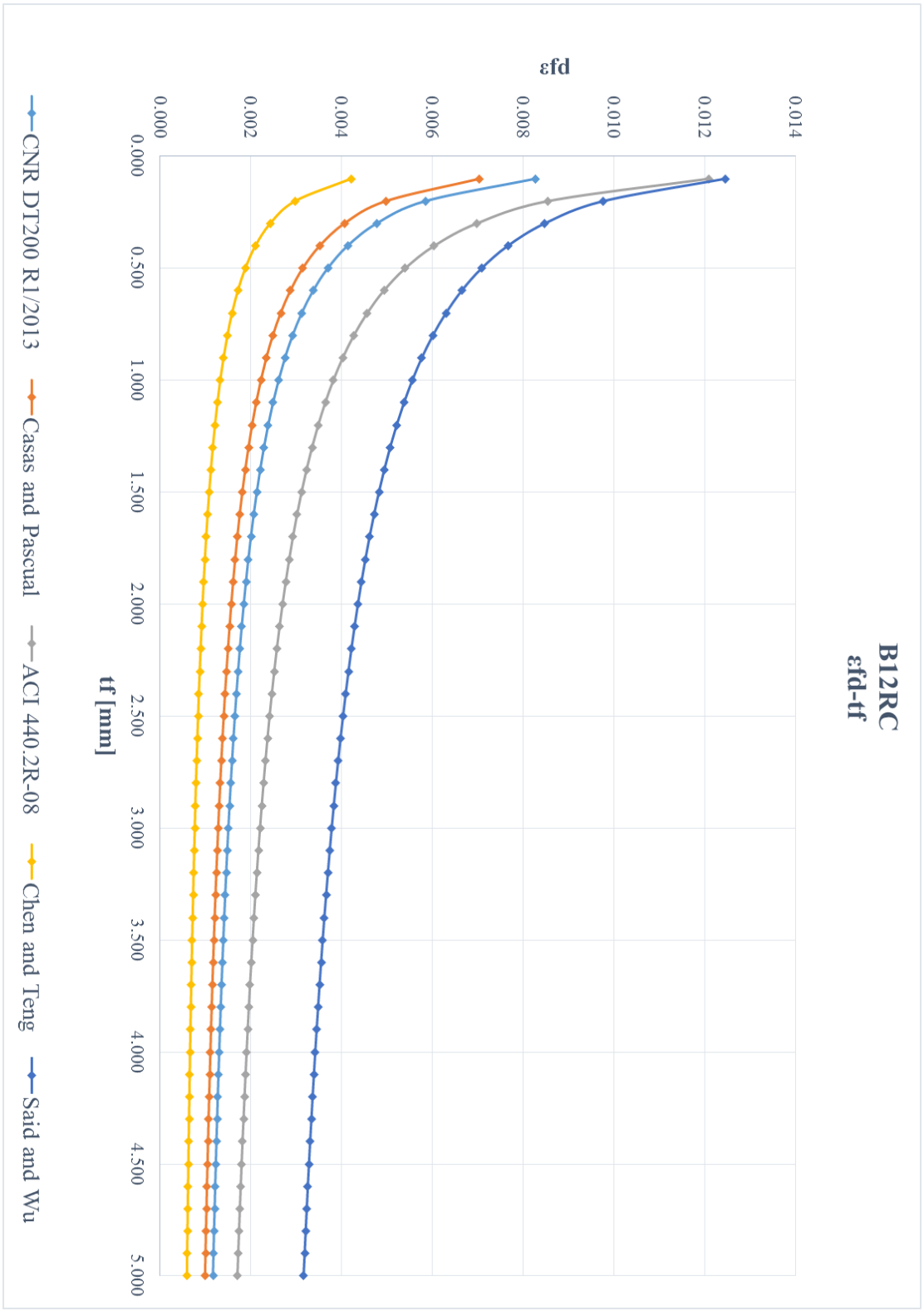

Figure 3.13. Debonding strain vs. fiber thickness for bridge B12RC.

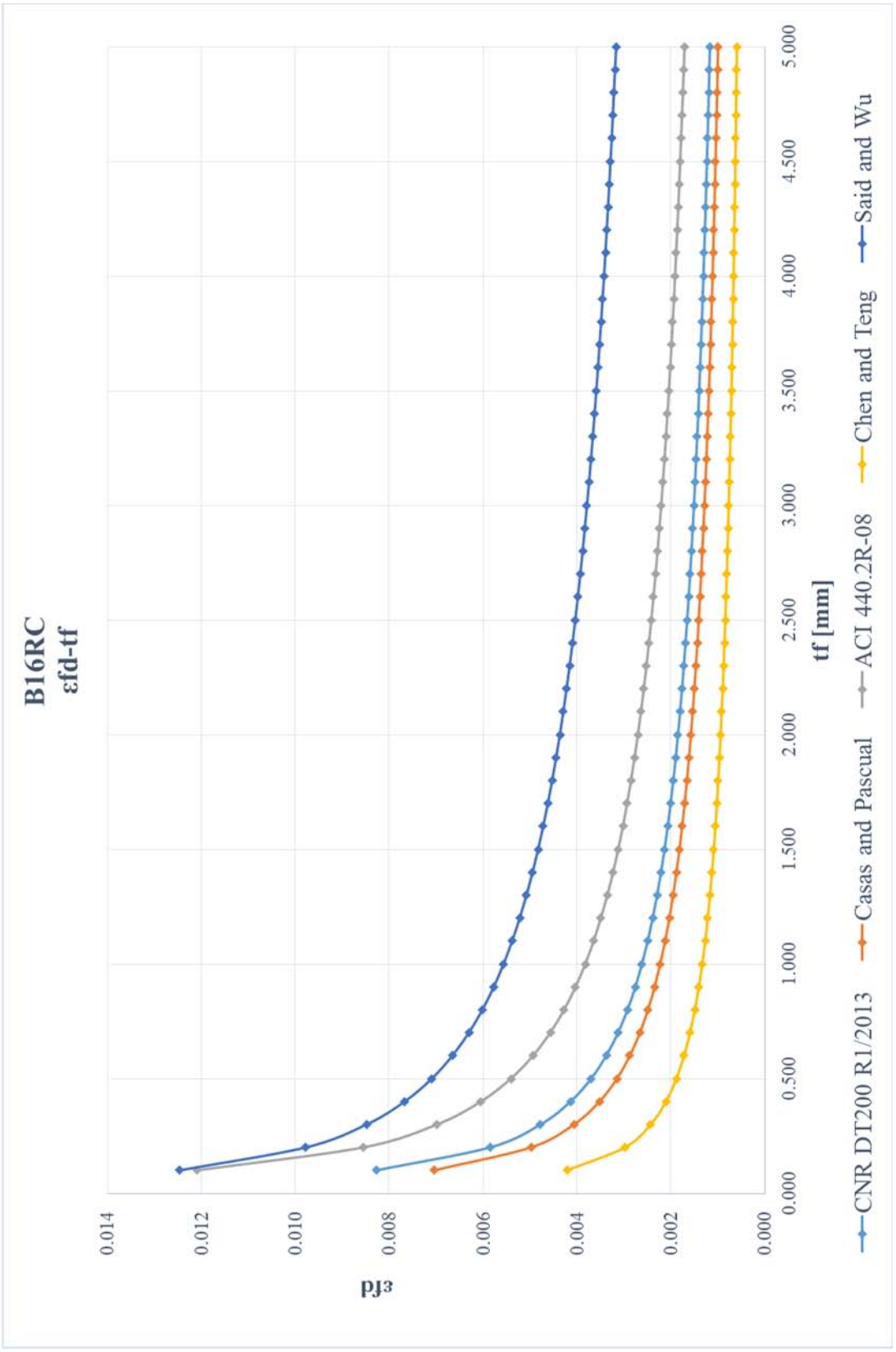

Figure 3.14. Debonding strain vs. fiber thickness for bridge B16RC.

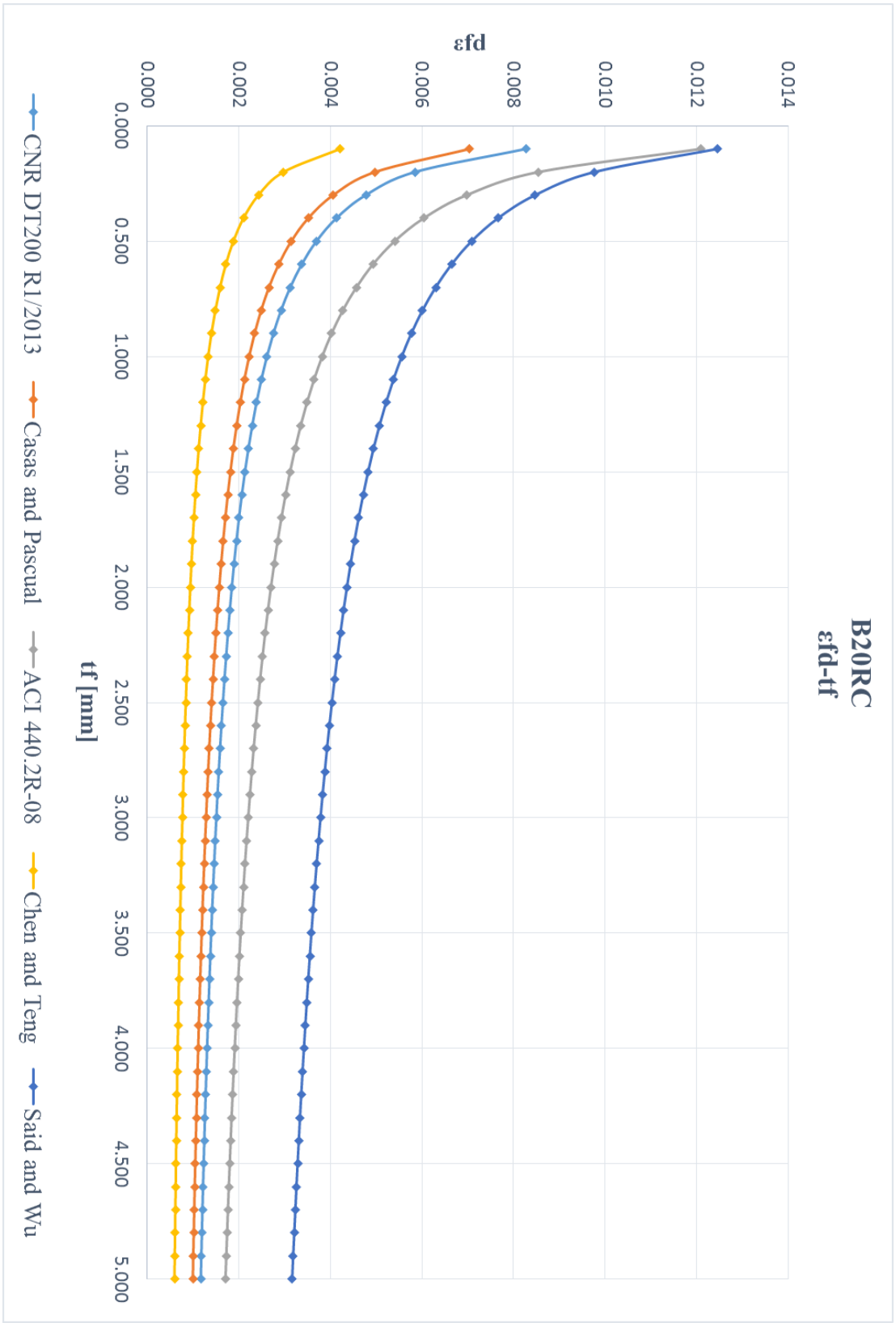

Figure 3.15. Debonding strain vs fiber thickness for bridge B20RC.

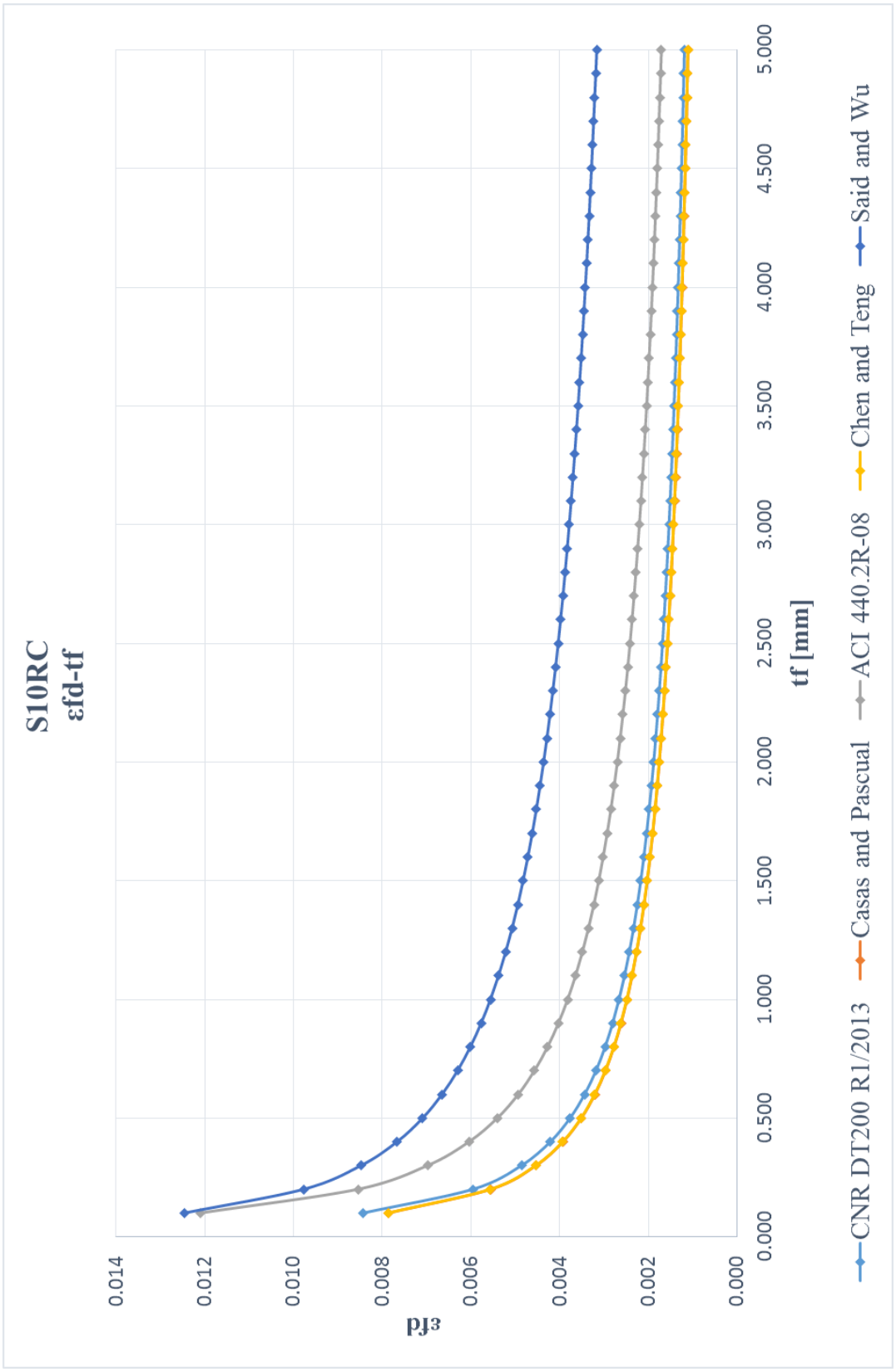

Figure 3.16. Debonding strain vs. fiber thickness for bridge S10RC.

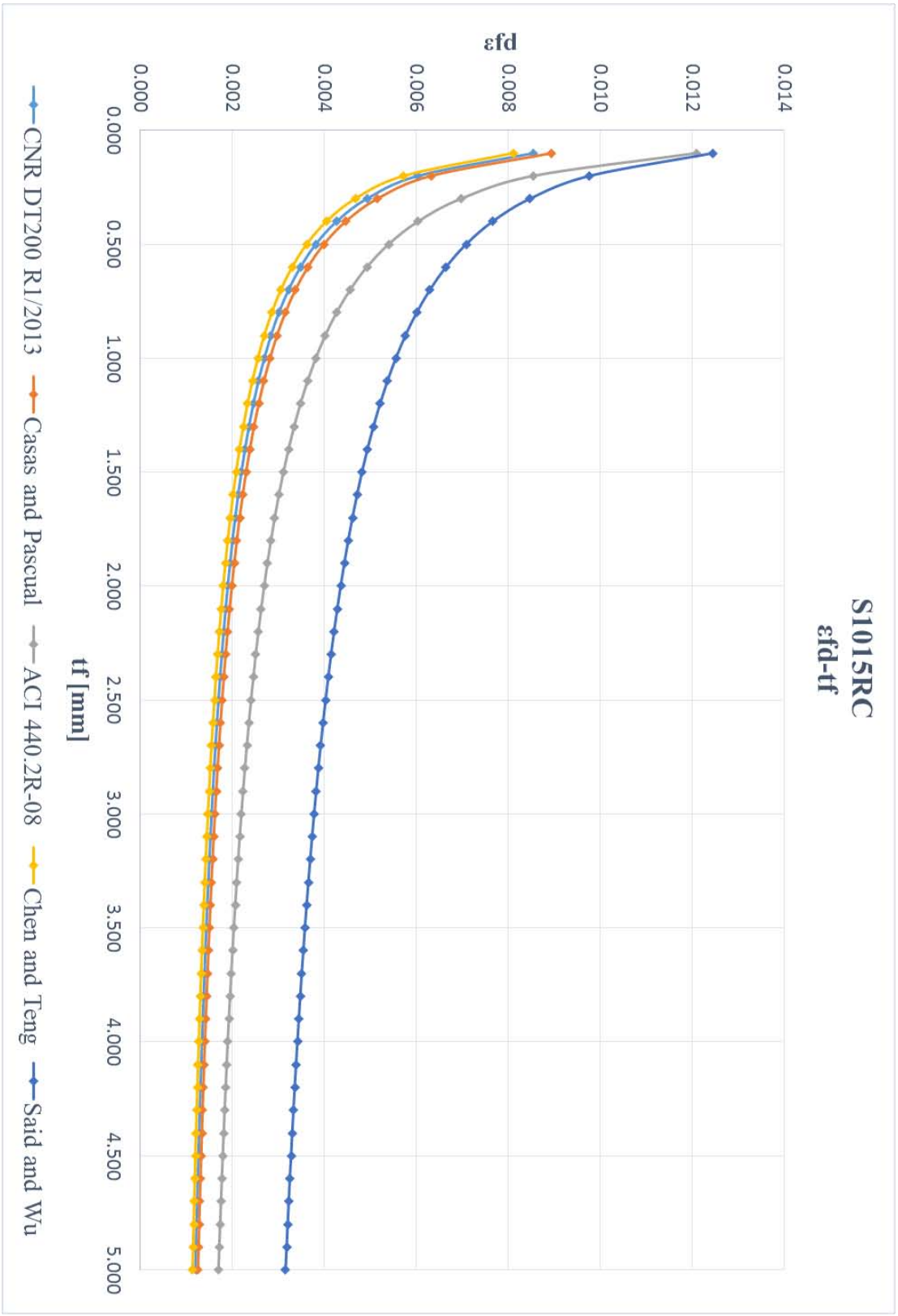

Figure 3.17. Debonding strain vs. fiber thickness for bridge S1015RC.

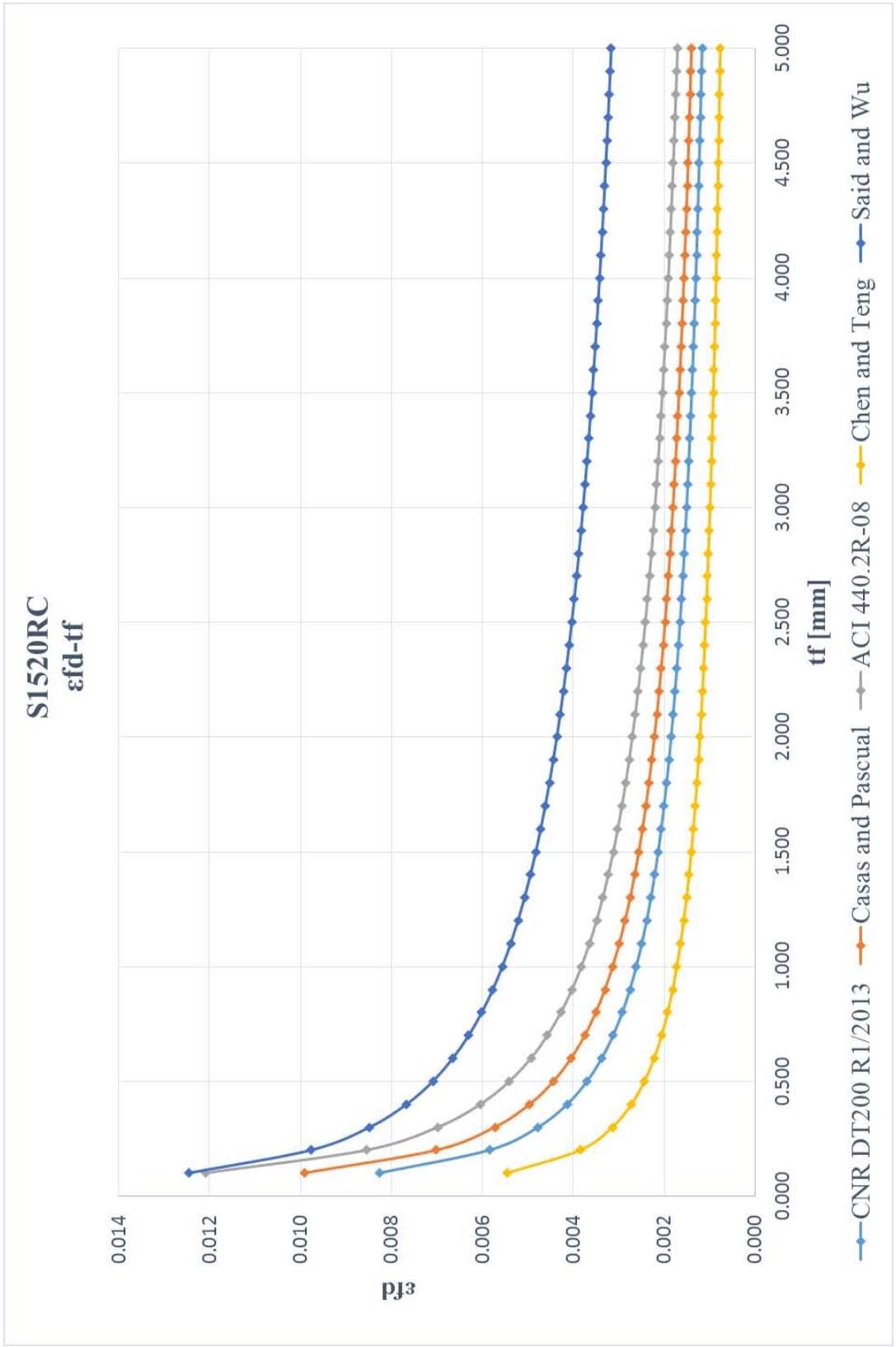

Figure 3.18. Debonding strain vs. fiber thickness for bridge S1520RC.

Chapter 4
Bridge strengthening design

4.1 Design assumptions

The bridge design is conducted according to CNR DT200 R1/2013. The assumptions made are:

a- Design calculations are based on the properties of the existing member being strengthened;
b- A plane section before loading remains plane after loading;
c- There is no relative slip between external FRP reinforcement and the concrete;
d- The shear deformation within the adhesive layer is neglected because of its thin and non-uniform thickness (this depends on the assumed debonding model, e.g., Casas and Pascual's model considers the effect of the resin layer);
e- The maximum compressive strain at failure in the concrete is 0,0035;
f- The tensile strength of concrete is neglected;
g- The FRP reinforcement has a linear elastic stress-strain relationship to failure.

The flexural strengthening is obtained by bonding a FRP plate to the soffit of the beam, through prefabricated or wet-lay up systems, already described in the previous chapter (*Figure 4.1*). The strengthening for the studied bridges is designed for both the systems.
The principles are the same as those for RC beams design. First, the neutral axis depth, x, is calculated from strain compatibility and internal force equilibrium, then the design moment is calculated by the rotational equilibrium around a certain point. The collapse can occur either for FRP rupture or concrete crushing, but also premature peeling failure has to be considered. Obviously the preferred mode of failure is that for concrete crushing following yielding of steel reinforcement, because it is the most ductile collapse.
However, due to the shape of the analyzed sections, the failure of the beams will always occur for FRP debonding, after yielding of the steel. This failure mode, although less ductile than the other one, occurs after the formation of flexural cracks, which give some warning of collapse.

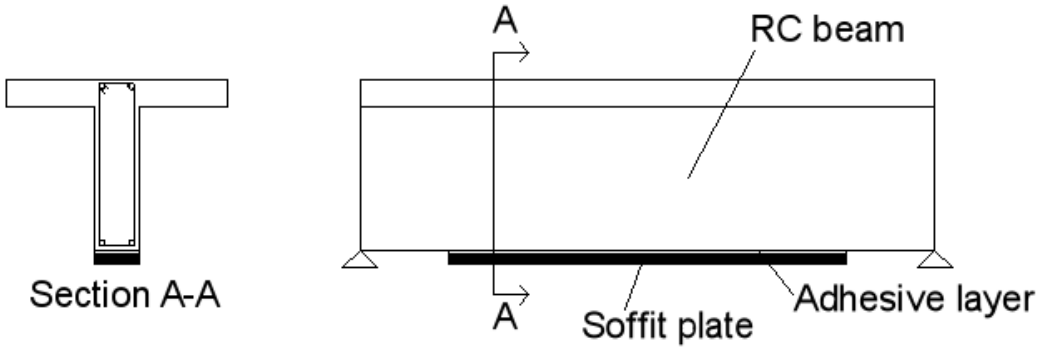

Figure 4.1. RC beam plated with prefabricated FRP.

4.2 Materials

Prior to the design of the flexural strengthening, it is necessary to describe the stress-strain relation for the materials involved in the problem.

4.2.1 Concrete

As the behavior of the FRP is brittle, the ultimate strain of concrete may not have been reached when the FRP ruptures or delamination occurs.

Actually this is what happens in the analyzed sections, because the debonding failure occurs before the concrete reaches the ultimate deformation $\varepsilon_{cu} = 0{,}0035$. Moreover, strains in the concrete at failure result very low for girder bridges, in the order of 0,3‰ to 0,7‰. This means that the use of the simplified rectangular stress-block for the concrete is no longer valid. Another type of relationship stress-strain may be considered, such as the parabola-rectangle or the bilinear ones.

In order to facilitate calculations a linear relation is taken, assumption legitimized by the small strain values. Results are then checked by the use of the software XTRACT in which a more precise constitutive relation is considered (the Mander's parabola-rectangle).

The simplification consists in taking a Young modulus of the concrete equal to $E_c = 9200\,MPa$ ($\approx \frac{1}{3}E_{cm}$, where E_{cm} is the mean secant elastic modulus according to the Eurocode [7]). This value, if the parabolic branch of the parabola-rectangle relation is

considered, corresponds to the secant modulus at the strain 0,00075, that is the maximum strain of the concrete reached in the analyzed sections (*Figure 4.3*). The considered parabola-rectangle relation is that suggested by NTC2008 [25] (*Figure 4.2*):

$$\sigma_c = 2\frac{f_{cd}}{\varepsilon_{c2}}\left(\varepsilon_c - \frac{{\varepsilon_c}^2}{2\varepsilon_{c2}}\right) \qquad 0 \le \varepsilon_c \le \varepsilon_{c2} \qquad (4.1)$$

where $\varepsilon_{c2}$is equal to 0,2% .

It can be seen from the graph (*Figure 4.2*) that the difference between taking the parabolic relation or the linear one is minimum. This choice is done in order to simplify the iterative procedure of the Monte Carlo simulation, since a parabolic relation would have been much more laborious in computational terms.

A coherence of the adopted constitutive relations is necessary between design and statistical simulation. Therefore, for the Monte Carlo simulation, which is performed by referring to the material characteristics as random variables, the Young modulus will be a random variable with a mean value equal to the secant modulus at the strain 0,00075 ($E_{cm} = 22750\ MPa$). The parabola, from which the secant modulus is calculated in the simulation, ends at a maximum compressive concrete resistance that is the mean one ($f_c = 28\ MPa$). However, this assumption will be explained more in details in Chapter 6. For now, only the design parabola and its corresponding secant elastic modulus are taken into consideration.

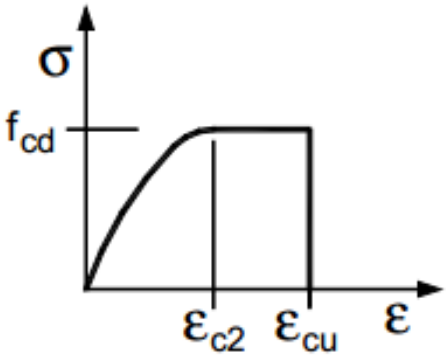

Figure 4.2. Parabola-rectangle stress-strain relation proposed by the NTC08.

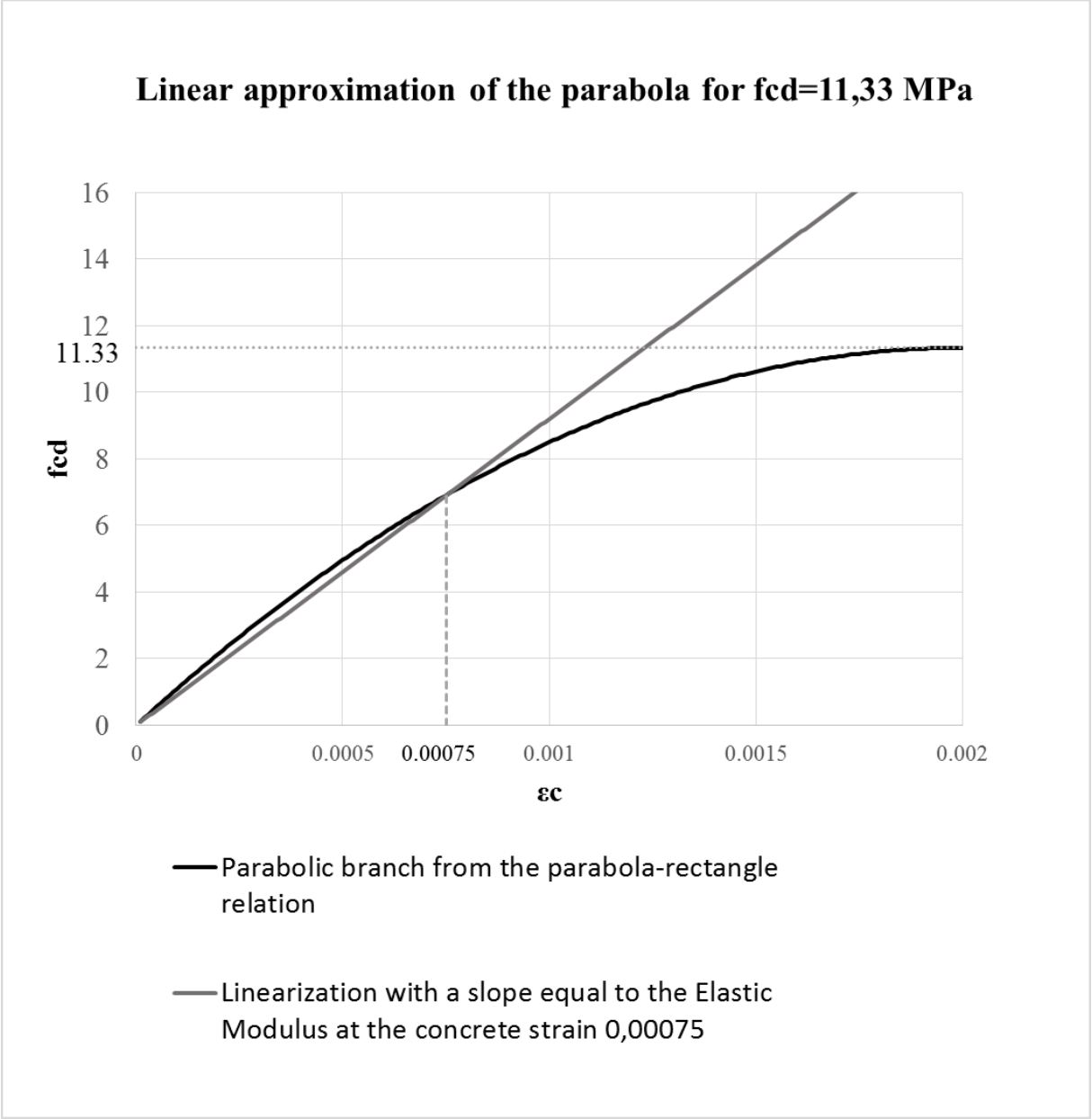

Figure 4.3. Linear approximation of the parabola for $f_{cd} = 11.33\ MPa$.

4.2.2. Steel

For the steel, it is assumed a bilinear stress-strain relation (*Figure 4.4*). The values adopted in the calculations are summarized in *Table 4.1*.

Characteristic values

ε_{yk}[‰]	1,08
ε_{uk}[‰]	67,5
f_{yk}[MPa]	216

Design values

ε_{yd}[‰]	0,94
ε_{ud}[‰]	67,5
f_{yd}[MPa]	187,83

Table 4.1. Characteristic and design values for the steel.

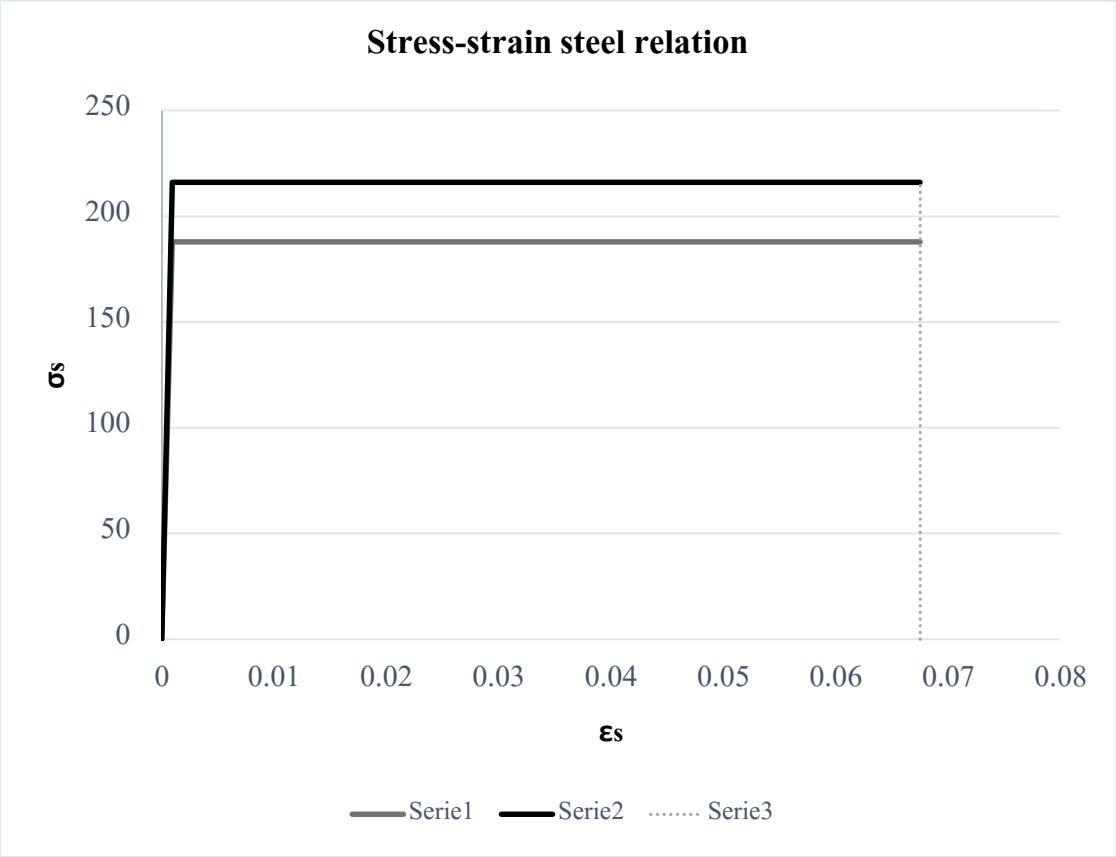

Figure 4.4. Stress-strain steel relation.

4.2.3. CFRP

The composite has a fragile behavior, hence the stress-strain relation of the material is linear till reaching the ultimate strain. Precured and wet lay-up systems present different characteristics, summarized in the following tables. It has to be minded that for precured systems the characteristics are those of the composite, while for wet-lay up systems, due to the uncertainty in the resin quantity, the data refer to the simple fiber. In order to underline this difference, a diverse nomenclature is used, that is the subscript *frp* for the composite and *f* for the fiber. The ultimate strain given in the tables ($\varepsilon_{frp,uk}$, $\varepsilon_{f,uk}$) is not the one resulting from an exact linear stress-strain relation (i.e., the ratio between the σ and E), but it is the real one, that it is lower. Anyway, the value in the *Tables 4.2* and *4.3* is that taken in the calculations and the stress-strain relation is assumed as linear until this ultimate strain is reached (*Figure 4.5*). Then the ultimate deformation is reduced in order to find its design value ($\varepsilon_{frp,ud}, \varepsilon_{f,ud}$), which is calculated according to the CNR DT200 R1/2013.

Precured system

E_{frp} [MPa]	160000
$\varepsilon_{frp,uk}$[%]	1,60
$\varepsilon_{frp,ud} = \eta_a \frac{\varepsilon_{frpuk}}{\gamma_{frp}}$ [%]	1,24
σ_{frpu} [MPa]	2560

Table 4.2. Main data for the precured system.

Where $\eta_a = 0{,}85$ is the environmental conversion factor (*table 3.2 CNR DT200 R1/2013)* and $\gamma_{frp,d} = 1{,}1$ is a factor which takes into account the material properties (*3.4.1,CNR DT200 R1/2013*).

Wet-lay up system

E_f [MPa]	230000
$\varepsilon_{f,uk}$ [%]	1,6
$\varepsilon_{f,ud} = \eta_a \frac{\varepsilon_{fuk}}{\gamma_f}$ [%]	1,24
σ_{fu} [MPa]	3680

Table 4.3. Main data for the wet-lay up system.

where $\gamma_f = \gamma_{frp}$. Obviously, the mechanical properties of the composite cannot be obtained by multiplying the area of the dry fiber for the elastic modulus or resistance of the fibers or of the composite. Indeed, the characteristics of the CFRP are extremely different. That is why, after the fiber thickness necessary for the flexural strengthening is found, it must be transformed in the equivalent composite thickness.

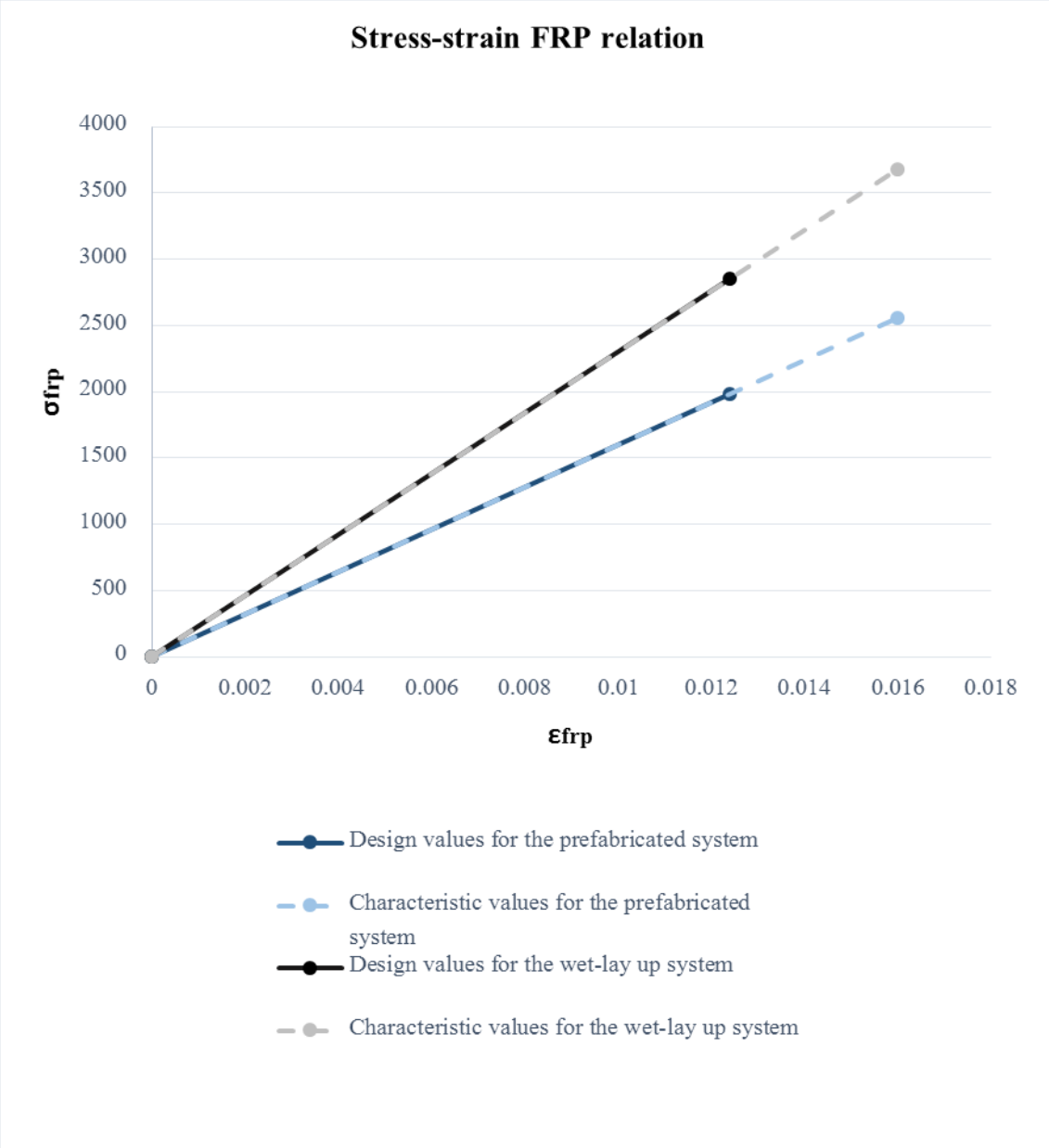

Figure 4.5. Stress-strain CFRP relation.

4.3 Design calculations

4.3.1. Design according to CNR DT200 R1/2013

The calculation of the neutral axis and resistant moment is performed in an Excel file, where the equilibrium equations necessary to solve the problem are set up. The followed method is well-represented by *Figure 4.6.*

Translational equilibrium

$$0 = A_c f_c + A_{s2}\sigma_{s2} - A_{s1}\sigma_{s1} - A_F\sigma_F \tag{4.1}$$

with

- A_c area of the concrete in compression and f_c compressive tension in the concrete (expressed as $\varepsilon_c E_c$);
- A_{s2} area of the steel in compression and σ_{s2} compressive tension in the steel, when present (i.e. only in girder bridges);
- A_{s1} area of the steel in tension and σ_{s1} tensile tension in the steel;
- A_F area of the composite/fiber (depending on the system applied) and σ_F tensile tension in the composite/fiber.

Rotational equilibrium (around the point where the tensile steel is placed).

$$M_{Rd} = \frac{1}{\gamma_{Rd}}[A_c f_c(d - \psi x) + A_{s2}\sigma_{s2}(d - d_2) + A_F\sigma_F d_1] \tag{4.2}$$

where

- $\gamma_{Rd} = 1$ is a partial factor which depends on the resistant model applied, in this case a flexural model (*Table 3.1, CNR DT200 R1/2013*);
- d is the effective depth;
- ψ is a coefficient which indicates the position of the force resulting from concrete compression compared to the neutral axis x;
- d_2 is the distance between the barycenter of the compressed steel and the upper section edge;

- d_1 is the distance between the barycenter of the tensile steel and the lower section edge.

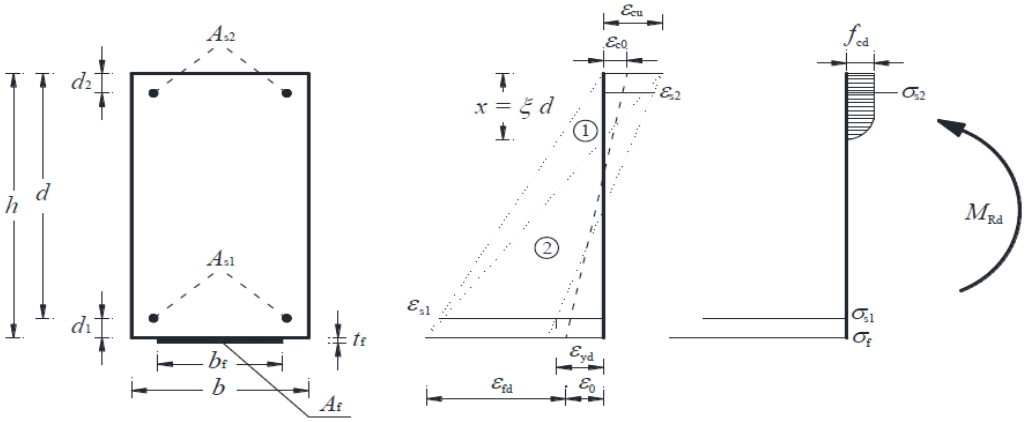

Figure 4.6. Collapse model for a RC section strengthened with FRP.

The two unknown terms are the neutral axis x, which appears in the translational equilibrium, and the thickness t_f of the fiber. Strains of steel and concrete are found by the fiber deformation, which is calculated for a series of t_f values, starting from 0,01 mm and increasing step by step the initial value of the quantity 0,01 mm. The relations between the strains are easily determined from the linearity of strain:

Concrete:

$$\varepsilon_c = (\varepsilon_{fd} + \varepsilon_0) \cdot \frac{x}{(h-x)} \leq \varepsilon_{cu}$$

Steel in compression:

$$\varepsilon_{s2} = (\varepsilon_{fd} + \varepsilon_0) \cdot \frac{x - d_2}{(h-x)}$$

Steel in tension:

$$\varepsilon_{s1} = (\varepsilon_{fd} + \varepsilon_0) \cdot \frac{d - x}{(h-x)}$$

In reality, the tensile steel reaches always its yielding point, hence the resistant stress is taken $f_y = f_{yd}$. Initial deformations ε_0 of the tensile edge prior to the composite application are considered equal to zero, since it is assumed that the bridges are unloaded.

Once calculated the neutral axis from the first equation, the resistant moment M_{Rd} is easily determined.

For girder bridges it is assumed a width of the composite equal to the width of the beam stem, $b_{frp} = b_f = 350\,mm$. This choice leads inevitably to lower admissible ultimate debonding deformations ($\frac{b_f}{b_c} = 1$), but it is forced by the excessive plate thickness that would result if a smaller CFRP width was taken. For slab bridges, an appropriate number of CFRP plates/sheets is taken, each with a width of 200 mm. For a better understanding, the reader should look at *Figure 4.7- 4.8*, where the FRP strengthening is drawn for each bridge (prefabricated system).

The results obtained according to CNR DT200 R1/2013 are listed in *Table 4.4*.

Bridge	Precured: $t_{frp}[mm]$	Wet-lay up:$t_f[mm]$	Width $b_{frp} = b_f[mm]$
B10RC	3,28	2,28	350,000
B12RC	3,56	2,48	350,000
B16RC	4,46	3,10	350,000
B20RC	6,15	4,28	350,000
S10RC	3,80	2,65	4000,000
S1015RC	2,89	2,01	3600,000
S1520RC	5,22	3,63	2400,000

Table 4.4 CFRP thicknesses obtained by design according to CNR.

It can be seen from table 4.4 that for B20RC it is obtained a thickness higher than 5 mm. This result in practical applications should be avoided, because of the excessive restriction in the ultimate strain and the significant loss in ductility that its use entails. Anyway, the found values have been calculated in order to verify the goodness of the applied linear constitutive concrete relation rather than for a real strengthening.

The accuracy in the obtained thicknesses could be thought exaggerated and surely it would be impossible to achieve it in practical applications. The reason why this accuracy is chosen is because the results will be later insert in another Excel file, necessary for

calibration. When calibrating, the maximum accuracy is wanted, because even very small values can affect significantly the reliability calculation.

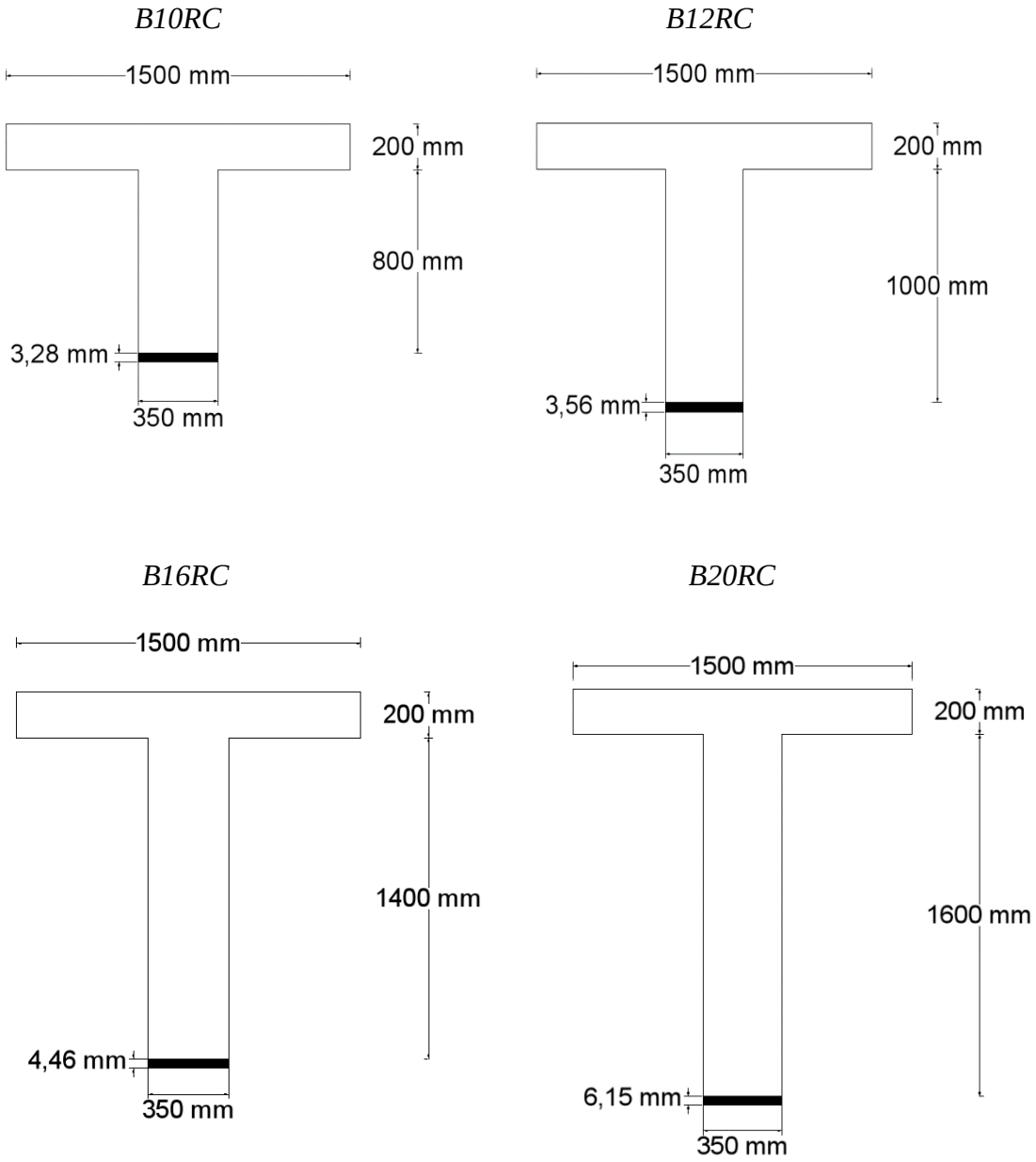

Figure 4.7. Strengthening for girder bridges (precured system).

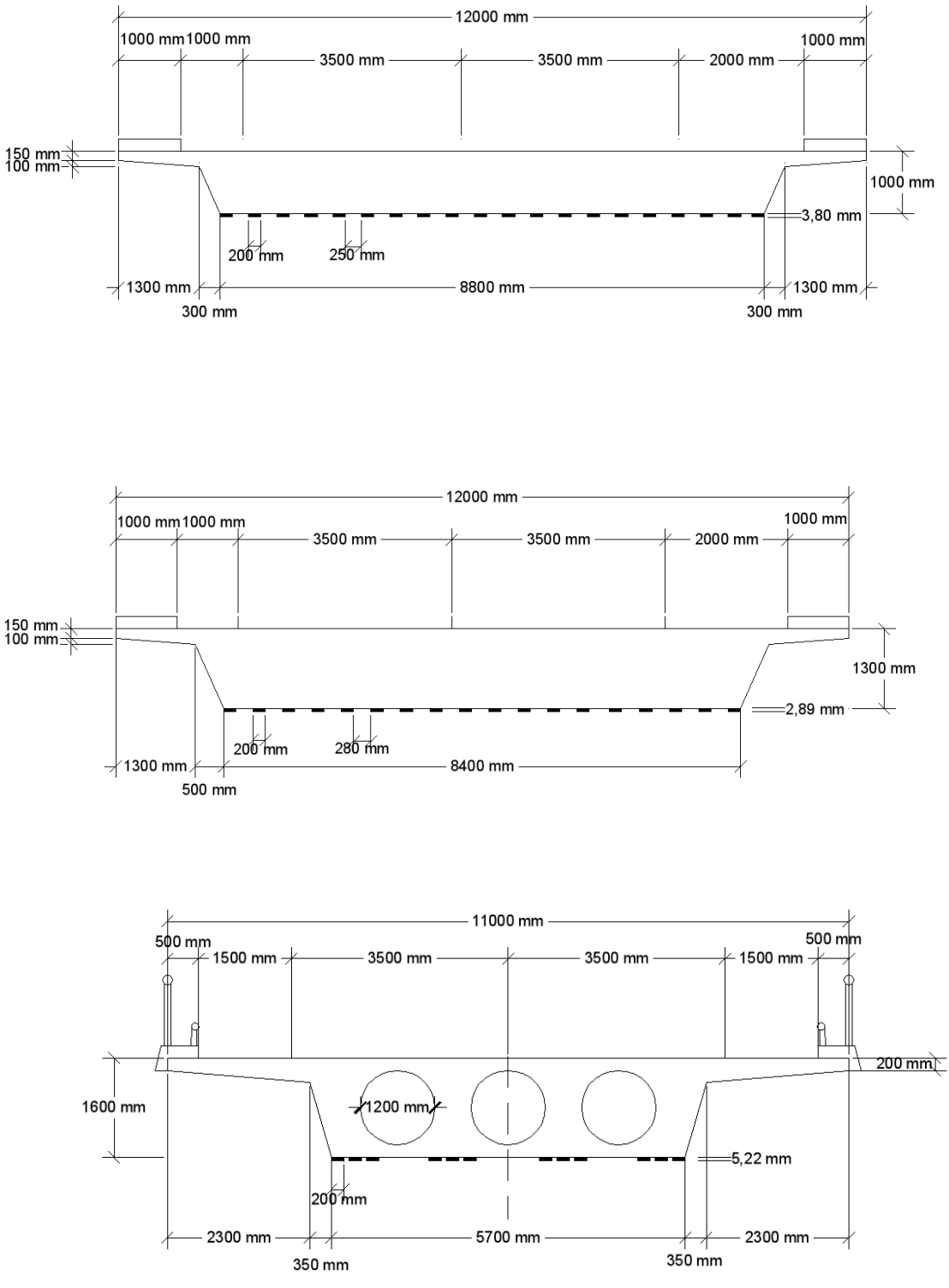

Figure 4.8. Strengthening for slab bridges (precured system). S10RC, S1015RC and S1520RC, going from top-down.

4.3.2. Design with the software XTRACT.

Results are checked with the American software XTRACT (*Table 4.5*), which allows to obtain the diagram Moment-Curvature for a section subject to an axial load and a flexural moment.

The program is used mainly in order to verify the reliability of the linear model assumed in the Excel files. The concrete constitutive relation assumed by the software is the parabolic-rectangle relation suggested by Mander et al . [22]. This means that the program assumes a resistance of the concrete in the parabolic branch that is a little higher than that hypothesized by the Italian Code (*Figure 4.9*).

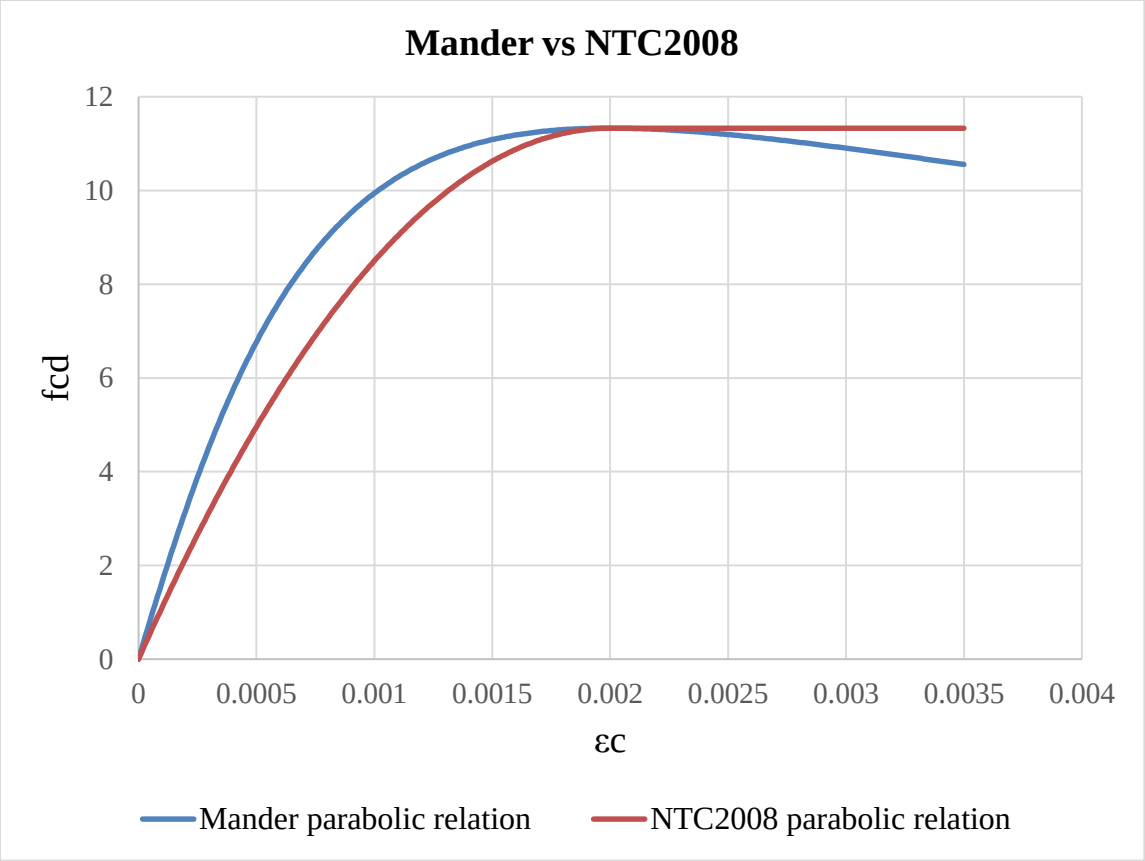

Figure 4.9. Parabolic concrete stress-strain relation according to Mander and NTC2008.

Bridge	Precured: $t_{frp}[mm]$	Wet-lay up:$t_f[mm]$	Width $b_{frp} = b_f[mm]$
B10RC	3,16	2,16	350
B12RC	3,37	2,34	350
B16RC	4,25	2,92	350
B20RC	6,12	4,25	350
S10RC	3,48	2,43	4000
S1015RC	2,65	1,85	3600
S1520RC	4,90	3,42	2400

Table 4.5 CFRP thicknesses obtained from the software XTRACT.

The difference between the results given by the excel files and the software XCTRACT is on the order of 5%, with a maximum of 8% for S10RC and S1015RC, probably due to the simplifications introduced in the model representation of the bridges. Moreover, because of the difference between the parabolic concrete stress-strain relation used by the software and that used in the design formula, it can be asserted that the difference between the XTRACT and Excel files results would be even lower. Hence, it can be said that the Excel files created can be used appropriately for the design and the Monte Carlo simulation carried out in the calibration. More detailed data and results obtained by XTRACT are given in *Annex B.*

Chapter 5

Reliability of structures

5.1 Introduction to the concept of reliability

Reliability is the property of an item or facility, which measures the ability to perform required functions under stated conditions for a specified period of time. For structures or structural components, the requirements which must be satisfied are termed by a limit state, that can be defined as (*Eurocode 0, 3.1-3.5*):

- **Ultimate limit state (ULS)**. It aims to the capacity for avoiding collapses, equilibrium loss and serious full or partial failures that could affect safety of people or lead to important economics losses, as well as relevant environmental and social damages.
  Examples. Tipping or sliding, rupture, progressive collapse, plastic mechanisms, instability, corrosion, fatigue, deterioration, fire, etc.

- **Serviceability limit state (SLS)**. It assures performances referred to operating conditions and it concerns the functioning of the structure or structural members under normal use, the comfort of people and the appearance of the construction works.
  Examples. Excessive deflections, vibrations, local damages, etc.

The "violation" of a limit state corresponds to the reaching of an undesirable condition for the structure and the aim of *structural reliability* consists indeed in the calculation and prediction of the probability of this limit state violation, the probability of failure p_f. Reliability r is therefore the complementary event of the probability of failure and can be defined as the probability of survival:

$$r = 1 - p_f \tag{1}$$

Reliability is not just a qualitative term, but is a measurable quantity and its measure may either derive from observations of the event conducted for a long period of time on similar structures or may be a simply estimation of its numerical value. Since it is not usually possible to examine a specific event for a long time, reliability is in reality determined by a combination of experimental data and subjective estimations.

5.2 The Limit State function and the probability of failure

The boundary between safe and unsafe states of a structure may be distinct or diffuse but generally codes of practice follow deterministic patterns and assume the former. Therefore the limit state is expressed by a function, the limit state function, which involves, in its simplest form, two terms, the load effect S and the resistance R, and can be defined as:

$$G = R - S \tag{2}$$

Each of S and R are two uncertain quantities described by a random variable with a known probability density function, $f_s()$ and $f_r()$ respectively. Indeed, loads, materials and geometry parameters are subject to uncertainties, which vary depending on their nature. It is important that $S$and R are expressed in the same units.

The probability of failure is:

$$p_f = P(R - S \leq 0) = \iint f_{RS}(r, s) dr\, ds \tag{3}$$

and when R and S are independent $f_{RS}(r, s) = f_R(r) f_S(s)$.

When the basic variables of the problem and their probability distributions are known, the limit state equation can be written in a generalized form. If **X** is the vector of the basic variables, then resistance and loads can be expressed as $R = G_R(\boldsymbol{X})$ and $S = G_S(\boldsymbol{X})$, so that the limit state function becomes:

$$G(\boldsymbol{X}) = R - S = G_R(\boldsymbol{X}) - G_S(\boldsymbol{X}) \tag{4}$$

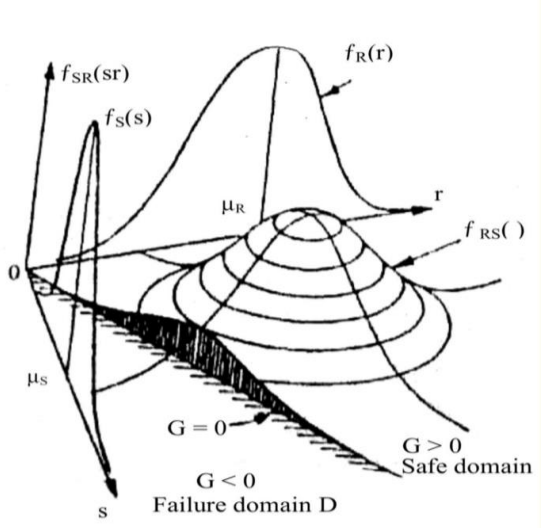

Figure 5.1. Region D of integration for failure probability determination (Melchers [5]).

As well known, a structure or a structural member is considered to fail when its resistance R is less than the force S acting on it. If x is a particular point, when the function $G(x)$ is higher than zero ($G(x) > 0$) the structure is in the safe domain, otherwise ($G(x) \leq 0$) the structure is in the unsafe domain (*Figure 5.1*).

It has to be said that, in reality, resistance and loads are generally functions of time. This implies that the uncertainty of prediction of both R and S increases with time and the probability density functions $f_R(r)$and $f_S(s)$ change. Since the parameter standard deviation (σ) increases, their curves become wider and flatter. Moreover, the mean value may change with time, because resistance tends to decrease, while loads tend to increase (*Figure 5.2*).

When the random variables defining the problem are many, it is necessary to express the probability of failure in a generalized form:

$$p_f = P[G(\boldsymbol{X}) \leq 0] = \int \dots \int_{G(\boldsymbol{X}) \leq 0} f_{\boldsymbol{X}}(\boldsymbol{X})\, d\boldsymbol{X} \qquad (5)$$

Where $f_{\boldsymbol{X}}(\boldsymbol{X})$ is the joint probability density function for the *n* vector **X** of basic variables. It is not necessary that R and S are independent, because the two functions are above described in terms of the basic variables **X**, while R and S are no more involved in the formulation. Anyway, it is preferable for the variables themselves to be independent.

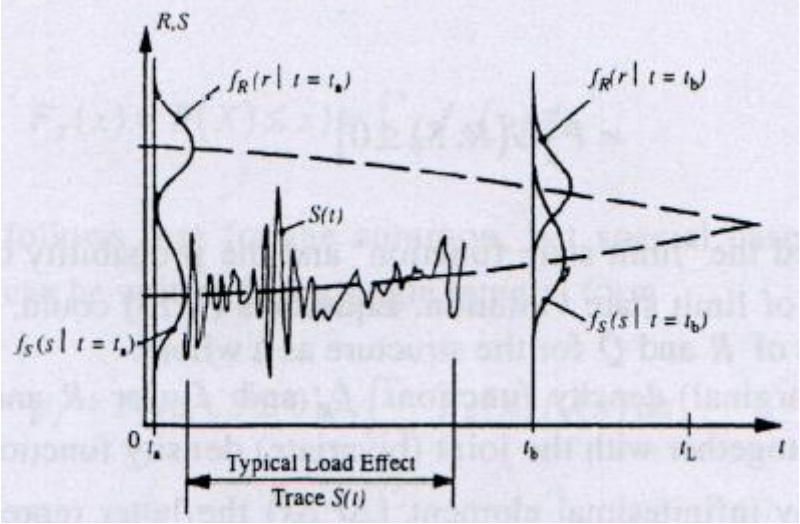

Figure 5.2. Schematic time-dependent reliability problem [23].

Usually it is assumed that neither R nor S is a function of time and the behavior of the structure is observed under a single load application. However, since there are loads, as the live load, that are applied more than once, their effect over the time should be considered by assuming for example a Gumbel or Frechet distribution. This allows to neglect the time effect in the reliability calculations, even if this simplification is not always possible.

5.3 The reliability index β

A standard reliability measure has been assumed, the so-called reliability index β, which is related to the probability of failure by the equation:

$$P_f = \Phi(-\beta) \tag{6}$$

Where Φ is the cumulative distribution function of the standardized Normal distribution (mean equal to 0 and standard deviation equal to 1), so that the relation between P_f and Φ can be easily found. Indeed if the limit state function follows a normal distribution, as it is generally possible to assume thanks to the central limit theorem, the probability of failure can be written as:

$$P_f = P(R - S \leq 0) = P(Z \leq 0) = \Phi\left(\frac{0-\mu_Z}{\sigma_Z}\right) \quad (7)$$

And so β is:

$$\beta = \frac{\mu_Z}{\sigma_Z} \quad (8)$$

where μ_Z is the mean value of the limit state function and σ_Z the standard deviation.

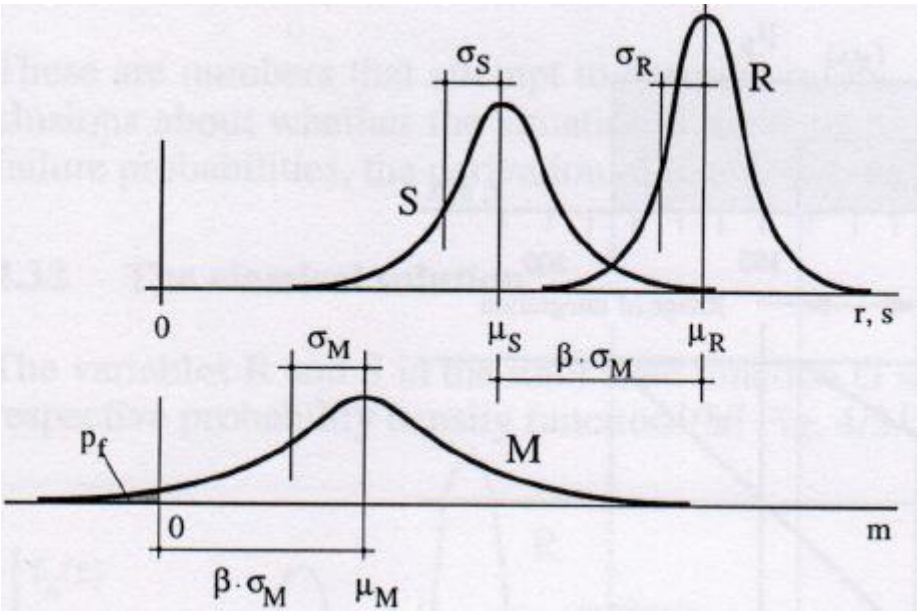

Figure 5.3. Graphical meaning of the reliability index β [30].

As it can be better understood from the image above (where $\sigma_M = \sigma_z$), the index βshows how many times the standard deviation of the variable limit state function Z (or safety margin) sets between zero and the mean value of the function (*Figure 5.3*). When the standard deviation σ_Z is higher than the mean value, the safety margin is crossed and the structure or structural component fails.

5.4 Reliability in the Eurocode

The Eurocode introduces the concept of reliability by describing two typologies of structural classes (*Annex B, B.3.1, Eurocode 0*):

- Consequences classes. They are determined depending on the consequences of failure and malfunction of the structure (*Table B1, Eurocode 0, Figure 2.4*);

Consequences Class	Description	Examples of buildings and civil engineering works
CC3	**High** consequence for loss of human life, *or* economic, social or environmental consequences **very great**	Grandstands, public buildings where consequences of failure are high (e.g. a concert hall)
CC2	**Medium** consequence for loss of human life, economic, social or environmental consequences **considerable**	Residential and office buildings, public buildings where consequences of failure are medium (e.g. an office building)
CC1	**Low** consequence for loss of human life, *and* economic, social or environmental consequences **small or negligible**	Agricultural buildings where people do not normally enter (e.g. storage buildings), greenhouses

Figure 5.4. Definition of consequences classes according to Eurocode 0.

- Reliability classes. They are associated with the consequences classes and defined by the introduction of the reliability index β, which, depending on the considered class, assumes a certain value. The higher this value is the higher the reliability of the structure or member is (*Table B2, Eurocode 0, Figure 5.5*).

Reliability Class	Minimum values for β	
	1 year reference period	50 years reference period
RC3	5,2	4,3
RC2	4,7	3,8
RC1	4,2	3,3

Figure 5.5. Recommended minimum values for reliability index β (Ultimate Limit State).

5.4.1 Target values of the reliability index (Eurocode)

Reliability class which usually designers refer to is RC2. Target values of index β are given by Eurocode for reference periods of 1 year and 50 years (*Eurocode 0, Annex C, C6, Table C2- Figure 5.6*).

Limit state	Target reliability index	
	1 year	50 years
Ultimate	4,7	3,8
Fatigue		1,5 to 3,8 [2)]
Serviceability (irreversible)	2,9	1,5

[1)] See Annex B

[2)] Depends on degree of inspectability, reparability and damage tolerance.

Figure 5.6. Target reliability index β for Class RC2 structural members.

5.5 Reliability in the assessment of existing structures

Eurocode and many other codes deal exclusively with design situations of new structures, but in the last years the assessment of existing structures has become more and more frequent, due to social and economical reasons. In reality, the reliability concept for existing and new structures is different, since there are parameters and sources of uncertainties that are different between the design and the assessment.

For example, when repairing and strengthening old structures, the designers have to mind that the analyzed facility was built following a code which could be different from the actual one. This adds uncertainties as regards the loads and the resistance parameters. Moreover, many times information and detailed documents about what was previously done lack and designers have to *interpret* old drawings and calculations. It is therefore evident that the probabilistic models used in assessment of structures generally represent only one part of the imperfect knowledge about the structure.

The only way to reduce the uncertainties due to lack of information is to proceed by a so-called Bayesian probabilistic reassessment. Based on the available prior information, a study of the structure and its behavior is conducted and a *priori* uncertainty model is used. By analyzing the building performance, it could be that new information about the structure are obtained. These can be used in order to update the previous uncertainty model and establish a new *a posteriori* model.

As for reliability of new structures, for assessment of facilities, a limit state equation has to be identified, which includes adverse and favorable events. The difference with limit

state functions for new buildings is that the study of the existing structures gives some more initial data that should be considered. For example, the presence of cracks in the concrete, the level of steel corrosion, even to know that the structure has not failed previously can help in establishing the formulation of the limit state equation. Obviously the latter can be formulated at any level of approximation, but generally in structural engineering the physical phenomena governing the problem is performed at an intermediate level (the so-called *meso-level*).

Once identified the limit state function, a probabilistic model should be determined in order to represent the basic variables appearing in the function. Uncertainties are due to geometry, material properties, loads and the assumed resistance model.

The last step is to fix a certain target reliability that eventually has to be checked. This would correspond to the end of reliability analysis for new structures, whereas for existing facilities it consists only in the end of a *prior* analysis, that, based on the obtained results, can be updated (for example by a linear regression) and done again as a *posterior* analysis, which leads the designer to achieve a safer assessment.

Another possible procedure is to perform a *posterior* analysis even before the first structural analysis has been conducted and to assume that the results obtained by this first analysis are those corresponding to the *prior* probabilistic model. This is an advanced procedure, defined as *pre-posterior* analysis.

5.5.1 Target values of the reliability index (Publication of the JCSS)

Differences between reliability problem for structures to be designed and structures which already exist have been illustrated. Hence reliability factor target values proposed by the Eurocode, which deals with the design of new structures, are no more valid. In addition to the usual parameters which influence the reliability index values, such as the failure modes considered, (structural o non-structural, individual or of a system) and the failure consequences, another important factor has to be considered. It is taken as reference a publication of the Joint Committee on Structural Safety (JCSS) [3], in which different target β values are suggested (*Table 5.1*). In reality, proposed values are valid both for new and existing structures. The new parameter is the relative cost of safety measure.

Indeed, most of the time target β value is the result of a decision based on an optimization of generalized benefits and cost including expected failure costs.

1	2	3	4
Relative cost of safety measure	Minor consequences of failure	Moderate consequences of failure	Large consequences of failure
Large (A)	$\beta = 3{,}1$ ($p_F \approx 10^{-3}$)	$\beta = 3{,}3$ ($p_F \approx 10^{-4}$)	$\beta = 3{,}7$ ($p_F \approx 10^{-4}$)
Normal (B)	$\beta = 3{,}7$ ($p_F \approx 10^{-4}$)	$\beta = 4{,}2$ ($p_F \approx 10^{-5}$)	$\beta = 4{,}4$ ($p_F \approx 10^{-6}$)
Small (C)	$\beta = 4{,}2$ ($p_F \approx 10^{-5}$)	$\beta = 4{,}4$ ($p_F \approx 10^{-5}$)	$\beta = 4{,}7$ ($p_F \approx 10^{-6}$)

Table 5.1. Tentative target reliability indices β (and associated target failure rates) related to one year reference period and Ultimate Limit State.

5.6 Evaluation of the structural reliability

Equation (5) can be solved by different methods, which are mainly grouped into two categories:

- Integration and simulation methods;
- Second-moment and transformation methods.

5.6.1 Integration and simulation methods

The principle hypothesis is that the probability density function of each basic variable is known and not approximated.

If R and S follow a normal distribution, then the integration region can be represented by a linear limit state function and the integral of equation (5) can be solved even if n-dimensional.

$$G(x) = Z = 0 = a_1 x_1 + a_2 x_2 + \cdots + a_n x_n \tag{9}$$

Most of the time, limit state functions are not linear, therefore it is preferable to proceed with another method, called Monte Carlo simulation. This method introduces approximate numerical solutions to the probability integral and can be applied to problems with limit state functions $G(x)$, which may have any form. Monte Carlo

simulation will be later illustrated in detail, being chosen for the calculation of the reliability of the studied bridges.

2.6.2 Second-moment and transformation methods

This time, the principle hypothesis is that the probability density function itself is simplified. In the so-called First Order Second Moment method (FOSM), each variable appearing in the limit state function is expressed by its two first moments (mean value and standard deviation of its probability distribution). Therefore, it is assumed to be a Normal distribution even if it is not (in fact, the only distribution that can exactly be represented by its mean value and standard deviation is the Normal distribution). This leads to the calculation of a probability of failure that is "nominal", precisely because to assume a variable described only by its two first moments, unless it has a normal distribution, means to make an approximation. The procedure is iterative and consists mainly in to approximate the limit state function $G(x)$ with a linear function, after transforming all the basic variables to their standardized form $N(0,1)$ (*Figure 5.7*).

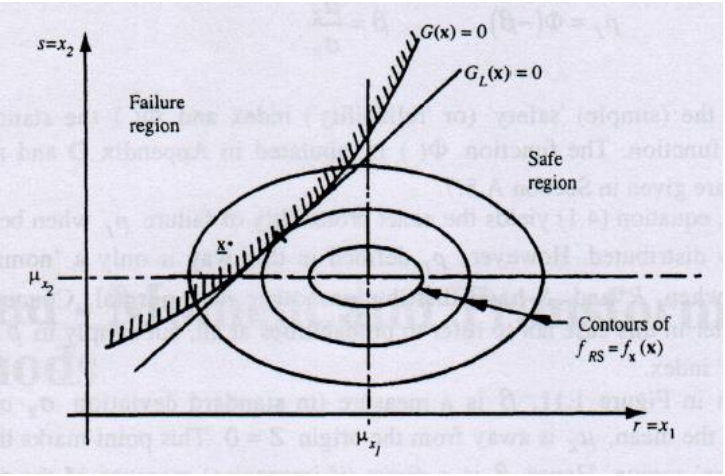

Figure 5.7. Limit state surface G(x)=0 and its linearized version $G_L(x) = 0$ in the space of the basic variables.

The transformation or First Order Reliability method (FORM) differs from the former because more information about the basic variables are known. These information should be incorporated in the reliability analysis and this can be done by transforming non-normal distributions into equivalent normal-distributions. It is done transformed at the so-called "design point" and the procedure is more complex than that of the FOSM method.

Eventually there is the so-called Second Order Reliability method (SOR) which is basically equal to the FOR method, with the difference that the limit state function $G(x)$ is approximated with a second order function and no more simply linearized.

5.7 The Monte Carlo simulation

The two physicists John von Neumann and Stanislaw Ulam were investigating in radiation shielding at Los Alamos scientific laboratory (1946) when they had the idea to solve a problem of lack of data by inventing the so called Monte Carlo simulation, which takes its name from the famous Monte Carlo Casino.

This method is largely used for structural reliability. It consists in sampling each random variable X_i that appears in the limit state function to give a sample value x_i that is briefly to simulate artificially a large number of experiments. Indeed in the limit state function, resistance and loads are assumed as random values with a specific statistical distribution. Depending on their combination the function will result greater or lower than zero.

To apply the Monte Carlo simulation means to simulate a certain number N of hypothetical trials, so that the probability of failure can be easily calculated as:

$$p_f = \frac{n(G \leq 0)}{N} \tag{10}$$

Where *n* is the number of trials for which $G \leq 0$. Number *N* value depends on the wanted accuracy.

5.7.1 Generation of random numbers

Generally basic variables acting in the structural reliability problem follow a nonuniform distribution. Their sample values are called "*random variates*" and can be found by different mathematical techniques. The most common procedure used is the "*inverse transform*" method. It is known that the cumulative distribution function $F_X(x_i)$ of a basic variable X_i assumes a value between 0 and 1. The inverse transform method consists in

generating a uniformly distributed random number $r_i$included in the interval (0,1) and equating this to $F_X(x_i)$.

$$F_X(x_i) = r_i \tag{11}$$

In this way, if the inverse function $F_X{}^{-1}(x_i)$ exists, the sample value x_i can be found (*Figure 5.8*).

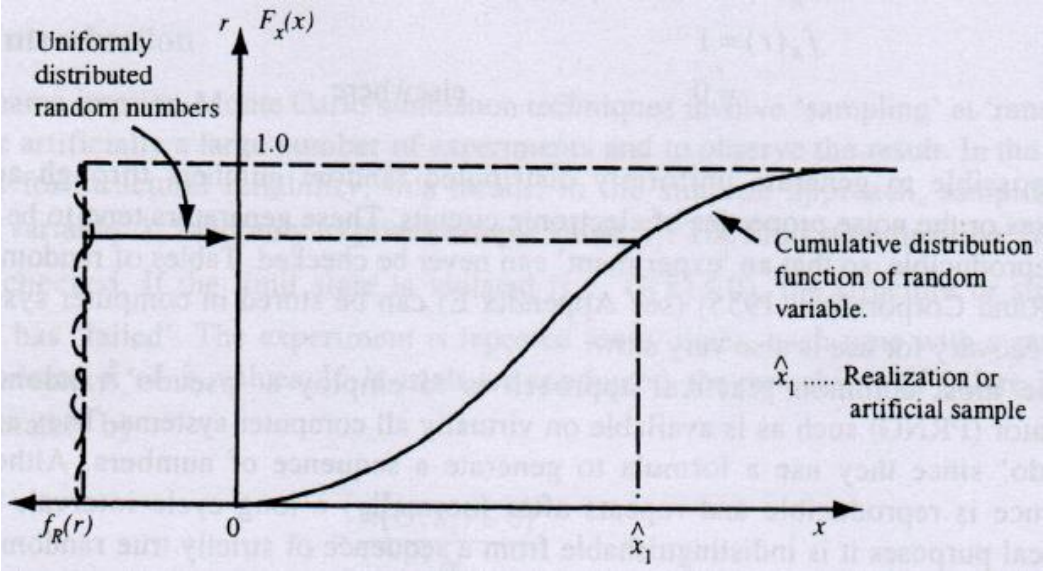

Figure 5.8. Inverse transform method for generation of random variates [23].

In order to generate the random numbers r_i automated roulettes or the noise properties of electronic circuits can be used. It is possible to store tables of random values in computer systems as well, but all these procedures are slow and not comfortable.

This is the reason why usually a pseudo random number generator (PRNG) is used, that is available in all computer systems. The word "*pseudo*" indicates that numbers are simulated by a formula and therefore they are not properly random values, but they follow a sequence which repeats after a long cycle interval.

Hence Monte Carlo methods using PRNGs are called more correctly "quasi Monte Carlo" methods. Anyway, the use of PNRG allows to get an uniform distribution and the reached accuracy is good.

5.8 Basic variables

Basic variables concurring in the structural reliability problem can be mainly divided into two groups, as seen in previous paragraphs:

- Resistance variables;
- Load variables.

5.8.1 Resistance variables

Structural resistance can usually be expressed in the following form:

$$R = M \cdot F \cdot D \cdot R_n \tag{12}$$

where

- R_n is the nominal resistance;
- M indicates the model uncertainty variable and it is called "professional" or "modelling" factor. This term summarizes the effect of the simplifications introduced by the mathematical model assumed in order to evaluate the resistance of the structure or structural component. For good models it results M≈ 1, but generally developed models are conservative, so that usually M > 1. Moreover the coefficient of variation is of a few percent if the model is good (e.g. bending resistance models), whereas for poor models (e.g. shear resistance models) its value sets between 10%-20%;
- F indicates material properties (strength, elastic modulus,…) . They should generally be derived from standardized tests (mostly tension and compression tests), performed under specified conditions. These tests have to be planned in order to get a realistic description of the material performance in real applications. The frequency of negative values is normally zero, hence material variables can be generally represented by a log-normal distribution.
- D indicates dimensions and derived quantities. This term can be important in concrete, because it is more easy to introduce dimensional variability, for example in the concreting phase. Generally dimensional variables can be modelled by normal or log-normal distributions. The standard deviations are of the order of

magnitude of the dimensional tolerances, therefore the coefficient of variation (mean value/standard deviation) is higher for smaller dimensions.

Factors M, F and D are usually ratios of actual to nominal values. If the resistance variables are independent and an assumption of second-order applicability is done (normal distribution for each variable), R could be expressed by a second-order format and its mean and coefficient of variation could be:

$$\mu_R \approx \mu_M \mu_F \mu_D R_n \tag{13}$$

$$V_R^2 \approx V_M^2 + V_F^2 + V_D^2 \tag{14}$$

where the letter μ denotes the sample mean of the quantity and V_i are the coefficients of variation.

If dimensional and material properties do not follow a normal distribution, simulation is generally the most viable approach for the derivation of member properties.

2.8.2 Load variables

Loads are the most uncertain factor in structural reliability, so that appropriate models should be developed in order to represent their values. It is not that simple though, indeed, loads are assumed to vary with time, so that they should be represented as a stochastic process. The different existing methods used for load modelling are not explained here in detail, since the aim of the author is to give an overview about the problem and the reader should consult the specialist literature for further in-depth analysis.

Loads can mainly be divided into two groups:

- Those due to natural phenomena (wind, waves, snow, earthquakes,…);
- Those due to man-imposed effects (dead loads and live loads).

For the formers observations of the phenomenon over a period of time are usually available, hence daily and yearly maxima can be generally identified and used for modelling extreme value distributions. For the latters, long term data are often insufficient and the statistical properties of the load distribution must be determined mathematically.

Leaving aside the first typology of load, some comments are given about loads due to man-imposed effects, which will take part into the Monte Carlo simulation developed in the next chapter.

Dead loads are the sum of *self-weight* and *permanent loads*. The *self-weight* is essentially constant during the life of the structure and there is just a small tendency to increasing values because of some factors, such as deformation of the shuttering, tolerances, etc.. Generally self-weight in concrete elements is represented by a Normal distribution, with a bias of 1,05 and a coefficient of variation of about 5%. *Permanent loads* are constant during a long time period too, but their coefficient of variation is usually higher than that of the self-weight, mainly because changes and alterations may occur (such as removal of pavement layers, …).

Live loads in buildings are generally of moderate extent and peaks showed by their distributions are mainly due to the possible presence of crowds of people. They can never assume a negative value and generally the live loads of a minor intensity, the so-called accompanying loads, assume a lognormal distribution. The leading loads instead, such as the crowd load, can be well represented by an extreme value distribution (Gumbel, Frechet, …). In bridges the leading live load is represented by the traffic load.

Chapter 6

Setting of the Monte Carlo simulation

6.1 The general Limit State function

To calculate the probability of failure of the strengthened bridge cross-sections and the corresponding reliability indexes β, it is chosen to perform a Monte Carlo simulation. Once defined R as the resistance and S as the loads acting on the section, the limit state equation can be written in a generic form as:

$$G = R - S = M_u - M_{dl} - M_{ll} = \tag{6.1}$$
$$= [A_{s1}\sigma_{s1}(d - d_c) + A_F\sigma_F(h - d_c) + A_{s2}\sigma_{s2}(d_c - d_2)] - M_{dl} - M_{ll}$$

where

- M_u is the resistant moment of the section calculated by imposing the equilibrium around the barycenter of the compressed concrete;
- M_{dl} is the acting moment due to the dead load;
- $M_{ll}$is the acting moment due to the live load;
- h is the height of the section and d the effective depth;
- d_c is the distance between the force resulting from compression in the concrete and the upper section edge;
- d_2 is the distance of the compressive steel barycenter from the upper edge;
- A_{s1}, A_{s2} and A_F are the areas of the tensile steel, compressive steel and composite/fiber, respectively;
- σ_{s1} and σ_{s2} are the stresses in the tensile and compressive steel;
- σ_F is the stress in the composite at debonding.

As already said in Chapter 5, in *Equation 6.1*, resistance and loads are assumed as random variables with a specific probability distribution. The main statistical properties of each random variable are discussed in this chapter, with the exception of the model error variable, which will be presented in details in Chapter 7.

6.2 Statistical properties of the resistance variables

6.2.1 Concrete compressive resistance and elastic modulus

a) The resisting stress of the concrete f_c follows a Lognormal distribution (*Table 6.1*).

Characteristic value f_{ck} [MPa]	20,00
Bias ϑ	1,40
Coefficient of variation COV	0,15
Mean value μ [MPa]	28,00
Standard deviation σ [MPa]	4,20

Table 6.1. Main statistical properties of the resisting concrete stress f_c.

Where the mean value is calculated as:

$$\mu = \vartheta f_{ck} \tag{6.2}$$

and the standard deviation is given by:

$$\sigma = \mu COV \tag{6.3}$$

The probability distribution of a variable x is a lognormal distribution if the variable $n = logx$ follows a standard normal distribution.

The mean value and variance of the x distribution are defined:

$$\mu_x = \exp(\lambda + \frac{1}{2}\xi^2) \tag{6.4}$$

$${\sigma_x}^2 = {\mu_x}^2(e^{\xi^2} - 1) \tag{6.5}$$

with

- λ is the mean value of the normal distribution of $n = logx$;
- ξ is the standard deviation of the normal distribution of $n = logx$.

The value of λ and ξ can be found by inverting the equations for μ_x and ${\sigma_x}^2$:

$$\lambda = \ln(\mu_x) - \frac{1}{2}\xi^2 = 3{,}321\ [\ln(MPa)] \tag{6.6}$$

$$\xi = \sqrt{\ln\left(\left(\frac{\sigma_x}{\mu}\right)^2 + 1\right)} = 0{,}149\ [\ln(MPa)] \tag{6.7}$$

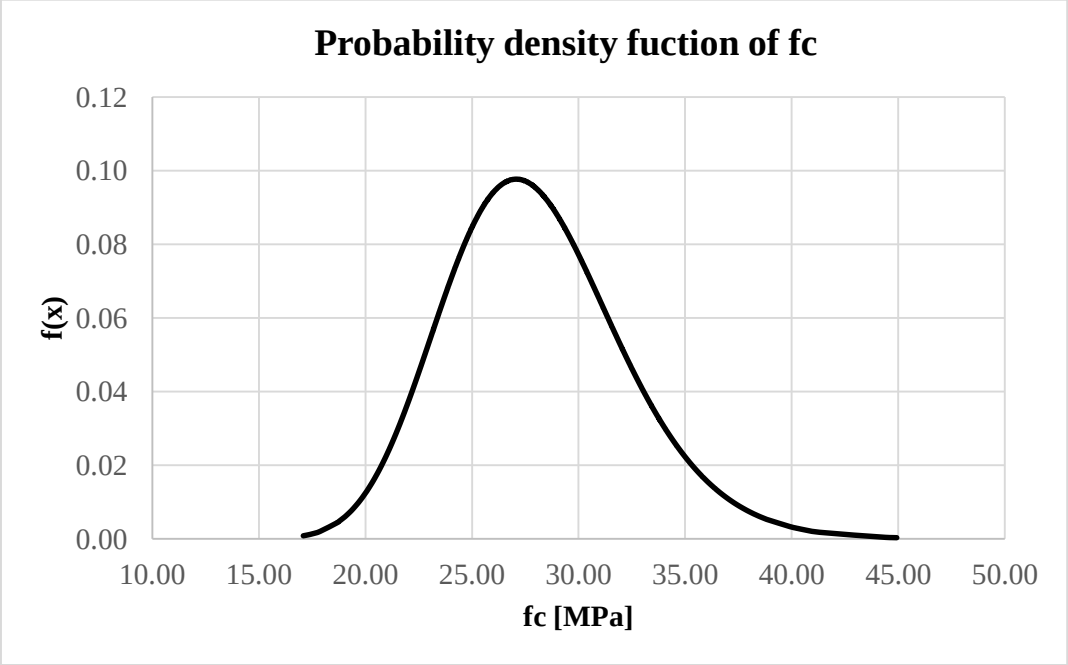

Figure 6.1. Probability density function of fc.

Since the value of ξ is very low (< 0,1 [lnMPa]), the distribution assumes a shape that is almost symmetric (*Figure 6.1*).
The probability density function equation is:

$$f(x) = \frac{1}{\sqrt{2\pi}x\xi} e^{\left[-\frac{1}{2}\left(\frac{lnx-\lambda}{\xi}\right)^2\right]} \qquad 0 \leq x < \infty \qquad (6.8)$$

It has to be stressed out that the compressive resistance of the concrete appears only in the equation of the applied debonding models and it is not taken for representing the resistance of the concrete at the compressed edge of the section. Indeed, due to the low strains, the concrete resistance is calculated by multiplying the strains for the elastic modulus of the material.

b) The concrete elastic modulus E_c follows a Lognormal distribution, too (*Table 6.2*). The value of the COV is taken from Atadero and Karbhari [3].

Mean value μ [MPa]	22750,00
Coefficient of variation COV	0,10
Standard deviation σ [MPa]	2275
Mean value λ [lnMPa]	10,03
Standard deviation ξ [lnMPa]	0,10

Table 6.2. Main statistical properties of the concrete elastic modulus E_c.

The mean value $E_{cm} = 22750$ MPa corresponds to the value of the secant modulus, when the compressive strains in the concrete are equal to 0,00075. In this case, the linearization is made by considering a parabolic stress-strain relation, which ends when the concrete stress is equal to the mean one ($f_c = 28$ MPa). For a better understanding, the secant modulus is represented in *Figure 6.2 Figure 6.3*, instead, represents the probability density function of the concrete elastic modulus.

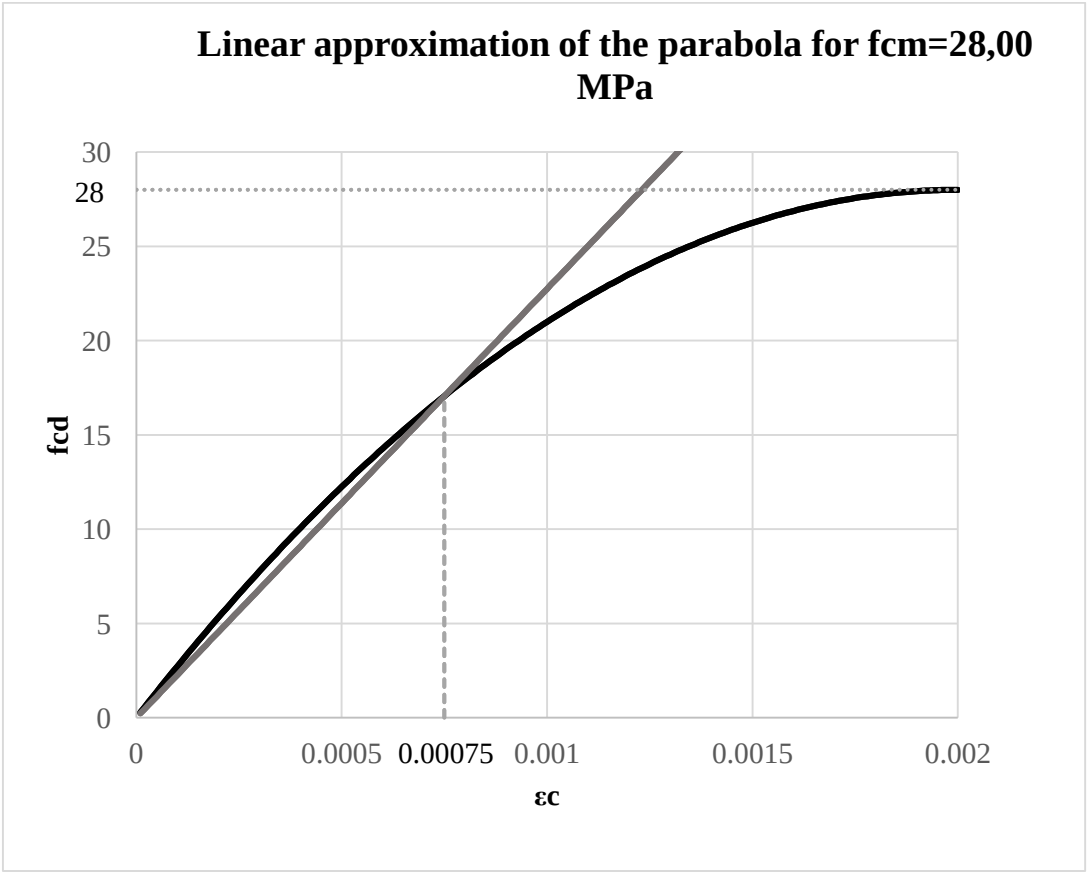

Figure 6.2. Linear approximation of the parabola stress-strain relation of the NTC08 for fcm=28 MPa.

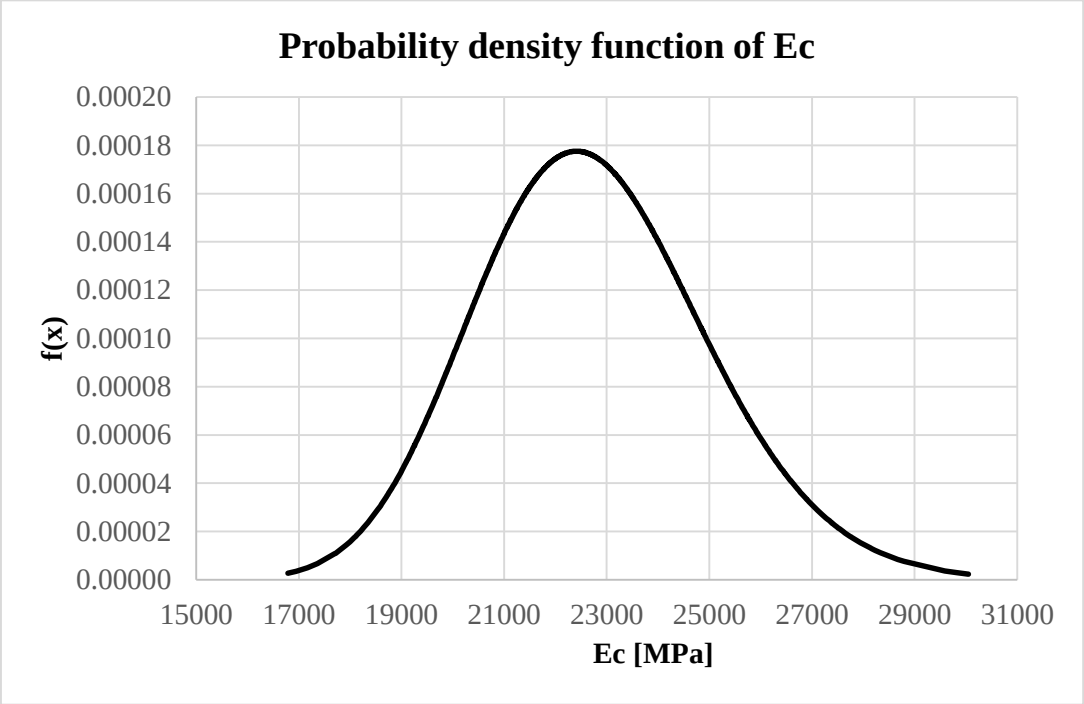

Figure 6.3. Probability density function of Ec.

6.2.2 Composite/Fiber elastic modulus and ultimate tensile resistance

a) The elastic modulus of the composite/fiber follows a Lognormal distribution. Bias and COV were taken from Ceci et al [12] (*Table 6.3*).

Statistical data	Precured	Wet-lay up
Characteristic value E_{frp} / E_f[MPa]	160000,00	230000,00
Bias λ	1,05	1,05
Coefficient of variation COV	0,09	0,15
Mean value μ_x [MPa]	168000,00	241500,00
Standard deviation σ_x [MPa]	15120,00	21735,00
Mean value λ [lnMPa]	12,03	12,39
Standard deviation ξ [lnMPa]	0,09	0,09

Table 6.3. Main statistical properties of the composite/fiber elastic modulus E_{frp}/E_f.

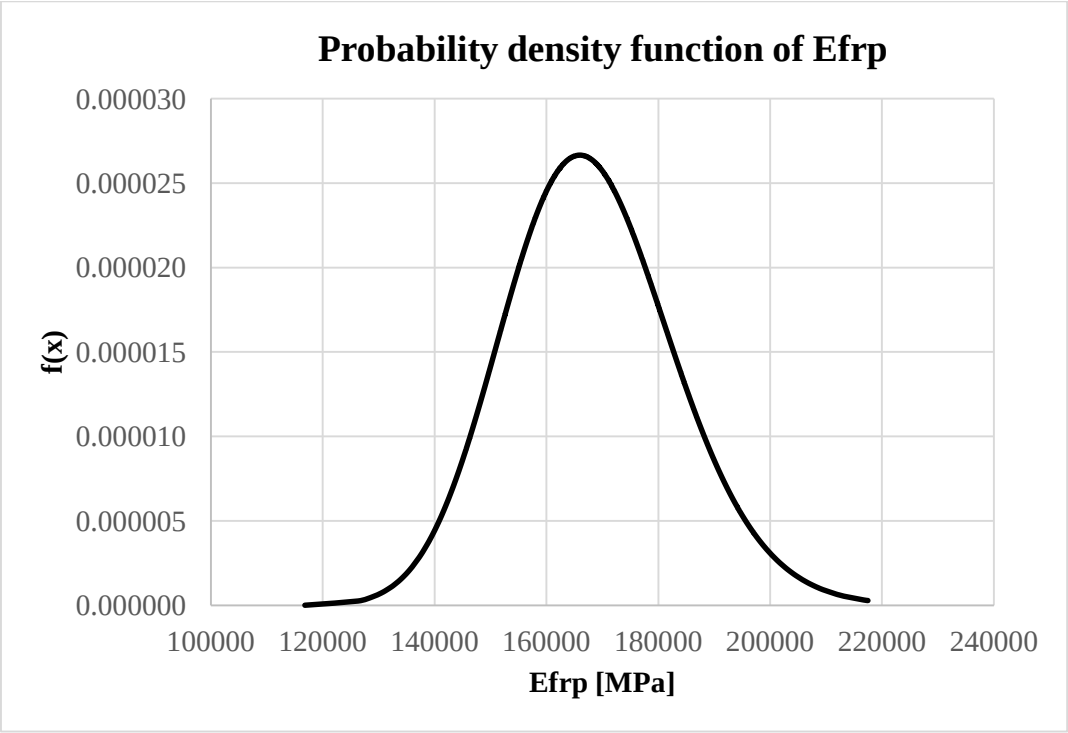

Figure 6.4. Probability density function of E_{frp}.

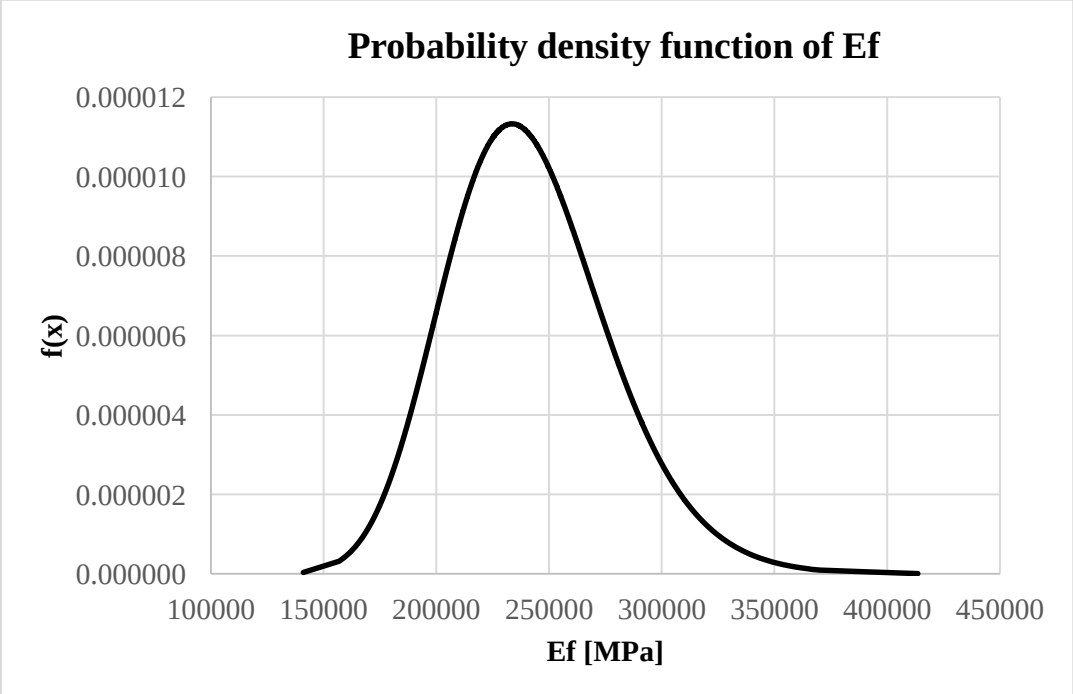

Figure 6.5. Probability density function of E_f.

A different coefficient of variation is taken for the composite and the fiber. Indeed, with a wet-lay up or field-manufactured application more uncertainties are introduced. They are related to the difficulty in combining the components of the resin in proper ratios, in controlling the quantity of resin within the composite. It is also more difficult to get a right alignment of the fibers and many times the environmental conditions have more effects on the reaching of the highest properties of the system. Bias and COV are taken from Atadero and Karbhari [21]. It can be seen from *Figure 6.4 and 6.5* that because of the lower COV, the probability density function of E for the precured system has a more symmetric shape than that for the wet-lay up system.

b) The ultimate tensile strength of the composite/fiber follows a Lognormal distribution (*Figure 6.6-6.7*) and its bias and COV are taken from Atadero et al. [21].
In reality, only the properties of wet-lay up systems are studied in the mentioned source. It is decided to take the lowest COV obtained in [21] for wet-lay up systems as the COV for the precured system (*Table 6.4*). Generally the COV for the precured systems is even lower than that adopted, but it is wanted to consider eventual uncertainties due to an inadequate control during the application phase.

Statistical data	**Precured**	**Wet-lay up**
Characteristic value σ_{frp} / σ_f[MPa]	2560,00	3680,00
Bias λ	1,10	1,10
Coefficient of variation COV	0,09	0,15
Mean value μ_x [MPa]	2816,00	4048,00
Standard deviation σ_x [MPa]	253,44	364,32
Mean value λ [lnMPa]	7,94	8,30
Standard deviation ξ [lnMPa]	0,09	0,09

Table 6.4. Main statistical properties of the composite/fiber ultimate tensile stress σ_{frp}/σ_f.

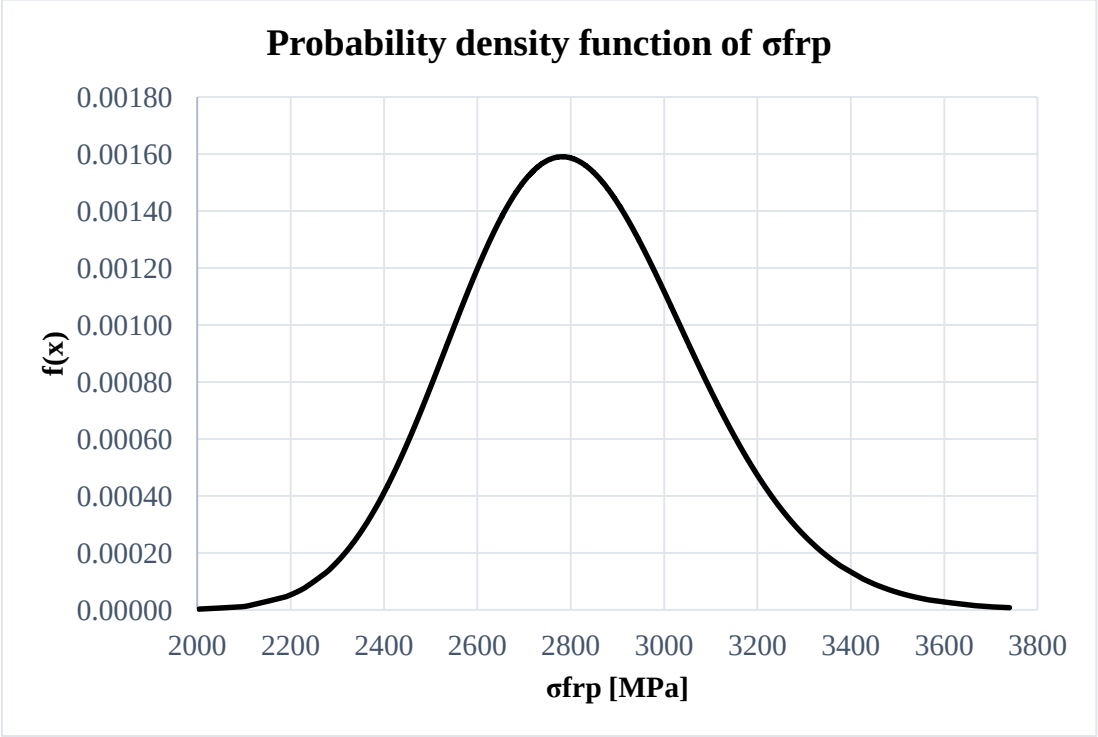

Figure 6.6. Probability density function of σ_{frp}.

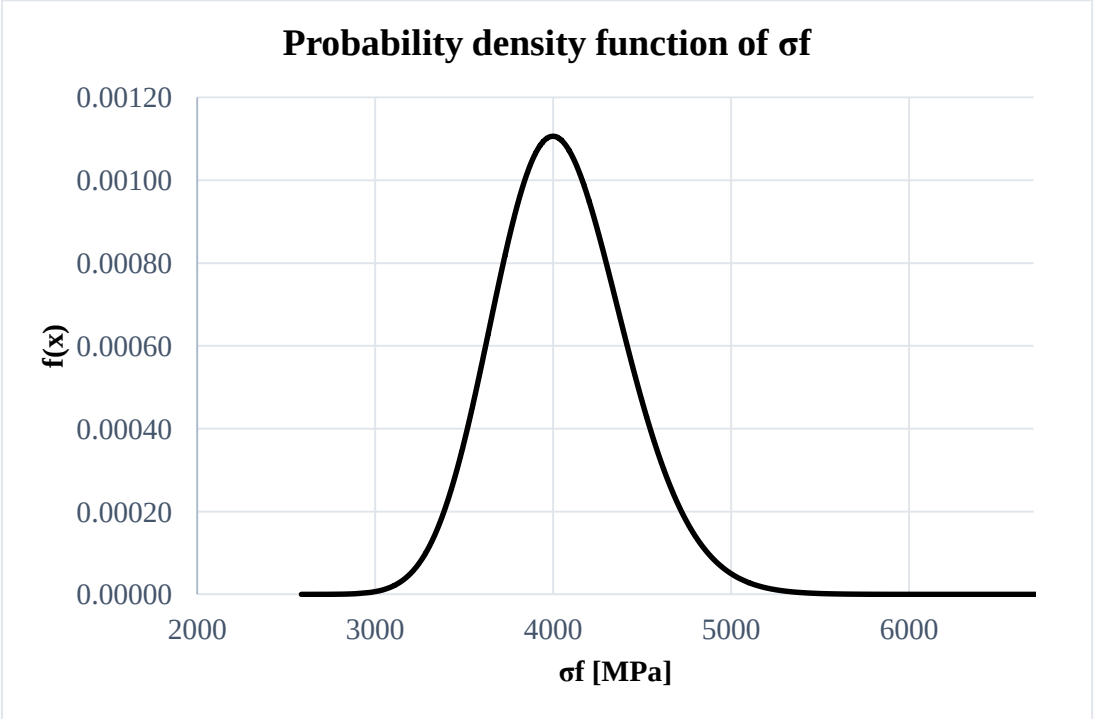

Figure 6.7. Probability density function of σ_f.

6.3.3 Steel yielding resistance

The yielding resistance f_y follows a Lognormal distribution (*Table 6.5*, *Figure 6.8*).

Characteristic value f_{yk}[MPa]	216,00
Bias λ	1,20
Coefficient of variation COV	0,08
Mean value μ_x [MPa]	259,20
Standard deviation σ_x [MPa]	20,70
Mean value λ [lnMPa]	5,55
Standard deviation ξ [lnMPa]	0,08

Table 6.5. Main statistical properties of the yielding tensile stress f_y.

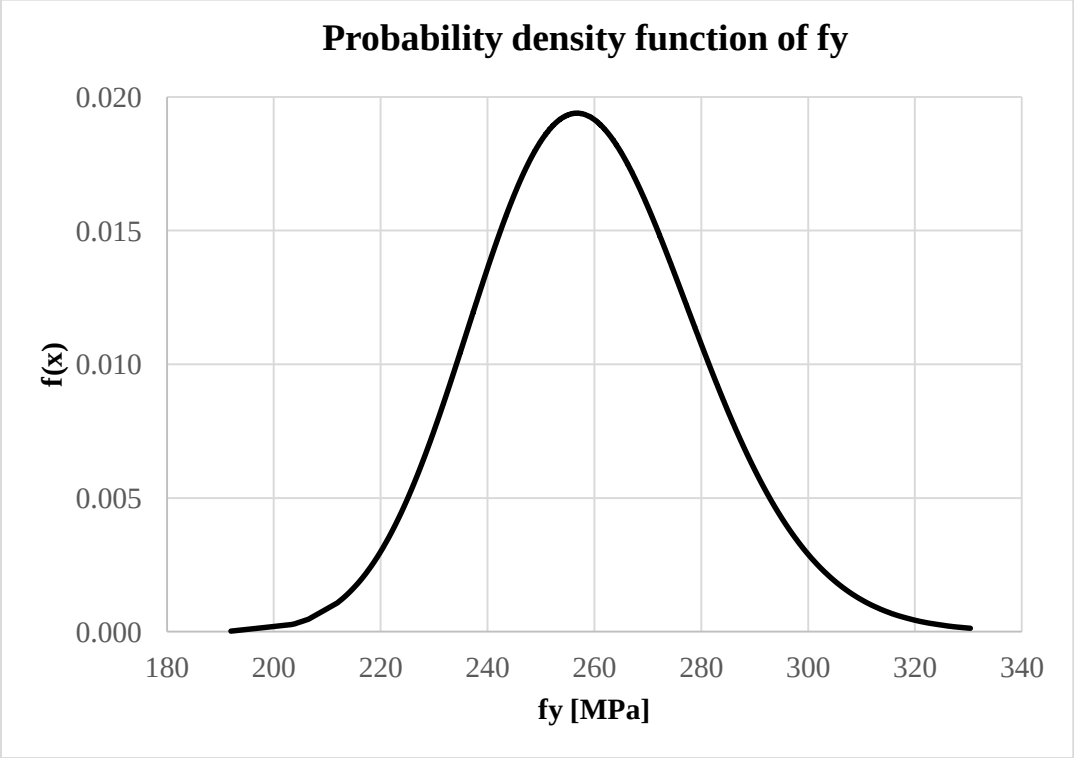

Figure 6.8. Probability density function of fy.

6.3 Statistical properties of the load variables

6.3.1 Dead Load

Dead loads result from the self-weights of the materials and from permanent installations, hence they do not vary significantly through the life of the structure. Dead loads can generally be closely approximated by a Normal distribution (*Table 6.6*). The mean is typically almost equal to the nominal load; in this case a bias λ=1,05 is taken, according to Ellingwood et al. [17]. The coefficient of variation generally assumes a value between 0,05-0,10 [30]. It is chosen a value of COV=0.08.

Since in girder bridges the strengthening with carbon fibers is calculated focusing on the single beam, dead loads are those acting on the beam. For slab bridges, instead, the dead load is that acting on the whole bridge.

For illustrative, the probability density function of the dead load acting on B10RC is represented in *Figure 6.9*.

The equation, which describes the probability density function, is:

$$f(x) = \frac{1}{\sqrt{2\pi}\sigma_x} e^{\left[-\frac{1}{2}\left(\frac{x-\mu_x}{\sigma_x}\right)^2\right]} \qquad -\infty \leq x \leq \infty \tag{6.8}$$

Girder bridges	**B10RC**	**B12RC**	**B16RC**	**B20RC**
Characteristic value M_{dlk}[KNm]	232,88	365,40	761,60	1365,00
Bias λ	1,05	1,05	1,05	1,05
Coefficient of variation COV	0,08	0,08	0,08	0,08
Mean value μ_x [KNm]	244,26	383,67	799,68	1433,25
Standard deviation σ_x [KNm]	19,56	30,96	63,97	114,66

Slab bridges	**S10RC**	**S1015RC**	**S1520RC**
Characteristic value M_{dlk}[KNm]	3384,38	3788,00	4150,00
Bias λ	1,05	1,05	1,05
Coefficient of variation COV	0,08	0,08	0,08
Mean value μ_x [KNm]	3553,59	3977,40	4357,50
Standard deviation σ_x [KNm]	284,29	318,19	348,60

Table 6.6. Statistical properties of the dead load acting on the bridges.

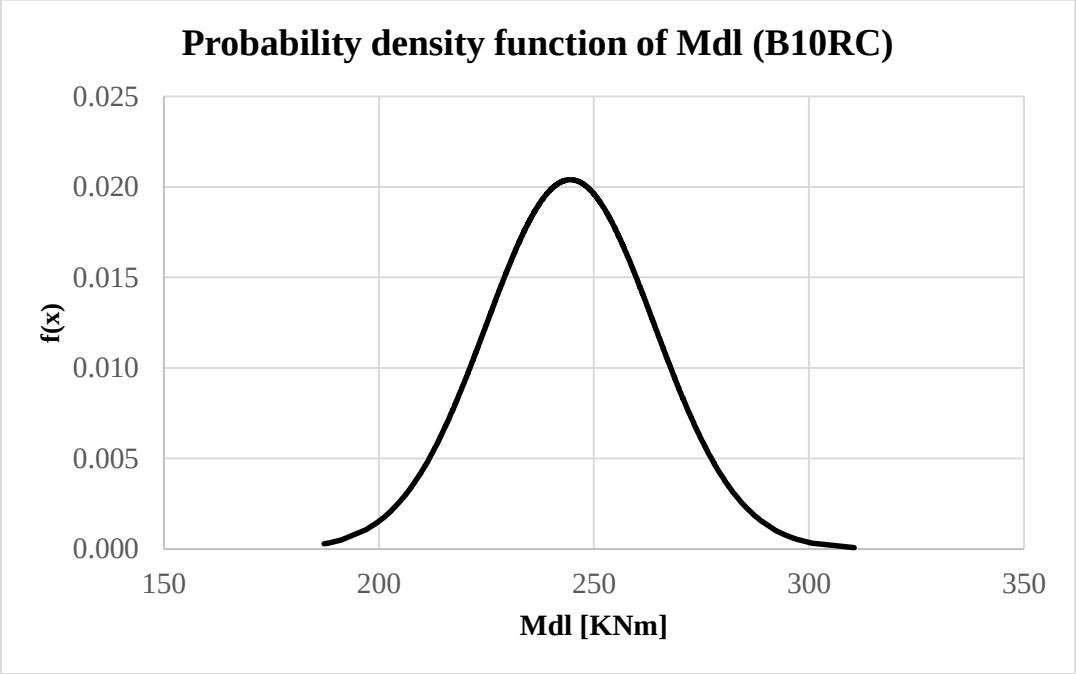

Figure 6.9. Probability density function of Mdl for B10RC.

6.3.2 Live loads

For traffic loads the important random variable is the magnitude of the largest extreme load that occurs during a specified reference period for which the probability of failure is calculated. For the analyzed bridges the reference period is of 50 years and the largest extreme follows one of the asymptotic extreme value distributions (Gumbel, Frechet). A Gumbel distribution is chosen.

The Gumbel distribution is also called Extreme value distribution type I and its cumulative distribution function is expressed by the following formula:

$$F_Y(x) = e^{[-e^{-\alpha(x-u)}]} \qquad -\infty < x < \infty \tag{6.10}$$

The parameters of the distribution are the mode u and α, which is the measure of the dispersion. They are related to the mean value μ_x and to the standard deviation σ_x by the equations:

$$u = \mu_x - \frac{\Upsilon}{\alpha} \tag{6.11}$$

where $\Upsilon = 0{,}5772156649$ ... is the Euler's constant.

$$\alpha = \frac{\pi}{\sqrt{6}\sigma_x} \tag{6.12}$$

In this case, only the nominal value M_{llk} and the COV are known, so that the calculation of the mean value and standard deviation is a little more complex.

Indeed, the nominal value is that calculated according to the Eurocode (M_{llk}), which corresponds to the 95% fractile for a 50 years reference period (return period of 1000 years). The COV is taken equal to 0,20, according to [10]. The high value of the COV takes into consideration the traffic variability, which depends on the type of studied road (e.g. a second class road, a local road, etc.), together with eventual amplifications of the loads and the girder distribution. Once the COV is known, the value of the bias can be extrapolated from the equation of the cumulative probability Gumbel distribution:

$$F_Y(x) = 0{,}95 = e^{[-e^{-\alpha(x-u)}]} = e^{\left[-e^{-\frac{\pi}{\sqrt{6}(0{,}2)\mu_x}\left(Mllk-(\mu_x-\frac{\gamma}{\pi}(\sqrt{6}(0{,}2)\mu_x)\right)}\right]} \qquad -\infty < x < \infty \tag{6.13}$$

The obtained value is λ=0,723. However, in order to take into account an increase in the traffic loads over the years, the bias value is taken equal to 0,9.

Now, it is easy to determine $\sigma_x = 0{,}2\mu_x = 0{,}2(0{,}9M_{llk})$ and eventually u and α (*Tables 6.7-6.8*).

Girder bridges	**B10RC**	**B12RC**	**B16RC**	**B20RC**
Characteristic value M_{llk}[KNm]	456,00	578,63	845,00	1140,63
Coefficient of variation COV	0,20	0,20	0,20	0,20
Mean value μ_x [KNm]	410,40	520,77	760,50	1026,57
Standard deviation σ_x [KNm]	97,54	104,15	152,10	205,31
Mode u [KNm]	366,50	473,90	692,05	934,17
Dispersion α [1/KNm]	0,013	0,012	0,008	0,006

Table 6.7. Statistical properties of the live load acting on girder bridges.

Slab bridges	S10RC	S1015RC	S1520RC
Characteristic value M_{llk}[KNm]	3258,80	3342,00	4953,00
Coefficient of variation COV	0,20	0,20	0,20
Mean value μ_x [KNm]	2932,20	3007,80	4457,70
Standard deviation σ_x [KNm]	586,44	601,56	891,54
Mode u [KNm]	2668,28	2737,07	4056,47
Dispersion α [1/KNm]	0,002	0,002	0,001

Table 6.8. Statistical properties of the live load acting on girder and slab bridges.

For illustrative, the probability density function of the live traffic load acting on B10RC is represented (*Figure 6.10*).

The equation is:

$$f_Y(x) = \alpha e^{[-\alpha(x-u)-e^{-\alpha(x-u)}]} \qquad -\infty < x < \infty \tag{6.14}$$

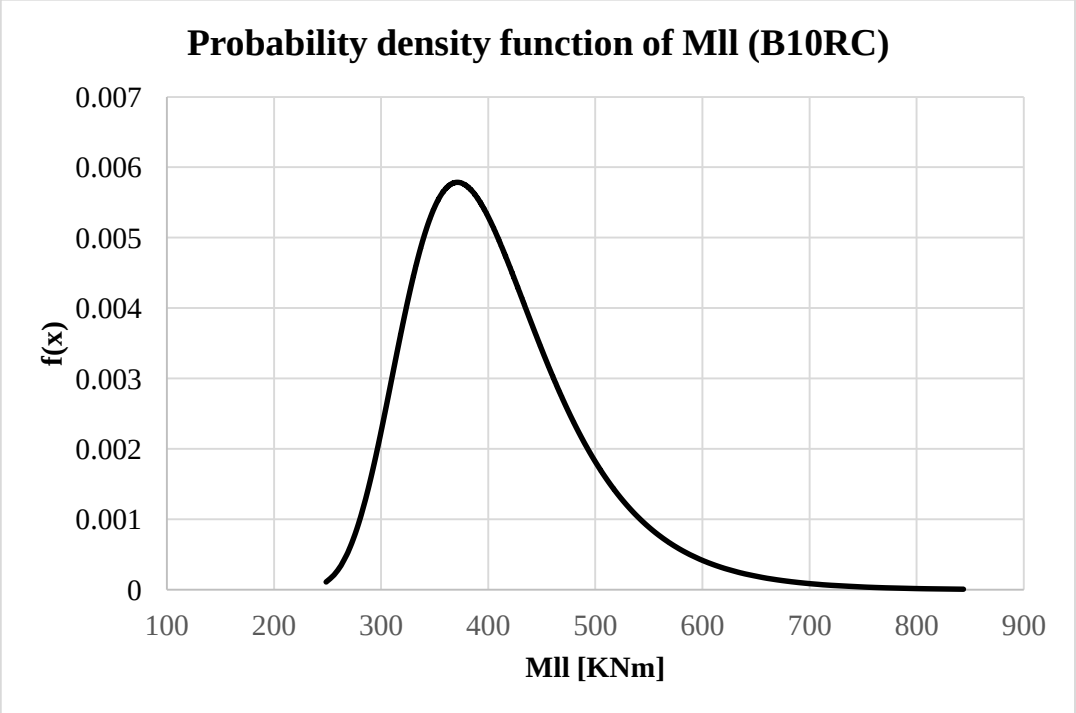

Figure 6.10. Probability density function of Mll for B10RC.

6.4 Implementation of the Monte Carlo

6.4.1 Setting of the problem

The Monte Carlo simulation is now performed. All the variables taking part into the simulation are known and it is necessary to generate from them a series of random variates, which simulates a certain number of fictitious trials. Since the principal parameters of each distribution are known, a random value of each variable defined in the previous sections can be generated artificially (§ 6.3 , 6.4).

Indeed, it is possible to reproduce fictitious values assumed by the cumulative distribution function of each variable through the function CASUAL of Excel, which allows to simulate uniformly distributed numbers between 0 and 1.

Next step is to calculate the value of the random variate by using an inverse cumulative distribution function (*inverse transform* method). This is done automatically by Excel for some distributions, such as the Normal and Lognormal, once the principal parameters are introduced as input (mean and standard deviation).For the Gumbel distribution, the inverse function is obtained by hand and it assumes the final form:

$$x = \frac{(\alpha u - \ln(-\ln(F_Y(x))))}{\alpha} \qquad 0 \leq F_Y(x) \leq 1 \qquad (6.15)$$

where $F_Y(x)$ is the cumulative distribution function.

Having all these input, it is possible now to set the equilibrium equations and both the neutral axis and the resistant moment are calculated.

Once calculated the resistant moment M_r the limit state function is written as:

$$G = M_r - M_{dl} - M_{ll} \qquad (6.16)$$

with M_{dl} is the acting moment due to dead loads and M_{ll} is the acting moment due to live loads.

If the limit state function is bigger than zero, then the structure is in the safe domain ($G \geq 0$), otherwise it is in the unsafe domain ($G < 0$). In order to count how many times a failure occurs, the Excel IF FUNCTION is used.

This function will assume a value equal to 1 if $G < 0$, 0 if $G \geq 0$.

Eventually all the failures are summed, so that the probability of failure can be easily calculated:

$$P_f = \frac{n}{N}$$

where n is the number of failures and N the number of trials.

Once P_f is known, it is possible to calculate the reliability factor β, assuming that, thanks to the central limit theorem, the function G has a normal distribution.

$$P_f = \Phi(-\beta)$$

6.4.2 Target reliability

The target reliability factor has to be set. It has be seen that its value is related to multiple aspects and that it assumes different values for structures to be designed and structures which already exist. For the strengthening of the studied bridges, it is not possible to refer to the Eurocode 0 [5] to fix the target reliability factor, because the Eurocode 0, as already explained, is thought for structure design and not for strengthening of existing constructions.

According to *Table 5.1* (Chapter 5), the target reliability factor is chosen. The table refers to a one year reference period though, whereas in this work a 50 years reference period is to be considered. It means that the target values of β are lower than those proposed in *Table 5.1*. As suggested in [16], the transition from a 1 year reference period to a 50 years reference period implies a decrease of the reliability factor approximately of 0,7.

So placing the studied bridges in a class that can be the Moderate or Large Consequences of Failure Class and assuming a Normal Relative Cost of Safety Measure, the target β can be set between 3,5-4. The Monte Carlo simulation will be conducted for both the extreme values of this interval.

6.4.3 Initial reliability

The first step consists in calculating the reliability factor $\beta$of the existing bridges, without considering any composite strengthening. It can be seen from *Table 6.9* that the initial

reliability is low and distant from the target value for all bridges, with the exception of B20RC, which has an initial β very close to the target value $\beta = 3{,}5$.

Bridge	**β value**
B10RC	2,680
B12RC	2,880
B16RC	3,209
B20RC	3,482
S10RC	2,514
S1015RC	2,420
S1520RC	2,756

Table 6.9. Initial values of the reliability index.

For the calibration, the β factor is obtained by implementing a Visual Basic file and performing a Monte Carlo simulation for 3,000,000 of trials. This number of trials was decided after some attempts, made to evaluate the variability of β across the number of fictitious tests, for the same t_{frp}/t_f. When the bridge is not strengthened yet, anyway, the reliability index tends to the target value after a much lower number of iterations, estimated to be around 150,000. For illustrative, the trend of the initial reliability factor for B10RC is showed in *Figure 6.11*; in *Figure 6.12* the trend of the difference between $\beta_i = \beta$ and $\beta_{i-1} = \beta_p$ (with i=number of trial) is represented.

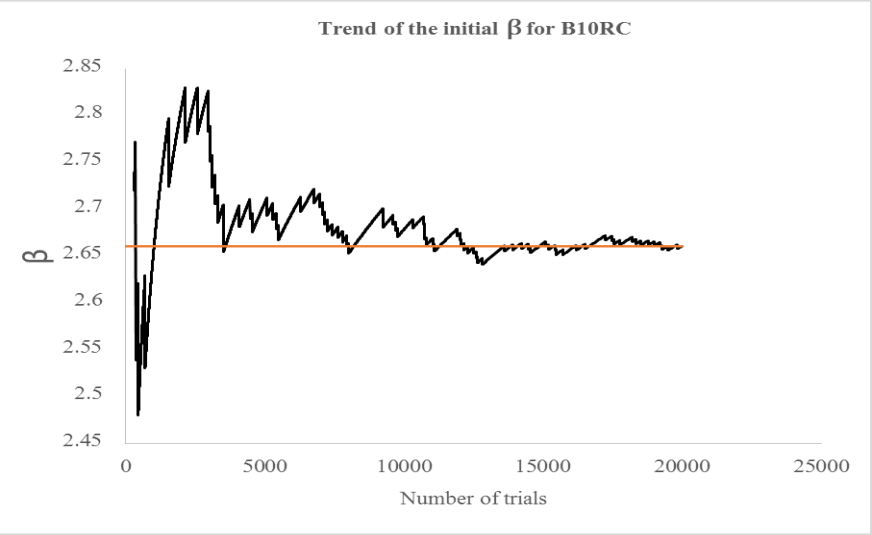

Figure 6.11. Trend of the initial reliability index for bridge B10RC.

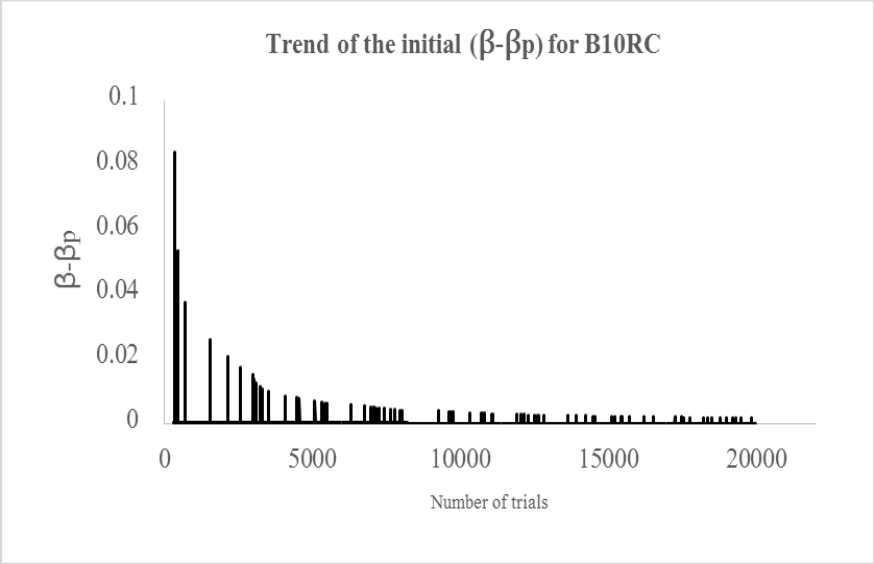

Figure 6.12. Trend of the scatter between $\beta_i = \beta$ and $\beta_{i-1} = \beta_p$.

A flow chart summarizing the procedure is represented in *Figure 6.13* :

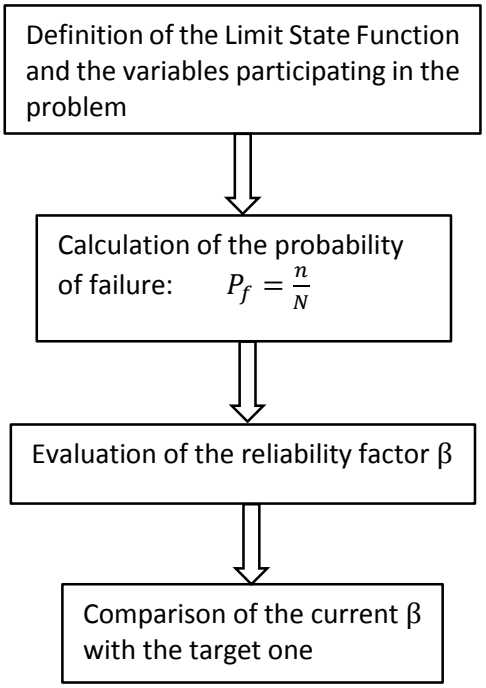

Figure 6.13. Summary of the procedure to obtain the initial reliability.

Chapter 7
Calibration of the safety factors

7.1 Introduction to the model error

The general procedure followed in order to develop the simulation of Monte Carlo has been explained. However, to calibrate a safety factor for Casas and Pascual's intermediate crack-induced debonding model and the other models, first of all, it is necessary to introduce another random variable which has to be inserted in the limit state equation, that is the *model error random variable* Φ. This variable derives from experimental data and indicates the reliability of the adopted resistance model. For Casas and Pascual, its value is taken from Ceci et al.'s [12] work, where the bias and the COV of the random variable are calculated. Together with the Casas and Pascual, other two models are analyzed and then compared with the first one: CNR DT200 R1/2013 model and Said and Wu's model. Of the latters, the statistical definition of Φ is available only for Said and Wu [29], because no specific tests were conducted (or at least they are not published and available) to verify the accuracy of the CNR DT200 R1/2013 model in statistical terms.

7.1.1 Evaluation of the model error

The model variability factor can be obtained by means of three typologies of tests (*Figure 7.1*):

- Single shear tests;
- Double shear tests;
- Beam tests.

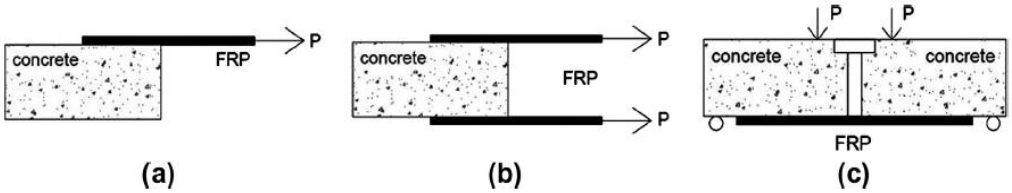

Figure 7.1 Test set-ups for the evaluation of the FRP concrete-bond strength: (a) single shear test, (b) double shear test, (c) bend test. [15]

Different test set-ups can significantly change the experimental results, but at present there is not a defined standard procedure to follow.

Single shear test consists in pulling the FRP sheet or plate and simultaneously pushing the concrete block strengthened with the composite. Double shear test is similar to the previous, but two FRP sheets or plates are bonded to the pushed concrete block. These tests are useful to determine the maximum plate-end debonding force that can be handled by the concrete-composite system.

Bend tests can instead be performed for both plate-end and intermediate debonding. The composite is bonded to the soffit of the beam, subject to a flexure induced by the application of external forces at specific points of the upper face. When these tests are conducted over small-scale specimens, a notch or hinge can be provided in order to initiate the debonding at a specific cross-section.

In Ceci et al. [12], to predict the intermediate crack-induced debonding, the loading configurations adopted in bend tests consisted of:

a) Four-point bending;
b) Three-point bending;
c) One-point bending of cantilevered beams.

The dataset included 187 beams reinforced with FRP, from 38 experimental programs carried out between 1996 and 2007. However, the model error which will be assumed in this work is that resulting from 22 tests, 20 on small-size specimens and 2 on large-size specimens. Indeed, Casas and Pascual contains in its formula the thickness of the matrix, which seldom if ever is known. Over 187 beams, only for 22 this data was available. Therefore, it can be understood already that this suggest the necessity to conduct more experiments to determine a more precise model error.

Said and Wu [29] collected a database of 200 flexural test specimens from the existing literature. All the specimens were strengthened at the bottom with nonprestressed FRP sheets/plates and tested under static loading. The specimens were beams or slabs from small scale to full scale and the load configurations consisted of four-, three- and two-point bending (cantilevers). Different strengthening materials were used for both the experimental programs, such as carbon, glass and aramid FRP. In both cases, the model error can be modeled by a Normal distribution (*Figures 7.2-7.3*).

The value of the model error is estimated by comparing the experimental bond strength predictions with the corresponding analytical results ($P_{exp.}/P_{pred.}$). The strengths are determined by considering the whole resisting system *concrete-steel-composite*. The ratio is calculated for each specimen and the obtained values are analyzed statistically. The results obtained for Casas and Pascual and Said and Wu are listed in *Table 7.1*.

Φ	Bias λ	COV	Mean Value	Standard deviation
Casas and Pascual	1,800	0,230	1,800	0,414
Said and Wu	1,000	0,092	1,000	0,092

Table 7.1. Statistical properties of the model error Φ.

It can be seen that the bias and COV are higher for Casas and Pascual's model. The high value of the bias is due to the fact that Casas and Pascual was calibrated on characteristic values (95% fractile), whereas Said and Wu was calibrated on mean values. This should be taken into account when interpreting the values of the partial safety factors derived in each case.

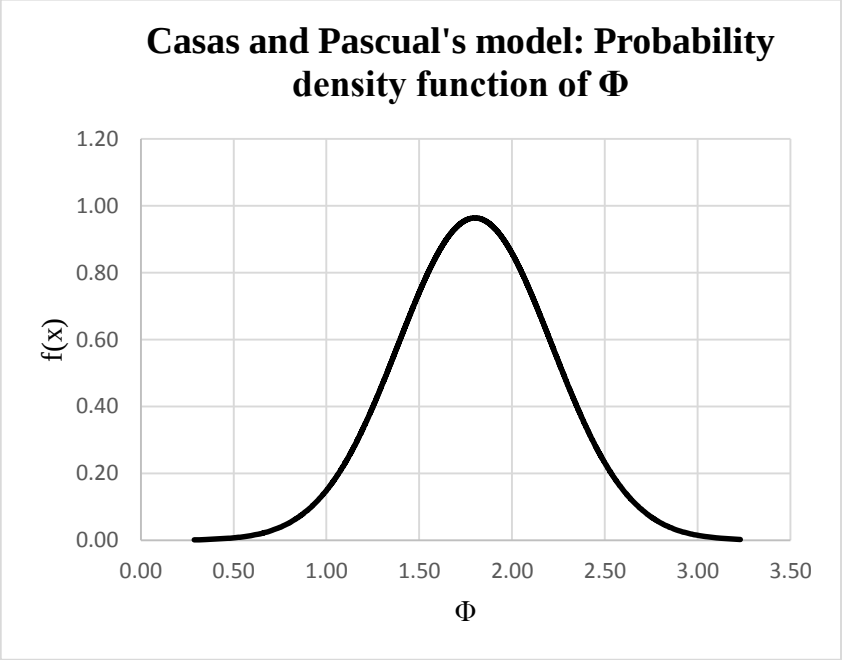

Figure 7.2. Probability density function of Φ for Casas and Pascual's model.

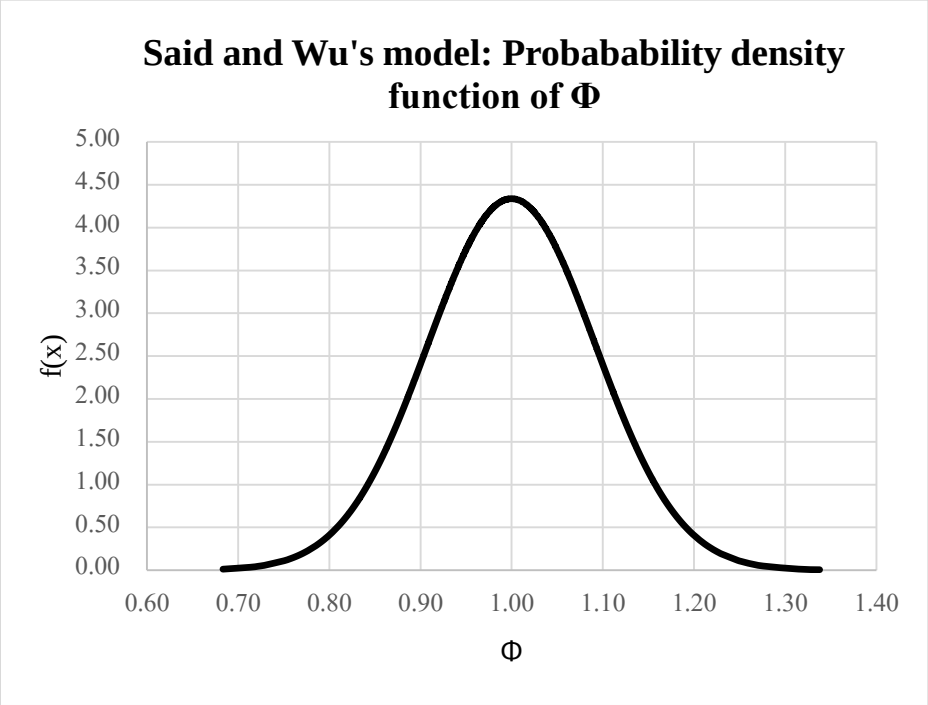

Figure 7.3. Probability density function of Φ for Said and Wu's model.

7.2 Calibration

Due to the lack of some data such as the model error for the Italian Code model, calibration is conducted in three different ways, which diverge one from the other depending on the position of the random variable "model error" in the limit state function, and, therefore, on the position of the safety factor in the corresponding design equation.

The general procedure consists in assuming at first a certain value for the safety factor γ appearing in the design equation. The design leads to a thickness t_{frp}/ t_f which is inserted in the Monte Carlo simulation and gives a specific P_f and β. If the reached β is the target one, then the procedure is stopped and the value of γ is found. Otherwise, the initial γ value is changed and another t_{frp}/t_f, $P_f$and β are located. Again, if the found β is not the target one, the procedure is conduced once more, till the t_{frp}/t_f and γ values which assure the minimum difference between the actual reliability and target reliability are achieved.

The following three cases are analyzed:

a) The model error is not considered, safety factors affect the material properties;

b) The model error affects the composite contribution, safety factors affect only the material properties;
c) The model error and safety factors affect the whole resistant moment M_r.

7.2.1 Method a

This procedure is not the proper one. It is performed in order to get a comparison between Casas and Pascual, Said and Wu and CNR DT200 R1/2013, since for the latter the model error is unknown and therefore it is not possible to compare the three models in the second and third studied cases (b, c).
If none model error is considered, it means that the models are assumed to be exact and the results should confirm what has been already seen in chapter [3], where the maximum debonding strains are compared.
Minding that compressive steel is present only in girder bridges, the governing equations are:

- *Design formula (Resisting moment):*

$$M_{rd} = A_s \frac{f_y}{\gamma_s}(d - \psi x) + A_{s2} \frac{f_s}{\gamma_s}(\psi x - d_2) + A_F \frac{\sigma_F}{\gamma_r} d_1 \tag{7.1}$$

where γ_s is the safety factor for the calculation of the design yielding steel strength, γ_r the safety factor for the composite; ψ is the ratio of the distance of the force resulting from compression in the concrete from the upper edge to the neutral axis x. The other terms have already been defined in chapter 6 (§6.1). The equilibrium equation is calculated around the point of application of the concrete compressive force.

- *Limit state function (Resisting moment):*

$$M_r = A_s f_s (d - \psi x) + A_{s2} f_{s2} (\psi x - d_2) + A_F \sigma_F d_1 \tag{7.2}$$

Where the random variables are f_s, E_F, f_c and E_c; the latter is the concrete elastic modulus, necessary to determine the concrete strength and therefore the neutral axis x. Indeed, as already explained in chapter 6 (§6.2.1), the resistance f_c is simply inserted in the debonding models equation and does not coincide with the effective resistance of the concrete at the compressed edge. The other terms are random variables, which depends on the values of the four main random variables.

The flow chart below (*Figure 7.4*) has the function to illustrate in a simple way the adopted method:

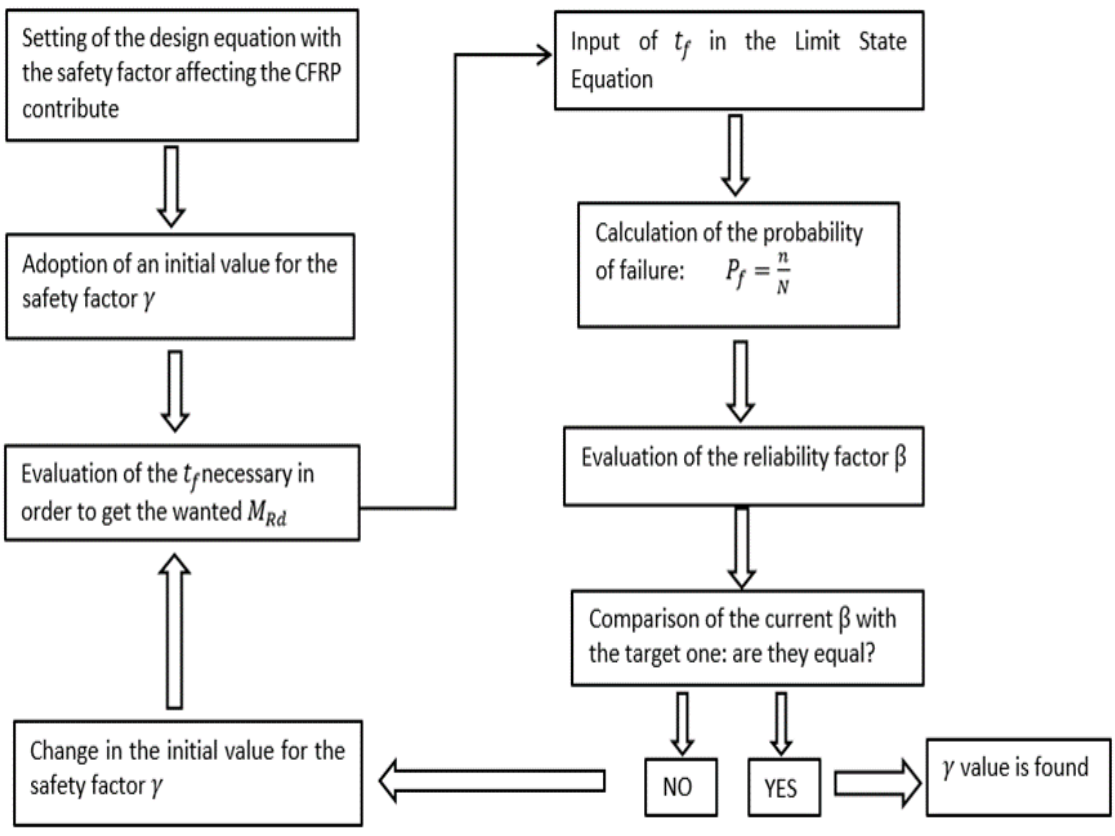

Figure 7.4. Summary of the first analyzed case (a).

Results

- $\beta = 3{,}5$

A) **CNR DT200 R1/2013.**

Bridge	**Precured**		**Wet-lay up**	
	γ_r	t_{frp} (mm)	γ_r	t_f (mm)
B10RC	0,904	1,620	0,908	1,140
B12RC	0,766	1,190	0,770	0,840
B16RC	0,455	0,420	0,453	0,290
B20RC	RUPTURE OF THE COMPOSITE		RUPTURE OF THE FIBER	
S10RC	0,652	0,810	0,665	0,590
S1015RC	0,638	0,640	0,649	0,470
S1520RC	0,671	1,330	0,682	0,960

B) Casas and Pascual's model.

Bridge	**Precured**		**Wet-lay up**	
	γ_r	t_{frp} (mm)	γ_r	t_f (mm)
B10RC	0,836	2,000	0,843	1,430
B12RC	0,720	1,530	0,720	1,050
B16RC	0,438	0,570	0,438	0,390
B20RC	RUPTURE OF THE COMPOSITE		RUPTURE OF THE FIBER	
S10RC	0,602	0,790	0,607	0,560
S1015RC	0,590	0,480	0,592	0,350
S1520RC	0,611	0,690	0,615	0,480

C) Said and Wu's model.

Bridge	**Precured**		**Wet-lay up**	
	γ_r	t_{frp} (mm)	γ_r	t_f (mm)
B10RC	0,845	0,360	0,855	0,260
B12RC	RUPTURE OF THE COMPOSITE		RUPTURE OF THE FIBER	
B16RC	RUPTURE OF THE COMPOSITE		RUPTURE OF THE FIBER	
B20RC	RUPTURE OF THE COMPOSITE		RUPTURE OF THE FIBER	
S10RC	RUPTURE OF THE COMPOSITE		RUPTURE OF THE FIBER	
S1015RC	RUPTURE OF THE COMPOSITE		RUPTURE OF THE FIBER	
S1520RC	RUPTURE OF THE COMPOSITE		RUPTURE OF THE FIBER	

Table 7.2. Results for case (a), target β=3,5.

- $\beta = 4{,}0$

A) CNR DT200 R1/2013

Bridge	Precured		Wet-lay up	
	γ_r	t_{frp} (mm)	γ_r	t_f (mm)
B10RC	1,368	4,530	1,393	3,300
B12RC	1,284	4,230	1,297	3,000
B16RC	1,028	3,020	1,054	2,230
B20RC	0,802	2,130	0,805	1,500
S10RC	0,958	2,120	0,962	1,490
S1015RC	0,940	1,600	0,953	1,120
S1520RC	1,079	4,060	1,086	2,880

B) Casas and Pascual's model.

Bridge	Precured		Wet-lay up	
	γ_r	t_{frp} (mm)	γ_r	t_f (mm)
B10RC	1,298	5,900	1,304	4,150
B12RC	1,196	5,280	1,196	3,650
B16RC	0,984	4,050	0,986	2,820
B20RC	0,775	2,930	0,763	1,950
S10RC	0,872	1,990	0,892	1,470
S1015RC	0,869	1,190	0,880	0,850
S1520RC	0,992	2,180	1,009	1,590

C) Said and Wu's model.

Bridge	Precured		Wet-lay up	
	γ_r	t_{frp} (mm)	γ_r	t_f (mm)
B10RC	1,328	0,790	1,358	0,580
B12RC	1,200	0,720	1,200	0,500
B16RC	0,948	0,570	0,928	0,380
B20RC	RUPTURE OF THE COMPOSITE		RUPTURE OF THE FIBER	
S10RC	0,884	0,440	0,891	0,310
S1015RC	0,870	0,390	0,887	0,290
S1520RC	1,024	0,750	1,044	0,540

Table 7.3. Results for case (a), target β=4..

The observations that will follow have to be taken as comments on fictitious results, since all models are treated here as they were characterized by equal bias and COV; this means

that the values obtained in *Tables 7.2-7.3* do not account for the real error variability of the applied model. Precisely, it is equal to consider the models with λ=1 and a COV= 0 %, as they were exact models. However, an analysis of these first results can be useful for a comparison with the values obtained in the next sections.

It can be seen that what emerged from the diagrams of the debonding strains (Chapter 3) is confirmed. Casas and Pascual turns out again to be the most conservative model for girder bridges, CNR DT200 R1/2013 for slab bridges, while Said and Wu gives smaller thicknesses for the same reliability target, as it emerges from results with β =4. It should be born in mind that Casas and Pascual's model was calibrated for characteristics results (95% percentile), while Said and Wu's model was calibrated at mean values.

It can be noticed that, even if Casas and Pascual's model is basically less conservative than the CNR model for slab bridges, because of the influence of the parameter t_{ce}, differently from what happens in the diagrams of the maximum debonding strains, the found thicknesses are much smaller than what could be expected by simply looking at the graphs.

This outcome can be explained. In fact, minding the equations of the two debonding models, in Casas and Pascual appears the characteristic value of the compressive concrete strength (f_{ck}), whereas in CNR DT R1/2013 the mean value of f_c is taken, together with the mean tensile strength. Therefore, when the Monte Carlo simulation is performed and f_c is considered as a random variable, the value assumed in the debonding formula, considering all the trials, is on the average equal to f_{cm}. This means that the equation for CNR DT200 R1/2013 does not change in the Monte Carlo simulation, while Casas and Pascual's model assumes values of the concrete resistance higher than those counted in its standard equation. The result is an higher admissible debonding strain in the simulation and therefore a lower probability of failure.

As underlined above, anyway, it would be necessary to compare the results by referring also to the error variability factor before drawing any conclusion on the conservatism of each model.

Unfortunately a comparison of Casas and Pascual, CNR DT200 R1/2013 and Said and Wu's model is not possible for a β=3,5. In fact, the low value of the target reliability index

can be satisfied with a small thickness of CFRP, which is less sensitive to the debonding problem.

When the Monte Carlo simulation was performed, for quite thin thicknesses, the ultimate tensile strain of the composite was exceeded a certain number of times over the 3,000,000 trials, because of the variability of the random variable *debonding strain*. When this happened, the trials were considered invalid and excluded from the studied population. Therefore, a higher number of trials was conducted, till the number of valid trials reached the value 3,000,000.

The terms "*rupture of the composite*" and "*rupture of the fiber*" mean that, when designing, the failure occurs because the ultimate limit strength of the composite/fiber is reached (this corresponds in the Monte Carlo simulation to a number of failures for ultimate limit strain that is much higher than that for debonding). It is meaningless going on with the calibration, since the Monte Carlo simulation is thought for a debonding failure mode: there are no more safety factors that need to be calibrated and the probability of failure is that of the rupture of the composite/fiber. This happens for Said and Wu's model more than for the others, since, being the least conservative model, the thickness that assures the wanted reliability index is lower.

From *Tables 7.2-7.3*, it can be noticed that the values obtained for the composite thicknesses from the Monte Carlo simulations vary differently, going from B10RC to B20RC and from S10RC to S1520RC, if compared with those given by the design done according to the CNR. In fact, as seen in chapter 4, the bridge that needs more strengthening, following the design formula of CNR DT200 R1/2013, is B20RC. This suggests that there is not accounting for the initial reliability of the bridges, but not real considerations can be done, since the model variability coefficient has not been taken into account. Results for slab bridges should not mislead, indeed, it has to be remembered that the width of the strengthening varies adapting to the different geometry of the cross-section.

One of the key objectives of reliability based-design is to give a level of reliability that is the most uniform as possible across many different design cases. Looking at the initial reliabilities, it is already possible to understand that the design formula proposed in CNR

DT200 R1/2013 is not well-calibrated, as the higher the initial reliability the higher the calculated t_{frp}/t_f. This would lead to different grades of reliability, depending on the cross-section dimensions of the bridge and acting loads, while a more unvarying value across different situations is desirable. Anyway, it has to be underlined that to speak of initial reliability in this case could be not properly correct, since the initial resisting behavior of the cross-section is radically changed when the strengthening is applied. In fact, if at the beginning there is an exploitation of the concrete compressive strength, when the CFRP is applied, the leading maximum strain becomes that of the composite and the resisting mechanism changes. However, it is clear that, even simply referring to the quantity of tensile steel, the thickness of the strengthening calculated for design follows a trend opposite to what should be expected, since the design formula gives higher thicknesses for bridges that are in safer initial conditions (higher amount of tensile steel).

The three models are compared for the precured system in *Figures 7.5-7.8*, in which the trend of β for the final thickness that assures the target index is represented as a function of the number of trials (β=4). It has been observed that the thicker the CFRP plate/sheet the higher number of iterations necessary to stabilize the reliability index, as it can be deduced from the graphs too. In general, it can be said that the variability and the way the β tends asymptotically to the wanted value depend on the characteristics of each single bridge, such as the material properties, the geometry, initial conditions, and by the model assumed to predict the resistance of the section. So, the behavior of the variability towards the number of trials will not be the same for all the bridges, even if 3,000,000 iterations result to be enough for assuring the target reliability index of each bridge. It has been noted that, except for small variations, the variability of all the applied debonding models can be considered to be of the same order.
Obviously the target value is reached before for prefabricated systems (COV of E_{frp} equal to 0,09) than for wet-lay up systems (COV of E_f equal to 0,15).

The proposed safety factors have to be taken as approximate values, that have been calculated in this section to see how they change later, when the random variable model error is considered. Contrarily to what could be expected, safety factors for Said and Wu's

model are not always the highest ones. This means that the resisting contribution of the composite given by Said and Wu's formula is not always the most reduced as it could be presumed. Indeed, a less conservatism of the model does not correspond necessarily to higher safety factors. In fact, the value of the safety factor is related to the applied resisting model, which affects the results both in the design and the Monte Carlo simulation. When Said and Wu is applied, the Monte Carlo gives lower thicknesses for the same bridge and target β, since the contribution attributed to the composite is higher according to the model formula. This leads to values of the safety factors that are proportioned to the composite thickness required and the resisting model adopted in the design.

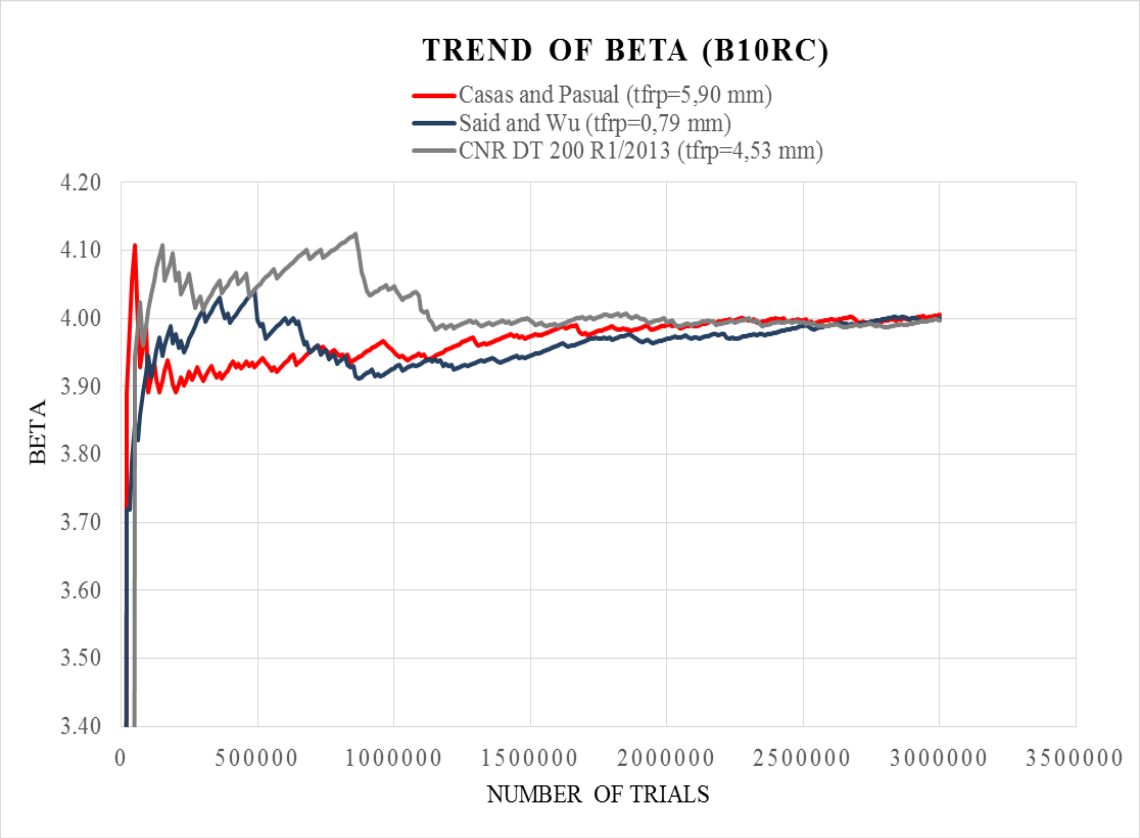

Figure 7.5. Trend of the reliability index over the number of trials for B10RC (precured system).

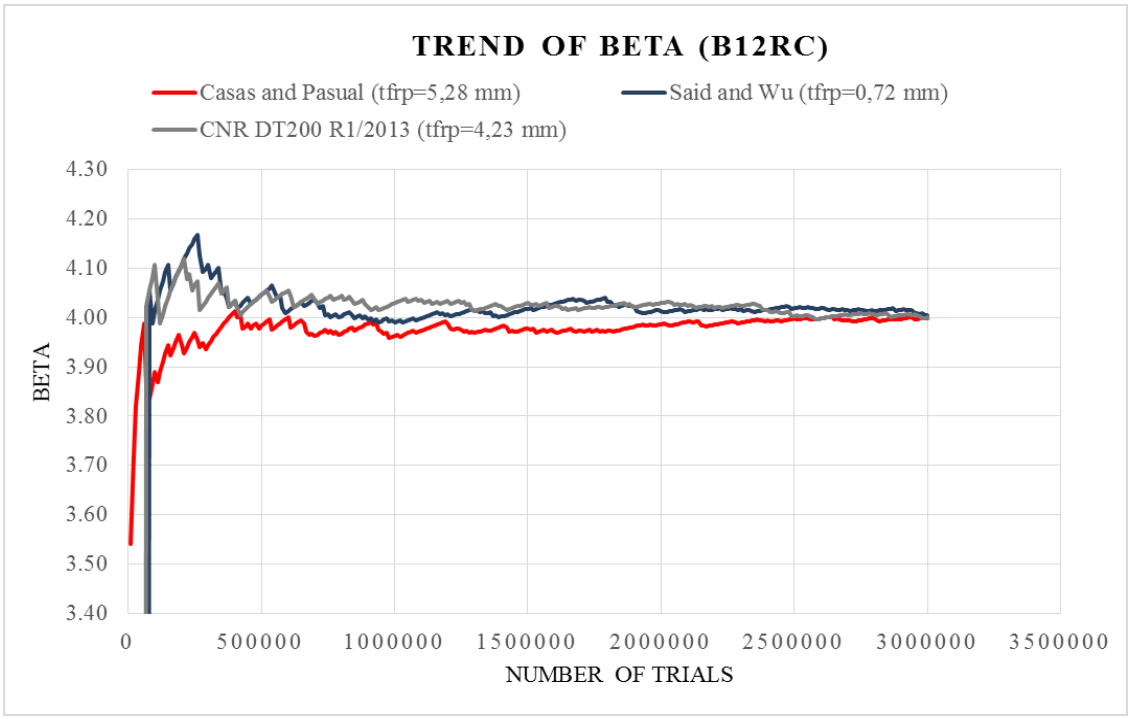

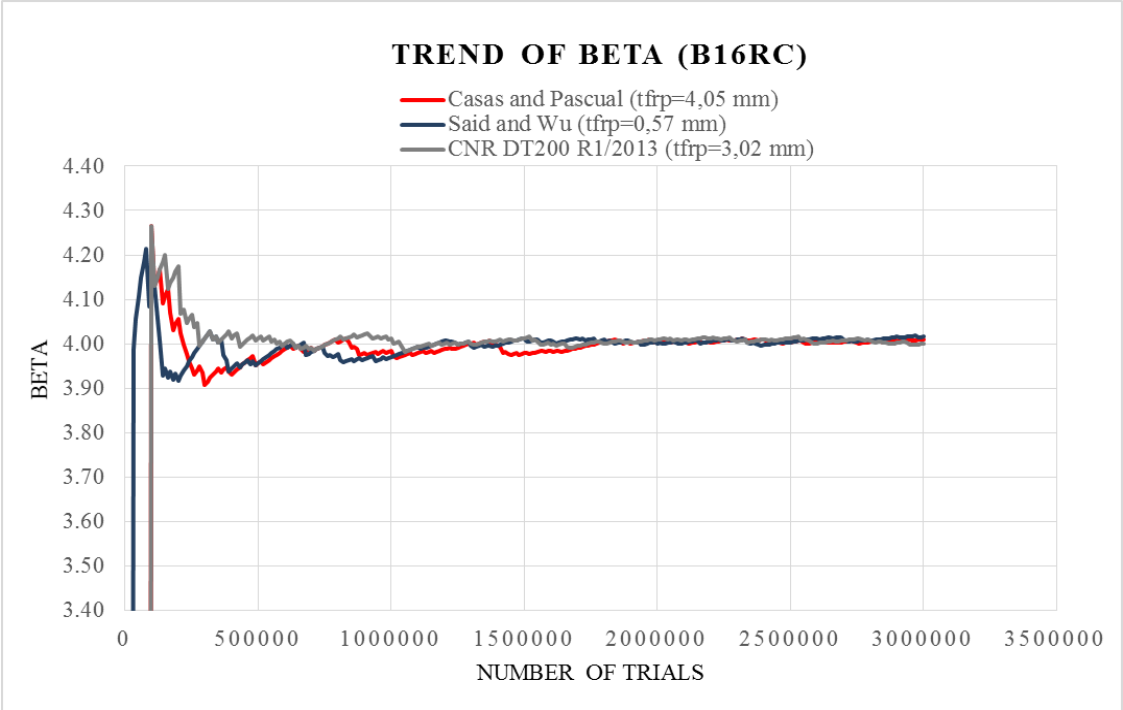

Figure 7.6. Trend of the reliability index over the number of trials for B12RC and B16RC (precured system).

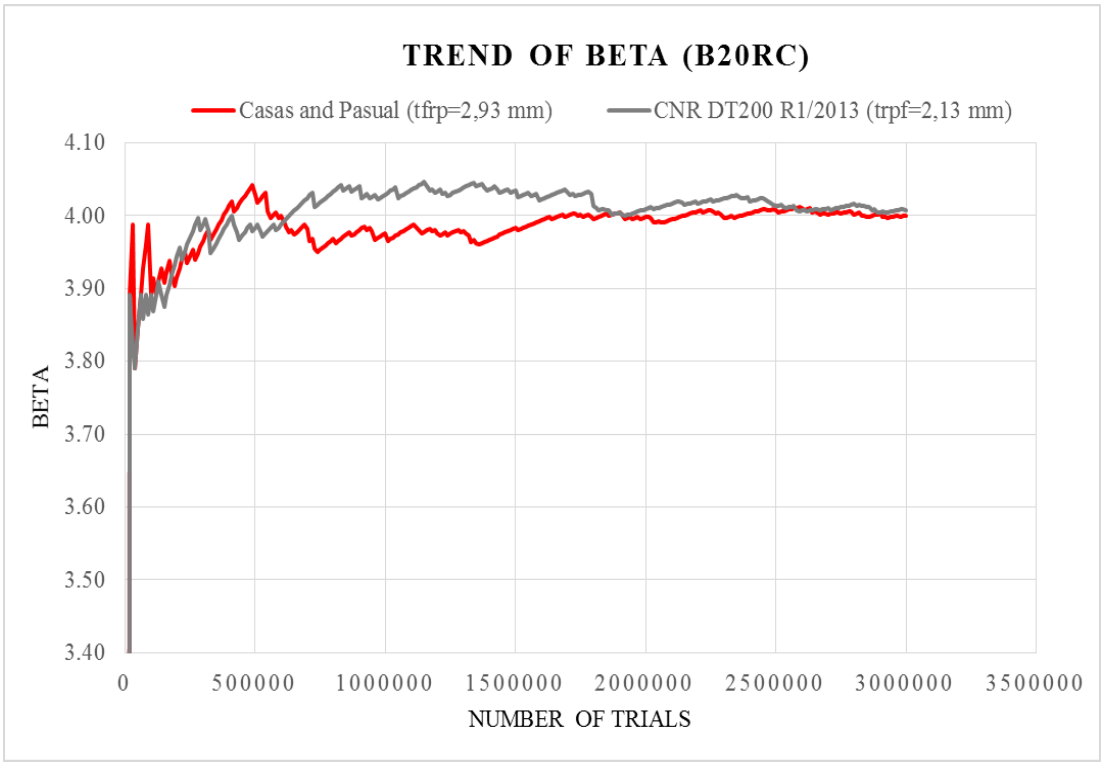

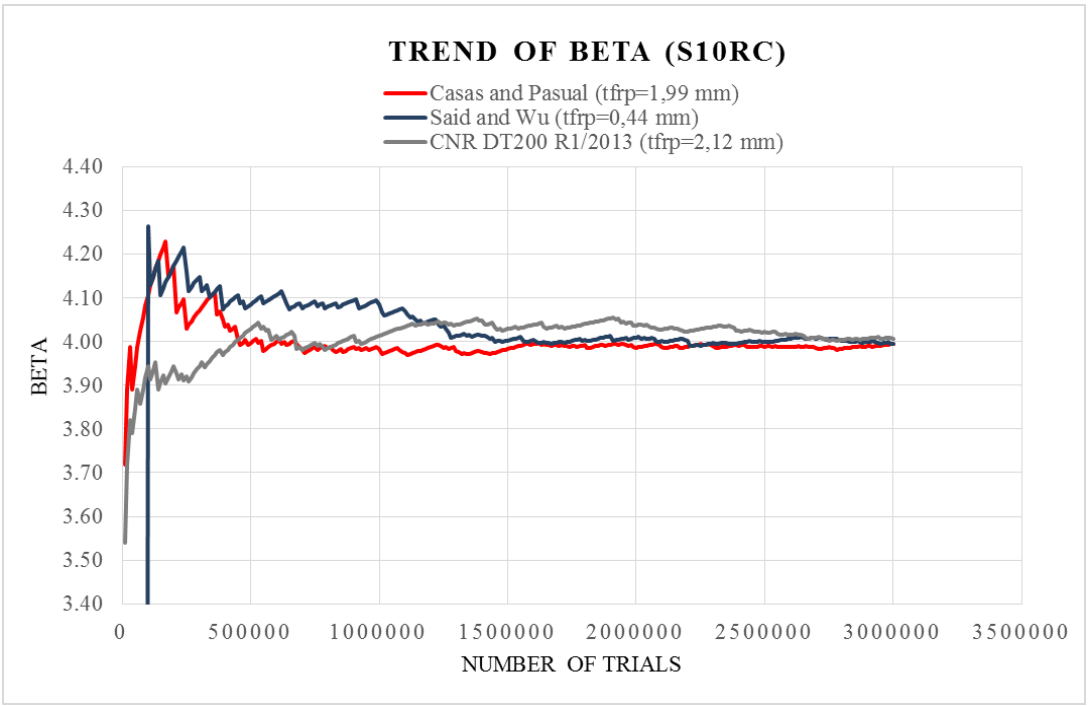

Figure 7.7. Trend of the reliability index over the number of trials for B20RC and S10RC (precured system).

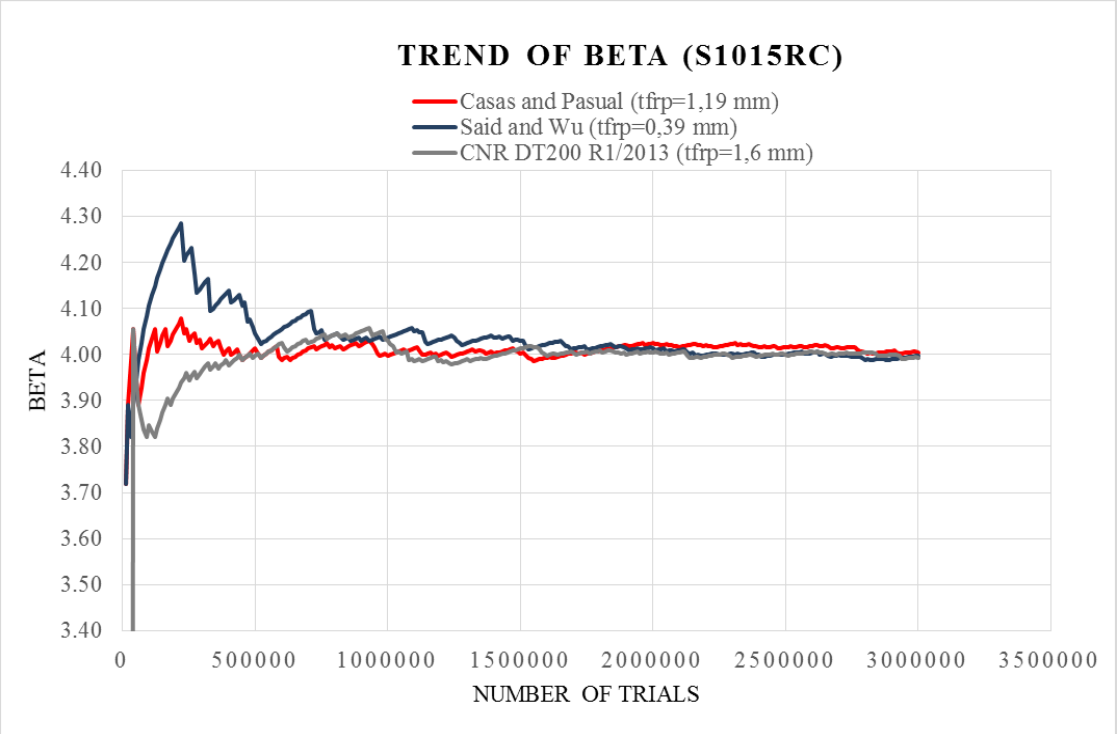

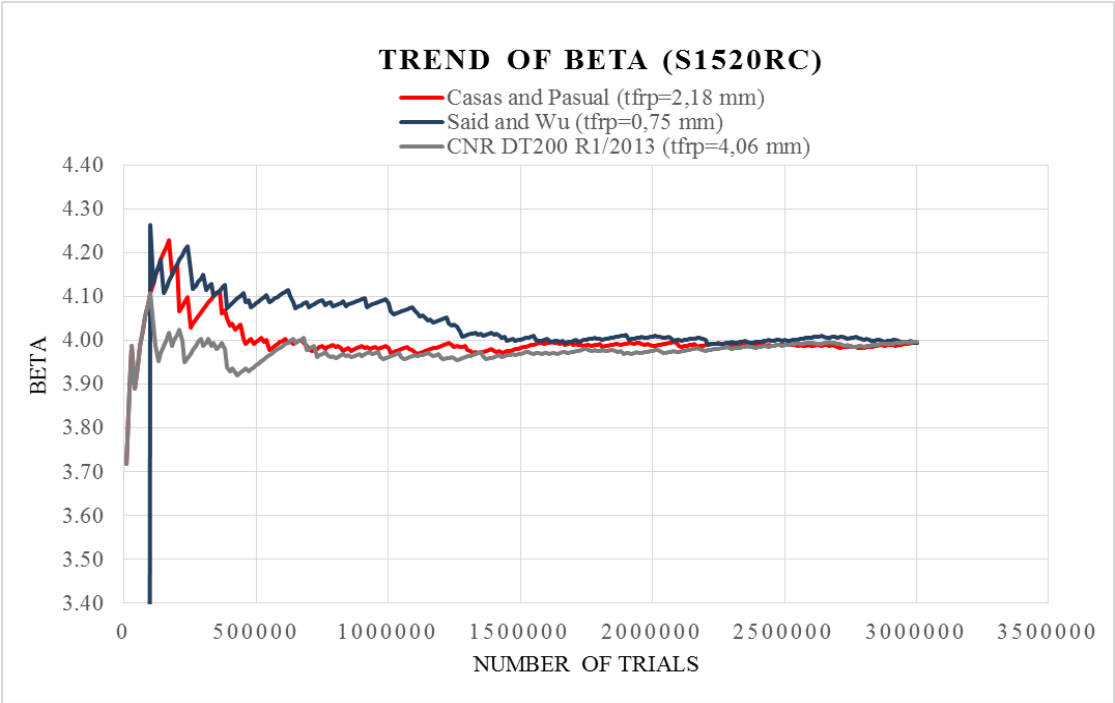

Figure 7.8. Trend of the reliability index over the number of trials for S1015RC and S1520RC (precured system).

It can be seen that the safety factors for prefcured systems are lower than those for wet-lay up systems. This is because wet-lay up systems have an elastic modulus with an higher coefficient of variation (COV=0,15), due to the larger number of uncertainties related to their application in situ.

As it can be seen by comparing the trend of β for B10RC with precured system and wet-lay up system (*Figure 7.9*), the change in the value of the COV does not affect significantly the layout of the reliability index trend, since the two coefficients of variation present close values.

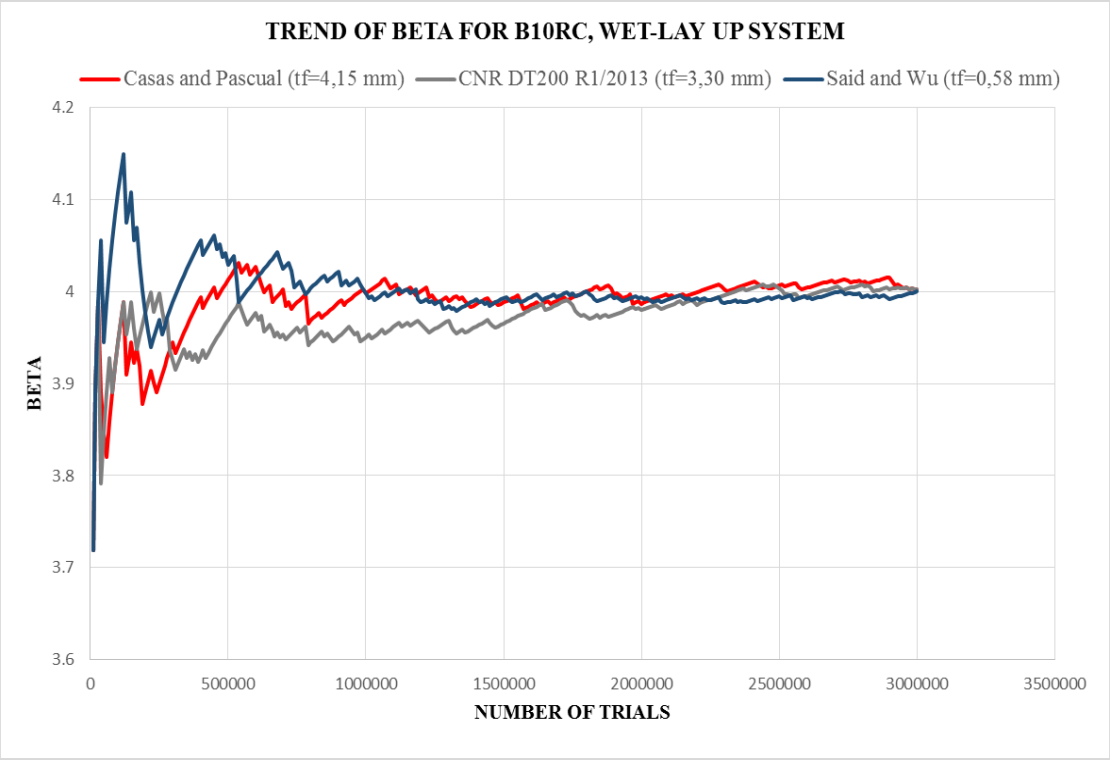

Figure 7.9. Trend of the reliability index over the number of trials for B10RC (wet-lay up system).

7.2.2 Method b

Since the random variable *model error* for the intermediate debonding model of the CNR DT200 R1/2013 is not available, this case is performed only for Casas and Pascual and

Said and Wu. The position of the model error variable adopted in this procedure is still not the correct one. Indeed, it has been explained how this error is determined (*§ 7.1.1*) and it appears clear that the random variable should affect the global resistant moment and not only the composite contribution.
However, it is interesting to notice how the introduction of the model error, even if in the wrong place, makes the results to vary a lot for Casas and Pascual's model.

- *Design formula*

$$M_{rd} = A_s \frac{f_y}{\gamma_s}(d - \varphi x) + A_{s2} \frac{f_s}{\gamma_s}(\varphi x - d_2) + A_F \frac{\sigma_F}{\gamma_r} d_1 \tag{7.3}$$

- *Monte Carlo simulation*

$$\begin{aligned} M_r &= A_s f_s (d - \varphi x) + A_{s2} f_{s2} (\varphi x - d_2) + \Phi A_F \sigma_F d_1 = \\ &= A_s f_s (d - \varphi x) + A_{s2} \varepsilon_{s2} E_s (\varphi x - d_2) + \Phi A_F \varepsilon_F E_F d_1 \end{aligned} \tag{7.4}$$

Where the random variables are f_s, E_F, f_c, E_c and Φ. The other terms are random variables, which depends on the four main random variables.

Results

- β = 3,5

A) Casas and Pascual's model

Bridge	Precured		Wet-lay up	
	γ_r	t_{frp} (mm)	γ_r	t_f (mm)
B10RC	0,524	0,610	0,531	0,440
B12RC	0,426	0,420	0,426	0,280
B16RC	RUPTURE OF THE COMPOSITE		RUPTURE OF THE FIBER	
B20RC	RUPTURE OF THE COMPOSITE		RUPTURE OF THE FIBER	
S10RC	RUPTURE OF THE COMPOSITE		RUPTURE OF THE FIBER	
S1015RC	RUPTURE OF THE COMPOSITE		RUPTURE OF THE FIBER	
S1520RC	RUPTURE OF THE COMPOSITE		RUPTURE OF THE FIBER	

Table 7.4. Results for case (b), Casas and Pascual, target β=3,5.

B) Said and Wu's model.

Bridge	Precured		Wet-lay up	
	γ_r	t_{frp} (mm)	γ_r	t_f (mm)
B10RC	0,865	0,370	0,871	0,260
B12RC	RUPTURE OF THE COMPOSITE		RUPTURE OF FIBER	
B16RC	RUPTURE OF THE COMPOSITE		RUPTURE OF FIBER	
B20RC	RUPTURE OF THE COMPOSITE		RUPTURE OF FIBER	
S10RC	RUPTURE OF THE COMPOSITE		RUPTURE OF FIBER	
S1015RC	RUPTURE OF THE COMPOSITE		RUPTURE OF FIBER	
S1520RC	RUPTURE OF THE COMPOSITE		RUPTURE OF FIBER	

Table 7.5. Results for case (b), Said and Wu, target β=3,5.

- $\beta = 4{,}0$

A) Casas and Pascual's model

Bridge	Precured		Wet-lay up	
	γ_r	t_{frp} (mm)	γ_r	t_f (mm)
B10RC	0,950	2,750	0,950	1,910
B12RC	0,843	2,250	0,852	1,600
B16RC	0,648	1,470	0,648	1,020
B20RC	0,439	0,750	0,449	0,550
S10RC	0,751	1,070	0,753	0,750
S1015RC	0,641	0,580	0,652	0,420
S1520RC	0,689	1,010	0,698	0,660

B) Said and Wu's model

Bridge	Precured		Wet-lay up	
	γ_r	t_{frp} (mm)	γ_r	t_f (mm)
B10RC	1,363	0,830	1,382	0,590
B12RC	1,213	0,730	1,242	0,530
B16RC	0,927	0,540	0,960	0,400
B20RC	RUPTURE OF THE COMPOSITE		RUPTURE OF THE FIBER	
S10RC	0,907	0,460	0,923	0,330
S1015RC	0,883	0,400	0,905	0,290
S1520RC	1,024	0,750	1,066	0,560

Table 7.6. Results for case (b), target β=4.

For a target β=3,5, it is almost impossible to get some values for both models. Indeed, in this case, also Casas and Pascual, due to the high mean of the model error ($\mu_{\Phi} = 1{,}8$), needs lower composite/fiber thicknesses to reach the wanted reliability, thicknesses that are subject to rupture for ultimate tensile stress of the composite before intermediate crack-induced debonding occurs.

The decrease in the needed composite/fiber thickness can be observed from results for β=4,0. It can be understood that, even if the COV for Casas and Pascual has a high value, what influences more the results is the mean of the model error, significantly increased. This happens because the model error is applied only to the composite/fiber term, which gives a small contribution to the resistance if compared to the reinforcing steel. That is why, even if small values of the composite/fiber contribution are relatively often obtained due to the high dispersion of the data (COV=0,23), this does not have a so much significant effect on the reliability of the structure.

The results for Said and Wu' model do not vary much, since the mean of the model error is equal to 1 and the COV is very low. So, for most of the bridges, the composite/fiber thickness is slightly increased in respect to the values obtained for case (a) and this variation depends exclusively on the COV of the model error.

Considering the underlined differences between case (a) and (b), it is possible to understand that the introduction of the model error is fundamental to have an idea of the real conservatism and goodness of the considered model. If for case (a) Said and Wu's model seemed to be much less safe than Casas and Pascual, now, though actually Casas and Pascual is confirmed more conservative, the difference between the two models is reduced. However, the difference still remains significant. This is mainly due to the fact that Casas and Pascual is calibrated for characteristic values, whereas Said and Wu for mean values.

Regarding the safety factors their behavior reflects what has been already seen for the composite/fiber thicknesses. For Casas and Pascual, the values of the safety factors decrease, which means that, since the coefficient γ_r is at the denominator of the term $1/\gamma_r$, the allowable stress in the composite/fiber is higher. On the contrary, for Said and Wu, the safety factors slightly decrease and the allowable stress in the composite/fiber is lower.

The introduction of the model error, though altering substantially the results, does not modify significantly the variability of the β trend, since, as already pointed out, it affects only composite/fiber contribution.

7.2.3 Method c

The model error is now applied to the whole resisting moment in the Monte Carlo simulation. This is the proper procedure, since the random variable Φ has been evaluated referring to the global system *concrete-steel-composite* and counts for the uncertainties due to all the materials and assumed resistance models.
The position of the safety factor is the same adopted by the American code [1] in the Load and Resistance Factor Design (LRFD) methodology. The resistance factor φ, here called γ to not confuse it with the model error Φ, in LFRD is used to consider all sources of uncertainty in the resistance, such as variation in material properties, the error of the models used for design and possible geometric variations.
The traditional design equation is given by:

$$\sum \gamma_i Q_i \leq \chi R \tag{7.5}$$

where γ_i are the load factors corresponding to the loads Q_i, R is the resistance and χ the safety factor, specific to the limit state being considered. In this case χ is evaluated for the single ultimate limit state (ULS).

- *Design formula*

$$M_{rd} = \gamma\left[A_s f_y (d - \varphi x) + A_{s2} f_{s2} (\varphi x - d_2) + A_F \sigma_F d_1\right] \tag{7.6}$$

No safety factors are used in the term between the parenthesis and the tensile steel stress f_y is the characteristic value, not the design one (f_{yd}).

- *Monte Carlo simulation*

$$\begin{aligned} M_r &= \Phi[A_s f_s (d - \varphi x) + A_{s2} f_{s2} (\varphi x - d_2) + A_F \sigma_F d_1] = \\ &= \Phi[A_s f_s (d - \varphi x) + A_{s2} \varepsilon_{s2} E_s (\varphi x - d_2) + A_F \varepsilon_F E_F d_1] \end{aligned} \tag{7.7}$$

Where the random variables are f_s, E_F, E_c and Φ. The other terms are random variables, which depends on the four main random variables.

Results

- β=3,5

Bridge	Precured		Wet-lay up	
	γ	t_{frp} (mm)	γ	t_f (mm)
B10RC	0,839	0,700	0,838	0,490
B12RC	0,861	0,640	0,855	0,470
B16RC	0,893	0,560	0,887	0,400
B20RC	0,910	0,500	0,908	0,360
S10RC	0,899	0,510	0,893	0,370
S1015RC	0,904	0,460	0,904	0,320
S1520RC	0,882	0,750	0,880	0,530

- β=4,0

Bridge	Precured		Wet-lay up	
	γ	t_{frp} (mm)	γ	t_f (mm)
B10RC	0,744	1,370	0,743	0,960
B12RC	0,766	1,360	0,764	0,960
B16RC	0,799	1,320	0,802	0,920
B20RC	0,828	1,350	0,825	0,960
S10RC	0,812	0,900	0,808	0,640
S1015RC	0,820	0,780	0,815	0,560
S1520RC	0,790	1,460	0,790	1,010

Table 7.7. Results for case (c), target β=3,5 and 4

.

Results are found only for Said and Wu's model (*Table 7.7*), since for Casas and Pascual many difficulties were encountered, as explained in the next section.

The value of the thickness, needed to get the wanted reliability index, increases in comparison with that obtained from the previous procedure (b), and this is due to the fact that this time the model error is applied to the whole *concrete-steel-composite* system and not only to the composite term, which gives a smaller contribution to the global resistant

moment. Indeed, even if the mean value does not alter the results, being equal to 1, the COV introduces a larger dispersion of the data both to the composite and steel terms, which inevitably leads to a higher probability of failure, for the same composite thickness. Another observation can be done about the change in the composite thicknesses. In fact, the values of the composite thickness for B16RC and B20RC are now closer to those for B10RC and B12RC (actually they are almost the same), if compared to the results got from the other two procedures. The reason why this happens is explained in paragraph 7.2.3.2, since the phenomenon is more pronounced for Casas and Pascual and it is the cause of the impossibility to find the wanted results for the model. For now, it can be said that it depends on the change in the resisting behavior of the section when the strengthening is applied and on the geometry of the cross-section.

The values of the safety factors calculated for girder bridges are quite different one to each other, because of the already mentioned problem of the "balanced" design. The stem width remains the same, even if the height of the section increases significantly going from B10RC to B20RC. For slab bridges, instead, each design was realized by changing the number and width of the plates/sheets, without encountering any geometric restriction; this is why the safety factor values are closer one to each other.

7.2.3.1 Proposed design safety factor γ

The design value for the safety factor should be determined by taking into account the highest

number of different design cases, in order to find a coefficient that could be suitable to each situation.

The problem in determining a design value for the safety factor is that each γ is found here by referring to a particular design case, which differs from the others for shape of the section, type of bridge, composite system and level of initial tensile steel lack. Therefore, it is difficult to choose an appropriate range of design for the calibration of the safety factor. Anyway, the COV for precured and wet-lay up systems are very close (0,09 and 0,15 respectively), so that it is decided to propose the same design value of the safety factor for both systems. In this way, the number of the variable properties affecting the problem is reduced. As proposed even by Atadero et al. [3], the baseline for the design is

defined as the amount of steel lack compared to the steel quantity needed according to the Eurocode requirements. For slab bridges the choice of this baseline comes almost natural, since they presents the same percent of steel loss (32%).

Girder bridges, instead, results in having a different quantity of steel lack (going from B10RC to B20RC, 45,10 %, 30,85%, 26,68%, 25,20% respectively), hence, they should be divided in different groups. Looking at the results obtained, it has been decided to place B10RC and B12RC in two different pools (50%<steel lack<40%, 40%<steel lack<30%), while B16RC and B20RC are placed in the same group (30%<steel lack<20%).The design values are taken by rounding-down the found values of table 7.6, when necessary. The chosen safety factors are listed in *Tables 7.8 and 7.9* for each design group and target reliability index.

- β=3,5

Design group	**Proposed γ**
B10RC (50% < steel lack ≤ 40%)	$\gamma = 0{,}835$
B12RC (40% < steel lack ≤ 30%)	$\gamma = 0{,}850$
B16RC,B20RC (30%< steel lack ≤ 20%)	$\gamma = 0{,}885$
S10RC, S1015RC, S1520RC (35%<steel lack<30%)	$\gamma = 0{,}880$

T*able 7.8. Proposed design safety factors for Said and Wu, target β=3,5.*

- β=4,0

Design group	**Proposed γ**
B10RC (50% < steel lack ≤ 40%)	$\gamma = 0{,}740$
B12RC (40% < steel lack ≤ 30%)	$\gamma = 0{,}760$
B16RC,B20RC (30%< steel lack ≤ 20%)	$\gamma = 0{,}795$
S10RC, S1015RC, S1520RC (35%<steel lack<30%)	$\gamma = 0{,}790$

T*able 7.9. Proposed design safety factors for Said and Wu, target β=4,0.*

Looking at *Tables 7.8- 7.9,* a more simplified proposal for the safety factors to be considered is a value of 0,85 to get a reliability index of 3.5; and a value of 0,75 to get a reliability index equal to 4. Hence, the strength reduction factor of 0,75, suggested by Said and Wu themselves [29], assures a target β=4,0 even for high percent of tensile steel loss. Therefore, the recommended value, even if not based on a reliability analysis, already assured a high level of safety. The safety factor proposed by Said and Wu was based just on engineering judgment and available experimental results, without any scientific background. The results obtained in the present thesis confirm that the proposed safety factor derives on too high level of safety, which is clearly ant economical because of the high cost of the composites. So, the value of 0,85 corresponding to a reliability level of 3,5 is more reasonable to be applied in real applications.

7.2.3.2 Casas and Pascual: the high COV value

The model variability factor plays a very important role and the value of the COV=0,23 determines a high variability in the results. Even when the initial reliability of the bridge is very close to the target β=3,5, it is impossible to find a composite thickness that can satisfy the reliability requirements, indeed, the number of failures remains very high even for high thicknesses. When the bridge is strengthened with the composite, the existing equilibrium of the section is altered and the leading parameter becomes the FRP debonding strain, which assumes very low values, easily reached because of the T shape of the section. If moreover the applied model is conservative and therefore the debonding strain is even lower, it is very difficult to reach the target value. When the Casas and Pascual's model is applied, the initial reliability of the bridge can be improved, but not significantly, due to the value of the COV, that, though the high value of the mean, influences negatively the results. At the beginning this outcome was deemed to be related to the low amount of the tensile steel. In fact, as pointed out by Atadero et al. [3], when the amount of tensile steel is significantly lower than that needed according to the code, it may be impossible to apply enough FRP to bring the bridge up to the target β.

For a better understanding of the problem, an expedient was thought. The maximum achievable reliability index has been calculated for each bridge (*Table 7.10*), by applying Casas and Pascual and setting the value 5 mm as a limit for t_{frp}. The calculation has been

made only for the prefabricated system, since the problems, that come up when designing with the wet-lay up system, are the same.

Bridge	Initial β	Maximum achievable β
B10RC	2,661	3,076
B12RC	2,880	3,038
B16RC	3,209	2,951
B20RC	3,482	2,958
S10RC	2,514	3,087
S1015RC	2,420	3,187
S1520RC	2,752	3,119

Table 7.10. Maximum achievable β for t_{frp}=5 mm (prefabricated system).

A comparison between the results obtained for slab bridges is not immediate, due to the different width of the composite plates/sheets, hence the analysis will focus now on girder bridges, for which the web width is the same (and so the strengthening width).

As it can be seen, the difference between the maximum achievable reliability index and the initial β varies from bridge to bridge.

Looking at the results obtained, it seems that the higher the initial reliability the lower the scatter from the final reliability. This is obvious, since the failure without the CFRP strengthening was due to the concrete crushing; the application of the strengthening not only changes completely the resisting mechanism of the cross-section but also results to be more effective for those girders that have a smaller depth. Indeed, because of the debonding problem, the allowable strains on the lower edge are clearly reduced and sections with an high depth reach sooner high strains. This is why for B16RC and B20RC the final β is even lower than the initial one.

The phenomenon is also accentuated by the high value of the COV of the model error, so that, many times, the increase in the number of failures cannot be contrasted with the application of an higher composite thickness, but it is simply impossible to be contrasted. This trend has been already seen when results for Said and Wu's model were presented, but it is here much stronger because of the high COV.

Conclusions

A reliability-based analysis was performed to calibrate the design safety factors for two intermediate crack-induced debonding models, *Casas and Pascual* and *Said and Wu*. The models were applied to design the flexural strengthening of seven existing reinforced concrete bridges that present different percents of reinforcing tensile steel lack and different geometries.

The choice of designing the strengthening for bridges with different characteristics was not coincidence. Indeed, a reliability-based design has to give a level of reliability that is the most uniform as possible across many different design cases. This is translated in the necessity to determine a safety factor that assures an alike reliability index when applied to structures with a similar function, but diverse geometric characteristics.

The performed reliability-based analysis considered for the first time the model error as one of the main variables participating in the limit state function. The way the introduction of this variable affects the results was discussed in details by comparing the values obtained from three different applied methods, in which the model error was first not considered at all and then placed at different positions in the limit state equation.

The last method, which turned out to be the correct one, consisted in multiplying the model error variable for the entire resisting moment of the limit state equation; for the sake of coherence, the safety factor was placed before the whole resisting moment in the design formula.

Results were found only for Said and Wu's model, for two target reliability indexes, β=3,5 and β=4,0. The design values for the safety factors were determined by grouping the bridges on the base of their percent of steel lack. Indeed, using the same design safety factor for elements with different amounts of tensile steel – a mistake affecting several current guidelines - means to waste both material and monetary resources. The proposed values show that the design factor equal to 0,75, as already suggested by Said and Wu [29], assures a reliability index close to 4 for bridges with a steel lack ranging from 50% to 30%. Note that this value is excessive for bridges that present a lower percent of steel lack. This is why, a lower value of the target reliability index in the range of 3,5 or even lower is proposed as a result of the present work, which consists on a global safety factor

equal to 0,85 for both prefabricated and wet-lay up systems. Therefore, the proposed design equation for the resisting moment when strengthening with CFRP in bending for both prefabricated and wet-lay up systems is the following:

$$M_{rd} = 0{,}85\left[A_s f_y (d - \psi x) + A_{s2} f_{s2} (\psi x - d_2) + A_F \sigma_F d_1\right]$$

where

- A_s, A_{s2} and A_F are the tensile steel, compressive steel and composite/fiber areas, respectively;
- f_y and f_{s2} are the tensile and compressive strength of the steel;
- d is the effective depth of the cross-section;
- ψ is the ratio of the distance of the force resulting from compression in the concrete from the upper edge to the neutral axis x;
- d_2 and d_1 are the distance of the compressive steel barycenter from the upper edge (edge in compression) and the distance of the composite/fiber barycenter from the bottom edge (edge in tension).

The stress in the composite/fiber should be calculated according to Said and Wu's model, and the position of the neutral axis can be calculated using the simplified model for the concrete stress-strain relationship proposed in this thesis. Indeed, because of the T shape of the bridge cross-sections, but also because of the low ultimate strains imposed by the debonding failure, strains in the concrete were so small that the simplified rectangular stress-block could not be adopted. Hence, it was chosen a linear stress-strain relation with a concrete elastic modulus equal to the secant modulus at the strain 0,00075. The assumption was checked by comparing the results with those obtained from the software XTRACT. Since the difference between the values was very low (≈5%), the simplification made was considered admissible.

According to the Casas and Pascual's model, no results were drawn, as the high value of the coefficient of variation (COV=0,23) impeded to reach the fixed reliability targets. Not only the increment of the initial reliability was little for the majority of the bridges, but also, in some cases, the final reliability was lower than the initial one. This was due to both the geometry of the considered cross-section, and the high variability of the model.

It was seen that, for values of the COV not higher than 0,15-0,16, both the target indexes would have been reached, maintaining the mean error equal to 1,8. When the COV value got closer to 0,2, the probability of failure increased drastically, and a reliability index higher than 3 was not achievable. This behavior was noticed also in Said and Wu's model, for which a reliability index of 3,5 and 4,0 could be reached till a COV $\approx$0,15.

In the light of all these considerations and of what has been stressed out in Chapter 7, what emerges from the study is that:

1) A design safety factor equal to 0,85 (or even higher) should be used when designing a flexural strengthening of reinforced concrete structural elements with Said and Wu's model;
2) It is not always worth to strengthen in bending existing structures with FRPs. Indeed, if the variability of the resisting model applied is too high, the probability of failure can exceed that of the structural member at the initial conditions; this is mainly due to the fact that ultimate debonding strains are generally very low and easy to achieve. In particular for T-shape sections, the low strain in the tensile reinforcement (both existing steel and additional CFRP) produces also a low strain in the compressed concrete and, therefore, a lower resisting moment than in the case without CFRP strengthening. In fact, in the existing section the reinforcing steel achieves high values of strain, what derives in concrete developing the maximum compressive strength.
3) Even though in the beginning the bridges have a significant lack of tensile steel (according to the Eurocode), the initial reliability turns out to be quite high, showing an excessive conservatism of the Eurocode in the resistance requirements.
4) The value of the design safety factors is strictly related to the adopted debonding model, but it varies mainly depending on if the model is calibrated over mean values (Said and Wu) or characteristic values (Casas and Pascual).
5) If the reliability-based approach is to be implemented for bridges and of strategic structures in need of a higher level of reliability, the adopted intermediate crack-induced debonding model should have a model error with a maximum COV of about 0,15 (depending also on the mean value of the model error).

Further investigations

The following are recommendations for future works to be completed in this area:

- Regarding Casas and Pascual's model, further tests should be conducted in order to evaluate more precisely the model error, giving attention to the evaluation of the resin layer thickness. Indeed, the high value of the COV was found by considering only 22 bending tests, 20 on small-size specimens and 2 on large-size specimens [9]:- a number insufficient to determine accurately the model error variable.
- Casas and Pascual's model, which has the double feature of intermediate crack-induced debonding and plate-end debonding, should also be analyzed as a plate-end debonding model.
- It could be interesting to calibrate design safety factors for the two analyzed IC models with fixed reliability targets lower than 3,5.
- The model error variable should be estimated for many of the already developed debonding models.
- A reliability-based analysis should be performed for each of the debonding models used in the guidelines, as to correctly evaluate the corresponding design safety factors, extending the study also to the serviceability limit state.

Bibliography

1) American Association of State Highway Transportation Officials (AASHTO). *AASHTO LRFD Bridge Design Specifications* (2006). Washington DC.

2) American Concrete Institute (ACI). ACI 440.2R-08 (2008). *Guide for the design and construction of externally bonded FRP systems for strengthening of concrete structures*. Farmington Hill, Michigan.

3) Atadero, R.A., Karbhari, V.M. (2008). "Calibration of resistance factors for reliability based design of externally-bonded FRP composites". *Composites: Part B* (ELSEVIER), 39, 665-679.

4) Atadero, R.A., Karbhari, V.M. (2009). "Sources of uncertainty and design values for field-manufactured FRP." *Composite structures* (ELSEVIER), 89(1), 89-93.

5) BS EN1990:2002 (2002). *Eurocode 0: Basis of structural design*. European Committee for Standardization (CEN), Brussels, Belgium.

6) BS EN1991-2:2003 (2003). *Eurocode 1: Action on structures – Traffic loads on bridges*. European Committee for Standardization (CEN), Brussels, Belgium.

7) BS EN1992:2004 (2004). *Eurocode 2: Design of concrete structures*. European Committee for Standardization (CEN), Brussels, Belgium.

8) Casado, C.F. (1942). *Colección oficial de puentes de tramos recto. Tramos de un vano simplemente apoyados*. Ministerio de Obras Públicas. Madrid, Spain.

9) Casas, J.R., Pascual, J. (2007). "Debonding of FRP in bending: Simplified model and experimental validation". *Construction and Building Materials* (ELSEVIER), 21, 1940-1949.

10) Casas, J.R., Gomez, J.D. (2013). "Load rating of highway bridges by proof-load ing." *Journal of Civil Engineering* (ASCE), 17(3): 556-567.

11) Ceci, A. (2006). *Development of design specifications for strengthening deteriorated concrete bridge elements using externally applied FRP sheets*. Thesis defenced at the Faculty of Civil Engineering, L'Aquila, A.Y. 2005-2006.

12) Ceci, A., Casas, J.R., Ghosn, M. (2012). "Statistical analysis of existing models for flexural strengthening of concrete bridge beams using FRP sheets". *Construction and Building Materials* (ASCE), 27(1), 490-520.

13) Chen, J.F., Teng, J.G. (2001). "Anchorage strength models for FRP and steel plates bonded to concrete." *Journal of Structural Engineering* (ASCE), 127(1), 784 –791.

14) Consiglio Nazionale delle Ricerche (CNR). CNR DT200 R1/2013 (2013). *Istruzioni per la progettazione, l'esecuzione e il controllo di interventi di consolidamento statico mediante l'utilizzo di compositi fibrorinforzati*. Consiglio Nazionale delle Ricerche, Rome, Italy.

15) D'Antino, T., Pellegrino, C. (2014). "Bond between FRP composites and concrete: Assessment of design procedures and analytical models. *Composites: Part B* (ELSEVIER), 60, 440-456.

16) Diamantidis, D. (2001). *Probabilistic Assessment of Existing Structures – A publication of the Joint Committee on Structural Safety (JCSS).* 1st ed., RILEM Publications.

17) Ellingwood, B.R., Galambos, T.V., MacGregor, J.G., and Cornell, C.A. (1980). "Development of a probability based load criterion for American National Standard A58". NBS Special Publication 577, National Bureau of Standards, U.S. Department of Commerce, Washington, D.C..

18) Esquius Berengueras, M. (2012). *Estudi sobre la robustesa structural de ponts de formigó reforçats a flexió amb materials compostos*. Thesis defenced at the Faculty of Civil Engineering, Barcelona, A.Y. (2012-2013).

19) Fib Bulletin 14 (2001). *Externally bonded FRP reinforcement for RC structures*. Lausanne, Switzerland.

20) Harmon, T.G., Kim, Y.J., Kardos, J., Johnson, T., Stark, A. (2003). "Bond of surface-mounted fiber-reinforced polymer reinforcement for concrete structures". *Structural Journal* (ACI), 100(5), 557–564.

21) Holloway, L.C., Teng, J.G. (2008). *Strengthening and rehabilitation of civil infrastructure using fiber-reinforced polymer (FRP) composites*. 1st ed., Woodhead Publishing Limited.

22) Mander, J.B., Priestly, M.J.N. (1988). "Theoretical stress-strain model for confined concrete." *Journal of Structural Engineering* (ASCE), 114(8), 1804-1826.

23) Melchers, R.E. (1999). *Structural reliability analysis and Prediction*. 2nd ed., Wiley.

24) Monti, G., Santini, S. (2002). "Reliability based calibration of partial safety coefficients for fiber-reinforced plastic". *Journal of Composites for Construction* (ASCE), 6(3), 162–167.

25) D.M. 14 Gennaio 2008 (NTC2008). *Norme tecniche per le costruzioni*, chapters 4 and 12. Rome, Italy.

26) Oehlers, D.J. (1992). “Reinforced concrete beams with plates glued to their soffits”. *Journal of Structural Engineerin*g (ASCE), 118(8), 2023-2038.

27) Okeil, A.M., El-Tawil, S., Shahawy, M. (2002). “Flexural reliability of reinforced concrete bridge girders strengthened with carbon fiber-reinforced polymer laminates.” *Journal of Bridge Engineering* (ASCE), 7(5), 290–299.

28) Plevris, N., Triantafillou, T.C., Veneziano, D. (1995). “Reliability of RC Members Strengthened with CFRP Laminates”. *Journal of Structural Engineering* (ASCE), 121(7), 1037–1044.

29) Said, H. and Wu, Z. (2008). “Evaluating and Proposing Models of Predicting IC Debonding Failure.” *Journal of Composites for Construction* (ASCE), 12(3), 284-299.

30) Schnieder, J. (1997). *Introduction to Safety and Reliability of Structures*. 2nd ed. (2006), International Association for Bridge and Structural Engineering (IABSE), Zurich, Switzerland.

31) Smith, S.T., Teng, J.G. (2002). “FRP-strengthened RC beams: assessment of debonding strength models”. *Engineering structures* (ELSEVIER), 24(4), 397-417.

32) Teng, J.G., Chen, J.F., Smith, S.T., Lam, L. (2001). *FRP strengthened RC structures*. 1st ed., Wiley.

33) Teng, J.G., Smith, S.T., Yao, J., Chen, J.F. (2003). “Intermediate crack-induced debonding in RC beams and slabs”. *Construction and Building Materials* (ELSEVIER), 17, 447-462.

34) Triantafillou TC, Plevris (1992). “Strengthening of RC beams with epoxy-bonded fibre-composite materials”. *Materials and Structures* (RILEM), 25(4), 201-211.

35) Val, D.V. (2003). “Reliability of fiber-reinforced polymer-confined reinforced concrete columns”. *Journal of Structural Engineering* (ASCE), 129(8), 1122–1130.

Annex A

Design of the analyzed bridges according to the Eurocode

The bridges studied in this work are here described, starting from the materials of which they are made continuing to the loads to which they are subject. Live loads are calculated according to the *Eurocode 1 (Part 3)* and acting moments are obtained by hand calculations, then checked through the FEM program STAUS7 for continuous bridges. At first, the quantity of the needed reinforcement was roughly estimated by applying the pre-dimensioning formula:

$$A_s = \frac{M_{sd}}{0{,}9 d f_{yd}} \; [mm^2]$$

where M_{sd} is the global acting moment according to the Eurocode, d is the effective depth of the cross-section and f_{yd} is the yielding design strength of the steel.

Eventually the obtained results were checked by using the program GELFI. Here only hand calculations are reported.

A1. Materials

Concrete	*Symbol*	*Value*	*Units*
Characteristic compressive strength	f_{ck}	20,00	MPa
Specific weight of RC	ρ	25,00	KN/m^3
Partial factor	α_{cc}	0,85	
Partial safety factor	γ_c	1,50	
Design value	f_{cd}	11,33	MPa
Steel			
Design yielding strength	f_{yd}	187,83	MPa
Partial safety factor	γ_s	1,15	
Characeristic yielding strength	f_{yk}	216,00	MPa
Pavimentation specific weigth	ρ_p	20,00	KN/m^3

A2. Bridges

A2.1 B10RC

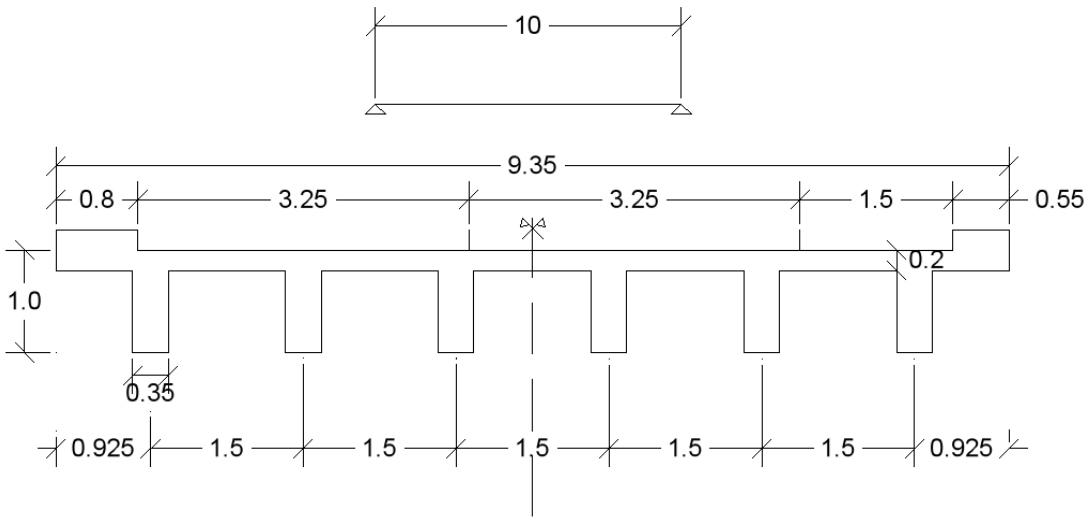

Figure A1. B10RC Cross-section (dimensions in m).

A2.1.1 Geometric characteristics

Cross section	*Symbols*	*Values*	*Units*
Base thickness	t_s	0,20	m
Tot Bridge width	B	9,35	m
Carriageway width	l_c	8,00	m
Beams width	b	0,35	m
Beams depth	h	0,80	m
N° of beams	n	6,00	m
Span lenght	L	10,00	m
Sidewalk height	h_s	0,20	m
Left sidewalk width	b_l	0,80	m
Right sidewalk width	b_r	0,55	m
Pavimentation height	t_p	0,08	m
Total area of the cross-section	$A_t = bhn + t_s b + h_s b_l b_r$		m^2
	3,82		

A.2.1.2 Loads according to the actual code (Eurocode)

Dead Loads (DL)

Loads	*Symbols*	*Values*	*Units*
Reinforced concrete	$q_{Rc} = A_s\rho$	95,50	KN/m
Pavimentation	$q_p = (t_p l_c)\rho_p$	12,80	KN/m
Guard Rail	q_g	3,00	KN/m
Total distributed dead load	q_{DLtot}	111,30	KN/m

- **Acting moment at mid span due to Dead Loads**

Moment at mid span	$M_{SdDL} = \frac{q_{DLtot}L^2}{8}$	1390,25	KNm

Live Loads (LL)

Geometrical assumptions	Symbols	Values	Units
Carriageway length	l_c	8,00> 6m	m
N° of conventional lines	$n_i = Int\left(\frac{l_c}{3}\right)$	2,00	
Width conv line	w_c	3,00	m
Remaining part length	$w_r = (l_c - w_c n_i) + bl + br$	3,35	m
Span length	L	10,00	m
Longitudinal eccentricity force from the support	a	4,40	m
Left sidewalk width	b_l	0,80	m
Right sidewalk width	b_r	0,55	m

Distributed and concentrated Live Loads

Line	Q_{ik} [KN]	q_{ik}[KN/m^2]
1	300,00	9,00
2	200,00	2,50
3	100,00	2,50
Others	0,00	2,50
Remaining part	0,00	2,50

Assumed longitudinal load distribution

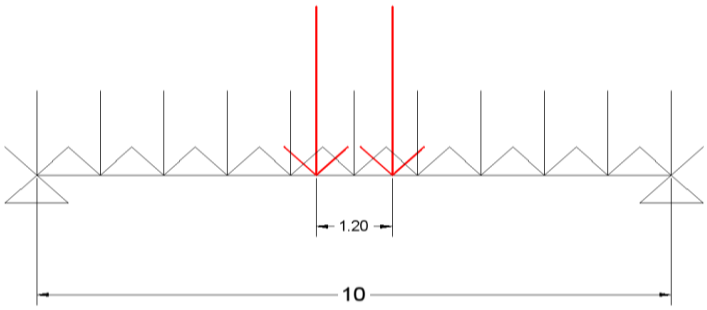

Figure A2. Assumed longitudinal load distribution (dimensions in m).

- **Acting moments at mid span due to Live Loads**

Concentrated loads		
$Q_{1k} + Q_{2k}$	500,00	KN
M_{Qk}	2200,00	KNm
Distributed loads		
$q_{1kl} = q_{1k}w_c$	27,00	KN/m
$q_{2kl} = q_{2k}w_c$	7,50	KN/m
$q_r = q_{rk}w_r$	8,38	KN/m
q_{tot}	42,88	KN/m
M_{qk}	535,93	KNm
Total moment		
M_{ll}	2734,94	KNm

- **Global actions (DL+LL)**

Total bending moment acting on the mid span section	$M_{tot} = M_{dd} + M_{ll}$	4125,19	KNm
Load combination factor	φ	1,35	
Total moment with safety factor	M_{ftot}	5569,70	KNm
N° of beams	n	6,00	
Mean moment for each beam	$M_{sm} = \frac{M_{ftot}}{n}$	928,28	KNm

Total tensile steel needed

$\boldsymbol{A_s}$	37000,00	mm^2
$\boldsymbol{M_{Rd,new}}$	6060,00	KNm

A2.1.3 Existing cross-section characteristics

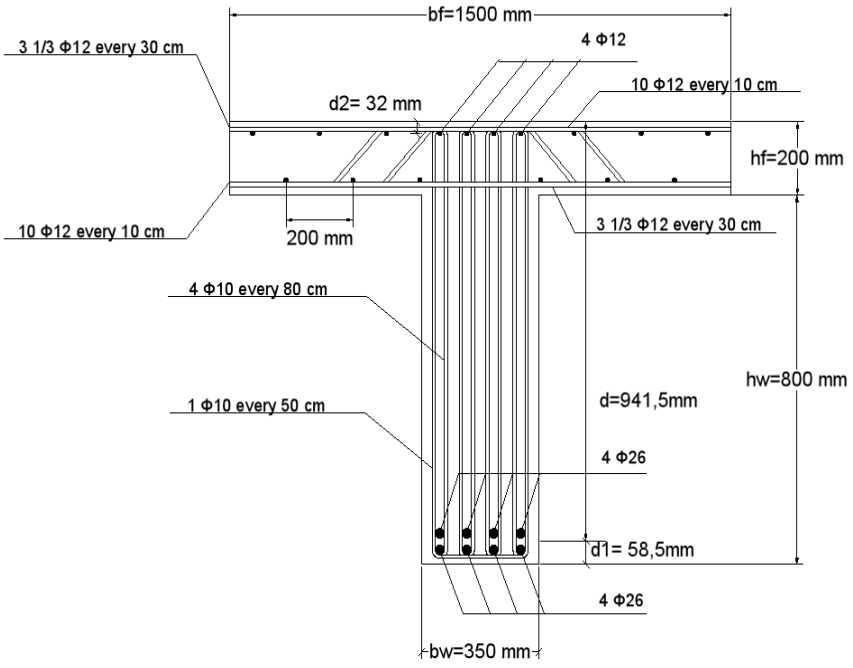

Figure A3. Cross-section of one of the girders.

Reinforcement and geometric characteristics

Depth of the web	h_w	800,00	mm
Width of the web	b_w	350,00	mm
Depth of the flange	h_f	200,00	mm
Width of the flange	b_f	1500,00	mm
Total heigth	h	1000,00	mm
Effective depth	d	941,50	mm
Distance from the bottom edge	d_1	58,50	mm
Distance from the upper edge	d_2	32,00	mm
Tensile steel	A_s	4247,00	mm^2
Tensile steel diameter	8Φ	26,00	mm
Compressive steel	$A_{s'}$	452,40	mm^2
Compressive steel diameter	4Φ	12,00	mm

Resistance of the existing section

Resisting moment at mid span $M_{Rd,old}$	4395,60	KNm
Mean resisting moment at mid span $M_{Rdm,old}$	732,60	KNm

A2.2 B12RC

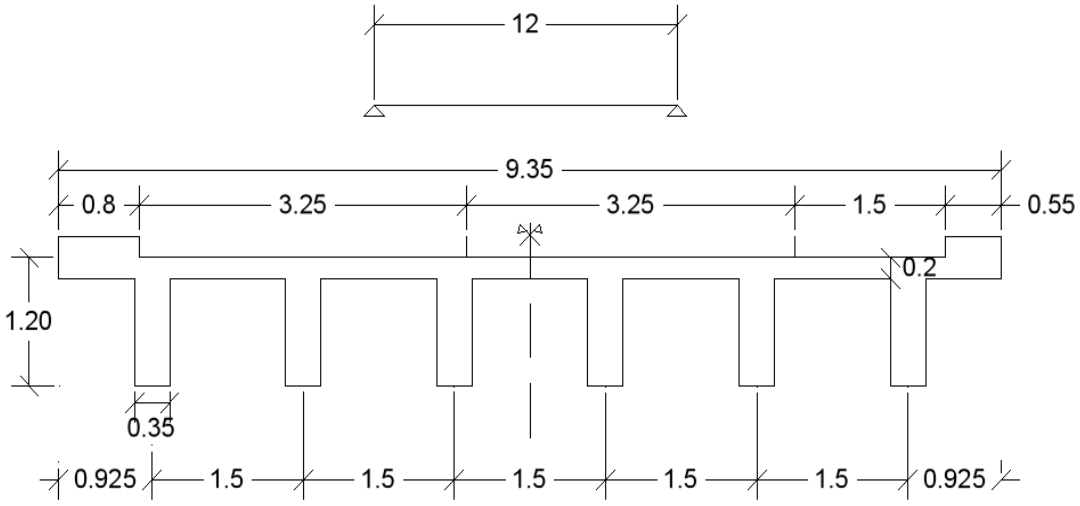

Figure A4. B12RC Cross-section (dimensions in m).

A2.2.1 Geometric characteristics

Cross-section	*Symbols*	*Values*	*Units*
Base thickness	t_s	0,20	m
Tot Bridge width	B	9,35	m
Carriageway width	l_c	8,00	m
Beams width	b	0,35	m
Beams depth	h	1,00	m
N° of beams	n	6,00	
Span lenght	L	12,00	m
Sidewalk height	h_s	0,20	m
Left sidewalk width	b_l	0,80	m
Right sidewalk width	b_r	0,55	m
Pavimentation height	t_p	0,08	m
Total area of the cross-section	$A_t = bhn + t_s b + h_s b_l b_r$		m^2
	4,24		

A.2.2.2 Loads according to the actual code (Eurocode)

Dead Loads (DL)

Loads	*Symbols*	*Values*	*Units*
Reinforced concrete	$q_{Rc} = A_s\rho$	106,00	KN/m
Pavimentation	$q_p = (t_p l_c)\rho_p$	12,80	KN/m
Guard Rail	q_g	3,00	KN/m
Total distributed dead load	q_{DLtot}	121,80	KN/m

- **Acting moment at mid span due to Dead Loads**

Moment at mid span	$M_{SdDL} = \frac{q_{DLtot}L^2}{8}$	2192,40	KNm

Live Loads (LL)

Geometrical assumptions	*Symbols*	*Values*	*Units*
Carriageway length	l_c	8,00> 6m	m
N° of conventional lines	$n_i = Int\left(\frac{l_c}{3}\right)$	2,00	m
Width conv line	w_c	3,00	m
Remaining part length	$w_r = (l_c - w_c n_i) + bl + br$	3,35	m
Span length	L	12,00	m
Longitudinal eccentricity force from the support	a	5,40	m
Left sidewalk width	b_l	0,80	m
Right sidewalk width	b_r	0,55	m

Distributed and concentrated Live Loads

Line	Q_{ik} [KN]	q_{ik}[KN/m^2]
1	300,00	9,00
2	200,00	2,50
3	100,00	2,50
Others	0,00	2,50
Remaining part	0,00	2,50

Assumed longitudinal load distribution

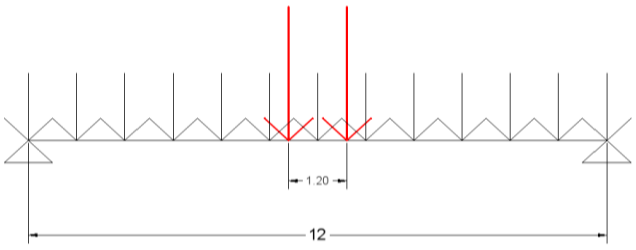

Figure A5. Assumed longitudinal load distribution (dimensions in m).

- **Acting moments at mid span due to Live Loads**

Concentrated loads		
$Q_{1k} + Q_{2k}$	500,00	KN
M_{Qk}	2700,00	KNm
Distributed loads		
$q_{1kl} = q_{1k} w_c$	27,00	KN/m
$q_{2kl} = q_{2k} w_c$	7,50	KN/m
$q_r = q_{rk} w_r$	8,38	KN/m
q_{tot}	42,88	KN/m
M_{qk}	771,75	KNm
Total moment		
M_{ll}	3471,75	KNm

- **Global actions (DL+LL)**

Total bending moment acting on the mid span section	$M_{tot} = M_{dd} + M_{ll}$	5664,15	KNm
Load combination factor	φ	1,35	
Total moment with safety factor	M_{ftot}	7646,60	KNm
N° of beams	n	6,00	
Mean moment for each beam	$M_{sm} = \frac{M_{ftot}}{n}$	1274,43	KNm

Total tensile steel needed

$\boldsymbol{A_s}$	38600,00	mm^2
$\boldsymbol{M_{Rd,new}}$	7722,00	KNm

A2.2.3 Existing section characteristics

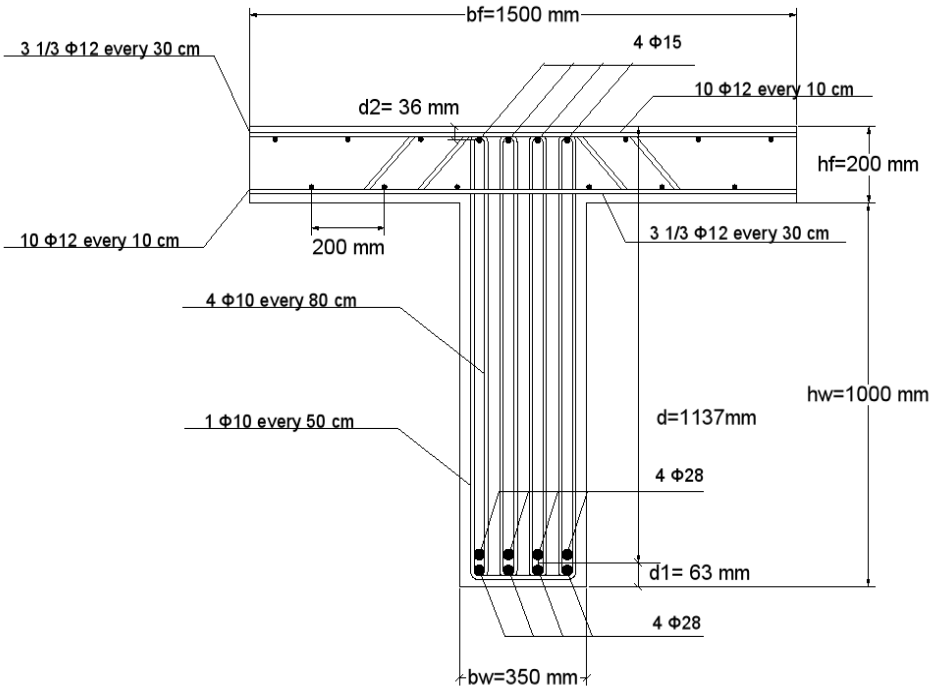

Figure A6. Cross-section of one of the girders.

Reinforcement and geometric characteristics

Depth of the web	h_w	1000,00	mm
Width of the web	b_w	350,00	mm
Depth of the flange	h_f	200,00	mm
Width of the flange	b_f	1500,00	mm
Total heigth	h	1200,00	mm
Effective depth	d	1137,00	mm
Distance from the bottom edge	d_1	63,00	mm
Distance from the upper edge	d_2	36,00	mm
Tensile steel	A_s	4926,00	mm^2
Tensile steel diameter	8Φ	28,00	mm
Compressive steel	$A_{s'}$	707,00	mm^2
Compressive steel diameter	4Φ	15,00	mm

Resististance of the existing section

Resisting moment at mid span $M_{Rd,old}$	6390,00	KNm
Mean resisting moment at mid span $M_{Rdm,old}$	1065,00	KNm

A2.3 B16RC

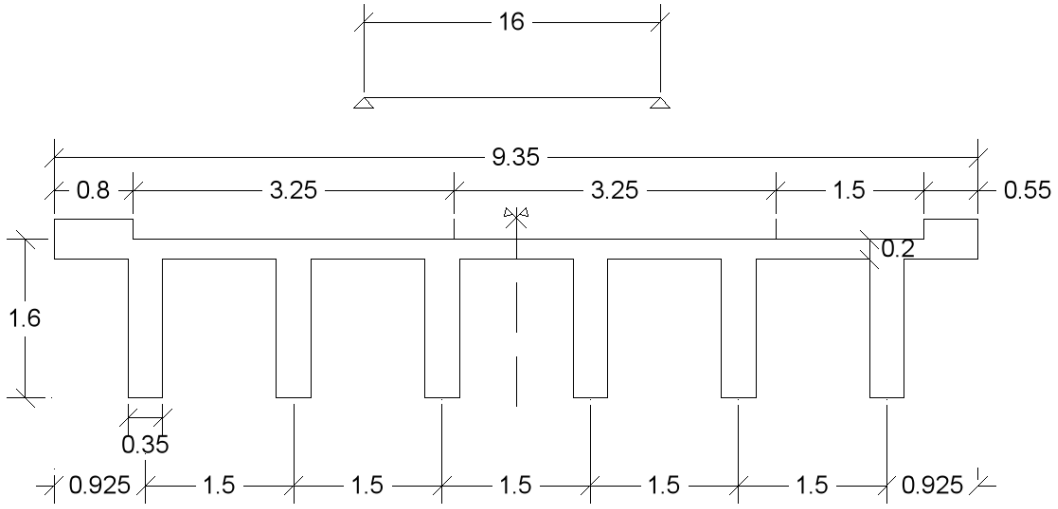

Figure A7. B16RC Cross-section (dimensions in m).

A2.3.1 Geometric characteristics

Cross-section	*Symbols*	*Values*	*Units*
Base thickness	t_s	0,20	m
Tot Bridge width	B	9,35	m
Carriageway width	l_c	8,00	m
Beams width	b	0,35	m
Beams depth	h	1,40	m
N° of beams	n	6,00	
Span lenght	L	16,00	m
Sidewalk height	h_s	0,20	m
Left sidewalk width	b_l	0,80	m
Right sidewalk width	b_r	0,55	m
Pavimentation heigth	t_p	0,08	m
Total area of the cross-section	$A_t = bhn + t_s b + h_s b_l b_r$		m^2
	5,08		

A.2.3.2 Loads according to the actual code (Eurocode)

Dead Loads (DL)

Loads	*Symbols*	*Values*	*Units*
Reinforced concrete	$q_{Rc} = A_s\rho$	127,00	KN/m
Pavimentation	$q_p = (t_p l_c)\rho_p$	12,80	KN/m
Guard Rail	q_g	3,00	KN/m
Total distributed dead load	q_{DLtot}	142,80	KN/m

- **Acting moment at mid span due to Dead Loads**

Moment at mid span	$M_{SdDL} = \frac{q_{DLtot}L^2}{8}$	4569,60	KNm

Live Loads (LL)

Geometrical assumptions	*Symbols*	*Values*	*Units*
Carriageway length	l_c	8,00> 6m	m
N° of conventional lines	$n_i = Int\left(\frac{l_c}{3}\right)$	2,00	
Width conventional line	w_c	3,00	m
Remaining part length	$w_r = (l_c - w_c n_i) + bl + br$	3,35	
Span length	L	16,00	m
Longitudinal eccentricity force from the support	a	7,40	m
Left sidewalk width	b_l	0,80	m
Right sidewalk width	b_r	0,55	m

Distributed and concentrated Live Loads

Line	Q_{ik} [KN]	q_{ik}[KN/m^2]
1	300,00	9,00
2	200,00	2,50
3	100,00	2,50
Others	0,00	2,50
Remaining part	0,00	2,50

Assumed longitudinal load distribution

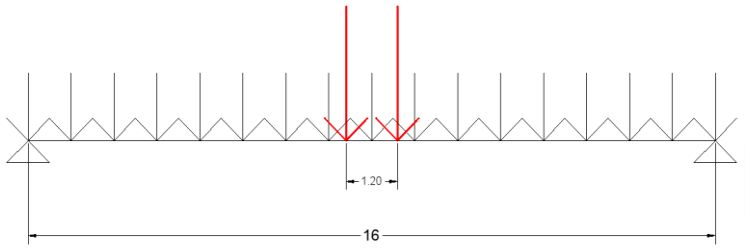

Figure A8. Assumed longitudinal load distribution (dimensions in m).

- **Acting moments at mid span due to Live Loads**

Concentrated loads		
$Q_{1k} + Q_{2k}$	500,00	KN
M_{Qk}	3700,00	KNm
Distributed loads		
$q_{1kl} = q_{1k}w_c$	27,00	KN/m
$q_{2kl} = q_{2k}w_c$	7,50	KN/m
$q_r = q_{rk}w_r$	8,38	KN/m
q_{tot}	42,88	KN/m
M_{qk}	1372,00	KNm
Total moment		
M_{ll}	5072,00	KNm

- **Global actions (DL+LL)**

Total bending moment acting on the mid span section	$M_{tot} = M_{dd} + M_{ll}$	9641,60	KNm
Load combination factor	φ	1,35	
Total moment with safety factor	M_{ftot}	13016,16	KNm
N° of beams	n	6,00	
Mean moment for each beam	$M_{sm} = \frac{M_{ftot}}{n}$	2169,36	KNm

Total tensile steel needed

$\boldsymbol{A_s}$	48900,00	mm^2
$\boldsymbol{M_{Rd,new}}$	13296,00	KNm

A2.3.3 Existing section characteristics

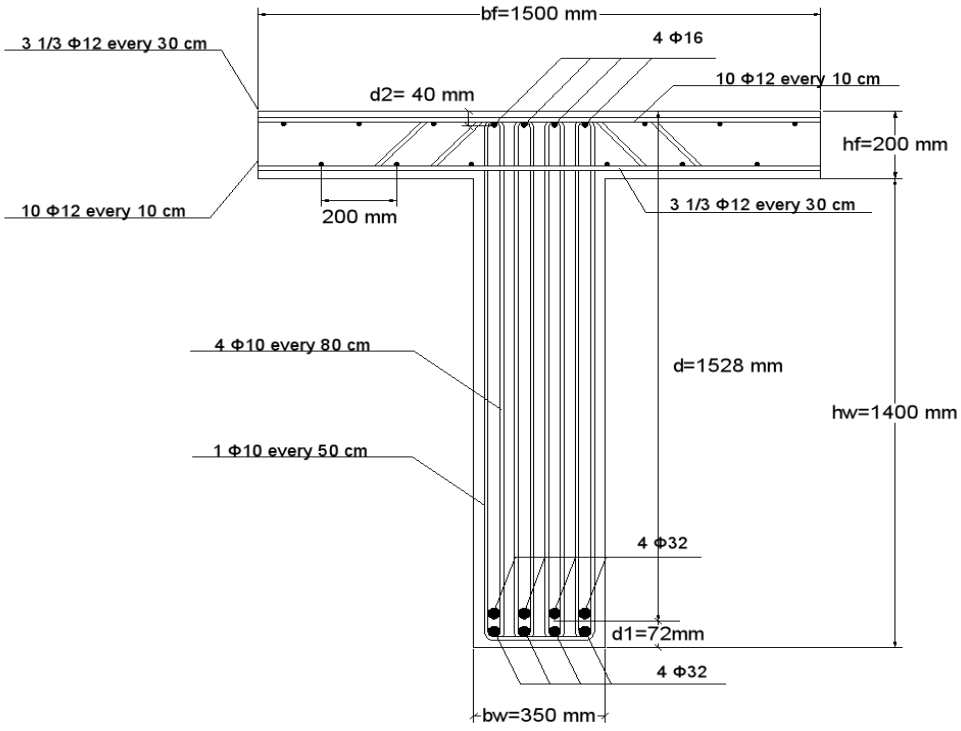

Figure A9. Cross-section of one of the girders.

Reinforcement and geometric characteristics

Depth of the web	h_w	1400,00	mm
Width of the web	b_w	350,00	mm
Depth of the flange	h_f	200,00	mm
Width of the flange	b_f	1500,00	mm
Total heigth	h	1600,00	mm
Effective depth	d	1528,00	mm
Distance from the bottom edge	d_1	72,00	mm
Distance from the upper edge	d_2	40,00	mm
Tensile steel	A_s	6433,33	mm^2
Tensile steel diameter	8Φ	32,00	mm
Compressive steel	$A_{s'}$	800,00	mm^2
Compressive steel diameter	4Φ	16,00	mm

Resistance of the existing section

Resisting moment at mid span $M_{Rd,old}$	10836,00	KNm
Mean resisting moment at mid span $M_{Rdm,old}$	1806,00	KNm

A2.4 B20RC

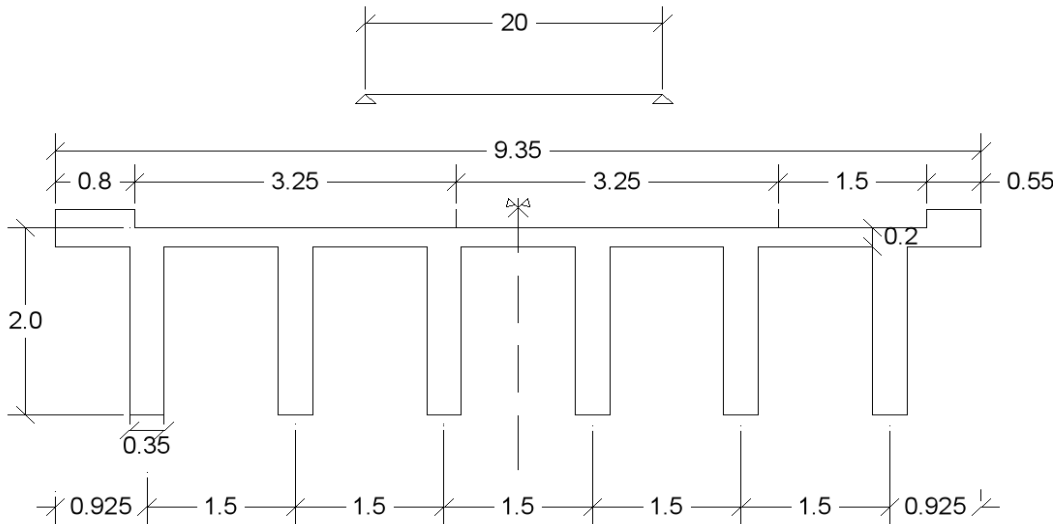

Figure A10. B20RC Cross-section (dimensions in m).

A2.4.1 Geometric characteristics

Cross section	*Symbols*	*Values*	*Units*
Base thickness	t_s	0,20	m
Tot Bridge width	B	9,35	m
Carriageway width	l_c	8,00	m
Beams width	b	0,35	m
Beams depth	h	1,80	m
N° of beams	n	6,00	
Span lenght	L	20,00	m
Sidewalk height	h_s	0,20	m
Left sidewalk width	b_l	0,80	m
Right sidewalk width	b_r	0,55	m
Pavimentation heigth	t_p	0,08	m
Total area of the cross-section	$A_t = bhn + t_s b + h_s b_l b_r$		m^2
	5,920		

A.2.4.2 Loads according to the actual code (Eurocode)

Dead Loads (DL)

Loads	*Symbols*	*Values*	*Units*
Reinforced concrete	$q_{Rc} = A_s\rho$	148,00	KN/m
Pavimentation	$q_p = (t_p l_c)\rho_p$	12,80	KN/m
Guard Rail	q_g	3,00	KN/m
Total distributed dead load	q_{DLtot}	163,80	KN/m

- **Acting moment at mid span due to Dead Loads**

Moment at mid span	$M_{SdDL} = \frac{q_{DLtot}L^2}{8}$	8190,00	KNm

Live Loads (LL)

Geometrical assumptions	*Symbols*	*Values*	*Units*
Carriageway length	l_c	8,00> 6m	m
N° of conventional lines	$n_i = Int\left(\frac{l_c}{3}\right)$	2,00	
Width conv line	w_c	3,00	m
Remaining part length	$w_r = (l_c - w_c n_i) + bl + br$	3,35	m
Span length	L	20,00	
Longitudinal eccentricity force from the support	a	9,40	m
Left sidewalk width	b_l	0,80	m
Right sidewalk width	b_r	0,55	m

Distributed and concentrated Live Loads

Line	Q_{ik} [KN]	q_{ik}[KN/m^2]
1	300,00	9,00
2	200,00	2,50
3	100,00	2,50
Others	0,00	2,50
Remaining part	0,00	2,50

Assumed longitudinal load distribution

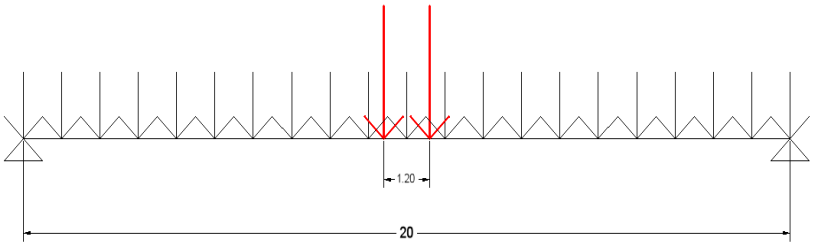

Figure A11. Assumed longitudinal load distribution (dimensions in m).

- **Acting moments at mid span due to Live Loads**

Concentrated loads		
$Q_{1k} + Q_{2k}$	500,00	KN
M_{Qk}	4700,00	KNm
Distributed loads		
$q_{1kl} = q_{1k}w_c$	27,00	KN/m
$q_{2kl} = q_{2k}w_c$	7,50	KN/m
$q_r = q_{rk}w_r$	8,38	KN/m
q_{tot}	42,88	KN/m
M_{qk}	2143,75	KNm
Total moment		
M_{ll}	6843,75	KNm

- **Global actions (DL+LL)**

Total bending moment acting on the mid span section	$M_{tot} = M_{dd} + M_{ll}$	15033,75	KNm
Load combination factor	φ	1,35	
Total moment with safety factor	M_{ftot}	20295,56	KNm
N° of beams	n	6,00	
Mean moment for each beam	$M_{sm} = \frac{M_{ftot}}{n}$	3382,59	KNm

Total tensile steel needed

$\boldsymbol{A_s}$	61100,00	KNm
$\boldsymbol{M_{Rd,new}}$	21150,00	KNm

A2.4.3 Existing section characteristics

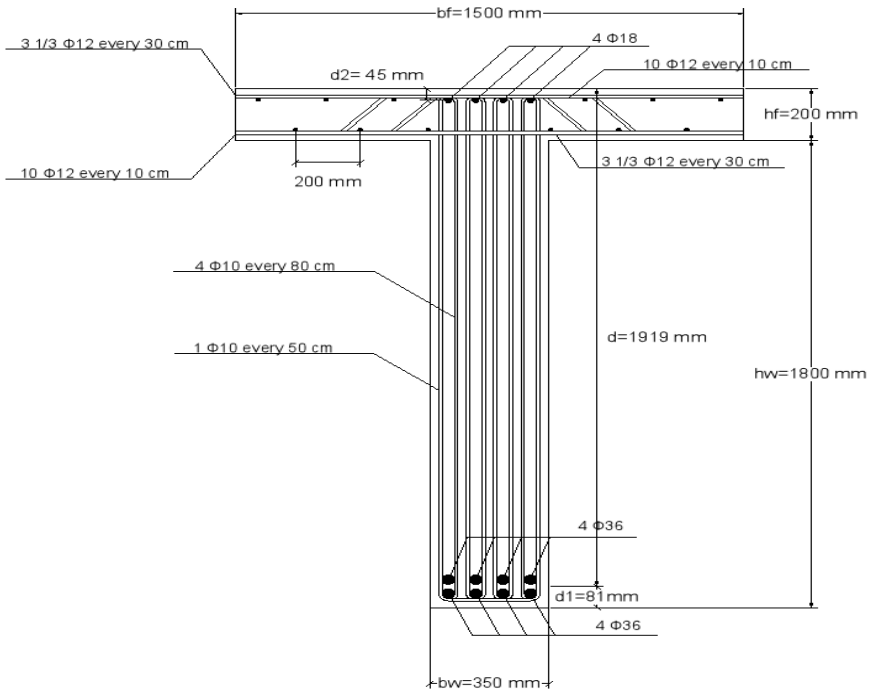

Figure A12. Cross-section of one of the girders.

Reinforcement and geometric characteristics

Depth of the web	h_w	1800,00	mm
Width of the web	b_w	350,00	mm
Depth of the flange	h_f	200,00	mm
Width of the flange	b_f	1500,00	mm
Total heigth	h	2000,00	mm
Effective depth	d	1919,00	mm
Distance from the bottom edge	d_1	81,00	mm
Distance from the upper edge	d_2	45,00	mm
Tensile steel	A_s	8133,33	mm^2
Tensile steel diameter	8Φ	36,00	mm
Compressive steel	$A_{s'}$	1016,67	mm^2
Compressive steel diameter	4Φ	18,00	mm

Resistance of the existing section

Resistant moment at mid span $M_{Rd,old}$	17208,00	KNm
Medium resistant moment at mid span $M_{Rdm,old}$	2868,00	KNm

A2.5 S10RC

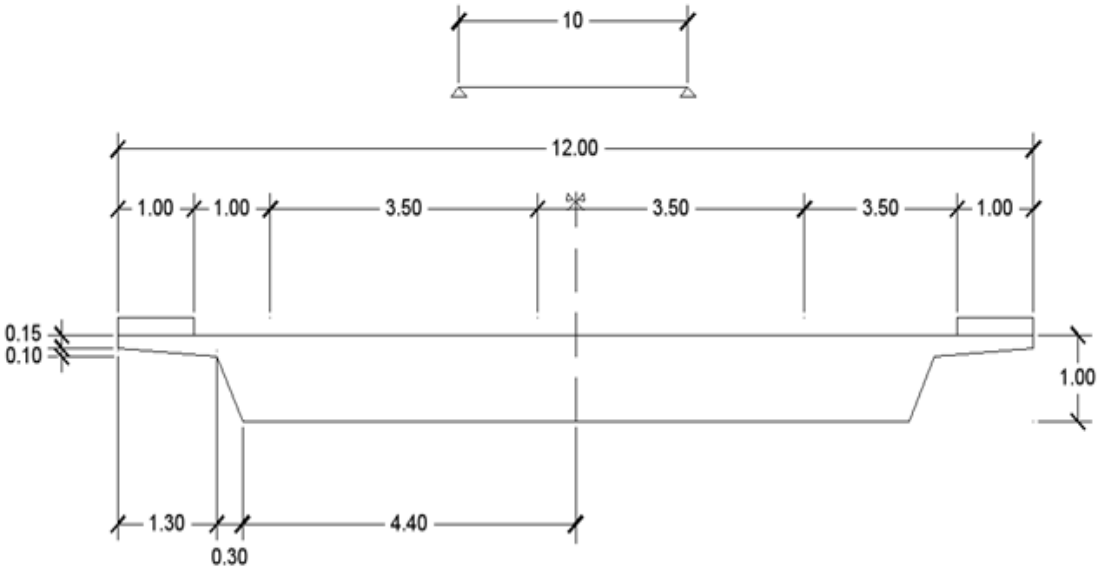

Figure A10. S10RC Cross-section (dimensions in m).

A2.5.1 Geometric characteristics

Cross-section	*Symbols*	*Values*	*Units*
Base thickness	t_s	0,15	m
Tot Bridge width	B	12,00	m
Carriageway width	l_c	10,00	m
Slab depth	h	0,85	m
Span lenght	L	10,00	m
Sidewalk height	h_s	0,20	m
Left sidewalk width	b_l	1,00	m
Right sidewalk width	b_r	1,00	m
Pavimentation heigth	t_p	0,08	m
Total area of the cross-section	A_{cs}	10,070	m^2

A.2.5.2 Loads according to the actual code (Eurocode)

Dead Loads (DL)

Loads	*Symbols*	*Values*	*Units*
Reinforced concrete	$q_{Rc} = A_s\rho$	251,75	KN/m
Pavimentation	$q_p = (t_p l_c)\rho_p$	16,00	KN/m
Guard Rail	q_g	3,00	KN/m
Total distributed dead load	q_{DLtot}	270,75	KN/m

- **Acting moment at mid span due to Dead Loads**

Moment at mid span	$M_{SdDL} = \frac{q_{DLtot}L^2}{8}$	3384,38	KNm

Live Loads (LL)

Geometrical assumptions	Symbols	Values	Units
Carriageway length	l_c	10,00> 6m	m
N° of conventional lines	$n_i = Int\left(\frac{l_c}{3}\right)$	3,33	
Width conv line	w_c	3,00	m
Remaining part length	$w_r = (l_c - w_c n_i) + bl + br$	3,00	m
Span length	L	10,00	m
Longitudinal eccentricity force from the support	a	4,40	m
Left sidewalk width	b_l	1,00	m
Right sidewalk width	b_r	1,00	m

Distributed and concentrated Live Loads

Line	Q_{ik} [KN]	q_{ik}[KN/m^2]
1	300,00	9,00
2	200,00	2,50
3	100,00	2,50
Others	0,00	2,50
Remaining part	0,00	2,50

Assumed longitudinal load distribution

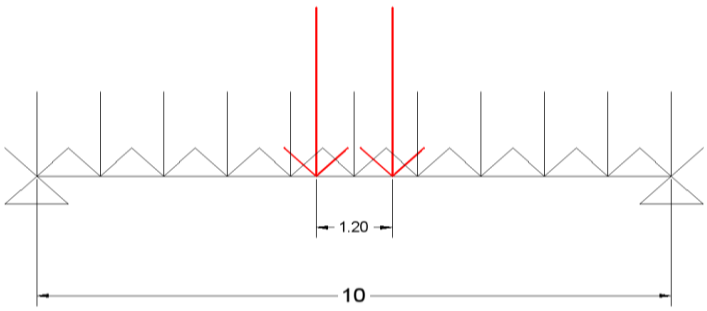

Figure A14. Assumed longitudinal load distribution (dimensions in m).

- **Acting moments at mid span due to Live Loads**

Concentrated loads		
$Q_{1k} + Q_{2k}$	600,00	KN
M_{Qk}	2640,00	KNm
Distributed loads		
$q_{1kl} = q_{1k} w_c$	27,00	KN/m
$q_{2kl} = q_{2k} w_c$	7,50	KN/m
$q_{3kl} = q_{3k} w_c$	7,50	KN/m
$q_r = q_{rk} w_r$	7,50	KN/m
q_{tot}	49,50	KN/m
M_{qk}	618,75	KNm
Total moment LL		
M_{ll}	3258,75	KNm

- **Global actions (DL+LL)**

Total bending moment acting on the mid span section	$M_{tot} = M_{dd} + M_{ll}$	6643,13	KNm
Load combination factor	φ	1,35	
Total moment multiplied for the safety factor	M_{ftot}	8968,22	KNm

Total tensile steel needed

$\boldsymbol{A_s}$	56548,00	mm^2
$\boldsymbol{M_{Rd,new}}$	9185,00	KNm

A2.5.3 Characteristics of the simplified "existing" section

A simplified T shape section is considered.

Depth of the web	h_w	800,00	mm
Width of the web	b_w	9000,00	mm
Depth of the flange	h_f	200,00	mm
Width of the flange	b_f	12000,00	mm
Total heigth	h	1000,00	mm
Effective depth	d	920,00	mm
Distance from the bottom edge	d_1	80,00	mm
Tensile steel	A_s	38872,00	mm^2
Tensile steel diameter	86Φ	24,00	mm

Resisting moment of the section

Resisting moment at mid span $M_{Rd,old}$	6519,00	KNm

A2.6 S1015RC

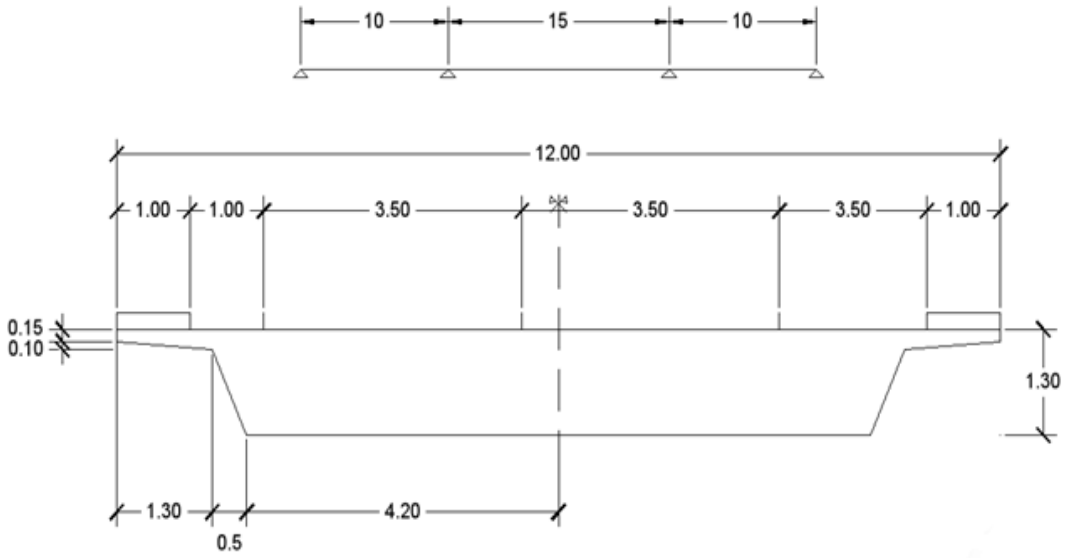

Figure A12. S1015RC Cross-section (dimensions in m).

A2.6.1 Geometric characteristics

Cross-section	*Symbols*	*Values*	*Units*
Base thickness	t_s	0,15	m
Tot Bridge width	B	12,00	m
Carriageway width	l_c	10,00	m
Slab depth	h	1,15	m
Span lenght	L	35,00	m
Sidewalk height	h_s	0,20	m
Left sidewalk width	b_l	1,00	m
Right sidewalk width	b_r	1,00	m
Total area of the cross-section	A_{cs}	12,65	m^2

A.2.6.2 Loads according to the actual code (Eurocode)

Dead Loads (DL)

Loads	*Symbols*	*Values*	*Units*
Reinforced concrete	$q_{Rc} = A_s\rho$	316,25	KN/m
Pavimentation	$q_p = (t_p l_c)\rho_p$	16,00	KN/m
Guard Rail	q_g	3,00	KN/m
Total distributed dead load	q_{DLtot}	335,25	KN/m

- **Acting moment at mid span due to Dead Loads**

Moment at mid span	$M_{SdDL} = \frac{q_{DLtot}L^2}{8}$	3788,00	KNm

Software FEM result (DL)

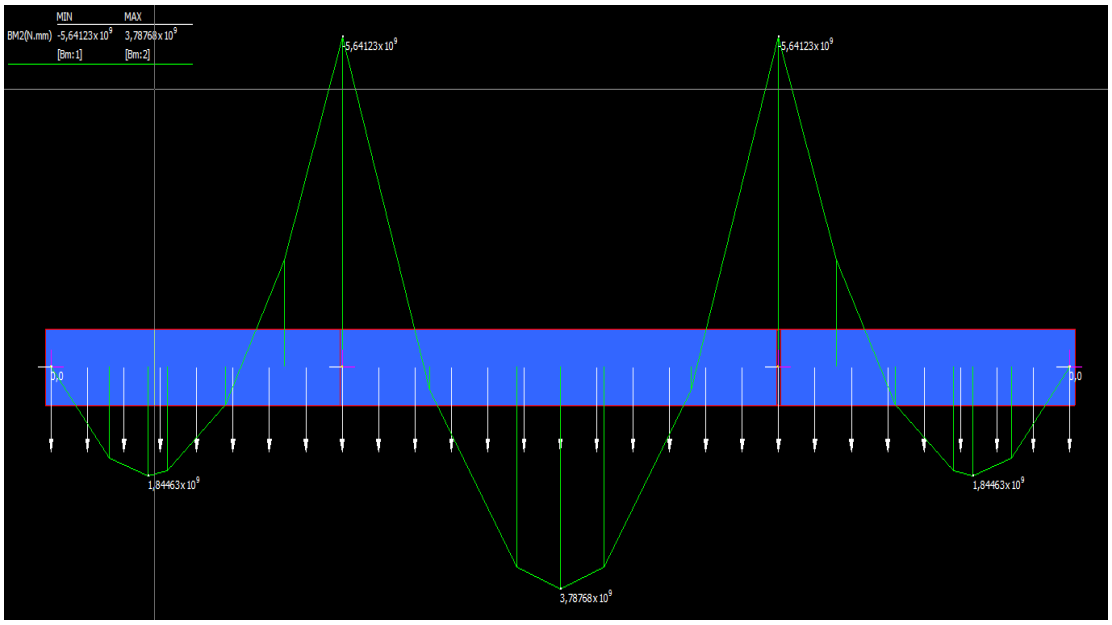

Figure A13. Acting moments due to the dead loads.

Live Loads (LL)

Geometrical assumptions	*Symbols*	*Values*	*Units*
Carriageway length	l_c	10,00> 6m	m
N° of conventional lines	$n_i = Int\left(\frac{l_c}{3}\right)$	3,33	
Width conv line	w_c	3,00	m
Remaining part length	$w_r = (l_c - w_c n_i) + bl + br$	3,00	m
Span length	L	15,00	m
Longitudinal eccentricity force from the support	a	6,90	m
Left sidewalk width	b_l	1,00	m
Right sidewalk width	b_r	1,00	m

Distributed and concentrated Live Loads

Line	**Q_{ik} [KN]**	**q_{ik}[KN/m^2]**
1	300,00	9,00
2	200,00	2,50
3	100,00	2,50
Others	0,00	2,50
Remaining part	0,00	2,50

Assumed longitudinal load distribution

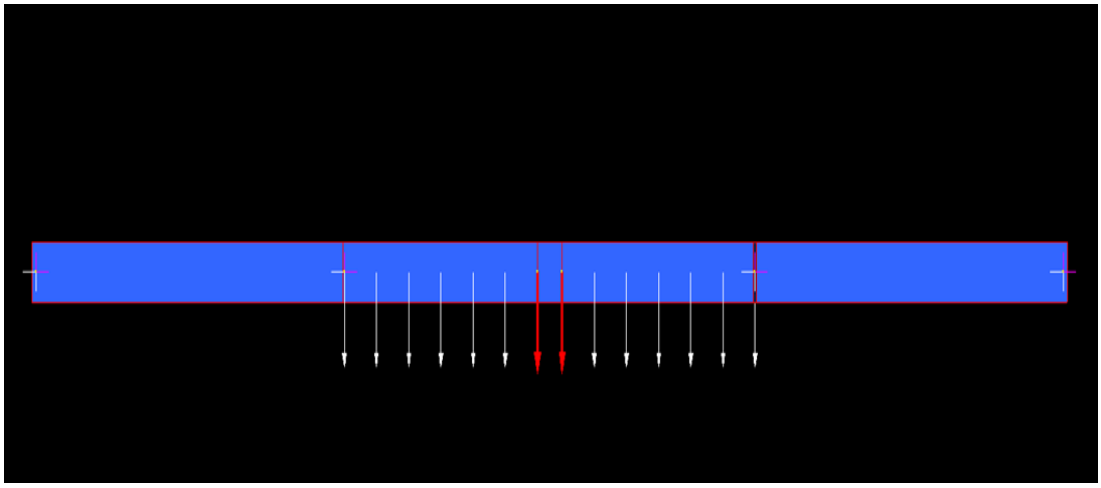

Figure A14. Assumed longitudinal live loads distribution.

- **Acting moments at mid span due to Live Loads**

Concentrated loads	*Values*	*Units*
$Q_{1k} + Q_{2k}$	600,00	KN
M_{Qk}	2592,00	KNm
Distributed loads		
$q_{1kl} = q_{1k} w_c$	27,00	KN/m
$q_{2kl} = q_{2k} w_c$	7,50	KN/m
$q_{3kl} = q_{3k} w_c$	7,50	KN/m
$q_r = q_{rk} w_r$	7,50	KN/m
q_{tot}	49,50	KN/m
M_{qk}	749,60	KNm
Total moment LL		
M_{ll}	3342,00	KNm

Software FEM results (LL)

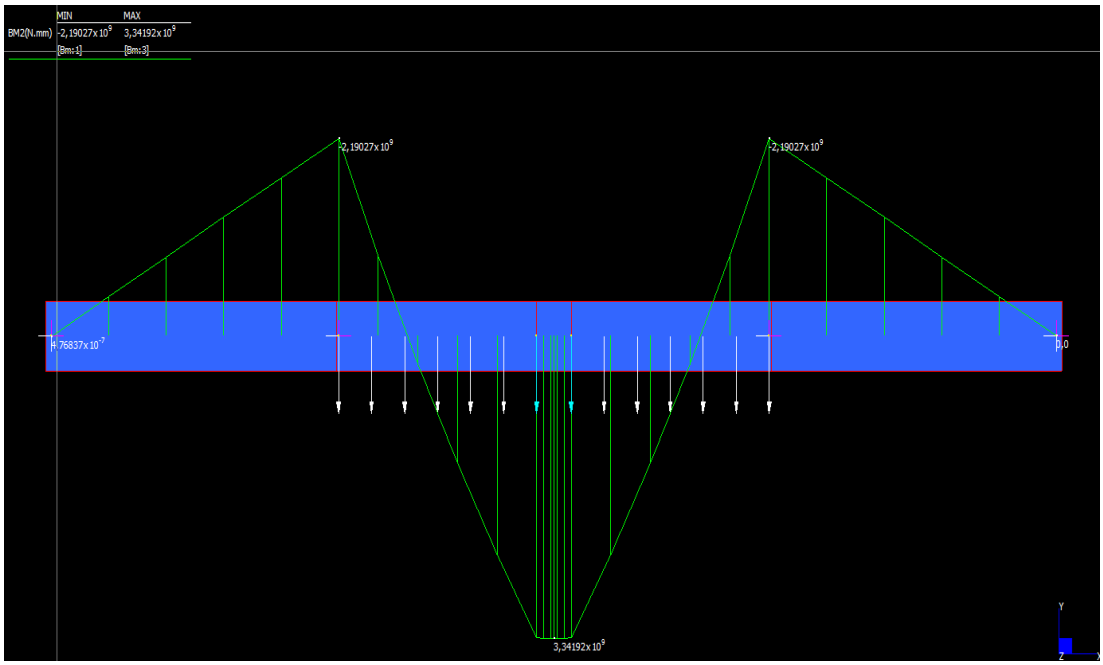

Figure A15. Acting moments due to the live loads.

- **Global actions (DL+LL)**

Total bending moment acting on the mid span section	$M_{tot} = M_{dd} + M_{ll}$	7130,00	KNm
Load combination factor	φ	1,35	
Total moment with safety factor	M_{ftot}	9625,50	KNm

A2.6.3 Characteristics of the simplified "existing" section

A simplified T shape section is considered.

Depth of the web	h_w	1100,00	mm
Width of the web	b_w	8900,00	mm
Depth of the flange	h_f	200,00	mm
Width of the flange	b_f	12000,00	mm
Total heigth	h	1300,00	mm
Effective depth	d	1217,00	mm
Distance from the bottom edge	d_1	83,00	mm
Tensile steel	A_s	30746,00	mm^2
Tensile steel diamter	69Φ	24,00	mm

Resisting moment of the section

Resisting moment at mid span $M_{Rd,old}$	6899,00	KNm

A2.7 S1520RC

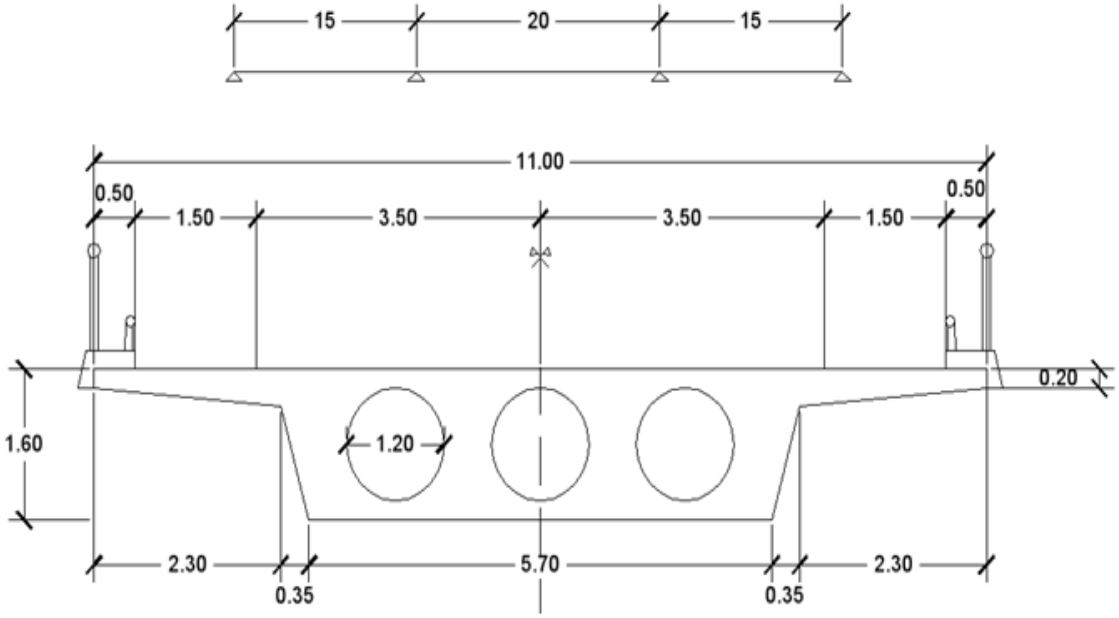

Figure A16. S1520RC Cross-section (dimensions in m).

A2.7.1 Geometric characteristics

Cross-section	*Symbols*	*Values*	*Units*
Base thickness	t_s	0,20	m
Tot Bridge width	B	11,00	m
Carriageway width	l_c	10,00	m
Slab depth	h	1,40	m
Span lenght	L	50,00	m
Sidewalk height	h_s	0,20	m
Left sidewalk width	b_l	0,50	m
Right sidewalk width	b_r	0,50	m
Total area of the cross-section	A_{cs}	8,14	m^2

A.2.7.2 Loads according to the actual code (Eurocode)

Dead Loads (DL)

Loads	*Symbols*	*Values*	*Units*
Reinforced concrete	$q_{Rc} = A_s\rho$	203,50	KN/m
Pavimentation	$q_p = (t_p l_c)\rho_p$	16,00	KN/m
Guard Rail	q_g	3,00	KN/m
Total distributed dead load	q_{DLtot}	222,50	KN/m

- **Acting moment at mid span due to Dead Loads**

Moment at mid span	$M_{SdDL} = \frac{q_{DLtot}L^2}{8}$	4150,000	KNm

Software FEM result (DL)

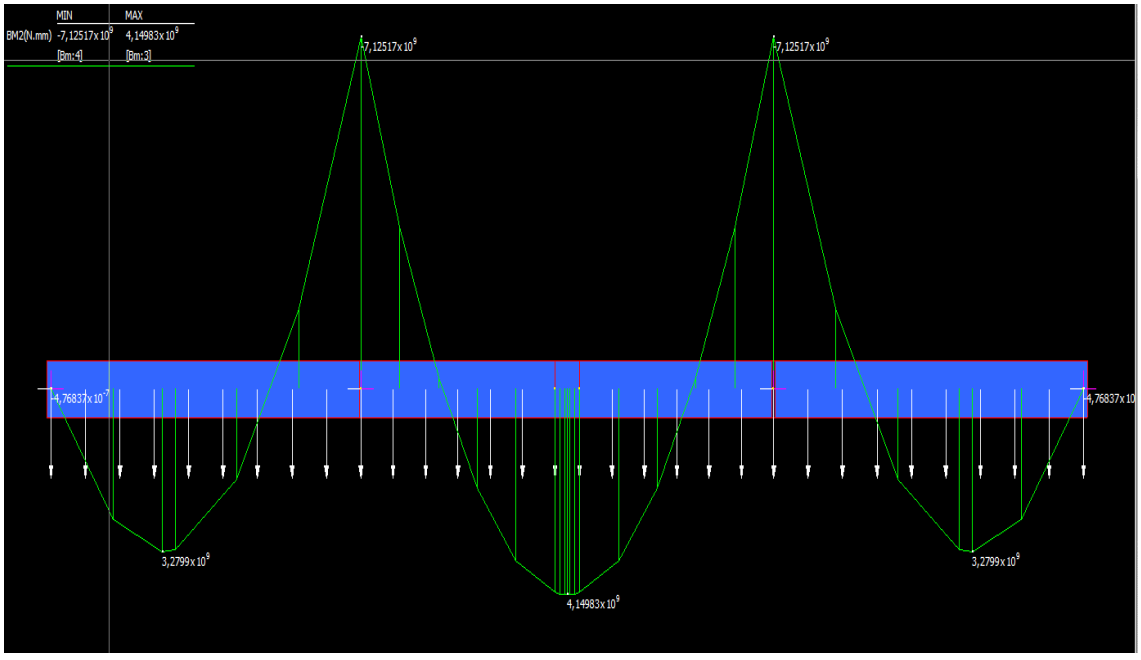

Figure A17. Acting moments due to the dead loads.

Live Loads (LL)

Geometrical assumptions	*Symbols*	*Values*	*Units*
Carriageway length	l_c	10,00> 6m	m
N° of conventional lines	$n_i = Int\left(\frac{l_c}{3}\right)$	3,33	
Width conv line	w_c	3,00	m
Remaining part length	$w_r = (l_c - w_c n_i) + bl + br$	2,00	m
Span length	L	15,00	m
Longitudinal eccentricity force from the support	a	6,90	m
Left sidewalk width	b_l	0,50	m
Right sidewalk width	b_r	0,50	m

Distributed and concentrated Live Loads

Line	**Q_{ik} [KN]**	**q_{ik}[KN/m^2]**
1	300,00	9,00
2	200,00	2,50
3	100,00	2,50
Others	0,00	2,50
Remaining part	0,00	2,50

Assumed longitudinal load distribution

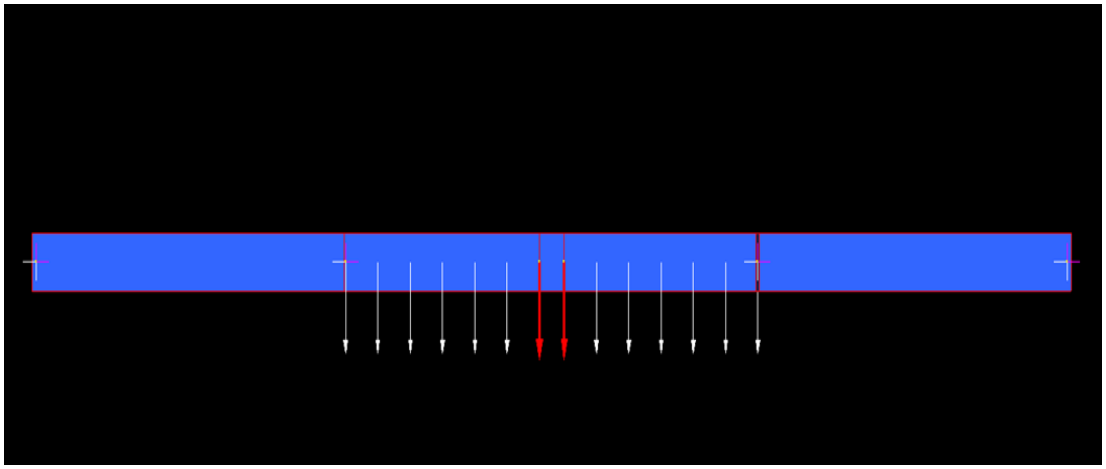

Figure A18. Assumed longitudinal live loads distribution.

- **Acting moments at mid span due to Live Loads**

Concentrated loads		
$Q_{1k} + Q_{2k}$	600,00	KN
M_{Qk}	3647,00	KNm
Distributed loads		
$q_{1kl} = q_{1k}w_c$	27,00	KN/m
$q_{2kl} = q_{2k}w_c$	7,50	KN/m
$q_{3kl} = q_{3k}w_c$	7,50	KN/m
$q_r = q_{rk}w_r$	5,00	KN/m
q_{tot}	47,00	KN/m
M_{qk}	1306,00	KNm
Total moment LL		
M_{ll}	4953,00	KNm

Software FEM results (LL)

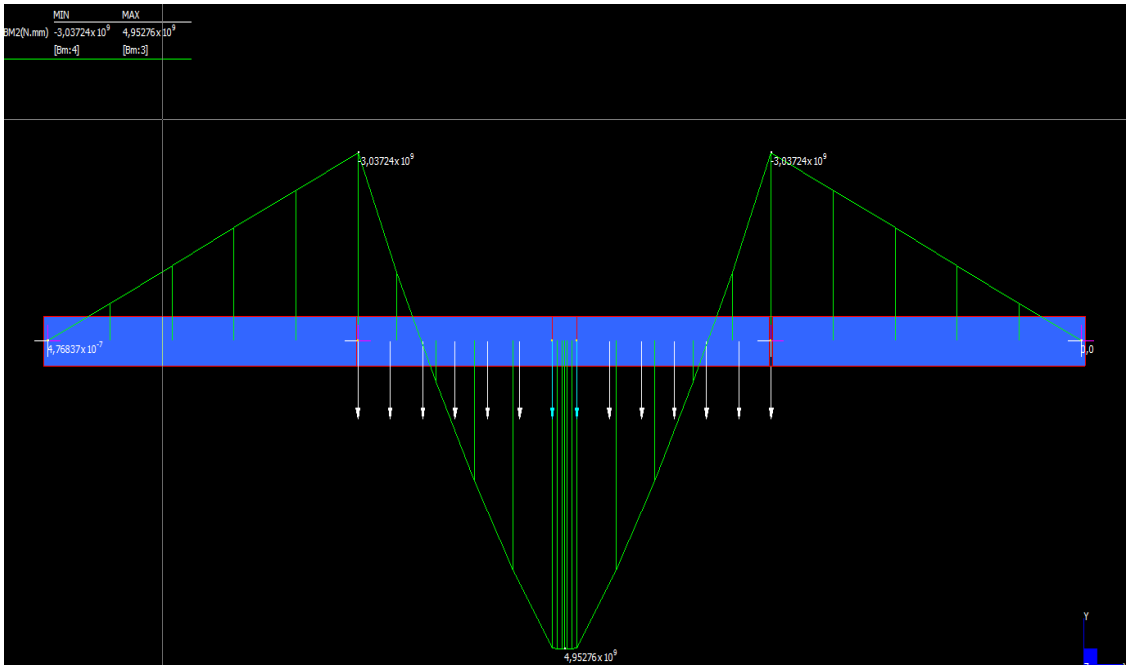

Figure A19. Acting moments due to the live loads.

- **Global actions (DL+LL)**

Total bending moment acting on the mid span section	$M_{tot} = M_{dd} + M_{ll}$	9103,00	KNm
Load combination factor	φ	1,35	
Total moment with safety factor	M_{ftot}	12289,05	KNm

A2.7.3 Characteristics of the simplified "existing" section

A simplified T shape section is considered.

Depth of the web	h_w	1350,00	mm
Width of the web	b_w	2450,00	mm
Depth of the flange	h_f	250,00	mm
Width of the flange	b_f	11000,00	mm
Total heigth	h	1600,00	mm
Effective depth	d	1516,00	mm
Distance from the bottom	d_1	84,00	mm
Tensile steel	A_s	33929,00	mm^2
Tensile steel diameter	75Φ	24,00	mm

Resisting moment of the section

Resisting moment at mid span $M_{Rd,old}$	9479,00	KNm

Annex B

Strengthening design with XTRACT

B. Results

The results obtained for the strengthening design with the software XTRACT are here shown for each bridge and CFRP system (precured and wet-lay up). Together with the Analysis Results given by the software in the so-called *Analysis Report*, the moment-curvature diagrams and the tensile steel and concrete strains are reported.

B.1 B10RC: $M_{sd} = 928,28\ KNm$

- **Prefabricated system:** $t_{frp} = 3,16\ mm$

Analysis Results:

Failing Material:	Fiber
Failure Strain:	1.470E-3 Tension
Curvature at Initial Load:	0 1/m
Curvature at First Yield:	-1.328E-3 1/m
Ultimate Curvature:	-1.888E-3 1/m
Moment at First Yield:	-831.1E+3 N-m
Ultimate Moment:	-931.5E+3 N-m
Centroid Strain at Yield:	.1886E-3 Ten
Centroid Strain at Ultimate:	.3252E-3 Ten
N.A. at First Yield:	-142.0 mm
N.A. at Ultimate:	-172.2 mm
Energy per Length:	1050 N
Effective Yield Curvature:	1.363E-3 1/m
Effective Yield Moment:	853.0E+3 N-m
Over Strength Factor:	-1.092
EI Effective:	6.26E+8 N-m^2
Yield EI Effective:	1.50E+8 N-m^2
Bilinear Harding Slope:	23.89 %
Curvature Ductility:	1.385

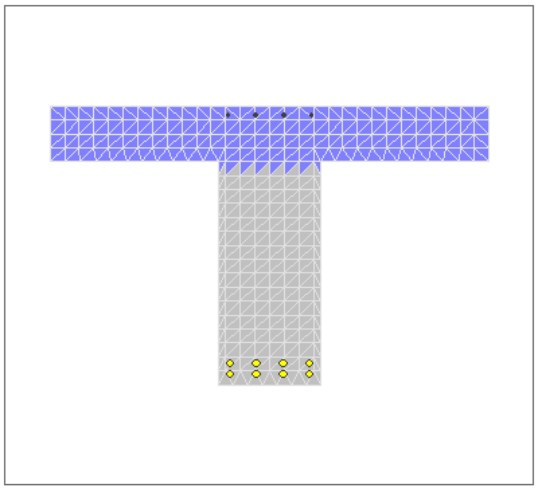

Figure B1. Analysis results and neutral axis position.

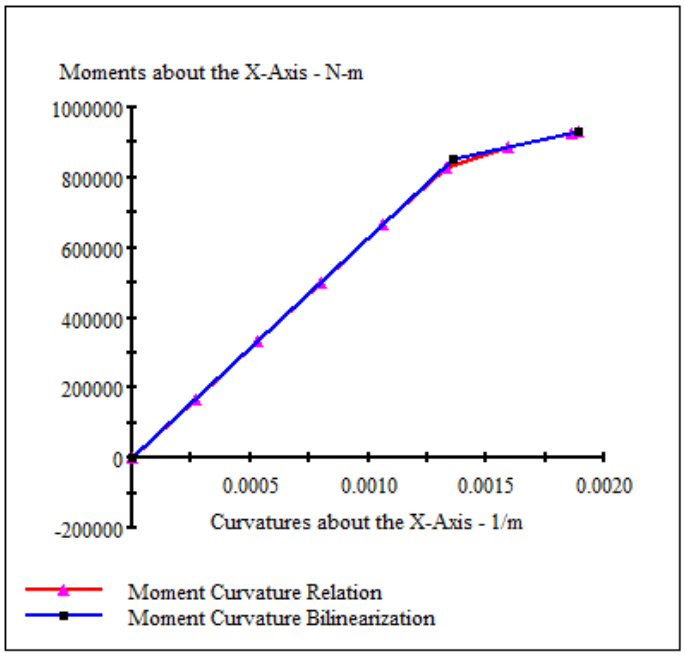

a)

Section	Section1
Loading	MC1
Units	strain
Data	
0	0
1	-60.47E-6
2	-.1227E-3
3	-.1853E-3
4	-.2497E-3
5	-.3152E-3
6	-.3536E-3
7	-.3870E-3
8	-.3909E-3

b)

Section	Section1
Loading	MC1
Units	strain
Data	
0	0
1	.1902E-3
2	.3787E-3
3	.5667E-3
4	.7530E-3
5	.9382E-3
6	1.150E-3
7	1.368E-3
8	1.392E-3

Figure B2. Moment-curvature diagram, minimum concrete strain (a) and maximum tensile steel strain (b).

- **<u>Wet-lay up system:</u>** $t_{frp} = 2,16\ mm$

Analysis Results:

Failing Material:	Fiber
Failure Strain:	1.480E-3 Tension
Curvature at Initial Load:	0 1/m
Curvature at First Yield:	-1.229E-3 1/m
Ultimate Curvature:	-1.901E-3 1/m
Moment at First Yield:	-807.3E+3 N-m
Ultimate Moment:	-929.5E+3 N-m
Centroid Strain at Yield:	.2115E-3 Ten
Centroid Strain at Ultimate:	.3287E-3 Ten
N.A. at First Yield:	-172.2 mm
N.A. at Ultimate:	-172.9 mm
Energy per Length:	1059 N
Effective Yield Curvature:	1.097E-3 1/m
Effective Yield Moment:	721.1E+3 N-m
Over Strength Factor:	-1.289
EI Effective:	6.57E+8 N-m^2
Yield EI Effective:	2.59E+8 N-m^2
Bilinear Harding Slope:	39.48 %
Curvature Ductility:	1.732

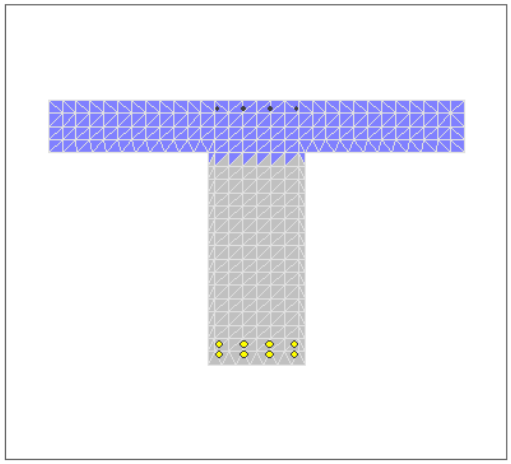

Figure B3. Analysis results and neutral axis position.

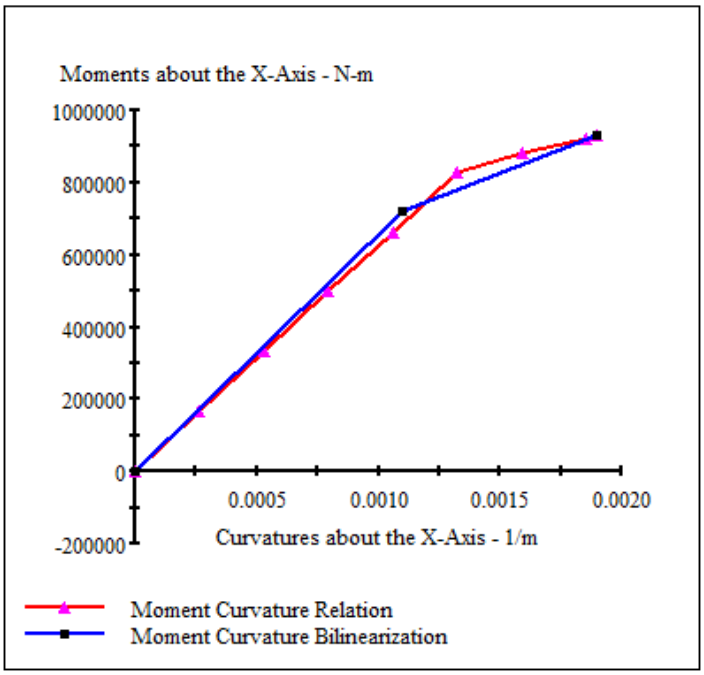

a)

Section	Section2
Loading	MC2
Units	strain
Data	
0	0
1	-61.56E-6
2	-.1229E-3
3	-.1849E-3
4	-.2492E-3
5	-.3146E-3
6	-.3534E-3
7	-.3864E-3
8	-.3916E-3

b)

Section	Section2
Loading	MC2
Units	strain
Data	
0	0
1	.1890E-3
2	.3783E-3
3	.5669E-3
4	.7532E-3
5	.9384E-3
6	1.150E-3
7	1.368E-3
8	1.403E-3

Figure B4. Moment-curvature diagram, minimum concrete strain (a) and maximum tensile steel strain (b).

B.2 B12RC: $M_{sd} = 1274,43\ KNm$

- **Prefabricated system: $t_{frp} = 3,37\ mm$**

Analysis Results:

Failing Material:	Fiber
Failure Strain:	1.424E-3 Tension
Curvature at Initial Load:	0 1/m
Curvature at First Yield:	-1.016E-3 1/m
Ultimate Curvature:	-1.525E-3 1/m
Moment at First Yield:	-1.129E+6 N-m
Ultimate Moment:	-1.275E+6 N-m
Centroid Strain at Yield:	.2255E-3 Ten
Centroid Strain at Ultimate:	.3336E-3 Ten
N.A. at First Yield:	-221.9 mm
N.A. at Ultimate:	-218.7 mm
Energy per Length:	1155 N
Effective Yield Curvature:	.8718E-3 1/m
Effective Yield Moment:	968.5E+3 N-m
Over Strength Factor:	-1.316
EI Effective:	1.11E+9 N-m^2
Yield EI Effective:	4.69E+8 N-m^2
Bilinear Harding Slope:	42.19 %
Curvature Ductility:	1.749

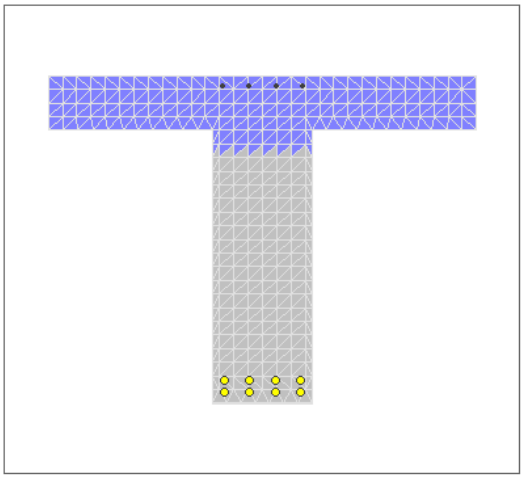

Figure B5. Analysis results and neutral axis position.

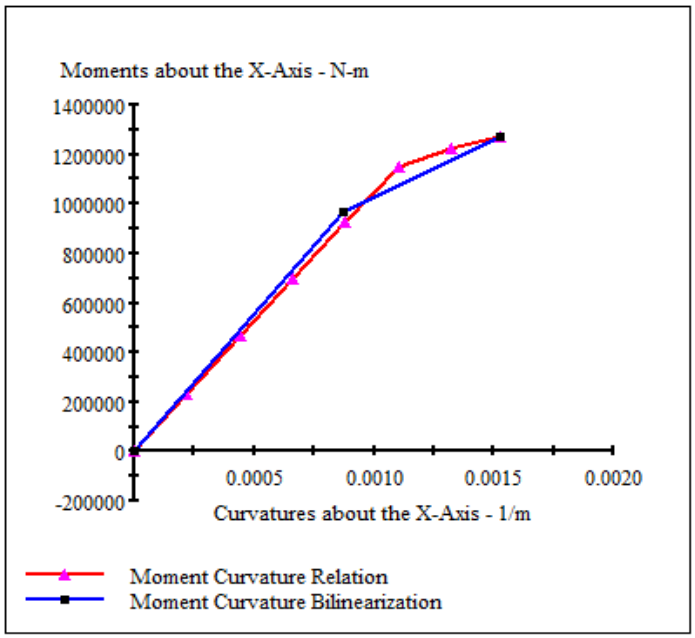

a)

Section	Section1
Loading	MC1
Units	strain
Data	
0	0
1	-62.01E-6
2	-.1243E-3
3	-.1875E-3
4	-.2527E-3
5	-.3190E-3
6	-.3550E-3
7	-.3842E-3

b)

Section	Section1
Loading	MC1
Units	strain
Data	
0	0
1	.1895E-3
2	.3788E-3
3	.5671E-3
4	.7535E-3
5	.9387E-3
6	1.154E-3
7	1.357E-3

Figure B6. Moment-curvature diagram, minimum concrete strain (a) and maximum tensile steel strain (b).

- **Wet-lay up system: $t_{frp} = 2,34\ mm$**

Analysis Results:

Failing Material:	Fiber
Failure Strain:	1.430E-3 Tension
Curvature at Initial Load:	0 1/m
Curvature at First Yield:	-1.015E-3 1/m
Ultimate Curvature:	-1.533E-3 1/m
Moment at First Yield:	-1.127E+6 N-m
Ultimate Moment:	-1.277E+6 N-m
Centroid Strain at Yield:	.2259E-3 Ten
Centroid Strain at Ultimate:	.3352E-3 Ten
N.A. at First Yield:	-222.5 mm
N.A. at Ultimate:	-218.7 mm
Energy per Length:	1164 N
Effective Yield Curvature:	.8739E-3 1/m
Effective Yield Moment:	970.2E+3 N-m
Over Strength Factor:	-1.317
EI Effective:	1.11E+9 N-m^2
Yield EI Effective:	4.66E+8 N-m^2
Bilinear Harding Slope:	41.98 %
Curvature Ductility:	1.754

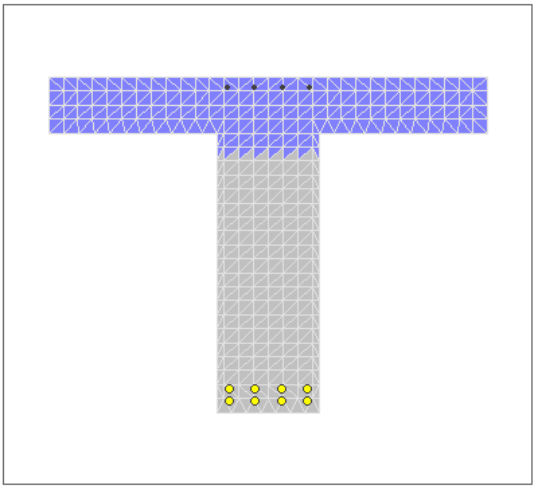

Figure B7. Analysis results and neutral axis position.

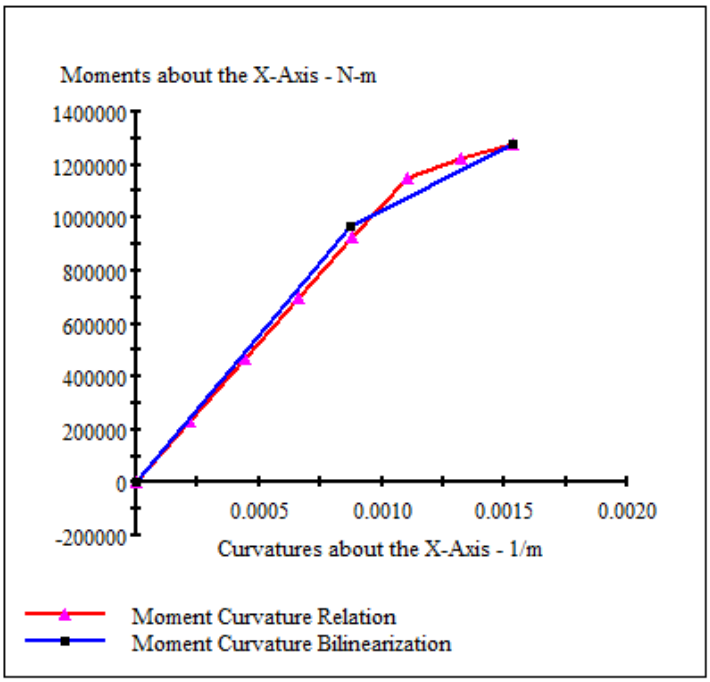

a)

Section	Section2
Loading	MC2
Units	strain
Data	
0	0
1	-61.83E-6
2	-.1241E-3
3	-.1875E-3
4	-.2527E-3
5	-.3192E-3
6	-.3551E-3
7	-.3862E-3

b)

Section	Section2
Loading	MC2
Units	strain
Data	
0	0
1	.1897E-3
2	.3790E-3
3	.5672E-3
4	.7535E-3
5	.9385E-3
6	1.154E-3
7	1.363E-3

Figure B8. Moment-curvature diagram, minimum concrete strain (a) and maximum tensile steel strain (b).

B.3 B16RC: $M_{sd} = 2169,36\ KNm$

- **Prefabricated system: $t_{frp} = 4,25\ mm$**

Analysis Results:

Failing Material:	Fiber
Failure Strain:	1.270E-3 Tension
Curvature at Initial Load:	0 1/m
Curvature at First Yield:	-.7677E-3 1/m
Ultimate Curvature:	-1.052E-3 1/m
Moment at First Yield:	-1.992E+6 N-m
Ultimate Moment:	-2.170E+6 N-m
Centroid Strain at Yield:	.2403E-3 Ten
Centroid Strain at Ultimate:	.3049E-3 Ten
N.A. at First Yield:	-313.0 mm
N.A. at Ultimate:	-289.9 mm
Energy per Length:	1301 N
Effective Yield Curvature:	.5734E-3 1/m
Effective Yield Moment:	1.487E+6 N-m
Over Strength Factor:	-1.459
EI Effective:	2.59E+9 N-m^2
Yield EI Effective:	1.43E+9 N-m^2
Bilinear Harding Slope:	55.01 %
Curvature Ductility:	1.834

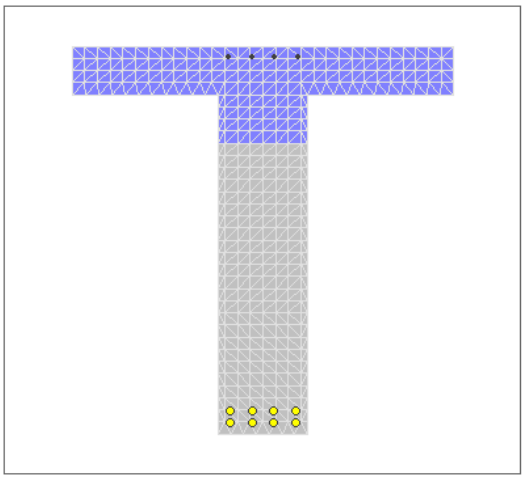

Figure B9. Analysis results and neutral axis position.

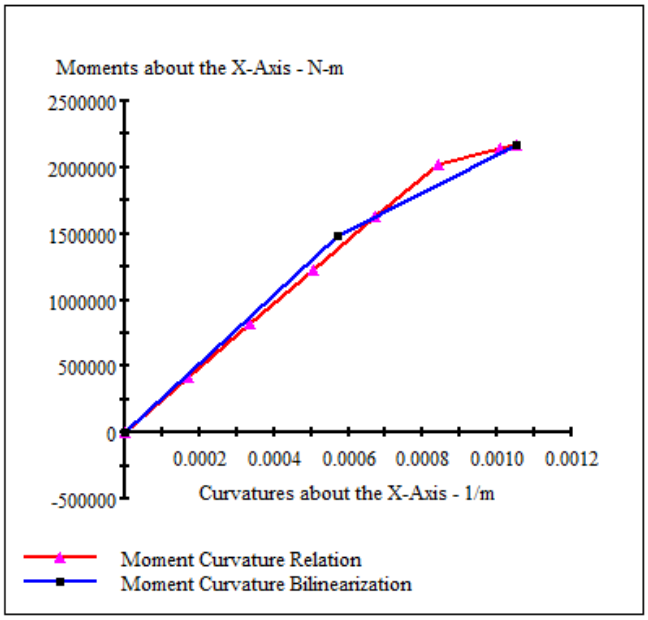

a)

Section	Section1
Loading	MC1
Units	strain
Data	
0	0
1	-67.77E-6
2	-.1365E-3
3	-.2061E-3
4	-.2778E-3
5	-.3524E-3
6	-.3896E-3
7	-.3980E-3

b)

Section	Section1
Loading	MC1
Units	strain
Data	
0	0
1	.1905E-3
2	.3799E-3
3	.5686E-3
4	.7551E-3
5	.9387E-3
6	1.160E-3
7	1.217E-3

Figure B10. Moment-curvature diagram, minimum concrete strain (a) and maximum tensile steel strain (b).

- **Wet-lay up system: $t_{frp} = 2,92\ mm$**

Analysis Results:

Failing Material:	Fiber
Failure Strain:	1.276E-3 Tension
Curvature at Initial Load:	0 1/m
Curvature at First Yield:	-.7685E-3 1/m
Ultimate Curvature:	-1.057E-3 1/m
Moment at First Yield:	-2.005E+6 N-m
Ultimate Moment:	-2.173E+6 N-m
Centroid Strain at Yield:	.2398E-3 Ten
Centroid Strain at Ultimate:	.3070E-3 Ten
N.A. at First Yield:	-312.1 mm
N.A. at Ultimate:	-290.5 mm
Energy per Length:	1312 N
Effective Yield Curvature:	.5614E-3 1/m
Effective Yield Moment:	1.465E+6 N-m
Over Strength Factor:	-1.484
EI Effective:	2.61E+9 N-m^2
Yield EI Effective:	1.43E+9 N-m^2
Bilinear Harding Slope:	54.80 %
Curvature Ductility:	1.882

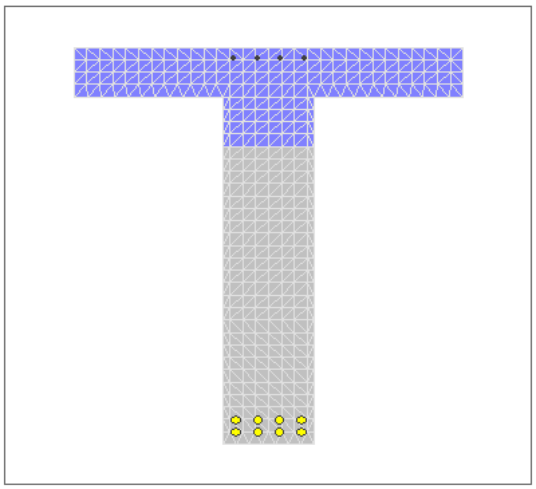

Figure B11. Analysis results and neutral axis position.

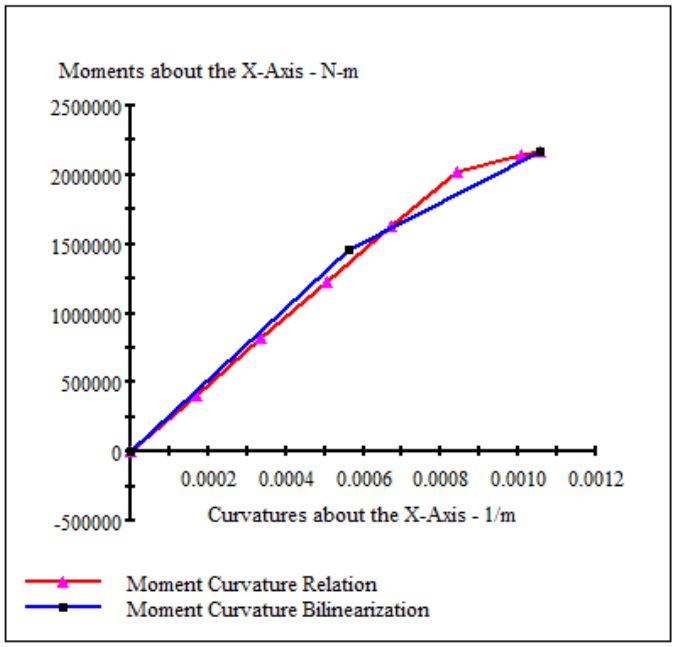

a)

Section	Section2
Loading	MC2
Units	strain
Data	
0	0
1	-67.55E-6
2	-.1364E-3
3	-.2069E-3
4	-.2778E-3
5	-.3520E-3
6	-.3902E-3
7	-.3994E-3

b)

Section	Section2
Loading	MC2
Units	strain
Data	
0	0
1	.1907E-3
2	.3800E-3
3	.5677E-3
4	.7551E-3
5	.9390E-3
6	1.159E-3
7	1.223E-3

Figure B12. Moment-curvature diagram, minimum concrete strain (a) and maximum tensile steel strain (b).

B.4 B20RC: $M_{sd} = 3382,59\ KNm$

- **<u>Prefabricated system:</u>** $t_{frp} = 6,12\ mm$

Analysis Results:

Failing Material:	Fiber
Failure Strain:	1.056E-3 Tension
Curvature at Initial Load:	0 1/m
Curvature at First Yield:	-.6948E-3 1/m
Ultimate Curvature:	-.7420E-3 1/m
Moment at First Yield:	-3.296E+6 N-m
Ultimate Moment:	-3.386E+6 N-m
Centroid Strain at Yield:	.2090E-3 Ten
Centroid Strain at Ultimate:	.2338E-3 Ten
N.A. at First Yield:	-300.8 mm
N.A. at Ultimate:	-315.1 mm
Energy per Length:	1321 N
Effective Yield Curvature:	.9678E-3 1/m
Effective Yield Moment:	4.591E+6 N-m
Over Strength Factor:	-.7375
EI Effective:	4.74E+9 N-m^2
Yield EI Effective:	5.34E+9 N-m^2
Bilinear Harding Slope:	112.5 %
Curvature Ductility:	.7667

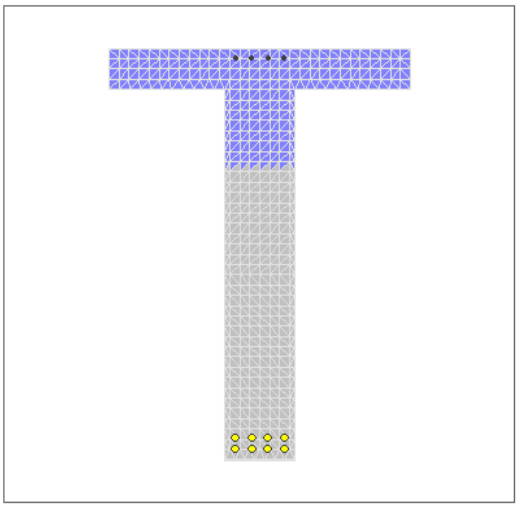

Figure B13. Analysis results and neutral axis position.

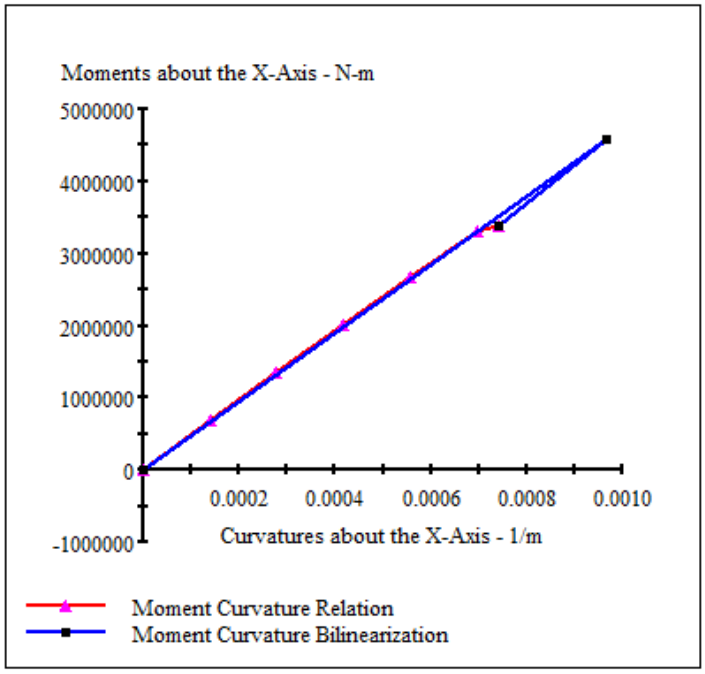

a)

Section	Section1
Loading	Moment
Units	strain
Data	
0	0
1	-77.03E-6
2	-.1554E-3
3	-.2351E-3
4	-.3173E-3
5	-.4040E-3
6	-.4187E-3

b)

Section	Section1
Loading	Moment
Units	strain
Data	
0	0
1	.1915E-3
2	.3817E-3
3	.5706E-3
4	.7570E-3
5	.9389E-3
6	1.013E-3

Figure B14. Moment-curvature diagram, minimum concrete strain (a) and maximum tensile steel strain (b).

- **Wet-lay up system:** $t_{frp} = 4,25\ mm$

Analysis Results:

Failing Material:	Fiber
Failure Strain:	1.057E-3 Tension
Curvature at Initial Load:	0 1/m
Curvature at First Yield:	-.7013E-3 1/m
Ultimate Curvature:	-.7430E-3 1/m
Moment at First Yield:	-3.649E+6 N-m
Ultimate Moment:	-3.384E+6 N-m
Centroid Strain at Yield:	.3017E-3 Ten
Centroid Strain at Ultimate:	.2345E-3 Ten
N.A. at First Yield:	-430.2 mm
N.A. at Ultimate:	-315.6 mm
Energy per Length:	1323 N
Effective Yield Curvature:	.2740E-3 1/m
Effective Yield Moment:	1.426E+6 N-m
Over Strength Factor:	-2.373
EI Effective:	5.20E+9 N-m^2
Yield EI Effective:	4.18E+9 N-m^2
Bilinear Harding Slope:	80.24 %
Curvature Ductility:	2.711

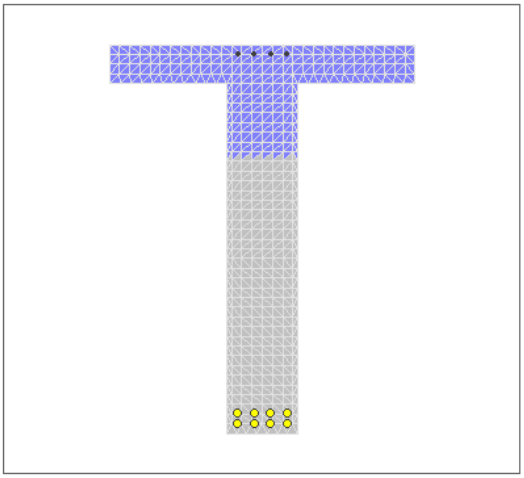

Figure B15. Analysis results and neutral axis position.

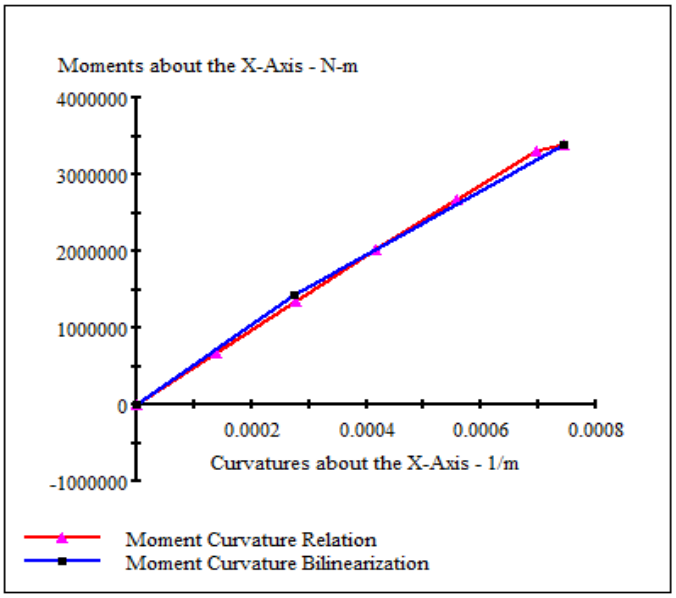

a)

Section	Section2
Loading	Moment 2
Units	strain
Data	
0	0
1	-76.96E-6
2	-.1553E-3
3	-.2349E-3
4	-.3176E-3
5	-.4033E-3
6	-.4187E-3

b)

Section	Section2
Loading	Moment 2
Units	strain
Data	
0	0
1	.1916E-3
2	.3818E-3
3	.5707E-3
4	.7565E-3
5	.9394E-3
6	1.015E-3

Figure B16. Moment-curvature diagram, minimum concrete strain (a) and maximum tensile steel strain (b).

B.5 S10RC: $M_{sd} = 8968,22\ KNm$

- **Prefabricated system: $t_{frp} = 3,48\ mm$**

Analysis Results:

Failing Material:	Fiber
Failure Strain:	1.427E-3 Tension
Curvature at Initial Load:	0 1/m
Curvature at First Yield:	-1.452E-3 1/m
Ultimate Curvature:	-1.910E-3 1/m
Moment at First Yield:	-8.131E+6 N-m
Ultimate Moment:	-8.971E+6 N-m
Centroid Strain at Yield:	.3261E-3 Ten
Centroid Strain at Ultimate:	.4711E-3 Ten
N.A. at First Yield:	-224.5 mm
N.A. at Ultimate:	-246.6 mm
Energy per Length:	9855 N
Effective Yield Curvature:	1.495E-3 1/m
Effective Yield Moment:	8.370E+6 N-m
Over Strength Factor:	-1.072
EI Effective:	5.60E+9 N-m^2
Yield EI Effective:	1.45E+9 N-m^2
Bilinear Harding Slope:	25.85 %
Curvature Ductility:	1.278

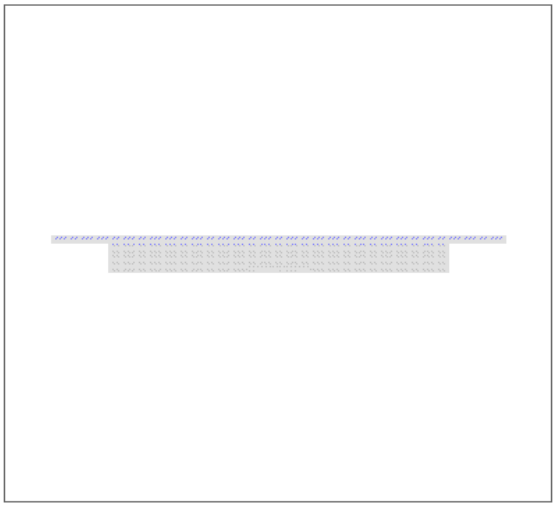

Figure B17. Analysis results and neutral axis position.

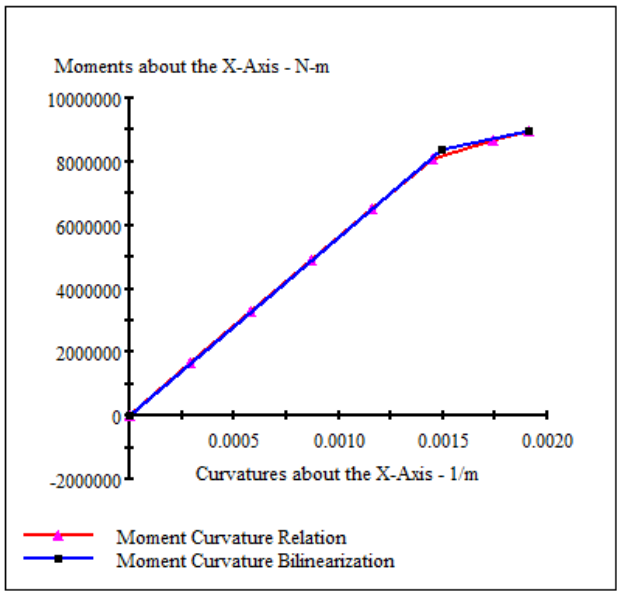

a)

Section	Section3
Loading	mc3
Units	strain
Data	
0	0
1	-68.43E-6
2	-.1376E-3
3	-.2081E-3
4	-.2801E-3
5	-.3538E-3
6	-.3992E-3
7	-.4238E-3

b)

Section	Section3
Loading	mc3
Units	strain
Data	
0	0
1	.1901E-3
2	.3795E-3
3	.5676E-3
4	.7542E-3
5	.9391E-3
6	1.152E-3
7	1.277E-3

Figure B18. Moment-curvature diagram, minimum concrete strain (a) and maximum tensile steel strain (b).

- **<u>Wet-lay up system:</u>** $t_{frp} = 2,43\ mm$

Analysis Results:

Failing Material:	Fiber
Failure Strain:	1.424E-3 Tension
Curvature at Initial Load:	0 1/m
Curvature at First Yield:	-1.452E-3 1/m
Ultimate Curvature:	-1.908E-3 1/m
Moment at First Yield:	-8.131E+6 N-m
Ultimate Moment:	-8.974E+6 N-m
Centroid Strain at Yield:	.3261E-3 Ten
Centroid Strain at Ultimate:	.4704E-3 Ten
N.A. at First Yield:	-224.5 mm
N.A. at Ultimate:	-246.5 mm
Energy per Length:	9844 N
Effective Yield Curvature:	1.499E-3 1/m
Effective Yield Moment:	8.392E+6 N-m
Over Strength Factor:	-1.069
EI Effective:	5.60E+9 N-m^2
Yield EI Effective:	1.42E+9 N-m^2
Bilinear Harding Slope:	25.38 %
Curvature Ductility:	1.273

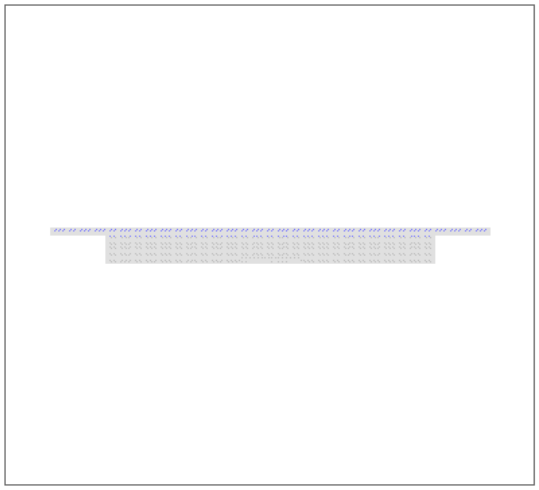

Figure B19. Analysis results and neutral axis position.

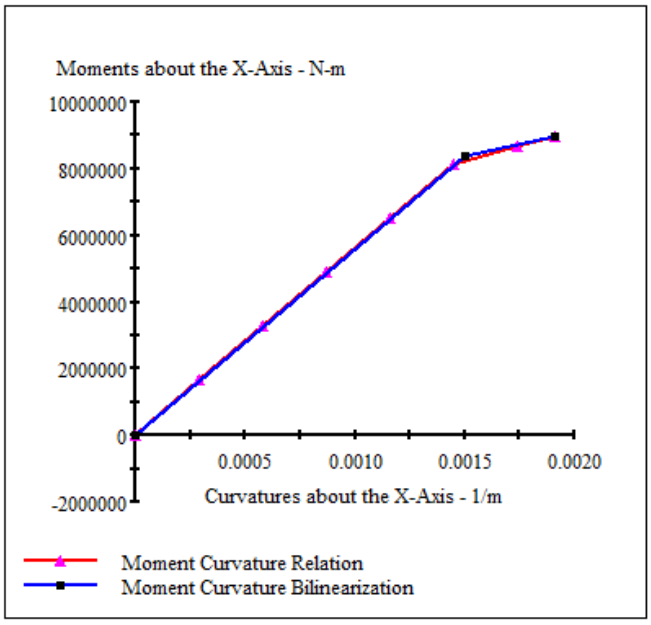

a)

Section	Section3
Loading	mc3
Units	strain
Data	
0	0
1	-68.41E-6
2	-.1376E-3
3	-.2081E-3
4	-.2802E-3
5	-.3539E-3
6	-.3993E-3
7	-.4237E-3

b)

Section	Section3
Loading	mc3
Units	strain
Data	
0	0
1	.1902E-3
2	.3795E-3
3	.5676E-3
4	.7542E-3
5	.9390E-3
6	1.152E-3
7	1.276E-3

Figure B20. Moment-curvature diagram, minimum concrete strain (a) and maximum tensile steel strain (b).

B.6 S1015RC: $M_{sd} = 9625,50\ KNm$

- **Prefabricated system:** $t_{frp} = 2,65\ mm$

Analysis Results:

Failing Material:	Fiber
Failure Strain:	1.661E-3 Tension
Curvature at Initial Load:	0 1/m
Curvature at First Yield:	-.9817E-3 1/m
Ultimate Curvature:	-1.572E-3 1/m
Moment at First Yield:	-7.927E+6 N-m
Ultimate Moment:	-9.629E+6 N-m
Centroid Strain at Yield:	.3550E-3 Ten
Centroid Strain at Ultimate:	.6268E-3 Ten
N.A. at First Yield:	-361.7 mm
N.A. at Ultimate:	-398.7 mm
Energy per Length:	9307 N
Effective Yield Curvature:	1.134E-3 1/m
Effective Yield Moment:	9.156E+6 N-m
Over Strength Factor:	-1.052
EI Effective:	8.08E+9 N-m^2
Yield EI Effective:	1.08E+9 N-m^2
Bilinear Harding Slope:	13.38 %
Curvature Ductility:	1.387

Figure B21. Analysis results.

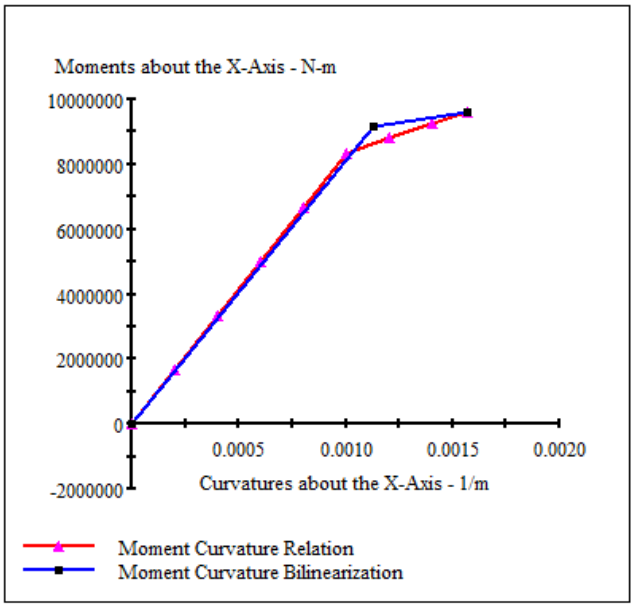

Figure B22. Moment-curvature diagram, minimum concrete strain (a) and maximum tensile steel strain (b).

a)

Section	Section3
Loading	mc3
Units	strain
Data	
0	0
1	-53.03E-6
2	-.1065E-3
3	-.1606E-3
4	-.2153E-3
5	-.2709E-3
6	-.3035E-3
7	-.3340E-3
8	-.3593E-3

b)

Section	Section3
Loading	mc3
Units	strain
Data	
0	0
1	.1889E-3
2	.3774E-3
3	.5654E-3
4	.7527E-3
5	.9390E-3
6	1.148E-3
7	1.360E-3
8	1.534E-3

- **<u>Wet-lay up system:</u>** $t_{frp} = 1,85\ mm$

Analysis Results:

Failing Material:	Fiber
Failure Strain:	1.657E-3 Tension
Curvature at Initial Load:	0 1/m
Curvature at First Yield:	-.9817E-3 1/m
Ultimate Curvature:	-1.570E-3 1/m
Moment at First Yield:	-7.927E+6 N-m
Ultimate Moment:	-9.634E+6 N-m
Centroid Strain at Yield:	.3550E-3 Ten
Centroid Strain at Ultimate:	.6253E-3 Ten
N.A. at First Yield:	-361.7 mm
N.A. at Ultimate:	-398.4 mm
Energy per Length:	9288 N
Effective Yield Curvature:	1.136E-3 1/m
Effective Yield Moment:	9.175E+6 N-m
Over Strength Factor:	-1.050
EI Effective:	8.08E+9 N-m^2
Yield EI Effective:	1.06E+9 N-m^2
Bilinear Harding Slope:	13.11 %
Curvature Ductility:	1.381

Figure B23. Analysis results.

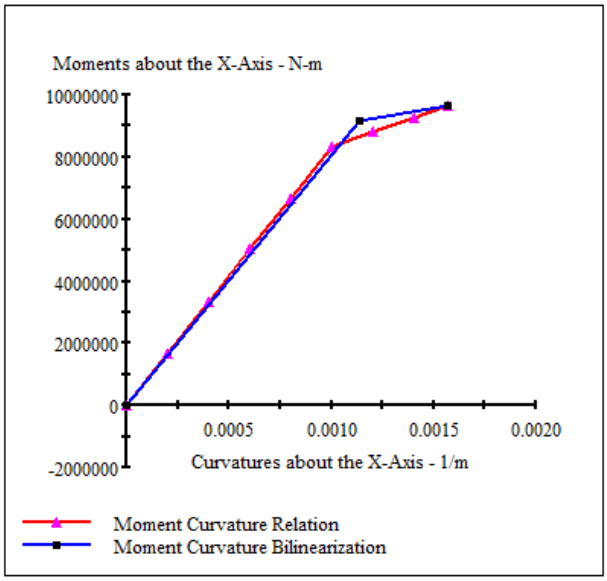

a)

Section	Section3
Loading	mc3
Units	strain
Data	
0	0
1	-53.02E-6
2	-.1065E-3
3	-.1606E-3
4	-.2154E-3
5	-.2710E-3
6	-.3036E-3
7	-.3342E-3
8	-.3592E-3

b)

Section	Section3
Loading	mc3
Units	strain
Data	
0	0
1	.1890E-3
2	.3775E-3
3	.5654E-3
4	.7526E-3
5	.9390E-3
6	1.148E-3
7	1.360E-3
8	1.531E-3

Figure B24. Moment-curvature diagram, minimum concrete strain (a) and maximum tensile steel strain (b).

B.6 S1520RC: $M_{sd} = 12289,05\ KNm$

- **Prefabricated system:** $t_{frp} = 4,90\ mm$

Analysis Results:

Failing Material:	Fiber
Failure Strain:	1.181E-3 Tension
Curvature at Initial Load:	0 1/m
Curvature at First Yield:	-.8148E-3 1/m
Ultimate Curvature:	-.9375E-3 1/m
Moment at First Yield:	-11.96E+6 N-m
Ultimate Moment:	-12.29E+6 N-m
Centroid Strain at Yield:	.2210E-3 Ten
Centroid Strain at Ultimate:	.2756E-3 Ten
N.A. at First Yield:	-271.3 mm
N.A. at Ultimate:	-294.0 mm
Energy per Length:	6297 N
Effective Yield Curvature:	.7277E-3 1/m
Effective Yield Moment:	1.07E+7 N-m
Over Strength Factor:	-1.150
EI Effective:	1.47E+10 N-m^2
Yield EI Effective:	7.64E+9 N-m^2
Bilinear Harding Slope:	52.01 %
Curvature Ductility:	1.288

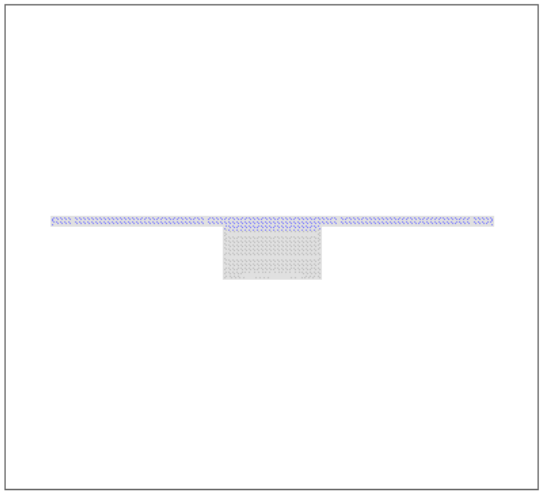

Figure B25. Analysis results and neutral axis position.

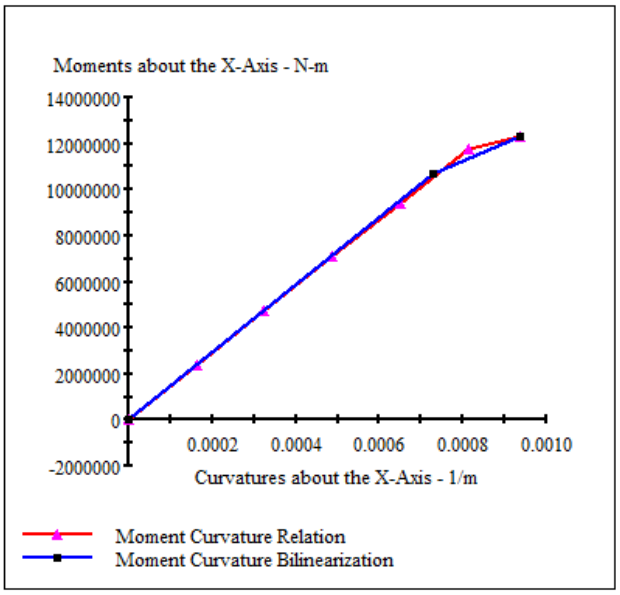

a)

Section	Section3
Loading	mc3
Units	strain
Data	
0	0
1	-52.31E-6
2	-.1050E-3
3	-.1584E-3
4	-.2129E-3
5	-.2687E-3
6	-.2908E-3

b)

Section	Section3
Loading	mc3
Units	strain
Data	
0	0
1	.1892E-3
2	.3781E-3
3	.5661E-3
4	.7532E-3
5	.9389E-3
6	1.103E-3

Figure B26. Moment-curvature diagram, minimum concrete strain (a) and maximum tensile steel strain (b).

- **Wet-lay up system: $t_{frp} = 3,42\ mm$**

Analysis Results:

Failing Material:	Fiber
Failure Strain:	1.179E-3 Tension
Curvature at Initial Load:	0 1/m
Curvature at First Yield:	-.8148E-3 1/m
Ultimate Curvature:	-.9368E-3 1/m
Moment at First Yield:	-11.96E+6 N-m
Ultimate Moment:	-12.29E+6 N-m
Centroid Strain at Yield:	.2210E-3 Ten
Centroid Strain at Ultimate:	.2752E-3 Ten
N.A. at First Yield:	-271.3 mm
N.A. at Ultimate:	-293.8 mm
Energy per Length:	6291 N
Effective Yield Curvature:	.7297E-3 1/m
Effective Yield Moment:	1.07E+7 N-m
Over Strength Factor:	-1.147
EI Effective:	1.47E+10 N-m^2
Yield EI Effective:	7.61E+9 N-m^2
Bilinear Harding Slope:	51.80 %
Curvature Ductility:	1.284

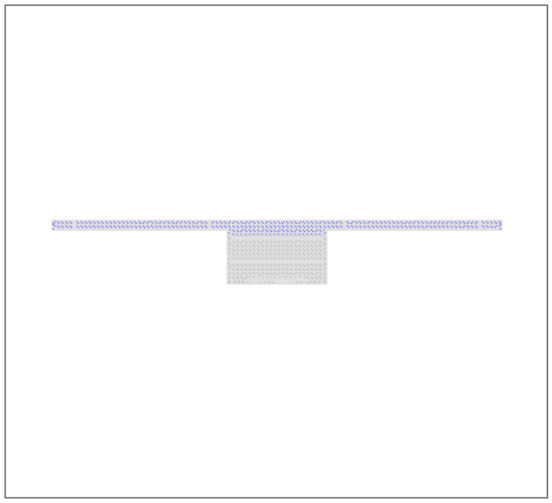

Figure B27. Analysis results and neutral axis position.

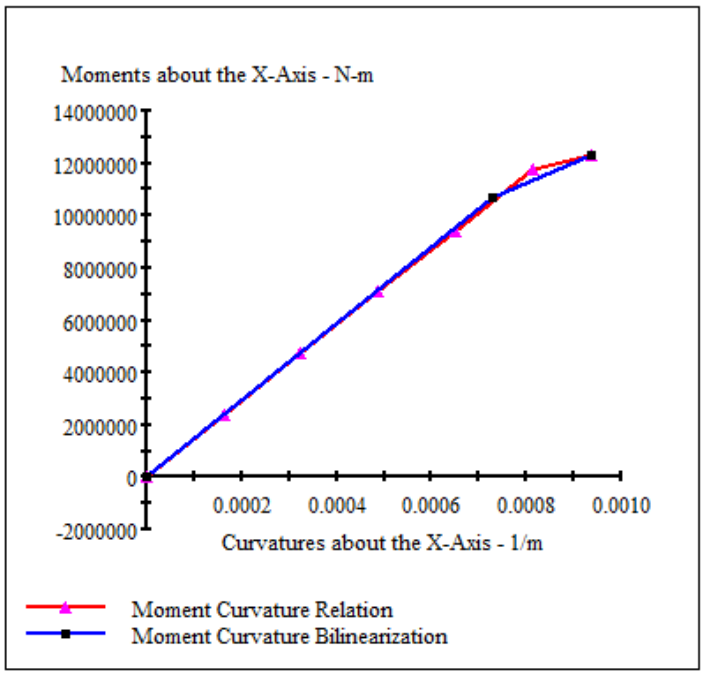

a)

Section	Section3
Loading	mc3
Units	strain
Data	
0	0
1	-52.25E-6
2	-.1051E-3
3	-.1585E-3
4	-.2130E-3
5	-.2687E-3
6	-.2908E-3

b)

Section	Section3
Loading	mc3
Units	strain
Data	
0	0
1	.1893E-3
2	.3780E-3
3	.5661E-3
4	.7532E-3
5	.9390E-3
6	1.102E-3

Figure B28. Moment-curvature diagram, minimum concrete strain (a) and maximum tensile steel strain (b).